Inaugural dissertation

for

obtaining the doctoral degree

of the

Combined Faculty of Mathematics, Engineering and Natural Sciences

of the

Ruprecht - Karls - University

Heidelberg

Presented by

M.Sc. Annalena Marie Meyer

born in Berlin, Germany

Oral examination: 05.12.2022

Nanodomain organization of the FGF2 secretory machinery

Referees: Prof. Dr. Walter Nickel

Prof. Dr. Michael Brunner

Table of Contents

Abstract *9*

Zusammenfassung *11*

1 Introduction *13*

1.1 Protein secretion **13**

1.1.1 Classical pathway of protein secretion 13

1.1.2 Unconventional protein secretion 16

1.2 Fibroblast growth factors **20**

1.2.1 The FGF family: properties and biological functions 20

1.2.2 Fibroblast growth factor 2 21

1.2.3 Type I UPS of FGF2 22

1.3 Heparan sulfate proteoglycans **24**

1.3.1 Biological functions of HSPGs 24

1.3.2 HS structure and synthesis 25

1.3.3 HSPG-protein interaction 26

1.3.4 Membrane bound HSPGs 27

1.4 Nanodomains and membrane organization **30**

1.4.1 Imaging membrane nanodomains 30

1.4.2 Proteins can associate with nanodomains 32

1.4.3 Caveolae and Caveolins 32

2 Aim of the thesis *35*

3 Materials and Methods *37*

3.1 Materials **37**

3.1.1 Chemicals, reagents, beads 37

3.1.2 Consumables 39

3.1.3 Kits and assays 40

3.1.4 Antibodies 41

3.1.5 Oligos and gRNAs 42

3.1.6 Plasmids 43

3.1.7 Cell lines 45

3.1.8 Technical devices 47

3.1.9 Software 47

3.2 Methods....48
3.2.1 Cloning....48
3.2.2 Cell culture....51
3.2.3 RT-qPCR....54
3.2.4 Biochemical methods....56
3.2.5 Microscopy....61
4 Results....63
4.1 The role of glypicans in FGF2 secretion....63
4.1.1 GPC1 is a rate-limiting factor in FGF2 secretion....63
4.1.2 GPC1 does not play a role in FGF2 endocytosis....66
4.1.3 Glypican-1, FGF2 and the α1 subunit of the Na,K-ATPase are in proximity to each other in HeLa S3 cells 68
4.1.4 HA-GPC1 expression levels can be correlated to FGF2-GFP secretion....80
4.1.5 Both GPC1 and GPC6 impact FGF2-GFP secretion in U2OS cells....81
4.1.6 Concluding remarks on glypicans in FGF2 secretion....88
4.2 Components involved in FGF2 secretion organize into membrane nanodomains....89
4.2.1 Proteins involved in FGF2 secretion are in proximity to each other in microscopy experiments 89
4.2.2 Proteins involved in FGF2 secretion localize together to detergent resistant membrane fractions 94
4.2.3 Concluding remarks on FGF2 secretion nanodomains....97
4.3 Caveolin-1 and Caveolin-2 might play a role in FGF2 nanodomain organization....98
4.3.1 Caveolin-1 did not impact FGF2-GFP secretion in HeLa S3 cells....98
4.3.2 Cav2 KO, not Cav1/2 dKO, reduced FGF2-GFP secretion in HeLa S3 cells....101
4.3.3 Caveolin-2 KO influenced protein localization into detergent resistant membrane fractions....103
4.3.4 Cav2 overexpression did not rescue the FGF2-GFP secretion phenotype....105
4.3.5 The order of caveolin KO altered secretion phenotypes....113
4.3.6 Caveolin-1 KO in U2OS FGF2-GFP did not impact FGF2 secretion in biotinylation, but did in TIRF 115
4.3.7 Overexpression of Cav1 or Cav2 in U2OS cells did not impact FGF2-GFP secretion in biotinylation 117
4.3.8 Neither Cav2 KO nor Cav1/2 dKO in U2OS altered FGF2-GFP secretion in biotinylation....118
4.3.9 Cav1 localization into liquid ordered membrane areas was not affected by Cav2 KO in U2OS.121
4.3.10 Concluding remarks on caveolin-1 and caveolin-2 in S3 or U2OS cells....123
4.4 The α1-subunit of the Na,K-ATPase interacts with $PI(3,4,5)P_3$....124
5 Discussion....127

5.1 Understanding UPS of FGF2 better 127

5.2 GPC1, GPC5 and GPC6 have different impacts on FGF2 secretion 128

5.3 PLA experiments showed proximity between proteins involved in FGF2 secretion 130

5.4 Components involved in FGF2 secretion localize into nanodomains 131

5.4.1 Proximity of components in PLA can reflect nanodomain organization 131

5.4.2 DRM experiments can demonstrate nanodomain organization 132

5.4.3 STED microscopy experiments can support the nanodomain hypothesis 133

5.5 Caveolins – interesting, yet complicated 134

5.5.1 Caveolin phenotypes in HeLa S3 cells 134

5.5.2 Caveolins and the nanodomain organization of the FGF2 secretory machinery 136

5.5.3 Caveolin phenotypes in U2OS cells 137

5.6 PI(3,4,5)P_3 interacts with the Na,K-ATPase 138

6 Future perspective 139

7 References 141

8 Abbreviations 153

9 Acknowledgements 157

Abstract

Fibroblast growth factor 2 (FGF2) is a potent mitogen involved in angiogenesis and tumor cell survival. Although a secretory protein involved in autocrine and paracrine signaling, FGF2 does not contain a signal peptide and bypasses the classical ER-Golgi-dependent route of protein secretion. In fact, FGF2 is secreted unconventionally (type I UPS) via direct translocation across the plasma membrane by self-sustained pores. FGF2 is recruited to the plasma membrane via interaction with the α1 subunit of the Na,K-ATPase. Thereafter FGF2 interacts with Tec kinase, which phosphorylates FGF2. FGF2 binds to the phosphoinositide $PI(4,5)P_2$, which drives its dimerization and oligomerization into membrane-spanning complexes. FGF2 is then captured on the cell surface through binding to heparan sulfate proteoglycans (HSPGs).

The GPI-anchored HSPG glypican-1 (GPC1) was identified in our laboratory via a genome-wide BioID screen. In the here presented thesis, GPC1 CRISPR-Cas9 knockout (KO) cell lines were shown to secrete significantly less FGF2 in cell surface biotinylation assays. GPC1 reintroduction and stable overexpression did not only restore secretion to wild-type levels but even further increased secretion. FGF2 endocytosis was not affected by GPC1 KO or overexpression. As I could correlate GPC1 levels to FGF2 secretion in TIRF microscopy, GPC1 can be considered a rate-limiting factor for FGF2 secretion. GPC5, another endogenously expressed glypican in HeLa cells, did not reduce FGF2 secretion when knocked out. Also, GPC5 could not compensate for loss of GPC1 in the here demonstrated data. GPC6 knockout in U2OS cells only led to a modest decrease in FGF2 secretion, yet further decreased FGF2 secretion in GPC1 KO cells in my experiments.

Organization of FGF2 and the components needed for secretion into nanodomains would facilitate fast FGF2 secretion from cells. FGF2, α1 and GPC1 were indeed shown to be in proximity to each other in the here conducted proximity ligation assays. Also, I found all three components in detergent resistant membrane (DRM) fractions, whereby GPC1 was the determining factor for FGF2 DRM localization. Super resolution STED experiments showed a homogenous distribution of α1 and GPC1 throughout the membrane. Interestingly, I found FGF2 and $PI(4,5)P_2$ in areas enriched in cholesterol detected via EGFP-$Gram_{1b}$ G187L transfection, which is supported by recent findings demonstrating that cholesterol promotes FGF2 secretion.

Caveolins, cholesterol-binding proteins that assemble into detergent resistant membrane fractions, were analyzed regarding their effect on FGF2 secretion. In my experiments caveolin-1 (Cav1) and -2 (Cav2) affected FGF2 secretion in HeLa S3 and U2OS. In HeLa cells, caveolin-2 KO cells showed reduced FGF2 secretion in biotinylation experiments. Intriguingly, caveolin-1 failed to localize into DRM fractions in this context and also α1 and FGF2 levels were reduced in liquid ordered detergent resistant fractions. Cav2 KO in U2OS on the other hand, did not impact FGF2 secretion in my hands, although TIRF data demonstrated Cav1 to be involved in FGF2 secretion. Caveolin function in FGF2 nanodomain organization remained unresolved.

Pulldown experiments I conducted using trifunctional lipid probes demonstrated an interaction between $PI(3,4,5)P_3$ and the α1 subunit of the Na,K-ATPase, further supporting the hypothesis of specialized membrane domains involved in FGF2 membrane translocation into the extracellular space.

Zusammenfassung

Der Fibroblasten-Wachstumsfaktor (FGF2) ist ein potentes Mitogen, welches an der Angiogenese und dem Überleben von Tumorzellen beteiligt ist. Obwohl FGF2 ein sekretorisches Protein ist, das an der autokrinen und parakrinen Signalübertragung beteiligt ist, enthält es kein Signalpeptid und umgeht den klassischen ER-Golgi-abhängigen Weg der Proteinsekretion. Tatsächlich wird FGF2 unkonventionell (Typ I UPS) durch direkte Translokation durch autarke Poren sezerniert. FGF2 wird durch die α1-Untereinheit der Na,K-ATPase an die Plasmamembran rekrutiert. Danach interagiert FGF2 mit Tec-Kinase, die FGF2 phosphoryliert. FGF2 bindet an das Phosphoinositid $PI(4,5)P_2$, das seine Oligomerisierung zu membrandurchspannenden Komplexen vorantreibt. FGF2 wird dann auf der Zelloberfläche durch Bindung an Heparansulfat-Proteoglykane (HSPG) eingefangen.
Das GPI-verankerte HSPG Glypican-1 (GPC1) wurde in unserem Labor über einen genomweiten BioID-Screen identifiziert. In der hier vorgestellten Arbeit wurde gezeigt, dass GPC1 CRISPR-Cas9 Knockout (KO) Zelllinien signifikant weniger FGF2 in Zelloberflächen-Biotinylierungsassays sezernieren. Die Wiedereinführung von GPC1 stellte nicht nur die Sekretion auf das Wildtypniveau wieder her, sondern erhöhte die Sekretion sogar noch weiter. Die FGF2-Endozytose wurde hingegen nicht beeinflusst. Da ich die GPC1-Spiegel mit der FGF2-Sekretion in der TIRF-Mikroskopie korrelieren konnte, kann GPC1 als geschwindigkeitsbegrenzender Faktor für die FGF2-Sekretion angesehen werden. GPC5, ein weiteres endogen exprimiertes Glypican in HeLa-Zellen, beeinflusste die FGF2-Sekretion nicht. GPC5 konnte den Verlust von GPC1 in den hier gezeigten Daten nicht kompensieren. GPC6-Knockout in U2OS-Zellen führte in meinen Experimenten nur zu einer bescheidenen Abnahme der FGF2-Sekretion, jedoch zu einer weiteren Abnahme der FGF2-Sekretion in GPC1-KO-Zellen.
Die Organisation von FGF2 und den für die Sekretion benötigten Komponenten in Nanodomänen würde eine schnelle FGF2-Sekretion aus Zellen erleichtern. In den hier durchgeführten PLA („proximity ligation assay“) Experimenten wurde gezeigt, dass FGF2, α1 und GPC1 nahe beieinander liegen. Außerdem fand ich alle drei Komponenten in Fraktionen mit Detergens-resistenten Membranen (DRM), wobei GPC1 der bestimmende Faktor für die Lokalisierung von FGF2 in DRM-Fraktionen war. STED-Experimente zeigten eine homogene Verteilung von α1 und GPC1 über die gesamte Membran. Interessanterweise fand ich FGF2 und $PI(4,5)P_2$ in Bereichen, die mit Cholesterin angereichert waren, nachgewiesen durch EGFP-Gram1b G187L-Transfektion, was durch neuere Erkenntnisse gestützt wird, die zeigen, dass Cholesterin die FGF2-Sekretion fördert.
Caveoline, cholesterinbindende Proteine, die sich zu Detergens-resistenten Membranfraktionen zusammenlagern, wurden hinsichtlich ihrer Wirkung auf die FGF2-Sekretion analysiert. In meinen Experimenten beeinflussten Caveolin-1 (Cav1) und -2 (Cav2) die FGF2-Sekretion in HeLa S3- und U2OS-Zellen. In HeLa-Zellen zeigten Caveolin-2 KO-Zellen in Biotinylierungsexperimenten eine reduzierte FGF2-Sekretion. Interessanterweise gelang es Caveolin-1 in diesem Zusammenhang nicht, sich in DRM-Fraktionen zu lokalisieren, und auch die α1- und FGF2-Level waren in Detergens-resistenten Fraktionen reduziert. Cav2 KO in U2OS hingegen hatte keinen Einfluss auf die FGF2-Sekretion in meinen Händen, obwohl TIRF-Daten zeigten, dass Cav1 an der FGF2-Sekretion beteiligt war. Die Caveolin-Funktion bei der Organisation von FGF2-Nanodomänen blieb ungelöst.
Pulldown Experimente mit trifunktionellen Lipidproben haben eine spezifische Interaktion zwischen α1 und $PI(3,4,5)P_3$ nachgewiesen. Dies unterstützt die Hypothese von organisierten Membrandomänen die auf die FGF2-Sekretion spezialisiert sind.

1 Introduction

1.1 Protein secretion

Soluble proteins or transmembrane proteins have to reach their final destination in order to exert their biological function. This means they have to be either transported and incorporated to the plasma membrane or they need to be secreted into the extracellular space. Secretion can be subdivided into the classical pathway via the Endoplasmic Reticulum (ER) – Golgi or unconventional protein secretion (UPS), where proteins bypass this classical route of secretion. It has been predicted that almost 14% of the human proteome is secreted by classical or non-classical secretory pathways [1].

1.1.1 Classical pathway of protein secretion

The classical secretory pathway implies transport through the rough ER, the ER exit sites (ERES), the ER to Golgi intermediate compartment (ERGIC), the Golgi complex and post Golgi network that carries the protein to its final location [2]. For details of ER-Golgi secretion, please refer to Figure 1.
Proteins carrying a signal peptide, a specific 16-30 amino acid long sequence containing 6-12 hydrophobic amino acids flaked by positively charged residues at the amino terminus of the nascent polypeptide chain, are recruited to the ER alongside with their bound ribosomes during translation [3]. The signal sequence is recognized by the signal recognition particle (SRP), a ribonucleoprotein complex of six proteins and an RNA scaffold. Elongation halts temporarily, but once the SRP has bound correctly to the SRP receptor, the polypeptide chain is translocated cotranslationally into the lumen of the rough ER through the trimeric Sec 61 α, β, γ translocon and SRP is released from the SRP receptor via GTP hydrolysis [4]. As the proteins enter the ER a signal peptidase associated with the translocon removes the signal peptide since this is no longer needed [5]. After full protein translation initial glycosylation, disulfide-bridge formation and other posttranslational modifications are performed in the ER.
Sugar must be added to glycoproteins before they can be secreted. N-linked glycosylation is highly conserved in all eukaryotes and requires glucose (Glc) and mannose (Man) chain addition to the N-acetylglucosamine (NAc) stem and later addition of the sugar chain to a target asparagine residue via an N-glycosidic bond [6]. This process begins in the cytosol via synthesis of a dolichol phosphate backbone, whereafter the entire lipid intermediate Man(5)GlcNAc(2)-PP-dolichol is translocated into the ER lumen [4]. Rft1, an ER membrane protein, has been proposed to mediate this translocation, as mutations in the human RFT1 gene are associated with diseases of N-glycosylation, yet functional flippase activity of Rft1 has not convincingly been demonstrated in reconstitution experiments [4, 7, 8]. After translocation four mannose and three glucose residues are added to form Glc(3)Man(9)GlcNAc(2)-PP-dolichol which is afterwards added to the asparagine residue (Asn-X-Ser/Thr whereby X ≠ P) on the acceptor glycoprotein by the oligosaccharide transferase (OST) once the target protein enters the ER [9, 10]. Glycosylation is essential for protein folding and quality control in the ER. The outermost glucose residues are removed by glucosidase I (GCSI) and II (GCSII),

allowing the monoglycosylated glycan to be recognized by the lectins calnexin (CNX) and calreticulin (CRT) which promote folding. Multiple rounds of glucose trimming and re-glycosylation are performed until the protein is released for further processing in the Golgi [11]. If proteins are not folded correctly the ER-associated degradation (ERAD) pathway becomes activated which recognizes the misfolded proteins, targets them for re-translocation into the cytoplasm or mediates ubiquitination and protein degradation via the proteasome [12].

O-linked glycosylation on the other hand is very diverse and is initiated by the transfer of a single monosaccharide to a hardly predictable serine or threonine residue within the target protein [4, 11]. Initiation can occur in the ER, but most modifications are carried out in the Golgi.

The oxidizing environment in the ER, which is established in part by the relatively high oxidized to reduced glutathione (GSSG:GSH) ratio, supports protein disulfide formation which is often required for correct folding and protein function [4]. Disulfide bridges can form co-translationally or after translocation to the ER. Protein disulfide isomerases (PDI) and endoplasmic reticulum oxidoreductases regulate disulfide bridge formation and the transport of electrons, whereby recent data show that oxidized Ero1 (endoplasmic reticulum oxidoreductin 1) first oxidizes PDI which in turn then oxidizes the substrate [13]. When non-native disulfide bridges form between adjacent cysteines co-translationally or as folding intermediate they must be isomerized by PDI to form the correct pair.

After correct folding proteins exit the ER at ER exit sites (ERES) via coat protein complex II (COPII) vesicles which are transported to the Golgi or fuse to form the ER Golgi intermediate compartment (ERGIC) and thereafter are directed to the Golgi [14, 15]. COPII vesicle formation is best understood in yeast where it is initiated by the activation of the small GTPase Sar1 [16]. The ER-bound guanine nucleotide exchange factor (GEF) Sec12 mediates conversion of Sar1-GDP to Sar1-GTP and allows for Sar1 insertion into the ER membrane [14, 17]. Inserted Sar1 can thereafter recruit Sec23-Sec24 heterodimer to together recruit cargo into the pre-budding complex [18]. The Sec13-Sec31 heterotetramer then forms the outer layer of the COPII coat and drives membrane deformation and budding via crosslinking of pre-budding complexes [14]. COPII vesicles are usually within 60-90 nm in diameter, which explains why additional proteins such as TANGO1 and cTAGE5 are necessary for transport of large proteins, such as collagens [19, 20].

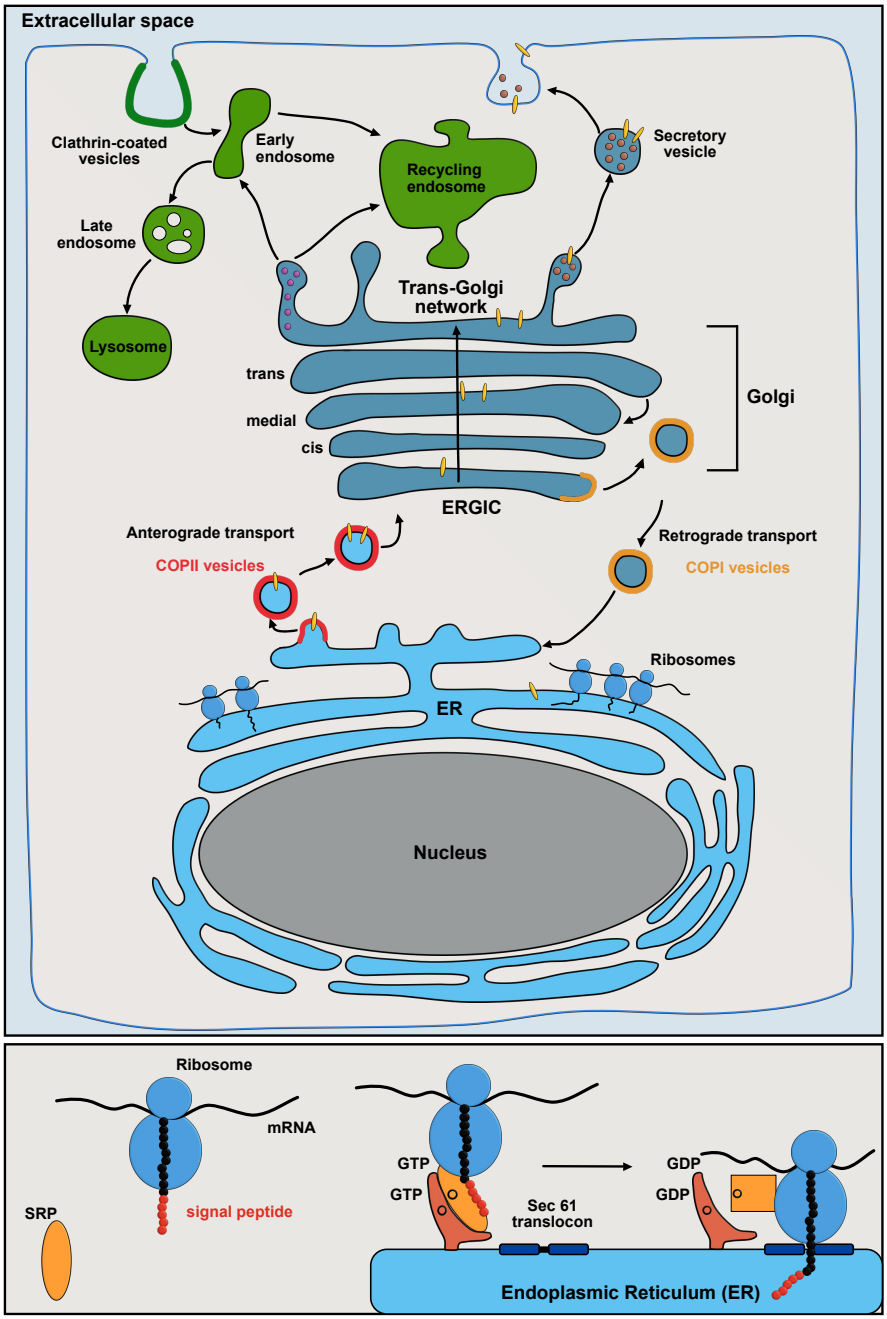

Figure 1: Classical ER-Golgi route of protein secretion. Top panel: The classical route of secretory proteins starts at the ER, where the polypeptide chain is co-translationally imported. After correct folding and initial modifications, proteins are transported to the ER-Golgi intermediate compartment (ERGIC) via anterograde transport within COPII vesicles. Further modifications are conducted at the Golgi until proteins are mature for secretion. Retrograde transport from the Golgi back to the ER is achieved via COPI vesicles. Mature proteins get sorted at the Trans-Golgi network (TGN) for secretion or transport into endosomes and lysosomes. Bottom panel: Polypeptide chains translated at the ribosome containing a signal peptide get recognized by the signal recognition particle (SRP). The ribosome gets recruited to the ER via the SRP receptor. Upon GTP hydrolysis, the Sec61 translocon allows for peptide import into the ER lumen and SRP dissociates from its receptor.

The Golgi apparatus consists of stacks formed of five to eight flattened cisternae, which can be subdivided into cis-, medial-, and trans-Golgi cisternae according to their functionality and location [21]. The cis-Golgi faces the ER and receives the newly folded proteins, whereas the trans-Golgi faces the plasma membrane. The Golgi is highly dynamic during the cell cycle as it disassembles in mitosis to be evenly distributed to both daughter cells and then has to reassemble in early interphase [21, 22].

Unstacking at mitosis is caused by phosphorylation of Golgi stacking and tethering proteins via cyclin-dependent kinase 1 (Cdk1) and polo-like kinase 1 (Plk1) which in turn leads to de-oligomerization of Golgi reassembly stacking protein of 65 kDa (GRASP65) [21, 23]. Dephosphorylation of GRASP65 and GRASP55 by protein phosphatase PP2A on the other hand leads to reassembly of the Golgi and cisternae stacking [24, 25]

Trafficking, glycan maturation and sorting of proteins occurs in the Golgi in a progressive fashion, which is achieved via distinct polarity of the cisternae in both structure and function [26]. As mentioned previously N-glycosylation and O-glycosylation is initiated in the ER, but proteins have to mature in the Golgi. Secreted or plasma membrane proteins get modified sequentially via removal of three additional mannose residues, sequential addition of N-acetylglucosamine (GlcNAc), removal of two mannose residues, addition of fucose and two GlcNAc, and final addition of three galactose and sialic acid residues [26].

Proteins are sorted for transport at the Golgi. Intra-Golgi transport, ensuring correct distribution of proteins within the stacks, or retrograde transport from the Golgi back to the ER is accomplished by COPI vesicles [27]. COPI coatomers, consisting of seven subunits, form the coat [28]. Arf1, a small GTPase of the Ras family, regulates COPI vesicle biogenesis by recruiting coatomers to the membrane, after it is inserted into the membrane via GDP-GTP exchange, catalyzed by the GEF GBF1 [29]. Coatomer recruitment also requires presence of members of the p24 family, which bind directly to coatomer and increase vesicle formation efficiency [30]. The tubular trans-Golgi network more specifically sorts proteins to different acceptor compartments such as: the plasma membrane, early or late endosomes, secretory granules and others [31]. Simultaneously it receives proteins from the endocytic pathway such as proteins internalized via clathrin-mediated endocytosis. Sorting signals involve: specific sorting motifs recognized by GTPases of the ARF and Rab family, posttranslational modifications such as glycosylation, phosphorylation and ubiquitination, protein complex formation, and increased affinities of sorted proteins for certain membrane domains enriched in sphingolipids or cholesterol [31]. As demonstrated the TGN is a complex organelle that involves diverse machineries and needs coordination of all processes.

All in all, the conventional secretory pathway has to be tightly regulated to ensure correct protein maturation and transport to the cell surface. Altered protein secretion or defects in the ER or Golgi can therefore be observed in a broad range of diseases.

1.1.2 Unconventional protein secretion

Many proteins are secreted from cells despite lacking a signal peptide, yet are not simply released via cell lysis or rupture. These regulated processes, including extracellular secretion of “leaderless proteins” that do not contain a signal peptide and cell surface transport of transmembrane proteins bypassing the Golgi route, are collectively termed unconventional protein secretion (UPS) [32-34]. UPS cargos share in common that they are insensitive to Brefeldin A, Monesin or Nocodazole, all drugs that block classical ER-Golgi mediated trafficking and secretion [35-37]. More than 17% of the human proteome have been predicted to be secreted in a non-classical manner by novel prediction tools [38]. UPS from cells is

largely triggered by stress, such as inflammation, ER stress, nutrient starvation and mechanical stress. Therefore, understanding UPS of different cargo proteins provides potential for novel therapeutic treatments, as many stresses are associated with diseases [32]. Alzheimer's disease, allergic and autoimmune diseases such as encephalomyelitis and atherosclerosis, and even diabetes are UPS-related diseases that trigger unconventional protein secretion [39-42]. UPS cargos such as heat shock proteins and growth factors regulate the progression of cancer, immunomodulation and stimulation of proliferation or angiogenesis [32, 43-45].

UPS proteins can be categorized into two superordinated groups: (1) soluble cytoplasmic proteins that do not contain a signal peptide and are active after plasma membrane translocation into the extracellular space via three different types of pathways (UPS type I, II or III) and (2) integral transmembrane or signal peptide-containing proteins that are inserted into the ER, but reach the cell surface without passing through the Golgi (UPS type IV) [33, 46]. The different pathways are depicted in Figure 2.

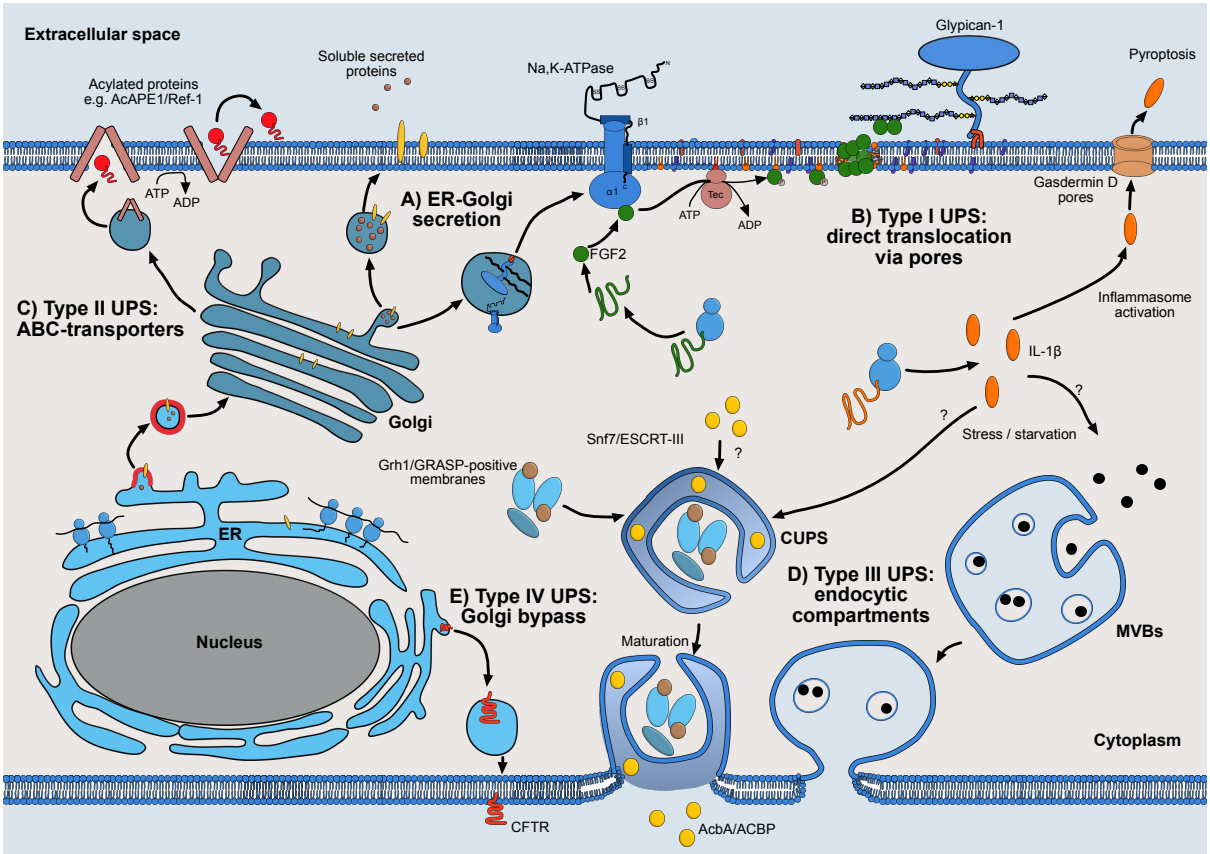

Figure 2: Different types of unconventional protein secretion exist. A) There is the classical ER-Golgi dependent route of protein secretion in contrast to four different types of unconventional protein secretion (UPS). B) Type I UPS describes proteins which translocate directly across the plasma membrane via pore formation. Examples are FGF2, which creates its own pores, and IL-1β which can be secreted via gasdermin D pores in the context of inflammasome activation and pyroptosis. C) Type II UPS corresponds to secretion of acylated proteins, such as AcAPE1/Ref-1, via ABC-transporters. D) Type III UPS is carried out via endocytic compartments. These can involve CUPS or MVB formation in the context of autophagy. IL-1β is proposed to alternatively use this form of protein secretion. Another well-studied cargo is AcbA/ACBP. E) Type IV UPS describes proteins that contain a signal peptide and reach the ER, yet are thereafter secreted bypassing the Golgi. An example is CFTR. Image adapted from [46].

1.1.2.1 Type I UPS: direct translocation via pores

Type I UPS involves protein translocation via direct plasma membrane pore formation, which can either be self-sustained or triggered by inflammation. FGF2 and HIV TAT are two well-studied proteins that are constitutively secreted from cells and are independent from stress. These proteins are recruited to the plasma membrane via interaction with the phosphoinositide $PI(4,5)P_2$ which induces self-oligomerization into membrane spanning lipidic pores with a toroidal structure [33, 47, 48]. After translocation FGF2 remains bound to cell surface heparan sulfate proteoglycans (HSPGs) and this interaction drives secretion [49-51]. Likewise, it has been shown that HIV TAT binds to HSPGs, yet whether this binding is necessary for secretion has not been shown [33, 52]. The unconventional secretion of FGF2 will be discussed later in more detail in 1.2.3.

Alternatively, type I UPS protein secretion is triggered by inflammation. Interleukin-1β (IL-1β) is a well-studied leaderless cytokine whose classification into type I or type III secretion is debated and the mode of secretion seems to be dependent on cell type or cell fate. When IL-1β is secreted from macrophages it is released via type I UPS via hyperpermeabilization of cells and subsequent cell lysis [53]. It does not bind to $PI(4,5)P_2$ and does not form self-sustained pores, despite having a β-barrel structure similar to FGF2 [53]. IL-1β is produced as inactive precursor pro-IL-1β. Cell exposure to pathogen-associated molecular patterns (PAMPs) causes inflammasome activation, which in turn causes activation of caspase-1 and maturation of pro-IL-1β into its active secreted form [54]. Caspase-1 activation also leads to pyroptosis, a form of programmed necrosis, where gasdermin D (GSDMD) is cleaved by caspase-1 into an N- and C-terminal fragment [55]. Under normal conditions N-gasdermin can bind to the plasma membrane via interaction with $PI(4,5)P_2$ and forms large oligomeric pores promoting fast cytokine release and cell lysis [56, 57]. Alternatively, IL-1β can be secreted via a GSDMD-dependent pathway which does not involve cell lysis from bone marrow derived macrophages and neutrophils [55]. In this process GSDMD is presumably only mildly activated or not expressed at very high levels.

Tau, the misfolded and hyperphosphorylated protein leading to tauopathies such as Alzheimer's disease, is also secreted via type I UPS. Tau interacts with phosphoinositides and more precisely can bind to $PI(4,5)P_2$ – containing large unilamellar vesicles (LUVs) in *in vitro* binding experiments [58]. The same study demonstrated that recombinant Tau can also disrupt the lipid bilayer when $PI(4,5)P_2$ is present in LUVs. Manipulating plasma membrane properties via increasing cholesterol and sphingomyelin promotes Tau secretion as Tau is recruited to microdomains at or near the plasma membrane [59]. Tau can bind to heparin and HSPGs have been implicated in the cellular uptake of Tau [60, 61]. It is therefore not surprising that cell surface biotinylation experiments detected a large portion of Tau, especially a phosphomimetic mutant, on the cell surface of living cells [58]. Tau is partially released to the cell medium after binding to HSPGs. Therefore, treatment of cells with $NaClO_3$, an inhibitor of heparan sulfate chain sulfation, does not only decrease surface Tau, but also to a big extent decreases soluble Tau in the cell supernatant and reduces cell-cell spreading of Tau [58]. It seems Tau is not only secreted by a single pathway though, as it has been described that Tau can also be secreted via type III and type IV secretion involving secretion via membranous organelle-based secretion and ectosome shedding [62].

Other, yet not very well-studied Type I UPS cargos, are FGF1, Annexin A1, Galectin-1 and TG2 [46].

1.1.2.2 Type II UPS: ABC-transporters

Type II unconventional protein secretion refers to proteins secreted via ATP-binding cassette (ABC-) transporters. ABC-transporters make up a large family of integral membrane proteins that can act both as exporters or importers via the hydrolysis of ATP and subsequent conformational change [63]. Not many proteins are known to be secreted by this mechanism. ABCA1 for instance promotes the secretion of acetylated apurinic endonuclease-1/redox factor-1 (AcAPE1/Ref-1), which in turn reduces proinflammatory responses and thereby promotes atherosclerosis [64]. Other cargos for unconventional protein secretion type II are Mat a, the mating pheromone a-factor of *S. cerevisae*, *Leishmania* hydrophilic acylated surface protein B (HASPB) and macrophage migration inhibitory (MIF) [65-67].

1.1.2.3 Type III UPS: Endocytic compartments and fusion with the plasma membrane

Type III UPS pathway is stress-dependent and includes proteins that are secreted via endosomes or autophagosomes which later fuse with the membrane [33, 68].
In *Dictyostelium*, cells fail to form viable spores under starvation conditions. Malhotra and colleagues discovered that the spore differentiation factor-2 (SDF-2), which is synthesized as part of the precursor protein acyl-CoA-binding protein (AcbA in *Dictyostelium,* Acb1 in yeast and ACBP in mammals), is not secreted form cells lacking GRASP [69]. The enzyme that converts AcbA to SDF-2 has its active center facing the extracellular space, indicating that AcbA must be secreted to the extracellular space for cleavage [46]. Since AcbA lacks a signal peptide, the secretion pathway was proposed to be unconventional. Studies of the yeast ortholog Acb1 showed that this protein is likewise secreted upon starvation and that secretion depends on the yeast GRASP orthologue Grh1 and the plasma membrane SNARE protein Sso1 [46]. Grh1 is necessary for formation of cup-shaped compartments, later termed compartments for unconventional protein secretion (CUPS), which are a characteristic for type III UPS. Grh1 relocates from the ER-Golgi to bigger cytoplasmic areas forming small vesicles that later fuse to a tubular compartment in an endosomal sorting complex required for transport (ESCRT)-I, -II, and -III dependent manner [33]. Mature CUPS are encased in a membrane-bound saccule and later fuse with the membrane in a Sso1-dependent manner to release Acb1 [46]. Alternatively secretory autophagosomes have been shown to be involved in Acb1 secretion [70].
Also, IL-1β has been proposed to be secreted upon starvation. IL-1β matures in the endosome or lysosome to it active form and is then secreted from cells via fusion with the membrane [71]. Secretion from non-macrophage cells requires GRASP proteins and multi-vesicular-body (MVB) formation [72]. Incubation of cells with the (not very specific) autophagy inhibitors Wortmannin and 3'-methyladenine inhibits secretion of IL-1β [72]. Mutations in Atg5, the main gene for autophagy, also lead to loss of IL-1β secretion from macrophages upon starvation [73]. It is unclear though whether this type of secretion involves CUPS formation as it is the case for Acb1 in yeast or whether this is merely secretory autophagy. In general, the mechanism by which IL-1β is secreted depends greatly on the cell type and

the mode of stress. Either it is starvation-induced autophagic secretion or inflammation induces inflammasome activation and GSDMD-dependent secretion of IL-1β followed by cell lysis in some cases.

1.1.2.4 Type IV UPS: Signal peptide-containing proteins bypassing the Golgi

Proteins containing a signal peptide or transmembrane domain can be secreted bypassing the Golgi via type IV UPS. These proteins are synthesized in the ER, yet reach the plasma membrane even in presence of Brefeldin A which blocks ER-Golgi transport [74]. A consequence of this bypass is that type IV secreted proteins contain ER high-mannose oligosaccharides that were not processed in the Golgi [74]. This bypass can be induced by ER stress or mechanical stress. Upon ER stress monomeric Golgi GRASP55 relocates to the ER and there mediates the encapsulation of cystic fibrosis transmembrane conductance regulator (CFRT) and its vesicular transport to the membrane [75]. Alternatively, the second sorting machinery at the ER, Hsp70, can also be used to mediate Golgi bypass of pendrin [76]. Mechanical stress can also induce Golgi bypass, yet the mechanisms are not fully understood. In *Drosophila* oogenesis integrins have been shown to bypass the Golgi upon mechanical stress in a dGRASP-dependent manner and also ciliary membrane proteins have been shown to bypass the Golgi [33, 77, 78].

1.2 Fibroblast growth factors

1.2.1 The FGF family: properties and biological functions

The first fibroblast growth factor family member was discovered in the 1970s, when Gospodarowicz and colleagues purified a mitogen from pituitary glands and showed it could stimulate DNA synthesis [79]. This molecule was named basic FGF (bFGF) due to its high isoelectric point (pI), while a later molecule with FGF activity was named acidic FGF (aFGF) due to its low pI [80-82]. As more and more FGFs were discovered, bFGF and aFGF were renamed to FGF2 and FGF1 respectively. Up to date 24 family members have been discovered in vertebrates and invertebrates, while 22 FGF family members are known in humans (FGF1-14 and FGF16-23) [83]. The FGF11 subfamily (FGF11-FGF14) refers to a small subfamily of fibroblast homology factors (FHFs) that are not secreted and do not bind to FGF receptors (FGFRs) [84]. Although binding to heparin with high affinity, these FHFs differ in their functional role from the other FGFs as they interact with voltage-gated sodium channels [85, 86]. FGF15/19, FGF21 and FGF23 are in another subfamily (FGF15/19 subfamily) and act in an endocrine fashion, whereas the other canonical secreted FGFs (involving 5 subfamilies) function in a paracrine or autocrine manner [86].

Fibroblast growth factors are 17-34 kDa in size and contain a conserved core region of 120-130 amino acids showing 16-65% sequence similarity, which organizes into three 4-stranded β-sheets that fold into a β-trefoil structure [87, 88]. Within the β1 and β2 loop FGFs contain a positively charged heparan sulfate glycosaminoglycan binding site [89]. The highly variable C- and N-terminus determine protein

functionality and have non-receptor binding functions [90]. In contrast to other FGFs, FGF1 and FGF2 lack a N-terminal secretory signal peptide, yet are transported to the extracellular space via direct translocation across the plasma membrane [91]. The FGF9 subfamily (FGF9, FGF16 and FGF20) also does not contain a classical N-terminal signal peptide, yet these ligands are guided through the ER and Golgi towards the plasma membrane via an internal non-cleaved hydrophobic sequence [92].

FGF ligands bind to FGFRs (FGFR1-4) of the receptor tyrosine kinase family in a heparan sulfate proteoglycan (HSPG) -dependent manner [89]. FGF receptors contain a large extracellular ligand-binding domain containing three immunoglobulin (Ig) -like domains, a transmembrane domain and a split intracellular tyrosine kinase domain [93]. Functional complexes that can induce FGF signaling are therefore composed of dimers or FGF-FGFR-HSPG (1:1:1) complexes. FGF pathway control is achieved by alternative splicing of the receptor [94]. The Ig-like domains I and III and the linker between them regulate ligand binding specificity, whereas Ig-like domain I and the linker between I and II inhibit ligand binding [95, 96].

Many signaling processes are activated upon FGF-FGFR interaction. Once activated, the cytosolic domains of the FGFR dimers get cross-phosphorylated and serve as docking site for proteins or enzymes containing Src homology-2 (SH2) or phosphotyrosine binding (PTB) domains. This leads to activation of the RAS/MAP kinase pathway, the PI3 kinase/AKT pathway and the phospholipase C-γ (PLC-γ) pathway leading to gene expression, cell growth and differentiation, and cell survival or apoptosis [97]. It is therefore not surprising that malfunctioning of FGF signaling is related to many diseases such as chronic kidney disease (CKD) and chronic obstructive pulmonary disease (COPD), obesity, dwarfism syndromes, and many tumor-related processes such as invasion, migration and angiogenesis [98, 99].

1.2.2 Fibroblast growth factor 2

Fibroblast growth factor 2 belongs to the FGF1 subfamily of canonical FGFs together with FGF1. As mentioned previously, these ligands to not contain a signal peptide that guides them through ER-Golgi mediated protein secretion.

FGF2 consists of 5 different isoforms with distinct molecular weights, which are all translated from the same *FGF2* gene as summarized by Liao and colleagues [100]. The smallest form is the 18 kDa big low molecular weight (LMW) FGF2 consisting of 155 amino acids which represents the core C-terminus also found in all other higher molecular weight (HMW) FGF2 isoforms. LMW FGF2 is translated from a conventional Kozak AUG start codon, while the HMWs are translated from alternative upstream CUG codons [100]. Four HMW FGF2 isoforms exist with the sizes: 34 kDa, 24 kDa, 22,5 kDa and 22 kDa. LMW FGF2 consists of 12 antiparallel β-sheets and has been crystalized in complex with FGFR1 and heparin in a 2:2:2 stoichiometry or with FGFR2 (2:2) [101, 102]. All FGF2 isoforms contain a short C-terminal nuclear localization signal (NLS), while the high molecular weight isoforms also contain a classical N-terminal NLS consisting of Glu/Arg repeats and 34 kDa FGF2 even has a third arginine-rich NLS [103-105]. Therefore, HMW FGF2 isoforms localize mostly to the nucleus and exert their function there, whereas 18 kDa FGF2 can localize both to the nucleus and to the cytoplasm [105]. LMW FGF2

can, to be exact, translocate to the nucleus after cellular HSPG-dependent internalization or can translocate directly after translation into the nucleus [106, 107]. When LMW FGF2 remains in the nucleus gene transcription is only mildly stimulated in contrast to extracellular activation of FGFR1 by FGF2 [100]. When FGF2 is secreted, it can bind to FGFR1 (IIIb and IIIc), FGFR2 and FGFR4, although it has been shown that LMW FGF2 binds preferentially and stronger to FGFR1 (IIIc) [108, 109]. FGF2 is involved in many signaling events within embryogenesis, wound repair and hematopoiesis, whereby internalization of FGF2-FGFR complexes leads to termination of signaling [108, 110]. Deregulation of these pathways in cancer can occur via upregulation of the transcription of FGFR1 and FGFR2 or via point mutations impairing receptor internalization and signaling termination [111, 112]. In addition to that, FGF2 itself is a very potent mitogen and pro-angiogenic growth factor. FGF2 mediated FGFR1 activation in endothelial cells leads to migration, proliferation, protease production and angiogenesis [110]. FGF2 levels are increased in blood serum derived from cancer patients and FGF2 levels can be correlated to tumor size, stage and metastasis for several cancer types [110]. It is therefore critical to target the FGF2-FGFR pathway in cancer via different therapy approaches involving not only the use of ligand inhibitory molecules but also to fully understand how increased FGF2 is secreted and exported from the cell to target this pathway.

1.2.3 Type I UPS of FGF2

Type I unconventional protein secretion of low molecular weight FGF2 has been extensively studied in our laboratory throughout the last years in order to understand the pathway into great detail and provide therapeutical approaches to inhibit FGF2 secretion and signaling. A model of the so far know components has been proposed and is pictured in Figure 3.
In order to examine FGF2 secretion in a simplified approach, an *in vitro* system using affinity-purified plasma membrane inside-out vesicles was established [113]. Here it was first shown that the direct translocation of FGF2 into the lumen of inside-out vesicles is unidirectional and requires the presence of an asymmetrical export machinery, as FGF2 could not enter the lumen of right side-out vesicles. Also, cytosolic factors seemed to be essential for FGF2 translocation. It was early questioned in what state FGF2 translocates across the plasma membrane, as import of classically secreted protein into the ER lumen via the protein channel Sec61 or transport across mitochondrial membranes requires proteins to be in an unfolded state [114, 115]. Experiments using FGF2-GFP-DHFR showed that treatment of cells with aminopterin, an inhibitor of DHFR unfolding, does not inhibit FGF2 secretion, demonstrating that FGF2 is exported unconventionally in a folded conformation [116].

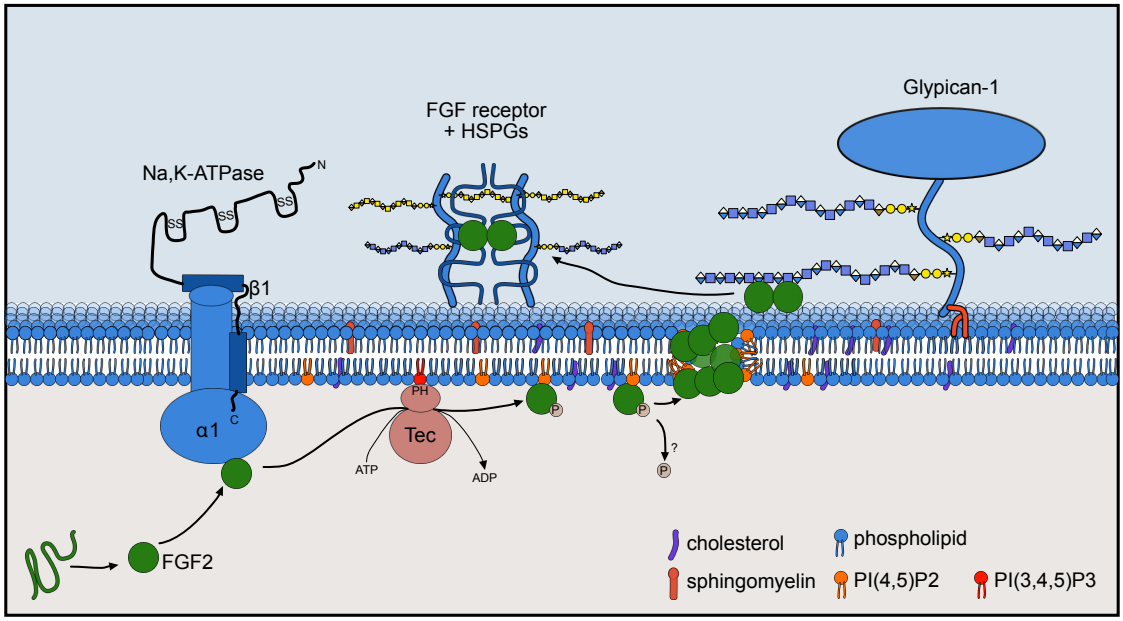

Figure 3: The type I unconventional protein secretion pathway of FGF2. FGF2 is recruited to the plasma membrane via interaction with the α1 subunit of the Na,K-ATPase. After phosphorylation by Tec kinase FGF2 binds to the phosphoinositide $PI(4,5)P_2$. This induces dimerization and oligomerization into membrane spanning complexes. FGF2 is retained at the cell surface via binding to HSPGs, namely GPC1. From there it can act in an autocrine or paracrine fashion via binding to FGF receptor-HSPG complexes. Adapted from [117].

FGF2 interacts at the plasma membrane with the α1 subunit of the sodium potassium (Na,K-) ATPase [118]. Even though FGF2 translocation was shown to be ATP independent *in vitro* [113], multiple pharmacological experiments have shown that the Na,K-ATPase is involved in FGF2 secretion. Treatment of cells with the Na,K-ATPase inhibitor ouabain blocks FGF2 export and this effect can be reversed when a ouabain-resistant mutant of the Na,K-ATPase is expressed [119-121]. Evidence for direct interaction or functional implication was missing at this point though. A genome-wide RNAi screen first identified that only the α1 subunit of the Na,K-ATPase is required for efficient secretion of FGF2 [118]. Removal of the β subunit does not impact FGF secretion, indicating that pump activity might not be essential for FGF2 secretion, as a functional Na,K-ATPase pump is composed of a heterodimer [122]. On the other hand, FGF2 secretion involves transient pore formation and pump activity might be needed to restore membrane potential and maintain cell viability. Furthermore, total internal reflection fluorescence (TIRF) microscopy experiments showed that α1 directly recruits FGF2 to the inner plasma membrane leaflet via interaction with two lysine residues (K54 and K60) on the surface of FGF2 and this interaction is needed for FGF2 secretion [123].

FGF2 is phosphorylated by Tec kinase at Y81 [124]. Down-regulation of Tec kinase via RNAi or pharmacological inhibition decreased FGF2 secretion in the same study. The precise function of Tec kinase and the organization within the secretory pathway of FGF2 remains debatable though.

FGF2 secretion requires interaction with the phosphoinositide $PI(4,5)P_2$, which is enriched at the inner plasma membrane leaflet [48, 125]. Although recombinant GFP-tagged FGF2 bound to multiple phosphoinositides immobilized on membranes, FGF2 is able to discriminate between different PIPs and binds to $PI(4,5)P_2$ with the highest affinity in plasma membrane-like liposomes [125]. Experiments also

showed that FGF2 binding to $PI(4,5)P_2$-containing liposomes is promoted by cholesterol-mediated clustering of $PI(4,5)P_2$ [125]. Temmerman and colleagues demonstrated that FGF2 binding to $PI(4,5)P_2$ is mediated by the K127, R128, K133 $PI(4,5)P_2$ binding pocket within FGF2, although K133 is also essential for HSPG binding of FGF2. FGF2 binding to $PI(4,5)P_2$ induces FGF2 dimerization and oligomerization into membrane spanning lipidic pores in reconstituted systems [48]. Disulfide bridge formation between cysteines 77 and 95 plays a pivotal role in oligomerization [126]. Once translocated to the cell surface, FGF2 localizes and remains bound to heparan sulfate proteoglycan-containing clusters on the cell surface [121, 127]. It was further shown that binding to HSPGs is not only important for FGF2 signaling or capturing, but also for secretion itself, as cell treatment with $NaClO_3$, which inhibits HS sulfation, drastically reduces surface FGF2 [127, 128]. Binding to HSPGs is mediated via the K133 residue within the $PI(4,5)P_2$ binding pocket of FGF2. Directionality of FGF2 secretion is achieved via higher affinity interaction with heparan sulfates (K_D ~ 100 nM) vs the interaction with $PI(4,5)P_2$ (K_D ~ 5-15 µM) and binding is mutually exclusive [129]. Whether FGF2 binds to a specific HSPG is part of the here presented thesis and results were published in collaboration with other members of the Nickel laboratory [51].

While FGF2 secretion is relatively slow in reconstituted systems, FGF2 secretion is a very dynamic and fast process in living cells and translocation takes place within ~200 ms [128]. This leads to the assumption that other regulatory or organizational mechanisms take effect within cells which must be further investigated.

1.3 Heparan sulfate proteoglycans

Heparan sulfate proteoglycans (HSPGs) are glycoproteins that have one or more heparan sulfate chain, a type of glycosaminoglycan (GAG), attached [130]. Cells have about 17 different HSPGs that can be classified according to their localization: membrane HSPGs, such as syndecans and glypicans, secreted HSPGs such as perlecans located in the extracellular matrix (ECM), and secretory vesicle HSPGs such as serglycin which are involved in inflammation amongst others [131]. Although very versatile in heparan sulfate (HS) chain number and length (size ranges between 20 – 150 nm), all HS and other sulfated GAGs have in common that are all highly negatively charged – a feature to keep in mind when working with HSPGs. The protein families of glypicans, syndecans and perlecans are highly conserved from vertebrates to the fruit fly *Drosophila* and the nematode *C. elegans* [132]. Not all HSPG members will be discussed in depth in this work.

1.3.1 Biological functions of HSPGs

Heparan sulfate proteoglycans, despite being few in number, play a role in many cellular processes as they are present in the extracellular matrix of every tissue and are practically on the cell surface of every organismal cell [133]. Extracellular matrix HSPGs, such as perlecan and agrin, help maintaining the integrity of the extracellular microenvironment by providing mechanical support and being a scaffolding component within the ECM [133-135]. Syndecans engage with components of the cytoskeleton, such

as α-actinin and integrins, and play a role in focal adhesions and stress fiber formation [136, 137]. HSPGs are essential for the regulation of development and regeneration, as they are key mediators of stem cell function and mediate cell fate decisions in embryonic stem cells [133]. It has been demonstrated in *Drosophila* and vertebrates that HSPGs, in particular glypicans, play a crucial role in many signaling pathways during development, such as Wnt/Wingless (Wg), Hedgehog (Hh), fibroblast growth factor (FGF) families and transforming growth factor-β (TGF-β) and are responsible for distribution of these signaling molecules [132, 138-141]. Many HS proteins serve as coreceptors and low affinity binders during such signaling events [133].
Above mentioned functions must be tightly regulated in order for proper HSPG performance. It is therefore not surprising that HS deregulation has been shown in various tumors and HS deregulation, either via altered HSPG levels or changes in HS biosynthesis and enzymes, contributes to cancer initiation and progression [142]. Glypican-1 for instance, is frequently overexpressed in tumors and has growth-promoting effects in pancreatic cancer, gliomas and breast cancer, where it stimulates angiogenesis and metastasis via prolonged signaling [143-146]. Reports even show the levels of glypican-1 are increased in the blood of patients, making this a promising biomarker in cancer diagnosis [147, 148].

1.3.2 HS structure and synthesis

Not only HS chains, but also chondroitin sulfate chains, are GAGs attached to proteoglycans. All GAGs are long unbranched polysaccharides consisting of repetitive disaccharide units. Heparan sulfate chains are composed of mostly of N-acetlyglucosamine (GlcNAc) and iduronic acid (IdoA) units, whereas chondroitin sulfate chains consist of N-acetylgalactosamine (GalNAc) and glucuronic acid (GlcA) (see Figure 4) [149]. Synthesis of both chain types begins similarly though via synthesis of a common tetrasaccharide. Xylose is added to a specific serine residue by xylosyl transferases 1 and 2 [150, 151], followed by addition of two galactose and one glucuronic acid residue. Thereafter, the characteristic disaccharide units for heparan sulfate or chondroitin sulfate are polymerized in the Golgi apparatus either via EXT family members or chondroitin sulfate synthases and transferases respectively [149]. The chain initiation step, so whether GlcNAc or GalNAc is added first, determines the chain type, yet not much is known about the mechanism or how the GAG type is chosen. After polymerization chains are modified via O- and/or N-sulfation, for GlcNAc and GalNAc respectively, and epimerization of glucuronic acid into iduronic acid which can also be sulfated [150, 151]. Sulfation extent and pattern, as well as epimerization, depends on the cell type and chains can vary according to growth conditions and growth factor stimulus [131].

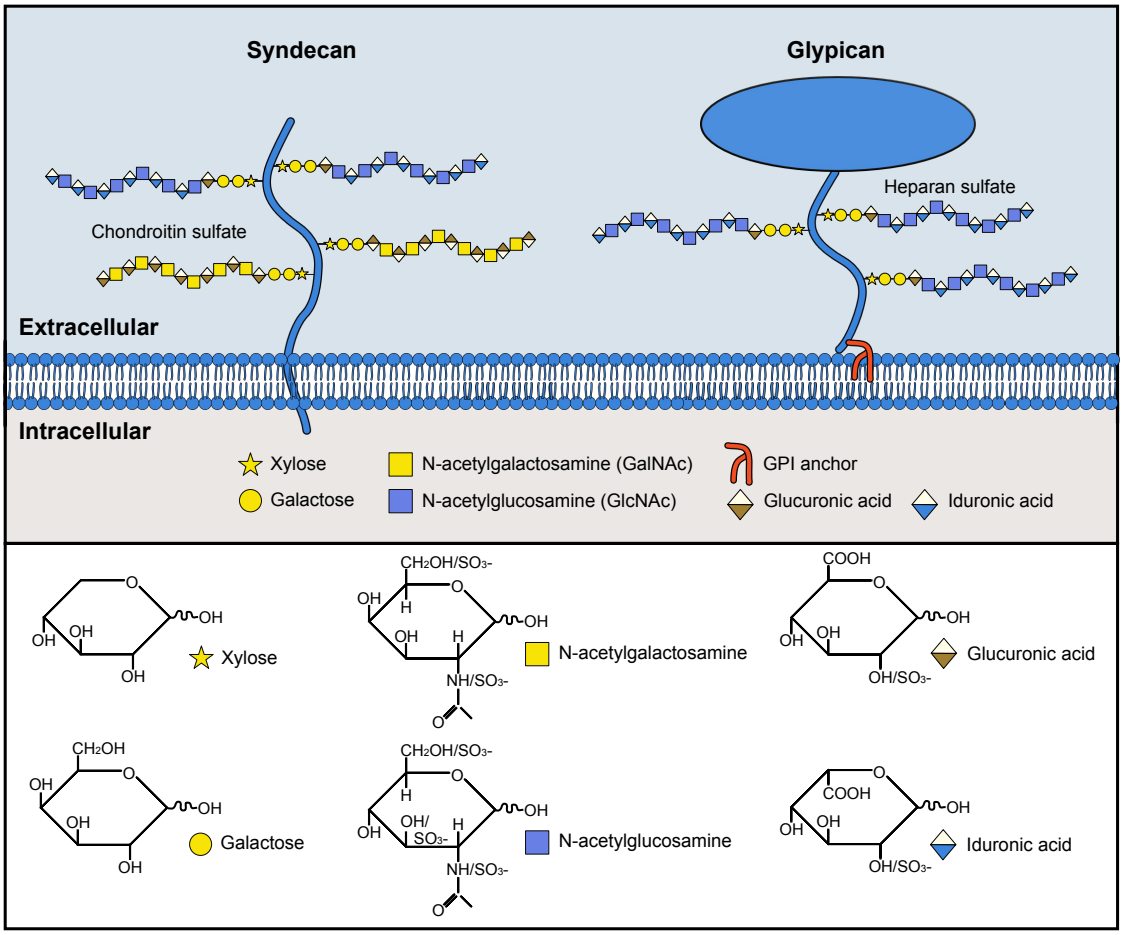

Figure 4: Structure of different HSPGs. Syndecans and glypicans both are heparan sulfate proteoglycans (HSPGs). While syndecans have a transmembrane domain, glypicans are linked to the plasma membrane via a GPI-anchor. The different components of the heparan sulfate or chondroitin sulfate chains are depicted.

1.3.3 HSPG-protein interaction

HSPGs bind a high variety of ligands such as growth factors, extracellular matrix proteins and cytokines. More than 100 GAG-binding proteins have been described in literature up to date [152]. Ligand binding is realized via the HS chains and binding depends on the arrangement of the sulfate groups. Sulfated groups are arranged into clusters along the chains, that are rich in mixes of glucuronic and iduronic acid. The clusters are then separated via regions lacking sulfation and containing mostly glucuronic acid [131]. For FGF2 it has been shown, that 2-O-sulfation of iduronic acid is sufficient for binding of FGF2, yet additional 6-O- and N-sulfation of GlcNAc is required for FGF2 induced activation of FGFR1 [153-155]. The minimum pentasaccharide binding motif for FGF2 is UA-GlcNS-UA-GlcNS-IdoA2S, containing N- and 2-O-sulfations [156]. Proteins binding to HSPGs do not possess a specific fold or amino acid consensus sequence but rather have surface grooves with positively charged amino acids that favor electrostatic interaction with the negative HS chains [152]. Network analyses screening 437 HS/heparin binding proteins for potentially conserved binding sequences revealed that these basic regions are highly variable and only contain very small conserved motifs [157]. Many small basic sequences might work in unison for efficient heparin binding. For FGF2 it has been shown that basic

residues in the C-terminus, with K133 as an essential amino acid, mediate the interaction with heparan sulfates [125, 158].

1.3.4 Membrane bound HSPGs

Membrane bound HSPGs are anchored to the plasma membrane via a type I oriented single membrane-spanning domain or a glycosylphosphatidylinositol (GPI) -anchor [130]. Most prominent amongst the membrane-bound HSPGs are the proteins families of syndecans and glypicans which will be mentioned here more in detail (for structural differences see Figure 4).

1.3.4.1 Syndecans

Syndecans have a small conserved cytoplasmic domain, a short hydrophobic transmembrane domain and a large extracellular domain containing GAG attachment sites [130, 159]. The syndecan family consists of four members (syndecan-1 to -4), which all differ in their GAG chains and vary significantly in their extracellular domains [160]. All syndecans have heparan sulfate chains at the distal part of the extracellular N-terminus, while syndecan-1 and -3 additionally carry chondroitin sulfate chains on membrane proximal sites opposed to syndecan-2 and -4 [130]. Syndecans can homodimerize via a GXXXG motif within their transmembrane domains creating a detergent-resistant complex implicated in syndecan function and syndecan protein-protein interaction [161]. Signal transduction occurs via ligand binding to HS chains and transmission into the intracellular environment directly via the syndecan cytoplasmic tail which interacts with several intracellular kinases and actin cytoskeleton components via its C-terminal PDZ domain [130, 160, 162]. The cytoplasmic domain is composed of the C1 and C2 conserved regions and a neighboring variable region (V), which is unique to each syndecan family member. The C1 region plays a role in endocytosis and cell cytoskeleton interactions, while the C2 region mediates recycling of syndecans [160] Ectodomain shedding of syndecans occurs via matrix metalloproteases, resulting in biologically active ectodomains carrying HS chains that can participate in ligand binding [130].

1.3.4.2 Syndecan-4 and FGF2 signaling in liquid ordered membrane compartments

Syndecans can be seen as low affinity receptors due to their ability to bind growth factors (GFs) via their heparan sulfate chains. By presenting growth factors to their corresponding growth factor receptors (GFR) and subsequent internalization, these HSPG-GF-GFR complexes play a key role in signal transduction and propagation. Recent studies suggest that signaling does not occur not via ligand HS binding, but rather via direct interaction of the syndecan cytoplasmic domain with effector proteins.
Syndecan-4 (SDC4), which is rather ubiquitously present in most cell types, can bind to $PI(4,5)P_2$ via a KKXXXKK motif within its variable (V) region and thereby mediates protein kinase C-alpha ($PKC\alpha$) activation and focal adhesion formation via activation of downstream signaling pathways [160, 163]. More precisely, FGF2 binding to its receptor mediates dephosphorylation of SDC4 via PP1/2A

phosphatase, which in turn leads to an increased binding affinity of SDC4 towards $PI(4,5)P_2$ [162]. This in turn facilitates multimerization and clustering of SDC4 and activates PKCα in membrane areas enriched in $PI(4,5)P_2$.

While unclustered SDC4 is predominantly present in non-raft compartments, it has been shown via confocal microscopy and sucrose gradient centrifugation that clustering induces extensive SDC4 redistribution into liquid ordered cholesterol-enriched membrane areas [164]. Caveolin-1, which promotes raft invagination and caveolae formation, moved together with SDC4 into detergent-resistant raft compartments, but SDC4 was not present in caveolae in these studies. SDC4 internalization via macropinocytosis occurs in raft microdomains and is independent from dynamin or clathrin [165]. This is congruent with studies demonstrating that FGFR1, a receptor activating mitogen-activated protein kinase (MAPK) pathway, is likewise localized to lipid raft-enriched membrane areas and FGFR1 endocytosis in these compartments requires cholesterol [166].

1.3.4.3 Glypicans

Glypicans, unlike syndecans, are linked to the plasma membrane via a glycosylphosphatidylinositol (GPI) -anchor and therefore do not contain a transmembrane and cytoplasmic domain. The glypican core protein, consisting of alpha helices, contains 14 conserved cysteine residues that are preserved in localization in all family members [138, 149]. All glypicans contain heparan sulfate chains, which are about 50 amino acids external to the GPI-anchor [167]. GPI-anchored proteins often localize to cholesterol-rich lipid rafts, therefore localizing to the apical membrane in polarized cells [168]. These domains facilitate certain protein-protein interactions and can function as transient cell signaling platforms [169]. Nevertheless, significant amounts of glypicans also localize to the basolateral membrane, which seems to be attributable to the heparan sulfate chains, since non-glycanated glypicans are sorted to the apical membrane of polarized cells, but glycanation seems to antagonize sorting [170]. Additionally, to their plasma membrane localization, glypicans can be found in the cytoplasm of cells and can also be shed into the extracellular space, via cleavage of their GPI anchor via phospholipases [171].

The glypican family consists of six members, glypican-1 to -6, each carrying two to five heparan sulfate chains [138, 139]. The family members can be further sub-divided into two groups based on similarity. Glypican-1, -2, -4 and -6 are in one group and glypican-3 and -5 are in another. Both groups only show about 25% sequence similarity [138].

1.3.4.3.1 Glypican-1

Glypican-1 (GPC1) is a ~ 62 kDa big member of the glypican family. Crystallization has revealed that the core protein is composed of 14 α-helices and three major loops [172]. Folded Glypican-1 is about 100 Å big, suggesting that the heparan sulfate chains can be up to 500 Å long, as eight disaccharide units have been proposed to be around 70 Å [172, 173]. GPC1 has three HS chains attached at sites

S486, S488 and S490 [147] and is the to date best described glypican concerning structural annotations.

GPC1 is important during embryonic development, where it is expressed in the central nervous system and the skeletal system, and is expressed in nearly all adult tissues [174]. It has been shown that deregulation of GPC1 expression occurs in a range of tumor tissues and is therefore associated with cancer [147]. GPC1 might play a role in initiation and progression of pancreatic cancer for example, since GPC1 is naturally overexpressed in these cells, but knockdown of GPC1 inhibits the mitotic response to FGF2 [175]. Other studies support this via the finding that GPC1 regulates proliferation and normal cell cycle progression of proliferating human glioma blood vessel endothelial cells if expressed in moderate levels [176]. This study demonstrated that constant overexpression on the other hand caused mitotic arrest and aneuploidy, while knockdown induced polyploidy possibly via G2 arrest or mitotic slippage, both indicating that optimal levels are required for correct cell cycle progression and deregulation to either side can promote cancer formation. GPC1 overexpression also results in increased angiogenesis in brain gliomas via ternary complex formation with FGF2 and FGF receptor-1, since FGF2 is known to be one of the most potent angiogenic factors in wound healing and tumorigenesis [177]. Since GPC1 on the cell surface is shed by lipases, it can be detected in the blood system. GPC1 present in exosomes has been reported to be used as a biomarker for pancreatic, colorectal, prostate and breast cancer since GPC1 was elevated in serum samples from patients [147]. Yet, there were also controversial results, indicating that further studies are needed to validate the clinical applicability of GPC1 as a biomarker for certain cancers.

1.3.4.3.2 Glypican-5

Glypican-5 (GPC5), a 63 kDa big protein, was first identified in 1997 by Veugelers and colleagues [178]. GPC5 expression was shown to be developmentally regulated in kidney, limb and brain tissues [179]. This is in agreement with *glypican-5* gene expression being localized to chromosome 13q31-32, deletions of which are associated with the developmental 13q syndrome. Transient transfection of GPC5 in COS-7 cells indicated that this HSPG might carry both heparan and chondroitin sulfate chains [179]. Different opposing roles for GPC5 in cancer have been proposed. On the one hand GPC5 is overexpressed in rhabdomyosarcoma and stimulated cell proliferation via hedgehog signaling [180]. GPC5 is also overexpressed during lymph node metastasis and promotes cell migration in non-small lung cell cancer (NSCLC) [181]. On the other hand, GPC5 overexpression inhibits migration and invasion in NSCLC and reduced GPC5 expression is associated with poor survival of breast cancer patients [182, 183]. As seen, GPC5 can inhibit or stimulate cell signaling activity and further investigation is required to fully understand its physiological role.

1.3.4.3.3 Glypican-6

Glypican-6 (GPC6) is a heparan sulfate-only containing 60 kDa big protein of the glypican family that is encoded by 6 exons [184]. GPC6 is homologous to GPC1, 2 and 4 (minimally 40% sequence similarity).

Although broadly expressed in adult and fetal tissue GPC6 mRNA is not ubiquitous and protein expression seems to be highly regulated during development [184]. GPC6 for instance plays a direct role in bone development by stimulating hedgehog signaling [185]. Cell adhesion and migration in melanoma samples can be correlated to GPC6 expression and GPC6 may play a role in tumor metastatic progression [186]. Glypican-6, same as GPC3, GPC4 and GPC2, can be cleaved post-translationally at an internal cleavage site and is therefore often detected as two fragments in Western blotting if lysate preparation was under reducing conditions [187-189].

1.4 Nanodomains and membrane organization

Cell membranes function in many cellular processes, such as signaling, endocytosis and exocytosis, there fulfilling essential physiological functions, like protection, compartmentalization, ion homeostasis and others. Therefore, the core of membranes, lipid bilayers, must be organized in a dynamic fashion in order to allow site specific or temporally controlled events to occur. Different super-resolution techniques and *in vitro* model membrane systems are amongst the approaches developed in the last years to examine and better understand membrane lipid heterogeneity, caused by variations in the major membrane lipids glycerophospholipids, sphingolipids and sterols (mainly cholesterol).
Membrane domains can be classified into different phases according to their composition and physical properties: the liquid disordered phase L_d, which is highly fluid due to unsaturated lipids, and the (at cold temperatures) detergent-resistant liquid ordered phase L_o or lipid rafts, enriched in higher order and saturated sphingolipids (mainly sphingomyelin) and cholesterol, which has reduced diffusion [190-192]. Lipid rafts are present both in the inner and outer plasma membrane leaflet and are presumably coupled across leaflets [193]. The raft hypothesis, erected by Simons and Ikonen, was supported by model membranes, where liquid-liquid phase separation was observed [194].

1.4.1 Imaging membrane nanodomains

Lipid rafts or membrane nanodomains, usually described as lipid compartmentalizations up to 200 nm in size, have been a source of many controversies and open questions, since their presence was mostly described via indirect methods, such as isolation of plasma membrane fractions. It was estimated that L_o fractions can range between 10 – 80% of cell membranes [195], which is why it is important to directly visualize membrane domains in intact cells via different imaging techniques.

1.4.1.1 Solvatochromic dyes

Fluorescent solvatochromic dyes can sense lipid order by sensing decreased local polarity in membrane regions having higher packed lipids and consequently higher exclusion of water molecules [196]. The spectral properties of these dyes depend on the lipid environment and shift to a longer emission wavelength in the L_d environment. Generalized polarization maps, depicting the phases, can thereby be created via ratiometric imaging. Many dyes, such as Prodan [197], Laurdan [198, 199], C-Laurdan

[200], Nile Red [195, 201] and others have been developed the last years and applied to both cell-based experiments and *in vitro* studies using unilamellar vesicles.
Laurdan, binds to the higher-ordered outer plasma membrane leaflet, which contains mainly sphingomyelin and phosphatidylcholine, but flips rapidly into the phosphatidylethanolamine and phosphatidylserine rich inner leaflet and is redistributed to intracellular membranes in living cells [198]. A moderate improvement and inhibition of internalization was achieved via introduction of a carboxyl-group, creating C-Laurdan [200]. Pro12A, a derivative of Prodan containing a membrane targeting moiety, is able to circumvent this problem and results in an outer membrane leaflet specific staining [196].
Potential nanodomains smaller than 200 nm are below the resolution limit of conventional light microscopy and therefore need high resolution microscopy techniques, such as STED microscopy. For this purpose, more photostable and exchangeable dyes, such as NR12S and NR4A [195, 202, 203] have been developed recently.

1.4.1.2 Cholesterol sensors

Cholesterol, being the most abundant lipid species and making up 25 – 50 % of the plasma membrane lipids depending on cell type, is localized up to 90% of its total cellular content at the membrane [204-207]. Therefore, it plays a major role in membrane lipid organization and is an attractive tool to examine nanodomains.
Most plasma membrane cholesterol is in complex with membrane lipids, such as sphingomyelin and phospholipids, and is therefore inactive and not available for intracellular transport [208, 209]. Free and active cholesterol however, making up around 15 mole % of plasma membrane lipids [210], can be detected in fixed cells by UV irradiation (360 nm) of the sterol-binding fluorescent antibiotic Filipin [211]. Alternatively, intrinsically fluorescent sterols, such as dehydroergosterol (DHE) and cholestatrienol (CTL) [212, 213], and cholesterol analogs containing fluorophores, for example BODIPY or NBD [211, 214-216], have been used with certain limitations for imaging of cellular cholesterol distribution.
The GRAM domain of the ER-anchored sterol transfer proteins GRAMD1 can detect both accessible cholesterol and anionic lipids, such as phosphatidylserine, and transports plasma membrane cholesterol to the ER if a threshold of above 25 mole % is reached [217, 218]. It has been shown that overexpression of the fluorescently-tagged GRAM domain of GRAM1b binds in a synergistic fashion to membranes that contain both cholesterol and anionic lipids in close proximity and this codistribution becomes more prominent when plasma membrane cholesterol is transiently increased via sphingomyelinase treatment and released from cholesterol-sphingomyelin complexes [217]. Furthermore, the study showed that a single point mutation (G187L) in the GRAM domain was able to promote hypersensitivity towards cholesterol, without affecting the binding to sphingomyelin, thereby inducing increased plasma membrane tethering and consequently showed increased staining in immunofluorescence microscopy.

1.4.2 Proteins can associate with nanodomains

Not only lipid composition is critical for nanodomain formation, but also certain proteins can characterize plasma membrane domains and are essential for the cellular processes occurring therein. Proteins can associate permanently or transiently to lipid rafts via different mechanisms, such as hydrophobic transmembrane domains, a hydrophobic protein tail (e.g. GPI-anchor attachment to membrane proteins, N-myristoylation of cytosolic protein or S-palmitoylation of integral and peripheral membrane proteins) or protein-protein and protein-lipid interactions [219]. Caveolin, which is permanently associated with lipid rafts, can potentially recruit other proteins via a caveolin-binding domain whereas lipids in rafts, such as $PI(4,5)P_2$, can recruit proteins containing Pleckstrin homology (PH) domains [219].

1.4.3 Caveolae and Caveolins

Caveolae are flask-shaped membrane invaginations at the cytosolic side composed of caveolin oligomers with a characteristic diameter ranging from 50 – 100 nm (see Figure 5) [220, 221]. Caveolae exist in most cell types, but are especially abundant in adipocytes and smooth muscle cells making up around 20% of the cell and endothelial cells can even contain 5000 – 10 000 caveolae per cell [221]. Mouse experiments have shown that these membrane domains, sometimes even described as organelles, play an important role in many cellular processes, such as signaling, transport, tumorigenesis and lipid regulation [219, 222-224].

Caveolae are composed of the membrane scaffolding proteins caveolin-1 (Cav1), caveolin-2 (Cav2) and caveolin-3 (Cav3), whereby Cav3 is muscle cell specific and more similar to Cav1 than Cav2 based on sequence homology as both proteins show 65% sequence equality [225]. Depending on the cell type Cav1 can form homooligomers or heterooligomers with Cav2 or Cav3 [221, 226, 227]. Caveolins can bind to a conserved caveolin binding motif (CBM) consisting of hydrophobic and aromatic residues ($\Omega x\Omega xxxx\Omega$, $\Omega xxxx\Omega xx\Omega$ or the combined sequence $\Omega x\Omega xxxx\Omega xx\Omega$, where Ω is phenylalanine, tryptophane or tyrosine and x can be any amino acid) which has been proposed to function in scaffolding and caveolin-protein interactions [221, 228]. Plentiful signaling and non-signaling proteins have been shown to interact with caveolin, not making it surprising that around 30% of all cellular proteins possess a CBM [228, 229]. Caveolin-1 also shows high-affinity binding to cholesterol and it has been shown, that caveolae formation and Cav1 expression levels are dependent on available cholesterol [230-232]. Many interplays between the three caveolins have been described using caveolin knockout (KO) mice and are hereafter summarized by Le Lay and Kurzchalia [227]. $Cav1^{-/-}$ mice are viable and lack caveolae in all non-muscle tissues, demonstrating the essential function of Cav1 in caveolae biogenesis. These mice show defects in lipid homeostasis, vascular system disfunctions, pulmonary diseases and are susceptible to tumorigenesis. Strikingly, caveolin-2 expression is drastically decreased in KO mice. It remains trapped in the Golgi, since Cav1 determines Cav2 localization and Cav2 is degraded via the proteasome in the absence of Cav1. In contrast, Cav1 levels and caveolae formation are not impaired in $Cav2^{-/-}$ mice. Depletion of caveolin-3 results in loss of caveolae in skeletal muscle fibers, without

affecting the other two or caveolae formation in non-muscle cells and results in mild cardiomyopathies. The loss of caveolae in all cell types can be achieved via generation of Cav1$^{-/-}$ / Cav3$^{-/-}$ double KO mice, which are viable, fertile and show similar lung, fat and skeletal defects to their single KO counterparts, yet develop more severe cardiomyopathies.

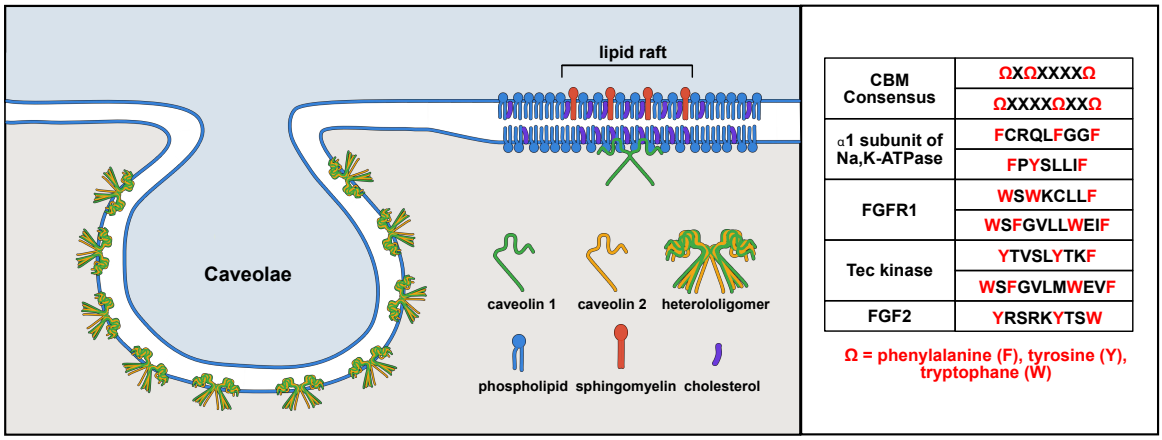

CBM Consensus	ΩXΩXXXXΩ
	ΩXXXXΩXXΩ
α1 subunit of Na,K-ATPase	FCRQLFGGF
	FPYSLLIF
FGFR1	WSWKCLLF
	WSFGVLLWEIF
Tec kinase	YTVSLYTKF
	WSFGVLMWEVF
FGF2	YRSRKYTSW

Ω = phenylalanine (F), tyrosine (Y), tryptophane (W)

Figure 5: Caveolae and caveolins. Left: Caveolin 1 and 2 can form heterooligomers to induce formation or caveolae. Caveolins also localize to lipid rafts/liquid ordered membrane areas. These are rich in cholesterol and sphingomyelin. Adapted from [233]. Right: Many proteins involved in FGF2 secretion contain a caveolin binding motif (CBM).

2 Aim of the thesis

The pathway of unconventional secretion of FGF2 has been extensively studied throughout the last years and more and more factors, such as the Na,K-ATPase, Tec kinase and $PI(4,5)P_2$, have been shown to be involved in FGF2 secretion via membrane spanning pores [234]. It has been known that cell surface heparan sulfate proteoglycans are not only important for FGF2 signaling and retention on the cell surface, but are actually required for efficient secretion [127, 128]. A BioID screen, conducted within the laboratory by Matthias Gerstner and Eleni Dimou, identified Glypican-1, a GPI-anchored HSPG, to be a potential new interaction partner of FGF2 [235]. The aim of my thesis was to validate and examine this protein target, in collaboration with Carola Sparn, Sabine Wegehingel and Roberto Saleppico. Experimental approaches involved the generation and biochemical analysis of different glypican knockout and overexpression cell lines and also different microscopy techniques.

Beyond this, it has remained unclear whether proteins involved in FGF2 secretion can form nanodomains. This would favor the very fast translocation of FGF2 seen in living cells [128] and explain why translocation in *in vitro* reconstitution systems is much slower. To gain support of this nanodomain hypothesis I employed several methods such as STED microscopy, proximity ligation experiments, and isolation of detergent resistant membrane fractions.

Within the experiments involved in nanodomain analysis, an interesting new target protein was discovered: caveolin. As caveolins are associated with liquid ordered nanodomains and caveolin-1 is a cholesterol-binding protein [230, 231], this seemed a promising protein family to investigate. Also, many proteins involved in FGF2 secretion contain a caveolin binding motif. To assess whether caveolin-1 or caveolin-2 play a role in FGF2 secretion I generated several knockout and overexpression cell lines. These were analyzed via cell surface biotinylation, microscopy and isolation of DRM fractions.

Trifunctional lipid probes have become a popular tool to study lipid-protein interactions [236]. These lipids have a coumarin cage, a diazirine group for photo-crosslinking and an alkyne for click chemistry. The Na,K-ATPase was identified in a mass spectrometry approach using synthesized trifunctional $PI(3,4,5)P_3$ in the laboratory of Carsten Schulz at EMBL [237]. It was my aim to conform this interaction in pulldown experiments.

3 Materials and Methods

3.1 Materials

3.1.1 Chemicals, reagents, beads

Reagent	Company	Order #
100 bp DNA Ladder	NEB	N3231
Acetic acid (AcOH)	Sigma-Aldrich	33209
Agarose	Invitrogen	16500-500
Amido black 10 B	Serva	12310.01
Ampicillin sodium salt	Gerbu	1046
Ascorbic acid	Sigma-Aldrich	33034
Bacto Agar	BD	214010
Bacto Yeast Extract	Gibco	80705
Biotin	Sigma-Aldrich	B4501
Blasticidin [10 mg/ml]	ChemCruz	SC-495389
Bovine serum albumin fraction V (BSA)	Carl-Roth	8076.2
Bromophenol blue-NA-salt	Serva	11447413
Calcium chloride ($CaCl_2$)	Sigma-Aldrich	31307
Cell dissociation buffer (CDB)	Gibco	13151-014
Chloroform	Sigma-Aldrich	32211-M
ChromoTek GFP-Booster AlexaFluor® 647	Chromotek/Proteintek	gb2AF647
Collagen R (0,2%)	Serva	47254.01
$CuSO_4$	Sigma-Aldrich	61245
DEAE-dextran	Sigma-Aldrich	78816
DMEM high glucose	Sigma-Aldrich	D6429
DMEM low glucose	Sigma-Aldrich	D6046
DMSO	Sigma-Aldrich	276855
Doxycycline	Clontech	564-25-0
Duolink® In Situ Detection Reagents FarRed	Sigma-Aldrich	DUO92013
Duolink® In Situ PLA® Probe Anti-Mouse MINUS	Sigma-Aldrich	DUO092004
Duolink® In Situ PLA® Probe Anti-Rabbit PLUS	Sigma-Aldrich	DUO092002
Ethanol absolute (EtOH)	Sigma-Aldrich	32205-M
Ethylenediaminetetraacetic acid (EDTA)	Honeywell	34549
EZ-Link-Sulfo-NHS-SS-Biotin	Thermo Fischer	21331
FACS clean buffer	BD	340346
FACS flow buffer	BD	342003

FACS rinse buffer	BD	340345
Fetal calf serum (FCS)	Biochrom AG	S0615
FGF2-GFP (recombinant, [5,71 mg/ml])	Carola Sparn, Nickel lab	-
G418	Sigma	G8168
Gel Loading Dye, Purple (6X, no SDS)	NEB	B7025
Glycerol	Sigma	15523
Glycine	Labochem	LC-4522.2
Heparinase III	NEB	P0737
HEPES	Sigma-Aldrich	3375
Hoechst 33342 stain	Thermo Fischer	62249
Kanamycin monosulfate	Sigma-Aldrich	25389-94-0
L-glutamine	Gibco	11539876
Live Cell Imaging Solution (LCIS)	Thermo Fischer	A14291DJ
Magnesium chloride ($MgCl_2$)	Sigma-Aldrich	63068
MEM-alpha modification	Sigma-Aldrich	M8042
MES SDS Running Buffer (20X)	Novex, Thermo Fischer	NP0002
Methanol (MeOH)	Honeywell	32213
Milk powder	Carl Roth	T145.2
Monosodium phosphate (NaH_2PO4)	Sigma-Aldrich	S0751
MOPS SDS Running Buffer (20X)	Novex, Thermo Fischer	NP0001
Mycoplasma Removal Agent (MRA)	MP Biomedicals	3050044
NP-40	Sigma-Aldrich	492016
OptiMEM™	Gibco	11058021
PageRuler™ prestained protein ladder	Thermo Fischer	26617
Paraformaldehyde (PFA) 16% solution	Electron Microscopy Sciences	15710
PBS	Sigma-Aldrich	D8537
Penicillin-Streptomycin (PenStrep)	Biochrom AG	P06-07050
Picolyl-azide-PEG4-Biotin (10 mM in DMSO)	Jena Bioscience	97995
Pierce™ Streptavidin UltraLink™ Resin	Thermo Fischer	53114
Pluronic® F-127	Sigma-Aldrich	P2443
Potassium chloride (KCl)	Sigma-Aldrich	31248
Potassium dihydrogen phosphate (KH_2PO_4)	AppliChem	A3620,1000
Protease inhibitor mix M	Serva	39102.02
Protease inhibitors	Roche	54925800
Quick-Load® Purple 1 kb DNA Ladder	NEB	N0552
QuickExtract DNA Extraction Solution	Lucigen	QE0905T
RedSafe dye	iNtROM	21141
Saccharose	Carl-Roth	4621.1
Saponin	Sigma-Aldrich	47036

SDS (sodium dodecyl sulfate)	Bio-Rad	1610301
Sodium chloride (NaCl)	Labochem	LC-59321)
Sodium hydroxide (NaOH)	Sigma-Aldrich	30620
Sodium-deoxycholate	Sigma-Aldrich	30970
Streptavidin Sepharose beads	Cytiva	17511301
TBTA	Sigma-Aldrich	678937
Transferrin AlexaFluor™ 546 conjugate	Thermo Fischer	T23364
Triethanolamine	Sigma-Aldrich	90278
Trifunctional PI(3,4,5)P_3	Rainer Müller, Laboratory of Carsten Schulz	-
Trifunctional PI(4,5)P_2	Rainer Müller, Laboratory of Carsten Schulz	-
Tris	Carl-Roth	4855.2
Triton X-100	Sigma-Aldrich	T8787
Trypsin EDTA 0,05%, phenolred	Gibco	11590626
Tryptone	Sigma-Aldrich	95039
Tween-20	Sigma-Aldrich	P9416
β-Mercaptoethanol	Merck	8.05740.0250

3.1.2 Consumables

Product	Company	Order #
35 mm Glass bottom dishes No 1,5, poly-d-lysine coated	MatTek	P35GC-1,5-10-C
6-, 12-, 24- and 96-well cell culture plates	Greiner Bio-one	-
Cell culture plates 100 and 60 mm	Greiner Bio-one	-
Cell scraper	Serva	99004
Cryotubes CryoS	Greiner Bio-one	122263
Falcons 15 ml	Greiner Bio-one	188271
Falcons 50 ml	Greiner Bio-one	227261
Glass beads 2,85-3,3 mm	Carl-Roth	A557.1
Glass Pasteur pipettes	Brand	747715
Immobilon®-FL PVDF Transfer Membrane	Millipore	IPFL00010
LUNA™ cell counting slides	Logos/ BioCat	L12001
Mobicol filters	MoBiTec	M1003
Nitril gloves	Starguard comfort	SG-C-S
NuPAGE™ 4-12% Bis-Tris-gels 1mm x 10 well	Thermo Fischer	NP0321

NuPAGE™ 4-12% Bis-Tris-gels 1mm x 15 well	Thermo Fischer	NP0323
NuPAGE™ 4-12% Bis-Tris-gels 1mm x 17 well	Thermo Fischer	NP0329
PCR plates	Greiner Bio-one	652260
PCR transparent foil	Axon Labortechnik	26979
PCR tubes	Kissler	S0141
Pipette 10 ml	Greiner Bio-one	607180
Pipette 25 ml	Greiner Bio-one	760180
Pipette 5 ml	Greiner Bio-one	606180
Pipette tips	Sarstedt	70.3030.XXX
Pipette tips filtered (for cell culture)	Greiner Bio-One	-
Reaction tube 1,5 ml	Sarstedt	72.690.001
Reaction tube 2 ml	Greiner Bio-one	623201
RT PCR plates	Applied Biosystems	4346906
SafeSeal reaction tube	Sarstedt	72.706
Syringe filter 0.20 µm	GE Healthcare	10462200
Syringe filter 0.45 µm	GE Healthcare	10462100
Ultracentrifuge tube (PC, 2 ml, thickwall)	Herolab	252020
Whatman paper 3 mm	Whatman	742118
µ-Slide 8 Well Glass Bottom Dishes	Ibidi	80827

3.1.3 Kits and assays

Product	Company	Order #
DNA Ligation Kit	Takara	6022
DNeasy® Blood and Tissue Kit	Qiagen	69504
FuGENE® HD Transfection Reagent	Promega	E2311
ImProm-II™ Reverse Transcription System	Promega	A3800
MBS Mammalian Transfection Kit	Agilent Technologies	200388
Nucleo Bond MIDI kit	Macherey-Nagel	740410
NucleoSpin Plasmid kit	Macherey-Nagel	740588
QIAquick Gel Extraction Kit	Qiagen	28706X4
QIAquick® PCR Purification Kit	Qiagen	28106
RNeasy Mini Kit	Qiagen	74104
TaqMan Gene Expression assay GAPDH	Applied Biosystems™	HS 02786624_g1
TaqMan Gene Expression assay GPC1	Applied Biosystems™	HS 00892476_m1
TaqMan Gene Expression assay GPC5	Applied Biosystems™	HS 00270114_m1
TaqMan Gene Expression assay GPC6	Applied Biosystems™	HS 00170677_m1
TaqMan™ Gene Expression Master Mix	Applied Biosystems™	4370048
Zero Blunt® PCR Cloning Kit	Invitrogen™	K270020

3.1.4 Antibodies

Antibody	Host	Supplier (#)	Dilution
10E4	Mouse	US Biological (H1890)	1:500
3G10	Mouse	Amsbio (370260)	1:500
Abberior STAR 580 anti-mouse IgG	Goat	Abberior (ST580-1001-500UG)	1:50
Abberior STAR 635P anti-rabbit IgG	Goat	Abberior (ST635P-1002-500UG)	1:100
AlexaFluor™ 488 anti-mouse IgG	Goat	Invitrogen (A11029)	1:500
AlexaFluor™ 488 anti-rabbit IgG	Goat	Invitrogen (A11034)	1:500
AlexaFluor™ 546 anti-mouse IgG	Goat	Invitrogen (A11030)	1:500
AlexaFluor™ 546 anti-rabbit IgG	Goat	Invitrogen (A11035)	1:500
AlexaFluor™ 647 anti-mouse IgG	Goat	Invitrogen (A21235)	1:500
AlexaFluor™ 647 anti-rabbit IgG	Goat	Invitrogen (A21244)	1:500
ATP1A1 (α1)	Mouse	Abcam (Ab7672)	1:200-1:500
ATP1A1 (α1)	Rabbit	Affinity purified antibody or unpurified serum	1:500
Caveolin-1	Rabbit	Thermo Fischer (PA1-064)	1:1000
Caveolin-1	Rabbit	Santa Cruz (N-20) discontinued	1:1000
Caveolin-2 SY-2205	Rabbit	Thermo Fischer (MA5-32083)	1:50 in IF and 1:1000 in Western blot
FGF2	Rabbit	Custom-made/Pineda	1:500
FGF2 (clone FB-8)	Mouse	Thermo-Fischer (MA1-24682)	1:500
Flag-M2	Mouse	Sigma (F1804-200)	1:500
GAPDH	Mouse	Invitrogen (AM4300)	1:20 000
HA	Rabbit	Sigma (H6908)	1:500
Mouse-APC	Goat	Invitrogen (A-865)	1:500
Pan-Cadherin	Mouse	Sigma (C1821)	1:1000
Rabbit-APC	Goat	Invitrogen (A-10931)	1:500

Streptavidin-AlexaFluor™ 680 conjugate	-	Invitrogen (S32358)	1:5000
TfR	Rabbit	Zymed (13-6800)	1:1000
Tubulin	Rabbit	Abcam (18251)	1:1000

3.1.5 Oligos and gRNAs

Name	Sequence (5' to 3')	Comments
Cav1 gRNA T3 fwd	CACCgAGTGTACGACGCGCACACCA	Cav1 KO in exon 2, 5'phosphate
Cav1 gRNA T3 rev	AAACTGGTGTGCGCGTCGTACACTC	Cav1 KO in exon 2, 5'phosphate
Cav2 Ex1 gRNA T1 fwd	CACCgCCGAGTCCGCGAACTTCTCG	Cav2 KO in exon 1, 5'phosphate
Cav2 Ex1 gRNA T1 rev	AAACCGAGAAGTTCGCGGACTCGGC	Cav2 KO in exon 1, 5'phosphate
Cav2 Ex1 gRNA T3 fwd	CACCgTCTCGGGGTCGGCGTACTCG	Cav2 KO in exon 1, 5'phosphate
Cav2 Ex1 gRNA T3 rev	AAACCGAGTACGCCGACCCCGAGAC	Cav2 KO in exon 1, 5'phosphate
Cav2 Ex2 gRNA T1 fwd	CACCgTCAAAGGAGTGCGTAGTCAC	Cav2 KO in exon 2, 5'phosphate
Cav2 Ex2 gRNA T1 rev	AAACGTGACTACGCACTCCTTTGAC	Cav2 KO in exon 2, 5'phosphate
GPC1 gRNA fwd	CACCGTGCAGCAGGTGTAGCCCTG	GPC1 KO in exon 2, 5'phophate (from Sabine Wegehingel)
GPC1 gRNA rev	AAACCAGGGCTACACCTGCTGCAC	GPC1 KO in exon 2, 5'phophate (from Sabine Wegehingel)
GPC6 Ex2 gRNA fwd	CACCgAATGGCTTGTCTCTTCCACA	GPC6 KO in exon 2, 5'phosphate
GPC6 Ex2 gRNA rev	AAACTGTGGAAGAGACAAGCCATTC	GPC6 KO in exon 2, 5'phosphate
GPC6 Ex3 gRNA fwd	CACCgCTGAAAAGGTACTACACTGG	GPC6 KO in exon 3, 5'phosphate
GPC6 Ex3 gRNA rev	AAACCCAGTGTAGTACCTTTTCAGC	GPC6 KO in exon 3, 5'phosphate
GPC6 Ex4 gRNA fwd	CACCgAGGCTGACCTCGACACAGAG	GPC6 KO in exon 4, 5'phosphate

GPC6 Ex4 gRNA rev	AAACCTCTGTGTCGAGGTCAGCCTC	GPC6 KO in exon 4, 5‘phosphate
SalI-KoGPC1SP-Flag-KflI-fwd	TCGACGAATTCGCCACCATGGAGCTC CGGGCCCGAGGCTGGTGGCTGCTAT GTGCGGCCGCAGCGCTGGTCGCCTG CGCCCGCGGGGATTACAAGGATGACG ACGATAAGGGG	For oligo annealing, Contains “digested” SalI and KflI flaking Kozak-GPC1 signal peptide-Flag tag
SalI-KoGPC1SP-Flag-KflI-rev	GTCCCCCTTATCGTCGTCATCCTTGTA ATCCCCGCGGGCGCAGGCGACCAGC GCTGCGGCCGCACATAGCAGCCACCA GCCTCGGGCCCGGAGCTCCATGGTG GCGAATTCG	For oligo annealing, Contains “digested” SalI and KflI flaking Kozak-GPC1 signal peptide-Flag tag
SalI-KoGPC1SP-HA-KflI-fwd	TCGACGAATTCGCCACCATGGAGCTC CGGGCCCGAGGCTGGTGGCTGCTAT GTGCGGCCGCAGCGCTGGTCGCCTG CGCCCGCGGGTACCCATACGATGTTC CAGATTACGCTGGG	For oligo annealing, Contains “digested” SalI and KflI flaking Kozak-GPC1 signal peptide-HA tag
SalI-KoGPC1SP-HA-KflI-rev	GTCCCCAGCGTAATCTGGAACATCGT ATGGGTACCCGCGGGCGCAGGCGAC CAGCGCTGCGGCCGCACATAGCAGCC ACCAGCCTCGGGCCCGGAGCTCCATG GTGGCGAATTCG	For oligo annealing, Contains “digested” SalI and KflI flaking Kozak-GPC1 signal peptide-HA tag

3.1.6 Plasmids

Name	Source	Comments
EGFP-Gram$_{1b}$ G187L	Kindly provided by the laboratory of Oliver Fackler, Heidelberg University Clinic	Original construct from Bilge Ercan and colleagues [217]
pEX-A128-SalI-Cav1-NotI	Custom-made, Eurofins	For cloning of Cav1 in pFB-Neo and pFB-Bsd
pEX-A128-SalI-Cav2-NotI	Custom-made, Eurofins	For cloning of Cav2 in pFB-Neo and pFB-Bsd
pFB-Bsd-Cav1	Created within this thesis	Via insertion of Bsd resistance cassette (from Sabine Wegehingel) for overexpression of Cav1 in U2OS

pFB-Bsd-Cav2	Created within this thesis	Via insertion of Bsd resistance cassette (from Sabine Wegehingel) for overexpression of Cav2 in U2OS
pFB-Bsd-Flag-GPC1	Created within this thesis	Via insertion of Bsd resistance cassette (from Sabine Wegehingel) for overexpression of GPC1 in U2OS
pFB-Bsd-GPC1	Created within this thesis	Via insertion of Bsd resistance cassette (from Sabine Wegehingel) for overexpression of GPC1 in U2OS
pFB-Bsd-HA-GPC1	Created within this thesis	Via insertion of Bsd resistance cassette (from Sabine Wegehingel) for overexpression of GPC1 in U2OS
pFB-Neo-Cav1	Created within this thesis	For overexpression of Cav1 in S3 cells
pFB-Neo-Cav2	Created within this thesis	For overexpression of Cav1 in S3 cells
pFB-Neo-Flag-GPC1	Created within this thesis	Via oligo annealing
pFB-Neo-GPC1	Created Created within this thesis together with Sabine Wegehingel	For overexpression of GPC1
pFB-Neo-GPC5	Nickel lab	For overexpression of GPC5
pFB-Neo-HA-GPC1	Created within this thesis	Via oligo annealing
pREV-TRE2 FGF2-GFP	Nickel lab	Doxycycline inducible overexpression of FGF2-GFP in U2OS
pSpCas9(BB)-2A-RFP	Sabine Wegehingel, Nickel lab	For ligation with all annealed gRNAs for knockout generation

3.1.7 Cell lines

Cell line	Source
CHO K1 FGF2-GFP	Nickel lab
CHO K1 FGF2-GFP + HA-GPC1 single clones	Created within this thesis together with Roberto Saleppico
HEK EcoPack 2-293	Clontech
HeLa MT FGF2-GFP	Nickel lab
HeLa S3 MT FGF2-GFP Caveolin-1 KO clones	Created within this thesis
HeLa S3 MT FGF2-GFP Caveolin-1/2 dKO clones	Created within this thesis
HeLa S3 MT FGF2-GFP Caveolin-2 KO clones & rescue of clones C2 and D7	Created within this thesis
HeLa S3 MT FGF2-GFP GPC1 KO B2	Nickel lab
HeLa S3 MT FGF2-GFP GPC1 KO B2 + GPC1 or + GPC5	Created within this thesis
HeLa S3 MT FGF2-GFP GPC1 KO B2 + HA-GPC1 or + Flag-GPC1	Created within this thesis
HeLa S3 MT FGF2-GFP GPC1 KO G4	Nickel lab
HeLa S3 MT FGF2-GFP GPC1 KO G4 + GPC1 or + GPC5	Created within this thesis
HeLa S3 MT FGF2-GFP GPC1 KO G4 + HA-GPC1 or + Flag-GPC1	Created within this thesis
HeLa S3 MT FGF2-GFP GPC1/5 dKO F2	Nickel lab
HeLa S3 MT FGF2-GFP GPC1/5 dKO F2 + GPC1 or + GPC5	Created within this thesis
HeLa S3 MT FGF2-GFP GPC1/5 dKO F2 + HA-GPC1 or + Flag-GPC1	Created within this thesis
HeLa S3 MT FGF2-GFP GPC5 KO B4	Nickel lab

HeLa S3 MT FGF2-GFP GPC5 KO B4 + GPC1 or + GPC5	Created within this thesis
HeLa S3 MT FGF2-GFP GPC5 KO C5	Nickel lab
HeLa S3 MT FGF2-GFP GPC5 KO C5 + GPC1 or + GPC5	Created within this thesis
HeLa S3 MT FGF2-GFP wt 3x pool	Nickel lab
HeLa S3 MT FGF2-GFP wt pool + Cav1 or + Cav2	Created within this thesis
HeLa S3 MT FGF2-GFP wt pool + HA-GPC1 or + Flag-GPC1	Created within this thesis
HeLa S3 MT FGF2-IRES-GFP	Nickel lab
U2OS MT cells	Nickel lab/ orginally from Brunner lab, BZH
U2OS MT FGF2-GFP Cav1 KO clones & rescue of clones B6 and B10	Created within this thesis
U2OS MT FGF2-GFP Cav1/2 dKO clones	Created within this thesis
U2OS MT FGF2-GFP Cav2 KO clones	Created within this thesis
U2OS MT FGF2-GFP D9 wt clone + HA-GPC1 or + Flag-GPC1	Created within this thesis
U2OS MT FGF2-GFP GPC1 KO clones	Created within this thesis
U2OS MT FGF2-GFP GPC1 KO D4 + HA-GPC1 or + Flag-GPC1	Created within this thesis
U2OS MT FGF2-GFP GPC1/6 dKO clones	Created within this thesis
U2OS MT FGF2-GFP GPC6 KO clones	Created within this thesis
U2OS MT FGF2-GFP wt + Cav1 or + Cav2	Created within this thesis
U2OS MT FGF2-GFP wt pool 3x sort	Created within this thesis
U2OS MT FGF2-Halo	Nickel lab

3.1.8 Technical devices

Device	Company
Centrifuge 5417R	Eppendorf
Centrifuge 5404R (cell culture)	Eppendorf
FACSCalibur™ Flow Cytometer	Becton Dickinson
Gel Doc™ XR + System	BioRad
Heraeus Megafuge 40R Centrifuge	Thermo Scientific
Infinite F50 plate reader	Tecan
LSM800	Zeiss
LUNA™ Automated Cell Counter	Logos Biosystems
Nanodrop ND-1000	Thermo Fischer
Odyssey CLx	LI-COR
Olympus xcellence TIRF/Scanner FRAP	Olympus
OptimaTM LE-80K Ultracentrifuge	Beckman Coulter
PCR cycler FG-TC01	FastGene
StepOne™ Real-Time PCR System	Applied Biosystems™
TCS SP8 STED 3X microscope with FALCON FLIM	Leica

3.1.9 Software

Software	Supplier
Affinity Designer	Serif Europe Ltd
Benchling	Benchling
Endnote 20	Endnote
Fiji	Schindelin 2012, [238]
Huygens Professional Deconvolution Software	Scientific Volume Imaging
Image Studio Lite	LI-COR Biosciences
Leica Application Suite X (LASX)	Leica
Microsoft Office	Microsoft
Olympus xcellence	Olympus
Prism 9	GraphPad
SnapGene	Dotmatics
ZEN (blue edition)	Zeiss

3.2 Methods

3.2.1 Cloning

Cloning was performed with DNA from ordered synthetic genes or with usage of vectors from a laboratory internal database. DNA was replicated for own usage via retransformation and DNA preparation from *E. coli*. DNA concentration was measured at an absorbance of 260 nm using a Nanodrop ND-1000 spectrophotometer.

3.2.1.1 Transformation into *E. coli*

For amplification of plasmids transformation into calcium competent DH5α *E. coli* (Life Technologies) was performed. Bacteria were thawed on ice and half of a ligation solution (see 3.2.1.8) or 1 µl of database DNA was added. In general, minimum 10-fold more bacterial solution than DNA was used. Bacteria were incubated with DNA on ice for 30 min followed by heat shock at 37°C for 20 sec and then placed back on ice. LB medium (5 g/l NaCl, 10 g/l Tryptone and 5 g/l yeast extract) was added to allow bacteria to recover for 1 h at 37°C shaking with 450 rpm. Bacteria were then plated out on LB-agar plates (LB + 16 g/l agar) at different concentrations for later picking of colonies or used for inoculation of liquid cultures if database DNA was retransformed. Plates and LB medium contained the appropriate antibiotics to select for plasmid presence (25 µg/ml Kanamycin or 100 µg/ml Ampicillin).

3.2.1.2 Plasmid isolation (miniprep or midiprep)

Plasmid isolation was performed from retransformed liquid bacterial cultures or from liquid cultures growing from single colonies for analysis of correct cloning. For cloning and plasmid storage DNA from small bacterial cultures of 4 ml were extracted via NucleoSpin Plasmid Kit (miniprep) according to manufacturer's protocol. DNA used for transfection and virus production was isolated from 100 ml liquid cultures via Nucleo Bond MIDI kit (midiprep) according to protocol. DNA concentration was measured at the Nanodrop and stored at -20°C for long-term storage or 4°C for subsequent cell transfection. Freshly cloned plasmids were sent for sequencing at Microsynth Seqlab.

3.2.1.3 PCR

PCR was used to amplify DNA fragments from existing vectors for subsequent cloning. Primers were designed to amplify the gene of interest with restriction enzyme sites suitable for later digest and ligation into predigested expression vectors. PCR mixes were prepared on ice with reagents from NEB as follows:

Reagents	Volume in µl for 1 reaction
Template DNA	50 – 100 ng
dNTP mix (10 mM each dNTP)	4
Forward primer [10 pmol/µl]	5
Reverse primer [10 pmol/µl]	5
Q5® 5X Reaction Buffer	10
Q5® High GC Enhancer	10
Q5® High-fidelity DNA Polymerase	0,5
Total sample volume in H_2O	50 µl

Duration	Temperature in °C
1 min	98
10 sec	98
20 sec	50-58 (depending on primers)
10 sec	72
2 min	72
∞	8

Marked steps were repeated for 30 cycles.

Correct PCR fragment size was verified via agarose gel electrophoresis before DNA extraction.

3.2.1.4 Agarose gel electrophoresis

For analysis of DNA agarose gel electrophoresis was performed. Therefore 1-2% agarose gels were prepared in 1X TAE buffer (1 mM EDTA, 40 mM Tris, 20 mM acetic acid) using 1:20 000 RedSafe dye. DNA samples were mixed with 6X loading dye from NEB and loaded on agarose gels together with 100 bp or 1kb ladder. Gels were run for 15-30 min at 120 V to separate the desired fragment sizes and imaged using a Gel Doc™ XR + system. DNA was extracted from cut out gel pieces using QIAquick Gel Extraction Kit. DNA was eluted in 20 µl H_2O and stored at -20°C for later use.

3.2.1.5 PCR blunt cloning

Blunt ended PCR fragments isolated from agarose gels were used for Zero Blunt® PCR Cloning to amplify fragment concentration. A 1:1 molar ratio of insert to vector was used and insert quantity was calculated via following formula:

$$ng\ of\ PCR\ fragment = \frac{size\ of\ PCR\ fragment\ (bp) * 25\ ng\ linearized\ pCR® - Blunt\ vector}{size\ of\ pCR® - Blunt\ vector\ (3500\ bp)}$$

Ligations were performed using a final reaction volume of 10 µl containing 1 µl (25 ng) pCR-Blunt, 1 µl ligation buffer and 1 µl T4 DNA Ligase. Mixes were incubated for 30 min at room temperature before half of the mix was transformed into DH5α and plated out on LB-Kanamycin plates. Single colonies were used for miniprep and analyzed via test digest with restriction enzymes and sequencing.

3.2.1.6 Restriction enzyme digest

For cloning of PCR fragments (in pCR-Blunt vector) into expression vectors both were digested with restriction enzymes. Test enzymatic digests were also performed to verify correct insert size into pCR-Blunt or expression vectors. For classical enzymatic digest, purified DNA (up to 5 µg) was digested in a total reaction volume of 25 µl. Except for KflI all enzymes were from NEB and up to 1 µl restriction enzyme were used for digest in CutSmart buffer. Enzymatic digest was performed for 1 h (4h for KflI) at 37°C. Vectors were treated with Quick CIP (calf intestinal phosphatase) according to NEB protocol to inhibit relegation of the backbone while inserts remained phosphorylated. Fragments and vectors were then prepared via agarose gel electrophoresis and DNA extraction to be used for subsequent ligation.

3.2.1.7 Oligo annealing

Some protein tags or fragments were too small for PCR amplification and detection via agarose gel electrophoresis. Therefore, oligo annealing was performed. In brief, oligos containing the desired tag/sequence were designed with restriction enzyme site overhangs in a “digested state” to be directly integrated into digested vectors. Either oligos were ordered with a 5’ phosphate and vectors were dephosphorylated or oligos without phosphate were ordered and ligated into non-dephosphorylated vectors. Forward and reverse oligos were mixed 1:1 (10 µl each of 1:1000 dilution of primer [100 µM]) and incubated for 2 min at 95°C in a PCR cycler. Afterwards the machine was switched off and left closed to allow for slow cooling down and annealing of oligos (approx. 1 h). 1 µl of oligo mix was used for subsequent ligation reaction.

3.2.1.8 Ligation

Ligation was performed using the T4 DNA ligation kit from Takara. Insert and vector were mixed in a 1:1 molar ration and amounts were calculated as follow:

$$ng\ insert = \frac{size\ of\ insert\ (bp) * 50\ ng\ linearized + CIP\ vector}{size\ of\ vector\ (bp)}$$

Vector and insert were mixed and Takara solution I containing T4 Ligase was added 1:1 to mix and incubated for 30 min at 16°C. Half of the ligation mix was used for transformation into DH5α and plating onto LB plates (+ antibiotic). Single colonies were used for miniprep and correct fragment insertion was

tested via test digest. Test enzymatic digest was performed as described above using NEB enzymes, only that a smaller volume of 0,2 µl enzyme were used per reaction. Clones with correct fragment sizes were also sent for sequencing at Microsynth.

3.2.2 Cell culture

3.2.2.1 Cultivation, thawing and freezing

All cell lines were cultivated in cell culture incubators at 37°C with 5% CO_2 and 95% humidity. HeLa S3 and HEK (Human Embryonic Kidney) EcoPack 2-293 cells were cultivated in 1g/l low glucose DMEM full medium containing 10% FCS and 100 IU/ml penicillin and 100 µg/ml streptomycin (full medium = + FCS, + PenStrep). HEK cells were cultivated on 0,02% collagen-coated plates when used for production of virus. U2OS (human bone osteosarcoma epithelial cells) were cultivated in high glucose (4,5 g/l) DMEM full medium and CHO K1 (Chinese Hamster Ovary) cells were cultivated in MEM-alpha modification full medium supplemented with 2 mM glutamine. Cells were cultivated until 80% confluent and then passaged via short incubation with trypsin or cell dissociation buffer (CDB) to detach cells.
For induction of FGF2-GFP protein expression 1 µg/ml doxycycline was added to cells for 20-24 h prior to experiments.
For thawing of cells cryotubes from -80°C or liquid nitrogen storage were taken out and wiped with ethanol. For quick thawing tubes were placed into a warm water bath until cells were almost completely thawed. Cells were transferred into a 50 ml falcon containing 10 ml warm full medium and centrifuged for 3 min at 1000 rpm to remove freezing medium containing DMSO. Cell pellets were resuspended in fresh warm full medium and transferred to cultivation plates. If cells were to be used for experiments, they were treated for 1 week with mycoplasma removal agent (MRA, 1:100 dilution) before use.
For cell freezing 80% confluent cells were detached with trypsin or CDB. Cells were pelleted in full medium via 3 min centrifugation at 1000 rpm. 2X freezing medium (containing 20% DMSO and 40% FCS) was prepared, filter sterilized (0,2 µm) and transferred to a cryotube. Cells were resuspended in fresh medium and mixed 1:1 with freezing medium. Cells were slowly frozen in Styrofoam containers at -80°C and transferred to liquid nitrogen after 2 days.

3.2.2.2 Transient transfection

For transient transfection with plasmids FuGENE® HD transfection reagent was used. Cells transfected for CRISPR-Cas9 knockout were transfected in 6-well plated and cells for microscopy were transfected in 8-well µ-slide ibidi chambers. Cells were transfected according to manufacturer's recommendations via mixing DNA diluted in OptiMEM in a 1:3 ratio with FuGENE® HD transfection reagent. After 5-15 min incubation at room temperature DNA mix was added to cells and transfected cells were analyzed 24h post transfection.

3.2.2.3 Virus production and transduction for stable cell lines

Stable cell lines were generated via viral transduction with Moloney murine leukemia virus as described previously [121]. HEK EcoPack 2-293 cells are designed for production of Moloney-based retroviral stocks by transfection with retroviral vectors (pFB-Neo for constituent expression or pRev TRE2 for doxycycline induction) containing the gene of interest. HEK EcoPack cells already express the MMLV Gag, Pol and Env proteins. Transfection was performed using the MBS Mammalian Transfection kit according to manufacturer's recommendations. In brief, HEK cells were plated onto collagen coated 10 cm plates and the subsequent day transfection was performed. Therefore, cell medium was changed to 6 ml MBS containing medium (DMEM + 7% modified bovine serum + 20 µM chloroquine) 20-30 min prior to transfection. 9 µg vector DNA were diluted in a final volume of 450 µl H_2O and mixed with 50 µl solution I and 500 µl solution II from the MBS kit. DNA was incubated for 10 min at room temperature. DNA solution was added to cells in a drop-wise fashion. 3 h after transfection medium was removed and replaced by 6 ml full medium containing 25 µM chloroquine. Another 6-7h later medium was again replaced by 6 ml full medium containing no chloroquine. After over-night incubation medium was replaced the subsequent morning with fresh medium. After 24-48 h of virus production target cells in a 6-well plate were transduced. Target U2OS or HeLa S3 cells expressed the Tet-on transactivator rtTA2-M2 and the murine cationic amino acid transporter MCAT-1 enabling activation of protein expression via the addition of doxycycline if containing a plasmid with FGF2-GFP [239, 240]. For transduction growth medium from target cells was removed and 2,5-5 ml virus-containing supernatant from HEK cells were passed through a 0,45 µm filter directly onto target cells. DEAE-dextran was added to a final concentration of 10 µg/ml. 3 h after transduction full medium was added 1:1 and cells were incubated for 72 h with viral particles before subsequent selection.

3.2.2.4 Cell line selection via FACS or antibiotics

Stable cell lines were either selected via antibiotic resistance (pFB-Neo or pFB-Bsd vectors) or FACS sort (pRev TRE2). Stable cell lines expressing pFB-Neo vectors were selected via incubation with 800 µg/ml G418 and cell lines expressing pFB-Bsd were selected via incubation with 10 µg/ml blasticidin. Cells were incubated with antibiotics until non-transduced control cells died (1 – 2 weeks).
For cells transduced with pRev TRE2 FGF2-GFP a FACS sort was performed at the ZMBH FACS facility. Therefore, cells were incubated with 1 µg/ml doxycycline 24h prior to sorting. For sorting cells were washed with PBS and detached from plates with CDB. Cells were pelleted and resuspended in sort medium containing no FCS and cells were sorted based on GFP expression levels. A pool of cells was collected and sorted again after 1 week incubation without doxycycline to select non-fluorescent cells. A third round of sorting with doxycycline was performed and GFP positive cells were then selected as final pool of cells expressing FGF2-GFP in a doxycycline inducible manner.

3.2.2.5 Generation of knockout cells

3.2.2.5.1 Design and cloning

Knockout cells were generated with CRISPR-Cas9 vectors existing in the laboratory or via own gRNA design. For design literature research was conducted on existing knockouts and corresponding gRNAs. Also, CCTop CRISPR-Cas9 online tool from COS Heidelberg was used. gRNAs from the first gene exons with the least off target effects and good efficiencies were selected. To verify whether the selected gRNA target sequence is present within cells, primers for genomic PCR of the selected exons for knockout were designed. Genomic DNA from cells growing on 10 cm dishes was extracted with DNeasy Blood and Tissue extraction kit according to manufacturer's recommendations. DNA was eluted in a final volume of 200 µl AE buffer and used for following PCR using Q5 polymerase and reagents from NEB:

Reagents	Volume in µl for 1 reaction
Template DNA	5 µl
dNTP mix (10 mM each dNTP)	4
Forward primer [10 pmol/µl]	5
Reverse primer [10 pmol/µl]	5
Q5® 5X Reaction Buffer	10
Q5® High GC Enhancer	10
Q5® High-fidelity DNA Polymerase	0,5
Total sample volume in H_2O	50 µl

Duration	Temperature in °C
1 min	98
10 sec	98
20 sec	50 – 58 (depending on primers)
10 sec	72
2 min	72
∞	8

Marked steps were repeated for 30 cycles.

Successful PCR amplification was verified via agarose gel and PCR fragments were purified via QIAquick® PCR Purification Kit. Amplified PCR fragments were then sequenced with self-designed primers using GATC supreme sanger sequencing service. After sequence verification forward and reverse gRNAs containing 5'-phosphate were ordered and annealed via 1:1 mix (10 µl of [100 µM] each) and heated 2 min at 95°C. Annealing was achieved via slow temperature decrease and cooling down of gRNA mix. 1 µl annealed gRNAs were mixed with 0,55 µl BbsI + CIP calf intestinal phosphatase

digested pSpCas9(BB)-2A-RFP vector ([96,1 ng/µl] from Sabine Wegehingel) and 1,55 µl Takara ligation solution I. Mixed were incubated for 30 min at 16° before transformation into DH5α competent bacteria. After colony inoculation and miniprep correct gRNA integration into Cas9 vector was verified via sequencing.

3.2.2.5.2 Transfection & selection

For Cas9-gRNA vector transfection FuGENE®-HD transfection reagent was used as mentioned previously. In brief, target cells were seeded into 6-well plates. 2 µg DNA were diluted in 104 µl OptiMEM and mixed with 6,6 µl FuGENE®-HD. DNA mix was incubated for 5 min at room temperature and added to cells in drops. The subsequent day cells were transferred to a 10 cm dish and doxycycline was added to induce FGF2-GFP expression. Cells were sorted into single clones for RFP and GFP at the ZMBH FACS facility into a 96-well plate.

3.2.2.5.3 Knockout validation

After 2-3 weeks of single clone growth viable single clones were selected and transferred to fresh 96-well plates at different dilutions. DNA of single clones was extracted using QuickExtract DNA Extraction Solution. Therefore, cells were detached and transferred to 96-well PCR plates. Pelleted cells were mixed with 10 µl QuickExtract solution and incubated for 6 min at 65°C followed by 2 min incubation at 98°C in a PCR cycler. Extracted DNA was stored at -20°C until used for genomic DNA PCR as described above. Afterwards PCR plates were sent for SupremeRun Multiprimer sequencing at GATC/Eurofins to validate knockout of the corresponding gene. Clones showing KO of desired protein were expanded and further validated via Western blotting or RT-qPCR.

3.2.3 RT-qPCR

To check for protein levels on RNA levels RT-qPCR was performed. 6 x 10^5 cells per 6-well were seeded to be analyzed. The subsequent day cells were washed once with PBS and RNA was extracted via RNeasy Mini Kit (Qiagen # 74104) according to manufacturer's recommendations.
For reverse transcription into cDNA the ImProm-II™ Reverse Transcription System (Promega #A3800) was used. In brief 1 µg extracted RNA was mixed with 1 µl Oligo$(dT)_{15}$ primer in a final volume of 5 µl H_2O and stored at 4°C. Mixes were heated at 70°C for 10 min using a PCR cycler and then placed back on ice. Per reaction the following transcription mixes were pipetted:

Reagents	Volume in µl for 1 reaction
$MgCl_2$	2,5
ImProm-II™ 5X Reaction Buffer	4
dNTP Mix	1
Recombinant RNasin Ribonuclease Inhibitor	0,5
ImProm-II™ Reverse Transcriptase	1
Total sample volume with RNA-oligo mix (in nuclease-free H_2O)	15 µl

Samples were reverse transcribed in a PCR machine with following settings:

Duration	Temperature in °C
10 min	25
60 min	42
5 min	95
∞	8

Readily transcribed cDNA was stored at –20°C and extracted RNA was stored at -80°C if needed for later use. RT-qPCR was performed using TaqMan Real-Time PCR Assays (Thermo Fischer). Gene Expression Master Mix (Thermo Fischer #4370048) and TaqMan assays coupled to FAM™ dye were ordered for the proteins to be analyzed (see 3.1.3). GAPDH assay was ordered as housekeeping and control protein. Per well of a 96-well PCR plate following mix was pipetted:

Reagent	Volume in µl
TaqMan master mix	10
TaqMan assay	1
H_2O	6,5
DNA (mixed 1:1 with H_2O)	2,5
Total sample volume	20 µl

For all proteins and cell lines technical triplicates were prepared. PCR plates were then sealed with transparent foil and RT-PCR was conducted using StepOne™ Real-Time PCR System (Applied Biosystems™) as using the predefined 2h program as follows:

Duration	Temperature in °C
2 min	50
10 min	95
15 sec	95
1 min	60

Marked steps were repeated for 40 cycles.

Mean CT (threshold cycle) values from three replicates of the individual proteins or cell lines were used to calculate relative cDNA replication. Therefore, GAPDH CT mean was subtracted from sample CT mean to calculate “delta CT” and an average from all sample “delta CTs” was calculated. Individual “delta CTs” were then subtracted from “delta CT average” to get X. Then 2^X was calculated and values were normalized to wt samples to get relative DNA/mRNA levels for all proteins.

3.2.4 Biochemical methods

3.2.4.1 FACS cell surface staining

For fluorescent activated cell sorting (FACS) 2 x 10^5 cells were seeded per well of a 12-well plate the day before the experiment. The next day cells were washed and detached with cell dissociation buffer (CDB) for 10 min at 37°C. Cells were transferred into a reaction tube and placed on ice. 1 ml cell culture medium (+ FCS) was added to the cells and cells were pelleted via 3 min centrifugation at 300 g. Cell pellets were then resuspended with 100 µl medium (+FCS) containing primary antibody (anti-rabbit HA or anti-mouse 10E4 antibody). Cells were incubated 1 h at 4°C while turning. 1 ml medium (+ FCS) was added to cells to wash and cells were again pelleted via centrifugation. Cell pellets were resuspended and incubated in 200 µl medium (+ FCS) containing secondary APC-linked antibody for 30 min at 4°C protected from light. Cells were washed and pelleted as described above and pellets were resuspended in 300 µl medium (no FCS) containing 5 % CDB. Cell fluorescence was measured using a FACSCalibur™ Flow cytometer.

3.2.4.2 Heparinase III digest

For heparinase III digest cells were detached from cell culture dishes via 10 min incubation with cell dissociation buffer at 37°C and pelleted together with cell culture medium (+FCS) at 300 g for 3 min. The supernatant was aspirated. For a 10 cm dish 40 µl heparinase solution were prepared using 10X heparinase buffer, H_2O and 0,5 µl heparinase III per 100 µl solution. Cells were incubated for minimum 4 h with heparinase solution at 30°C. Cells were pelleted to remove heparinase solution and lysed in 100 µl (for full 10 cm dish) RIPA buffer (150 mM NaCl, 1% NP-40, 0,5% sodium-deoxycholate, 0,1% SDS and 50 mM Tris pH 8) + protease inhibitors via 30 min incubation on ice. Cell debris was removed via 10 min centrifugation at 13 000 rpm at 4°C and supernatants were mixed 1:1 with 4 X sample buffer (40% Glycerol, 240 mM Tric-HCL pH 6,8, 8% SDS, 5% β-Mercaptoethanol, Bromophenol blue). Samples were boiled for 10 min at 95°C.
For other cell lysates not treated with heparinase, such as for KO validation, also a general RIPA lysis was performed. For 6-well plates lysis was performed in 30 µl RIPA + 30 µl 4X sample buffer.

3.2.4.3 SDS-PAGE and Western blotting

Proteins were separated according to their molecular weight via SDS-PAGE. Precasted NuPAGE™ 4-12% Bis-Tris-gels with different well number were used in Thermo Fischer Mini Gel Tanks. As reference 3 µl PageRuler™ were loaded and 10 – 30 µl protein lysate were loaded per rinsed pocket of a gel. MES or MOPS running buffers was used depending on protein sizes to be detected later. Gels were run at 200 V for 40 min (MES buffer) or 55 min (MOPS buffer).
Gels were then used for Western blotting for protein detection via antibody staining. Immobilon®-FL PVDF membrane was activated in methanol and wet in blot buffer (40 mM Glycine, 25 mM Tris pH 8,8, 20 % methanol). Western blot sandwiches were prepared as following from the side facing negative pole to positive side: one layer of Whatman paper, SDS gel, activated membrane, Whatman paper. Blots were run in blot buffer under cooling and stirring for 1h at 100V. Membranes were thereafter blocked 1 h with shaking in 5% milk-PBS (137 mM NaCl, 2,7 mM KCl, 10 mM Na_2HPO_4, 2 mM KH_2PO_4 pH 7,4) to reduce unspecific antibody binding. Membranes were thereafter incubated for 1 h at room temperature or over-night at 4°C with primary antibodies in 3% BSA-PBST (PBS + 0,05% Tween-20). After three 10 min washes with PBST, membranes were incubated for further 30 min with secondary antibodies in 3% BSA-PBST. Before imaging membranes were washed again three times in 3% BSA-PBST to remove all antibody. Membranes were imaged on a LI-COR Odyssey CLx using Image Studio Lite (version 5,2,5) software for imaging and analysis.

3.2.4.4 Cell surface biotinylation

For cell surface biotinylation experiments 3 x 10^5 cell were seeded per well of a 6-well plate two days before the experiment. One day before the experiment 1 µg/ml doxycycline was added to the cells to induce FGF2-GFP expression and cells were incubated 20-24 h. On the day of the experiment plates were placed on ice and cells were washed twice with 1 ml cold PBS-Ca/Mg (1 mM $MgCl_2$, 0,1 mM $CaCl_2$). Then cells were incubated 30 min on ice on a shaker with 600 µl of 1 mg/ml EZ-Link-Sulfo-NHS-SS-Biotin in cold incubation buffer (150 mM NaCl, 10 mM Triethanolamine pH 9, 2 mM $CaCl_2$). Cells were then washed once with cold quenching buffer (100 mM glycine in PBS-Ca/Mg) and then incubated further 20 min with 1 ml quenching buffer on ice under shaking to stop biotinylation. Cells were then washed twice with cold PBS to remove quenching buffer. For cell lysis cells were incubated 10 min at 37°C with 300 µl lysis buffer (62,5 mM EDTA pH 8, 50 mM Tris-HCL pH 7,5, 0,4% sodium-deoxycholate and 1% NP-40 + protease inhibitors). Cells were scrapped off the plates and resuspended via pipetting into a reaction tube. Samples were then sonicated in a sonification bath for 3 min prior to further cell lysis by 15 min incubation at room temperature and vortexing every 5 min. Cell debris was pelleted via 10 min centrifugation at 4°C and 13 000 rpm. An input sample of 15 µl was taken, mixed with 15 µl 4X sample buffer and boiled for 10 min at 95°C for later analysis. For pulldown of biotinylated protein 60 µl Pierce™ Streptavidin UltraLink™ Resin per sample were washed twice in lysis buffer. All bead centrifugation steps were carried out for 1 min at 3000 g. Washed beads were incubated with remaining lysate for minimum 1 h at room temperature under rotation. Beads were spun down and

washed once with wash buffer 1 (lysis buffer + 0,5 M NaCl) and three times with wash buffer 2 (lysis buffer without NP-40 + 0,5 M NaCl and 0,1% NP-40). Samples were eluted via boiling for 10 min at 95°C in 30 µl 4X sample buffer. 10 µl input and 10 µl eluate were used for SDS-PAGE and Western blot analysis (see 3.2.4.3). For quantification of FGF2-GFP secretion efficiency ratios between input and eluate were calculated (eluate/input) and normalized to wt cells. For absolute surface FGF2-GFP signal intensities were adjusted based on loading volume and original sample volume (3 x eluate/ 60 x input).

3.2.4.5 Isolation of detergent resistant membranes

For isolations of detergent resistant membrane (DRM) fractions cells were seeded on a 10 cm dish to reach 80-100% confluency on the day of the experiment. Cells were incubated with 1 µg/ml doxycycline for 20-24h prior to cell lysis if FGF2-GFP was to be detected. Cells were washed with PBS and detached from plates with 1 mM EDTA-PBS. Cell pellets were collected via centrifugation at 300 g for 5 min. After removal of the supernatant pellets were lysed in 120 µl of DRM lysis buffer (150 mM NaCl, 20 mM HEPES) containing 1% Triton X-100 and 1 X protease inhibitor mix on ice for 30 min. Samples were placed in an ultrasound bath for 3 min. Thereafter, 10 µl input sample was taken and boiled with 10 µl 4X sample buffer + 20 µl water. 80 µl lysate were mixed with 80 µl 80% sucrose in DRM lysis buffer (all sucrose buffers contained no Triton). 120 µl lysate-40% sucrose mix were placed into an ultracentrifugation tube and overlayed with 240 µl 30% sucrose and 240 µl 5% sucrose in DRM lysis buffer. Samples were ultracentrifuged overnight (around 16h) at 4°C and 50 000 rpm in a SW60 swing bucket. The subsequent day 60 µl fractions were collected from top to bottom and boiled for 10 min at 60°C with 4X sample buffer (20µl). For HeLa S3 cells 10 µl sample were analyzed via SDS-PAGE and Western blot. For U2OS samples were precipitated right after centrifugation and collection via methanol-chloroform-H_2O (see 3.2.4.6.4). Pellets were then dissolved in 20 µl sample buffer and loaded entirely on gels.

3.2.4.6 Trifunctional lipid probes pulldown

3.2.4.6.1 Preparation of cells and cell lysis

Cells were seeded on a 10 cm dish to reach 80% confluency on the day of the experiment in medium with FCS to let cells attach properly. The next day, trifunctional $PI(3,4,5)P_3$ or $PI(4,5)P_2$ (final concentration for cells 5 µM) was mixed 1:1 with 10% pluronic in DMSO and added to DMEM (no FCS). Cells were incubated over night with the lipid-DMEM solution. For pulldown experiment cells were washed with cold PBS, uncaged 90 s at 400 nm UV irradiation and directly afterwards crosslinked on a cold metal block for 5 min with 360 nm UV. Control cells were not crosslinked. Cells were scraped from plates and pelleted for 5 min at 300 g using a table top centrifuge. Pellets were resuspended in 100 µl lysis buffer (0,1% SDS, 1 % Triton X-100 + protease inhibitors from Serva) and sonified in a sonification bath for 5 min (put ice into bath). Cells were then further lyses via 1 h incubation at 4°C under rotation.

Debris was pelleted via 5 min centrifugation at 14 000 g at 4°C and supernatant was thereafter transferred to a new tube. Protein concentration was determined via amido black analysis.

3.2.4.6.2 Amido black protein concentration determination

For both standard and sample measurements technical replicates were prepared. A serial dilution of BSA standard using a 0,1 mg/ml stock solution was prepared via mixing 0 µl, 25 µl, 50 µl, 75 µl and 100 µl BSA standard solution with H_2O to reach a final volume of 100 µl. 2,5 µl sample from cell lysis were also mixed with H_2O to reach 100 µl. 400 µl amido black 10b solution ([1 g/l] in wash solution) were added to all samples and solutions were vortexed followed by 5 min incubation at room temperature. Samples were centrifuged at 14 000 rpm for 5 min and supernatant was aspirated. Stained pellets at the side of the reaction tube were washed twice with 500 ml wash solution (MeOH:AcOH 9:1) and centrifuged each time. Pellets were dissolved in 300 µl 0,1N NaOH and 150 µl were spotted into a 96 well plate to measure absorbance at 550 nm in a plate reader. Protein concentration was calculated based on standard BSA curve.

3.2.4.6.3 Biotin click

Samples were adjusted to 200 µg protein in 100 µl lysis buffer. Biotin click master mix was prepared for samples as followed:

Biotin master mix for 4 samples	Final concentration	Volume (µl)
$CuSO_4$ (50 mM in H_2O)	200 µM	4
TBTA (2 mM in DMSO)	20 µM	10
Ascorbic acid (50 mM in H_2O, fresh!)	200 µM	4
Picolyl-azide-PEG4-Biotin (10 mM in DMSO)	100 µM	10
Total volume for 1 sample		7

7 µl biotin lick mix were added to each 100 µl lysate and incubated 1 h at 37°C while shaking at 400 rpm.

3.2.4.6.4 Protein precipitations

Next protein was precipitated twice to remove click reagents. For the first precipitation 400 µl ice-cold MeOH, 100 µl ice-cold $CHCl_3$ and 300 µl ice-cold H_2O were added to samples and vortexed. Samples were centrifuged at 14 000 g for 2 min at 4°C. The upper phase was discarded and the protein pellet remained floating on the lower phase. 400 µl ice-cold MeOH were added and samples were vortexed briefly before centrifugation for 3 min at 4°C and 14 000 g. The supernatant was discarded and the protein pellet dissolved in 100 µl 2% SDS-PBS while shaking at 37°C. The second precipitation was

performed same as the first. Here the final protein pellet was air dried for 10 min to remove MeOH fully. Pellets were then dissolved in 200 µl 0,2% SDS-PBS via shaking at 37°C or in a sonification bath.

3.2.4.6.5 Immunoprecipitation

20 µl input sample were taken and frozen for later analysis. 20 µl streptavidin sepharose beads (#17511301, Cytiva) were washed and equilibrated with 0,2% SDS-PBS. All bead centrifugation steps were carried out at 1000 g for 30 sec. Samples after protein precipitations and input removal were added to the beads and incubated over night at 4°C under turning.

3.2.4.6.6 Washing and elution

The next day beads were centrifuged for 30 sec at 1000 g and the supernatant was removed. 20 µl of that supernatant were used for later analysis as unbound flow through. Beads were washed twice with wash solution 1 via 5 min incubation while turning and then twice with wash solution 2. Wash solution was fully removed and beads were eluted via addition of 20 µl elution buffer and incubation at 60°C for 15 min. Samples were passed through small Mobicol filters to remove beads. 7 µl 4X sample buffer were added to eluate sample, input and flow through and boiled for 10 min at 60°C. Entire fractions were loaded on SDS-PAGE and analyzed via Western blotting.

Wash buffer 1	Final concentration: 2% SDS
Wash buffer 2	Final concentration: 50 mM HEPES 1 mM EDTA 500 mM NACl 1% Triton X-100 0,1% sodium-deoxycholate
Elution buffer	Final concentration: 10 mM Tris pH 7,4 2% SDS 5% β-Mercaptoethanol 2 mM Biotin

3.2.5 Microscopy

3.2.5.1 Immunofluorescence staining

Cells were seeded onto 35 mm Glass bottom dishes No 1,5 or µ-Slide 8 Well Glass Bottom Dishes to reach about 80% confluency the day of the experiment. If desired, 1 µg/ml doxycycline was added to cells to induce FGF2-GFP expression. Cells were washed 2-3 times with PBS and fixed with 4% PFA for 20 min at room temperature. If cells were permeabilized, they were incubated for 10 min with 0,05% Saponin in PBS at room temperature. Then cells were washed twice with PBS before 30 min blocking in 1% BSA-PBS. Cells were incubated with primary antibodies in 1% BSA-PBS for 1h. Primary antibodies were removed via 3 washings with PBS. Secondary antibodies in 1% BSA-PBS were added to the cells and incubated for 30 min or 60 min (for STED Abberior antibodies) in the dark. Cells were washed three times before 15 min incubation with Hoechst (1:50 000 from [10 mg/ml]) if nuclei were stained. Nuclei were never stained for STED microscopy to inhibit channel crosstalk. Cells were imaged in PBS on a Zeiss LMS800 confocal microscope or on a TCS SP8 STED 3X microscope with FALCON FLIM from Leica. Image analysis was performed using Fiji [238]. STED images were beforehand subjected to standard deconvolution in express deconvolution option using Huygens Professional Deconvolution Software (Scientific Volume Imaging, http://svi.nl).

3.2.5.2 Duolink® proximity ligation assay

For Duolink® proximity ligation assays (PLA) cells were seeded onto 35 mm Glass bottom dishes No 1,5 the day before experiments to reach 60-80% confluency the next day and incubated with 1 µg/ml doxycycline if desired. Cells were washed twice with PBS (all washing with 1,5 ml) and fixed for 20 min in 4 % PFA in PBS. Cells were then permeabilized with 0,05 % saponin in PBS for 10 min. Fixed cells were washed twice with PBS and then blocked for 30 min in 1 % BSA in PBS. Cells were then incubated for 1 h with primary antibodies diluted in 1% BSA-PBS (only 50 µl onto center of sample area) in a wet chamber. PLA probe solutions (40 µl per sample, same for all further PLA reagents) were prepared via 1:5 dilution of PLA anti-rabbit PLUS and 1:5 dilution of PLA anti-mouse MINUS in 1% BSA-PBS. Solutions were incubated for 20 min at room temperature before use. Primary antibodies were removed and samples were washed 3 times with PBS before 40 µl probe solution was added to the cells. Cells were incubated for 1 h at 37°C in a wet chamber. PLA probes were removed and cells were washed twice for 5 min shaking with wash buffer A (10 mM Tris-HCL pH 7,5, 159 mM NaCl and 0,05% Tween20). Ligation stock was diluted 1:5 in H_2O and ligase was added 1:40. Cells were incubated for 30 min at 37°C with ligation solution in a wet chamber. Solutions were removed and cells were washed twice for 2 min with wash buffer A. Amplification stock was diluted 1:5 in H_2O together with polymerase which was diluted 1:80. Cells were incubated for 100 min with amplification solution in the dark at 37°C in a wet chamber. Amplification solution was removed and cells were washed twice for 10 min shaking with wash buffer B (0,1 M NaCl, 0,2 M Tris-HCL pH 7,5). Cells were then washed once with wash buffer B diluted 1:100 in H_2O. Cells were then stained with Hoechst (1:50 000 from [10 mg/ml]) for 15 min at

room temperature followed by 3 washes with PBS. Cells were then imaged in PBS on a Zeiss LMS800 confocal microscope. For quantification of PLA signals spots per cell were counted using the TrackMate plugin from Fiji [238, 241].

3.2.5.3 TIRF translocation and recruitment assay

Total internal reflection fluorescence (TIRF) translocation and recruitment experiments were conducted by Roberto Saleppico at the ZMBH imaging facility using an Olympus IX81 xCellence TIRF microscope using an Olympus PLAPO ×100/1.45 Oil DIC objective lens and a Hamamatsu ImagEM Enhanced (C9100-13) camera. TIRF experiments were conducted using an established protocol developed in the laboratory before [123, 128].

For translocation experiments cells were seeded onto µ-Slide 8 Well Glass Bottom Dishes from ibidi to reach 60-80% confluency on the day of the experiment and incubated for 24h with 1 µg/ml doxycycline. Cells were washed three times with live cell imaging solution (LCIS) and incubated on ice 30 min while shaking with membrane impermeable anti-GFP nanobodies labeled with AlexaFluor®-647. Cells were again washed three times with LCIS and fixed for 20 min at room temperature with 4% PFA before imaging of nanobody fluorescence using the Olympus 640 nm 140mW diode laser. Images were there analyzed and quantified using TrackMate and Fiji [238, 241]. The cell outline was therefore determined using widefield imaging and nanobody particles per cell were normalized to the cell surface (in μm^2). Nanobody number for each cell and cell line was normalized to wt nanobody average.

For recruitment experiments cells were seeded as mentioned above, yet not incubated with doxycycline to allow for single particle analysis. GFP fluorescence was detected using the Olympus 488 nm 100 mW diode laser. Recruitment of FGF2-GFP particles was imaged in TIRF time-lapse videos. For quantification cell outline was detected via widefield imaging. GFP particles detected in all frames were normalized to cell surface (in μm^2) and to FGF2-GFP expression levels (average intensity with average background subtraction). Particles for each cell were again normalized to average wt conditions.

4 Results

As elaborated previously, the unconventional secretory pathway of fibroblast growth factor 2 has been extensively studied in the last years. Essential components needed for FGF2 translocation have been identified with the phosphoinositide $PI(4,5)P_2$ at the inner plasma membrane leaflet and heparan sulfate proteoglycans on the cell surface being the driving forces of productive FGF2 toroidal pore formation and FGF2 translocation [234]. The role of the α1 subunit of the Na,K-ATPase being required for efficient FGF2 secretion and recruiting FGF2 to the inner plasma membrane leaflet, preceding the interaction with $PI(4,5)P_2$, has been explored [118, 123], yet the full mechanistic action of the ATPase is not well understood. Likewise, it has been known for a long time that heparan sulfate proteoglycans not only act in FGF2 signaling or binding on the cell surface, but are also essential for FGF2 secretion [127, 128], but it was not known whether a specific protein group or single protein is involved.
A proximity-based BioID labeling approach, performed in the laboratory by Matthias Gerstner and Eleni Dimou, was used to discover new interaction partners of FGF2 [235]. In this screen the promiscuous biotin ligase BirA* [242, 243] was fused to different FGF2 mutant versions and biotinylated proteins were identified via streptavidin affinity capture and mass spectrometry analysis. A GPI-linked HSPG, named Glypican-1, was identified and represented an attractive potential new interaction partner of FGF2. The role of GPC1 in FGF2 secretion was investigated in the here presented thesis in collaboration with Carola Sparn and also Sabine Wegehingel and Roberto Saleppico. The data were collectively published beginning of 2022 [51].

4.1 The role of glypicans in FGF2 secretion

4.1.1 GPC1 is a rate-limiting factor in FGF2 secretion

To investigate GPC1 impact on FGF2 secretion CRISPR-Cas9 GPC1 knockout cell lines in HeLa S3 expressing FGF2-GFP in a doxycycline-dependent manner were generated by Sabine Wegehingel (for details see 3.2.2.3 and 3.2.2.5, clone name refers to well number) and validated via genomic DNA sequencing and Western blot analysis. I digested samples with heparinase III to remove the highly negatively charged heparan sulfate chains and obtain accessibility to the unsaturated uronic acid 3G10 epitope recognized by the corresponding 3G10 antibody (therefore declared as ΔHS/ 3G10 ab). GPC1 KO was validated for the two single clones B2 and G4 in Western blot analysis (Figure 6A.) According to gene expression data HeLa cells not only express GPC1, but also GPC5 as only other glypican family member. Therefore, also GPC5 CRISPR-Cas9 KO (single clones B4 and C5) and GPC1/5 dKO (single clone F2) cell lines were generated by Sabine and successful knockout was confirmed via Western blot analysis following heparinase III digest (Figure 6A.). Additionally, I generated stable cell lines overexpressing GPC1 or GPC5 in all KO cell lines to gain further insights. As seen in Figure 6A. GPC1 and 5 were clearly visible when overexpressed and GPC5 ran slightly higher than GPC1 in MOPS SDS running buffer.

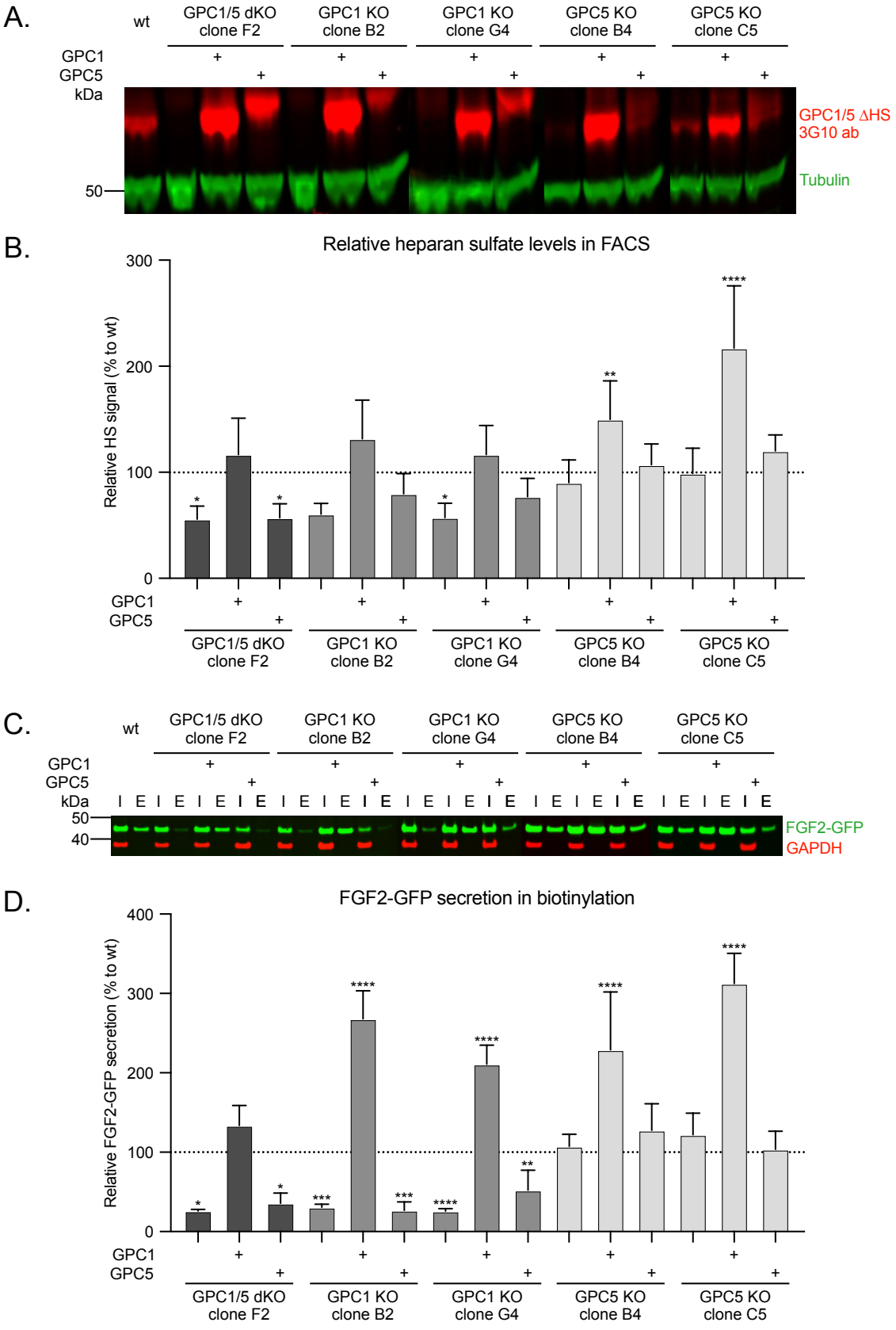
A.
wt
GPC1/5 dKO clone F2
GPC1 KO clone B2
GPC1 KO clone G4
GPC5 KO clone B4
GPC5 KO clone C5
GPC1
GPC5
kDa
50
GPC1/5 ΔHS 3G10 ab
Tubulin
B.
Relative heparan sulfate levels in FACS
Relative HS signal (% to wt)
300
200
100
0
GPC1
GPC5
GPC1/5 dKO clone F2
GPC1 KO clone B2
GPC1 KO clone G4
GPC5 KO clone B4
GPC5 KO clone C5
C.
wt
GPC1/5 dKO clone F2
GPC1 KO clone B2
GPC1 KO clone G4
GPC5 KO clone B4
GPC5 KO clone C5
GPC1
GPC5
kDa
I E I E I E I E I E I E I E I E I E I E I E I E I E I E
50
40
FGF2-GFP
GAPDH
D.
FGF2-GFP secretion in biotinylation
Relative FGF2-GFP secretion (% to wt)
400
300
200
100
0
GPC1
GPC5
GPC1/5 dKO clone F2
GPC1 KO clone B2
GPC1 KO clone G4
GPC5 KO clone B4
GPC5 KO clone C5

Heparinase III digested samples did not fully reflect absolute protein levels though due to possible variations in enzymatic digest efficiency. Relative heparan sulfate levels of the different knockout and overexpression cell lines were therefore also analyzed via FACS. Here, cells were not digested with heparinase III but instead the 10E4 antibody detecting epitopes on native heparan sulfate chains, including N-sulfated glucosamine residues, was used. As seen in Figure 6B. overall HS levels in the different cell lines differed form wild-type (wt) cells. GPC1 KO reduced overall HS levels, whereas GPC5 KO HS levels did not differ significantly from wt cells. Overexpression of GPC1 in GPC5 KO cells on top of endogenous GPC1 significantly raised heparan sulfate levels above wt levels. Heparan sulfate chains are not only present in glypicans though, but also other HSPGs such as syndecans have attached HS chains, explaining remaining HS signals in GPC1/5 dKO. Cells were furthermore analyzed via cell surface biotinylation to assess FGF2-GFP secretion. In brief, FGF2-GFP expression was induced via addition of 1 µg/ml doxycycline (for details please refer to 3.2.4.4) 20-24h prior to the experiment. Cells were incubated with membrane-impermeable NHS-coupled biotin to biotinylate primary amines in surface proteins. Following cell lysis, biotinylated proteins were captured via streptavidin affinity capture and surface protein (eluate) was compared to total protein levels (input taken before bead addition) via SDS-PAGE and Western blot analysis to determine FGF2-GFP secretion efficiency. GAPDH was used as loading control and to monitor cell integrity during biotinylation (intracellular GAPDH should not be in surface eluate). Representative blots are shown in Figure 6C. Quantification from 4 experiments showed a significant reduction of surface FGF2-GFP by 60% and 65% in GPC1 KO clones B2 and G4 respectively (Figure 6D.). Reintroduction and stable overexpression of GPC1 could rescue the observed phenotype not only back to wt levels, but even above two-fold higher, indicating that GPC1 is a rate-limiting factor for FGF2 secretion. Overexpression of GPC5, belonging to a different subclass of glypicans [138], did not compensate for loss of GPC1. Likewise, GPC5 KO did not reduce FGF2-GFP secretion. Consequently, a dKO of GPC1 and GPC5 showed a similar phenotype to GPC1 KO.

Figure 6: Analysis of GPC1 and GPC5 knockout cell lines and rescue cell lines. HeLa S3 FGF2-GFP cell lines with CRISPR-Cas9 GPC1 KO (single clones B2 and G4), GPC5 KO (single clones B4 and C5) GPC1/5 dKO (single clone F2) and associated GPC1/GPC5 overexpression were tested in all experiments. A. Representative Western blot analysis after digest with heparinase III to detect GPC1 or GPC5 via 3G10 antibody (in red) and tubulin loading control (in green). B. Quantification of heparan sulfate levels in FACS via cell surface staining with 10E4 antibody and secondary APC antibody. Relative HS levels of the different cell lines were normalized to wild-type (wt) cells for n = 5 and SD are shown. Statistical analysis via one-way Anova combined with Tukey's post hoc test (ns $p > 0,05$; * $p \leq 0,05$; ** $p \leq 0,01$; *** $p \leq 0,001$, **** $p \leq 0,0001$). C. Representative Western blot images for cell surface biotinylation experiments. Both inputs (I) and eluates (E) were loaded for the different cell lines. Overexpressed FGF2-GFP, induced via 24h incubation with 1 µg/ml doxycycline, was detected via anti-rabbit FGF2 antibody (in green) and anti-mouse GAPDH (in red) was used as endogenous loading control and cell integrity control. D. Quantification of FGF2-GFP secretion efficiency of the different cell lines via ratio between surface FGF2-GFP (eluate after streptavidin capture) and total FGF2-GFP expression levels (input) normalized to wild-type cells. Data for n = 4 experiments and SDs are shown. Statistical analysis via one-way Anova combined with Tukey's post hoc test (ns $p > 0,05$; * $p \leq 0,05$; ** $p \leq 0,01$; *** $p \leq 0,001$, **** $p \leq 0,0001$). Partially published in [51].

As mentioned previously, the enzymatic digest with heparinase III only gave an approximation of GPC1/5 levels on the cell surface. Alternatively, GPC1/5 mRNA levels were assessed via RT-qPCR as shown in Figure 7.

For RT-qPCR mRNA was extracted from HeLa S3 FGF2-GFP wt, GPC1/5 dKO and dKO + GPC1 or + GPC5 cells and reverse transcribed into cDNA. The cDNA was then amplified via Taqman™ RT PCR assays (Figure 7A., for details see 3.2.3) and DNA amplification was compared between cell lines. Both GPC1 and GPC5 were significantly reduced by more than 75% in GPC1/5 dKO cells (Figure 7B.). In overexpression cell lines mRNA levels for GPC1 and GPC5 exceeded wt levels by 9- and 5-fold, respectively. Also, this did not reflect protein amount on the cell surface though, as artificial overexpression can often induce intracellular protein aggregation, as has been observed for different bigger GPC1 fusion constructs (data not shown) and not all protein matures correctly and reaches the cell surface. Yet this offered an additional quantification method opposed to heparinase III digest.

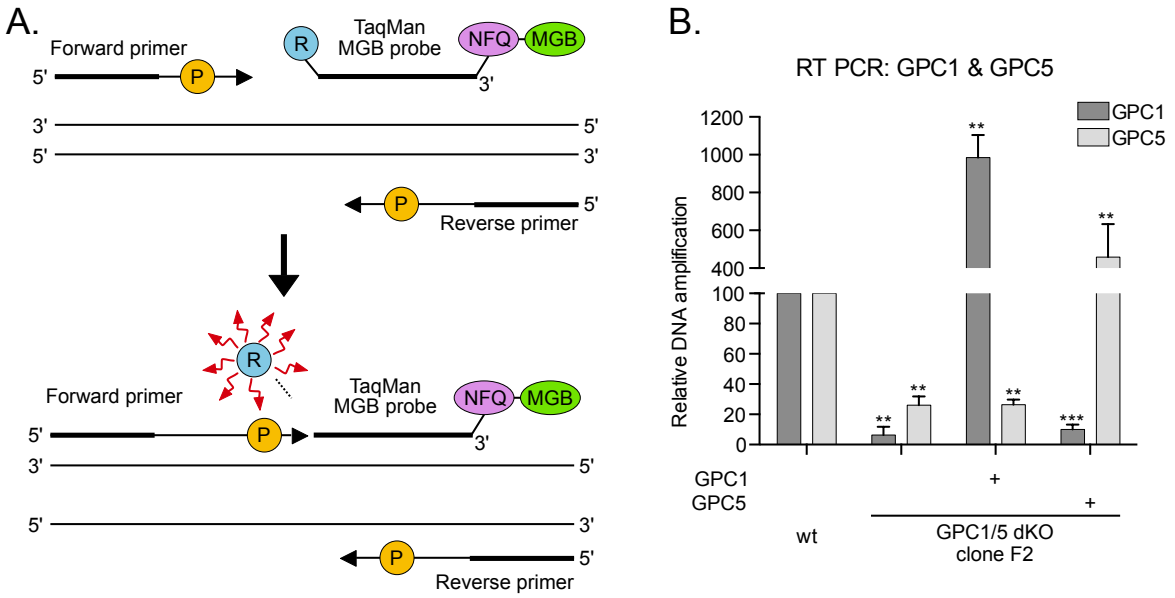

Figure 7: RT-qPCR of GPC1/5 mRNA levels. A. Working model for Taqman™ RT-qPCR from Thermo Fischer Scientific. Genomic RNA is extracted from cells and reserve transcribed into cDNA. Taqman™ RT-qPCR uses primers directed against the protein of interest and a Taqman™ probe containing a reporter dye (R), a non-fluorescent quencher (NFQ) and a minor groove binder (MGB) which binds to the cDNA. Upon binding of primers and chain extension by AmpliTaq gold polymerase (P) the reporter dye is cleaved off from the quencher and fluorescence correlates to DNA amplification. B. RT-qPCR was performed for HeLa S3 wt cells, GPC1/5 dKO and dKO + GPC1/GPC5 using Taqman™ assays directed against GPC1, GPC5 and GAPDH as housekeeping gene. Quantification from 3 experiments showed high increase of GPC1 and GPC5 RNA in overexpression conditions in relation to wt cells. Statistical analysis was performed via unpaired t-test with Welch's correction to wt conditions for the corresponding protein (ns $p > 0,05$; * $p \leq 0,05$; ** $p \leq 0,01$; *** $p \leq 0,001$, **** $p \leq 0,0001$).

4.1.2 GPC1 does not play a role in FGF2 endocytosis

FGF2 gets secreted from cells via direct translocation across the plasma membrane and then remains bound to HSPGs on the cell surface. GPC1 overexpressing cells contained more surface FGF2-GFP detected via biotinylation (Figure 6D.), whereas GPC1 KO reduced surface FGF2-GFP levels. To assess whether this was due to a secretion phenotype and not due to varied endocytosis, I performed

fluorescence microscopy endocytosis experiments with recombinant protein. In brief, HeLa S3 FGF2-GFP wt, GPC1 KO G4 and GPC1 KO G4 + GPC1 cells were cultivated without doxycycline and incubated with 5 µg/ml recombinant FGF2-GFP and 25 µg/ml transferrin coupled to AlexaFluor546® as control protein. Live cell imaging was performed for 20 min (data not shown, published in [51]) and experiments with incubation up to 1 h were performed in fixed cells (Figure 8).

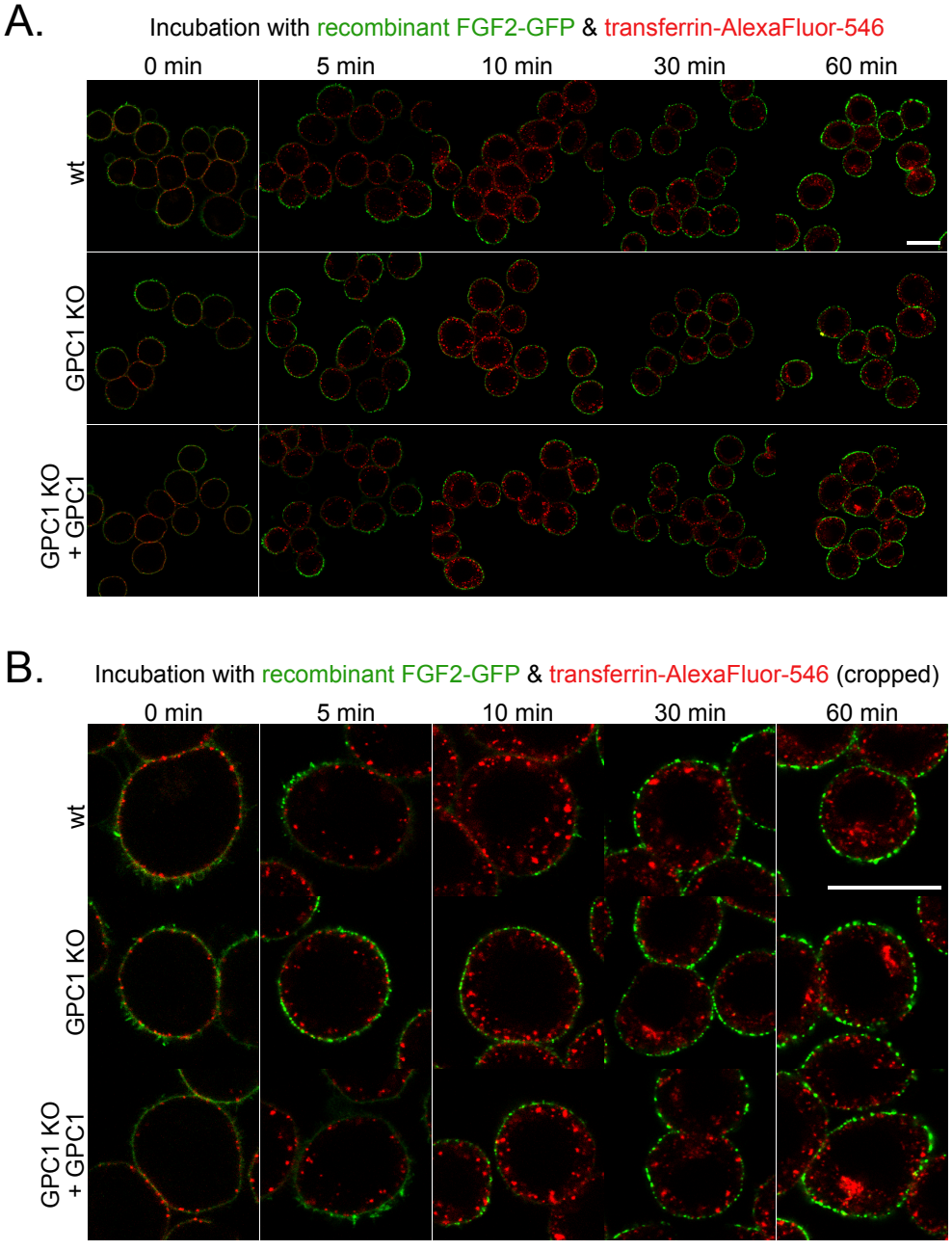

Figure 8: Endocytosis experiments showed no difference in FGF2-GFP uptake in GPC1 KO or overexpression conditions. HeLa S3 FGF2-GFP (no dox) wt, GPC1 KO clone D4 and GPC1 KO D4 + GPC1 cells were used for fluorescence microscopy experiments on a Zeiss LSM800 confocal microscope. Cells were incubated for the depicted timepoints with 5 µg/ml FGF2-GFP (in green) and transferrin-AlexaFluor546® (in red) before fixation with 4% PFA. Panel B. shows cropped images of A. Images at shorter incubation times were acquired with different settings, due to lower signal intensity. Scale bar 20 µm in both panels.

Iron-transporting transferrin functioned as control, as it binds to the transferrin receptor and complexes are internalized via clathrin-mediated endocytosis and subsequently localize to endosomes where the acidic pH liberates iron. Transferrin-receptor complexes are eventually degraded via endosome maturation into lysosomes or complexes are recycled to the cell surface [244].
As seen in Figure 8 FGF2-GFP bound broadly to the cell surface of cells, due to the abundant and long heparan sulfate chains bound to HSPGs at the cell surface, while transferrin localized in puncta along the membrane. While transferrin was readily endocytosed within 5 min, FGF2-GFP remained bound to the cell surface. Even after longer incubation up to 60 min FGF2-GFP was not endocytosed while transferrin accumulated intracellularly, presumably in endosomes. These experiments demonstrated that reduced FGF2-GFP levels on the cell surface in biotinylation were not due to varying endocytosis, but could be accounted for by the altered secretion in FGF2-GFP.

4.1.3 Glypican-1, FGF2 and the α1 subunit of the Na,K-ATPase are in proximity to each other in HeLa S3 cells

I demonstrated that GPC1 KO or overexpression greatly impacts FGF2-GFP secretion. GPC1 was also detected via a BioID screen as interaction partner of FGF2. To gain further insight into the interactions between FGF2, GPC1 and the α1 subunit of the Na,K-ATPase, I performed Duolink® proximity ligation assays (PLA) to probe for protein-protein distances within 40 nm. As GPC1 can only be detected via 3G10 or 10E4 antibody, which are directed against all heparan sulfate chain-containing proteins, GPC1 fusion constructs were cloned to enable specific antibody recognition of GPC1. Therefore, GPC1 was fused to small HA- or Flag-tags via oligo annealing and subcloning into GPC1 expression vectors and used for generation of stable cell lines in HeLa S3 FGF2-GFP wt (for details see 3.2.2.3), which were validated via heparinase III digests and Western blotting. A clear increase in GPC1 levels was observed (Figure 9A. and B.) both by eye and quantification following heparinase III digest and Western blot analysis. As seen in Figure 9C. and D. Flag- and HA-GPC1 fusion constructs were functional, as FGF2-GFP secretion was increased in cell surface biotinylation experiments to a similar extent as cell lines expressing untagged GPC1 (see Figure 6). GPC1 fusion constructs were expressed nicely on cell surfaces as seen in Figure 9E. The small Flag- or HA-tags did not interfere with proper protein maturation and transport to cell surfaces as no big intracellular aggregates were seen.

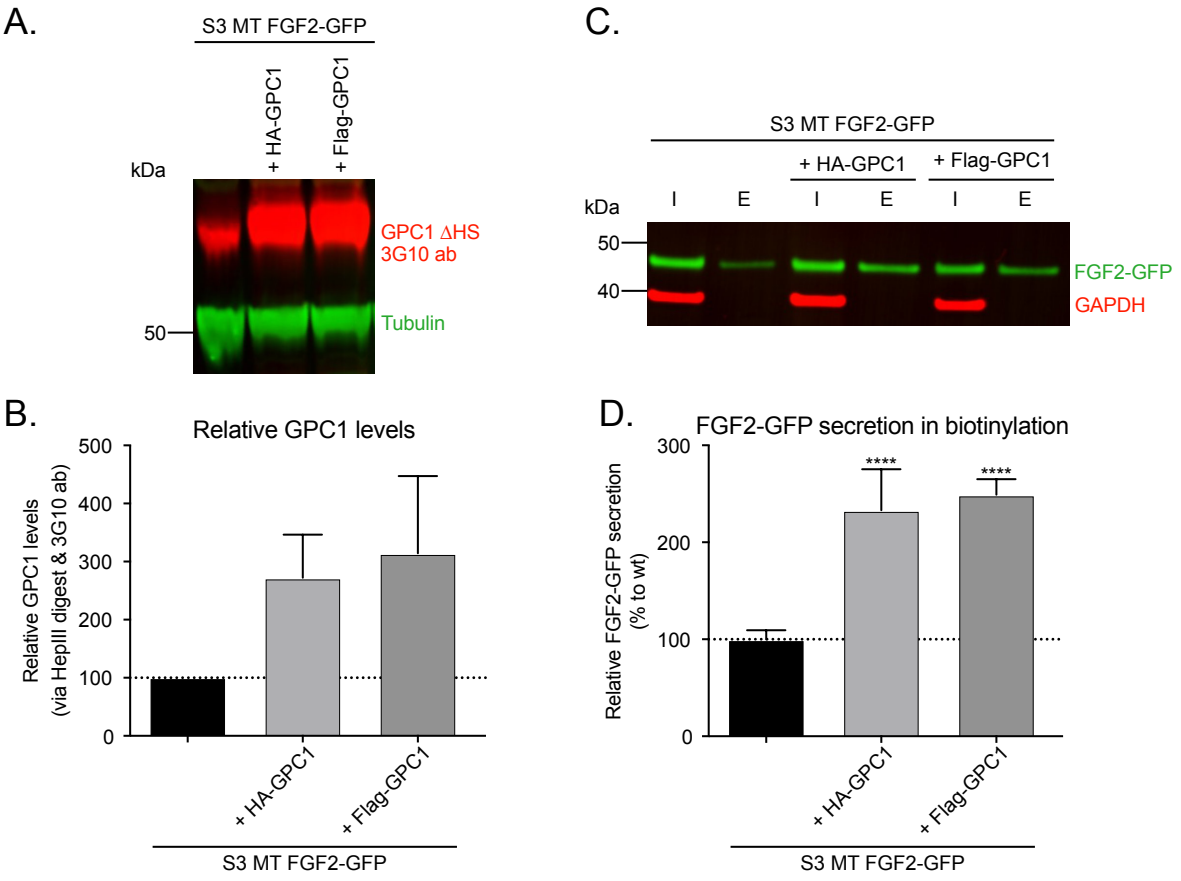
A.
S3 MT FGF2-GFP
+ HA-GPC1
+ Flag-GPC1
kDa
GPC1 ΔHS
3G10 ab
Tubulin
50
C.
S3 MT FGF2-GFP
+ HA-GPC1
+ Flag-GPC1
I
E
I
E
I
E
kDa
50
40
FGF2-GFP
GAPDH
B.
Relative GPC1 levels
Relative GPC1 levels
(via HepIII digest & 3G10 ab)
500
400
300
200
100
0
+ HA-GPC1
+ Flag-GPC1
S3 MT FGF2-GFP
D.
FGF2-GFP secretion in biotinylation
Relative FGF2-GFP secretion
(% to wt)
300
200
100
0
****
****
+ HA-GPC1
+ Flag-GPC1
S3 MT FGF2-GFP

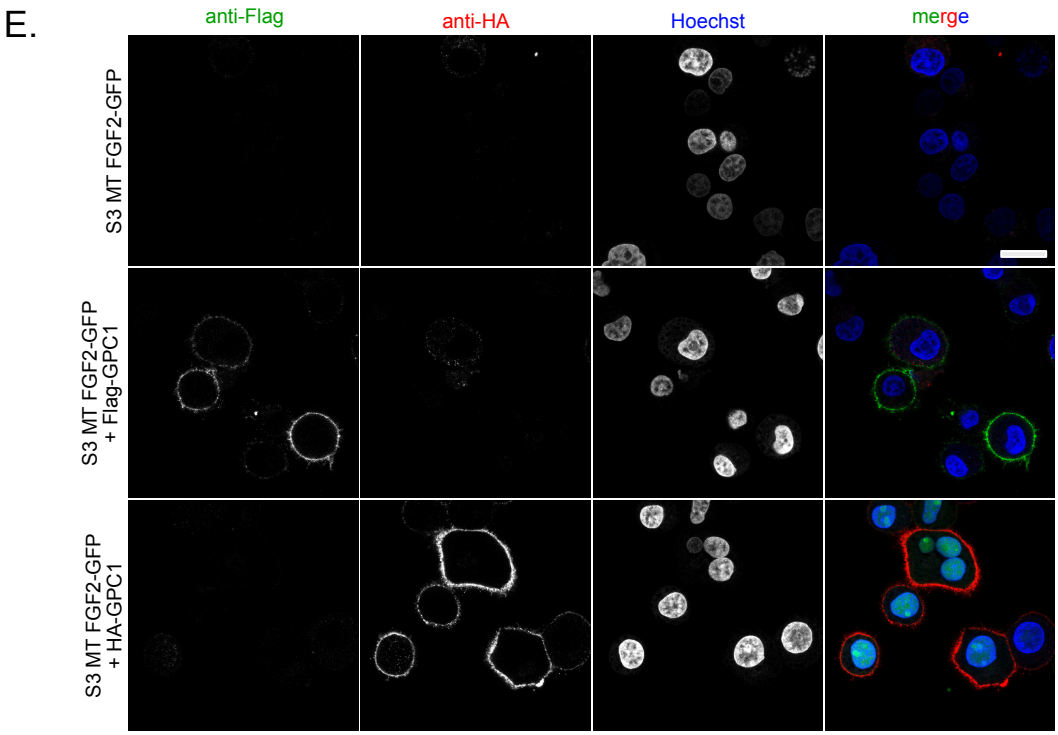
E.
anti-Flag
anti-HA
Hoechst
merge
S3 MT FGF2-GFP
S3 MT FGF2-GFP
+ Flag-GPC1
S3 MT FGF2-GFP
+ HA-GPC1

After cell line validation, Duolink® PLA experiments were conducted. For proximity ligation fixed and permeabilized cells were incubated with primary antibodies directed against the proteins of interest and subsequently incubated with anti-mouse and anti-rabbit plus and minus PLA DNA probes (see Figure 10A.). Ligation of both DNA strands when within 40 nm of each other resulted in incorporation of fluorescent probes and amplification of the signals.

Proximity between FGF2 and the α1 subunit of the Na,K-ATPase has been demonstrated before and this interaction was shown to decrease upon ouabain treatment, a known inhibitor of the Na,K-ATPase [118, 123]. For HeLa S3 FGF2-GFP wt cells overexpressing HA-GPC1 different experimental conditions were tested to examine GPC1 and α1 proximity, since it was of particular interest whether proximity events could be observed between two proteins on different sides of the membrane. S3 FGF2-GFP + HA-GPC1 cells were incubated with both anti-mouse α1 and anti-rabbit HA antibodies and single antibodies as controls. As seen in Figure 10B. the overall number of spots per cell in one focal plane was relatively low in HeLa S3 cells, despite overlapping α1 and HA signals in immunofluorescence staining (Figure 10D.). Yet proximity signals were clearly distinguishable from single antibody controls and cells not overexpressing HA-GPC1, where the antigen was missing (Figure 10C.). Overexpression of FGF2-GFP did not significantly alter proximity between α1 and HA-GPC1 (Figure 10C.), but might be explained by the fact that both are abundant (one even overexpressed) proteins, with the α1 subunit of the Na,K-ATPase having many different biological functions in cells. Potentially only a subpopulation might be involved in FGF2-GFP secretion, and stimulation of FGF2 secretion does not alter protein localization and proximity significantly at the plasma membrane.

Figure 9: S3 FGF2-GFP wt cells expressed HA-/Flag-tagged GPC1. Stable S3 FGF2-GFP cell lines overexpressing Flag-GPC1 or HA-GPC1 were generated and tested for functional protein expression. A. Representative Western blot analysis after digest with heparinase III to detect Flag-GPC1 or HA-GPC1 via 3G10 antibody (in red) and tubulin loading control (in green). B. Quantification of GPC1 levels after heparinase III digest from 3 experiments showing SD. C. Representative Western blot image for cell surface biotinylation experiments. Both inputs (I) and eluates (E) were loaded for the different cell lines. Overexpressed FGF2-GFP, induced via 24h incubation with 1 µg/ml doxycycline, was detected via anti-rabbit FGF2 antibody (in green) and anti-mouse GAPDH (in red) was used as endogenous loading control and cell integrity control. D. Quantification of FGF2-GFP secretion efficiency of the different cell lines via ratio between surface FGF2-GFP (eluate after streptavidin capture) and total FGF2-GFP expression levels (input) normalized to wild-type cells. Data for n = 3 experiments and SDs are shown. Statistical analysis via one-way Anova combined with Tukey's post hoc test (ns $p > 0,05$; * $p \leq 0,05$; ** $p \leq 0,01$; *** $p \leq 0,001$, **** $p \leq 0,0001$). E. Immunofluorescence images taken using a Zeiss LSM800 confocal microscope. Cell lines were stained with anti-mouse Flag (in green), anti-rabbit HA (in red) and Hoechst (in blue, nuclei). Scale bar 20 µm.

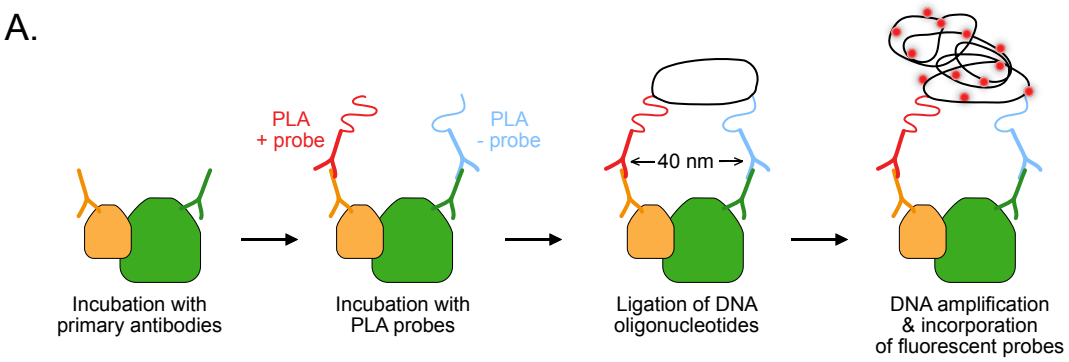
A.
PLA
+ probe
PLA
- probe
40 nm
Incubation with
primary antibodies
Incubation with
PLA probes
Ligation of DNA
oligonucleotides
DNA amplification
& incorporation
of fluorescent probes

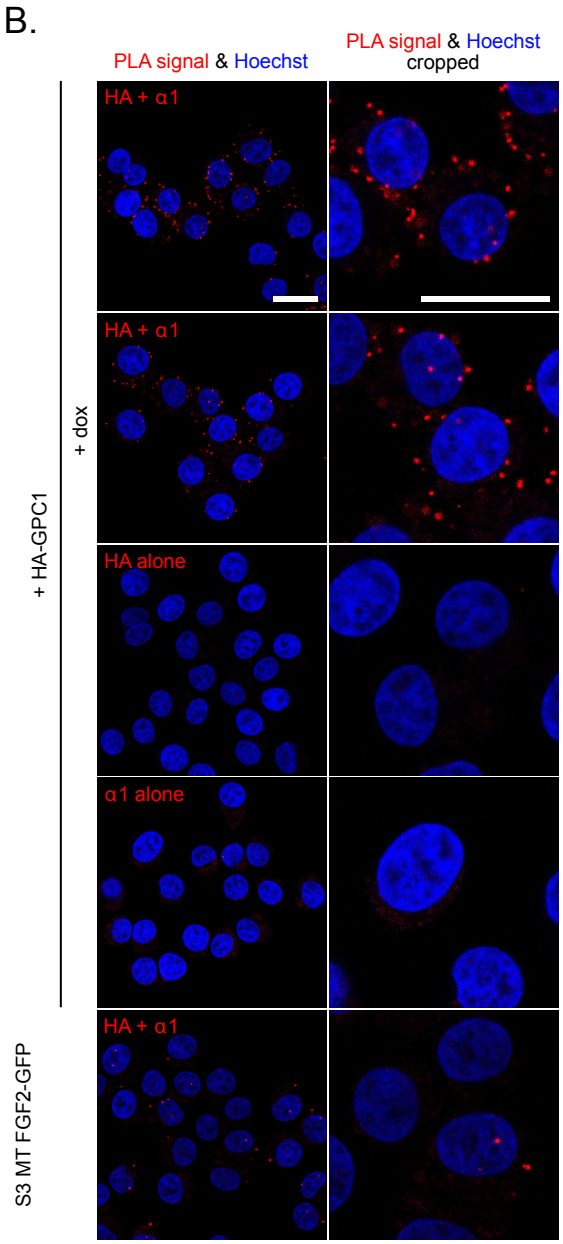
B.
PLA signal & Hoechst
PLA signal & Hoechst
cropped
HA + α1
HA + α1
HA alone
α1 alone
HA + α1
+ dox
+ HA-GPC1
S3 MT FGF2-GFP

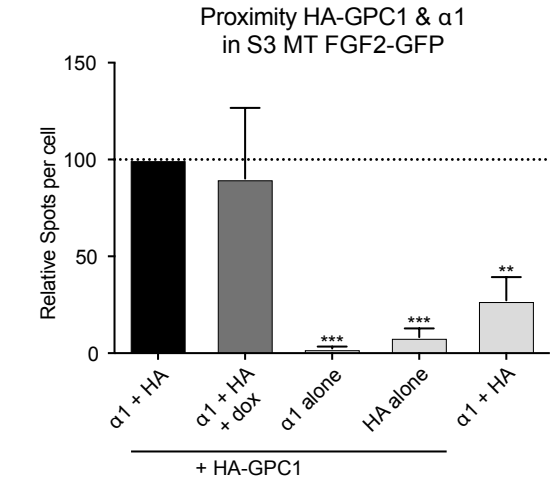
C.
Proximity HA-GPC1 & α1
in S3 MT FGF2-GFP
Relative Spots per cell
150
100
50
0
***
***
**
α1 + HA
α1 + HA
+ dox
α1 alone
HA alone
α1 + HA
+ HA-GPC1

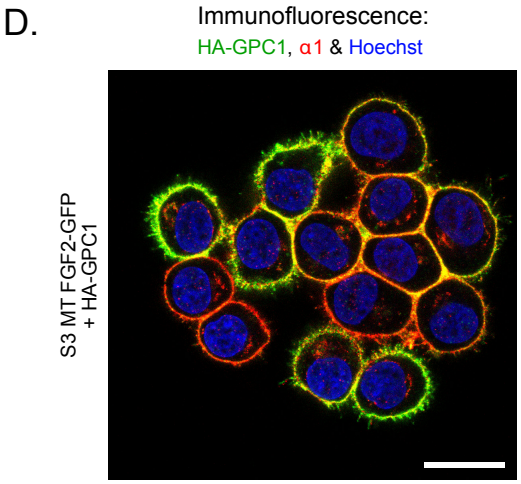
D.
Immunofluorescence:
HA-GPC1, α1 & Hoechst
S3 MT FGF2-GFP
+ HA-GPC1

Likewise, HeLa S3 FGF2-GFP wt cells overexpressing Flag-GPC1 were tested for proximity between Flag-GPC1 and α1 (Figure 11).

Proximity event abundance seen in Figure 11A. did not alter much from results seen before for HA-GPC1. In contrast to the previous experiment, the usage of both Flag and α1 antibodies in wt cells not expressing Flag-GPC1 led to higher background signals relative to control conditions. Also, here overexpression of FGF2-GFP did not significantly alter proximity between Flag-GPC1 and α1 (Figure 11B.) It's also worth mentioning that α1 immunofluorescence staining for the rabbit α1 antibody looked different from beforehand used mouse α1 antibody. The mouse monoclonal antibody showed almost exclusive membrane staining while the rabbit antibody showed higher intracellular signal.

Figure 10: HA-GPC1 and α1 showed proximity in HeLa S3 FGF2-GFP cells. A. Working model for Duolink ® proximity ligation assay. Fixed cells were incubated with primary antibodies directed two proteins of interest and PLA plus and minus DNA probes. When epitopes are within 40 nm of each other DNA probes were ligated. Afterwards fluorescent probes were incorporated and signals were amplified via polymerase reaction. B. Representative images showing PLA signal (in red) and Hoechst nucleus staining (in blue) for wt + HA-GPC1 cells using anti-rabbit HA antibody and anti-mouse α1 antibody. Single antibody samples and cells not expressing HA-GPC1 incubated with both antibodies were used as control. C. Quantification of relative dots per cell per condition normalized to S3 FGF2-GFP wt + HA-GPC1 conditions for 3 experiments + SDs. Statistical analysis via one-way Anova combined with Tukey's post hoc test (ns $p > 0,05$; * $p \leq 0,05$; ** $p \leq 0,01$; *** $p \leq 0,001$, **** $p \leq 0,0001$). D. Control immunofluorescence image showing antibody staining for HA-GPC1 (in green) and α1 (in red) together with Hoechst nucleus staining (in blue). Scale bar in all Zeiss LSM800 microscope images 20 µm.

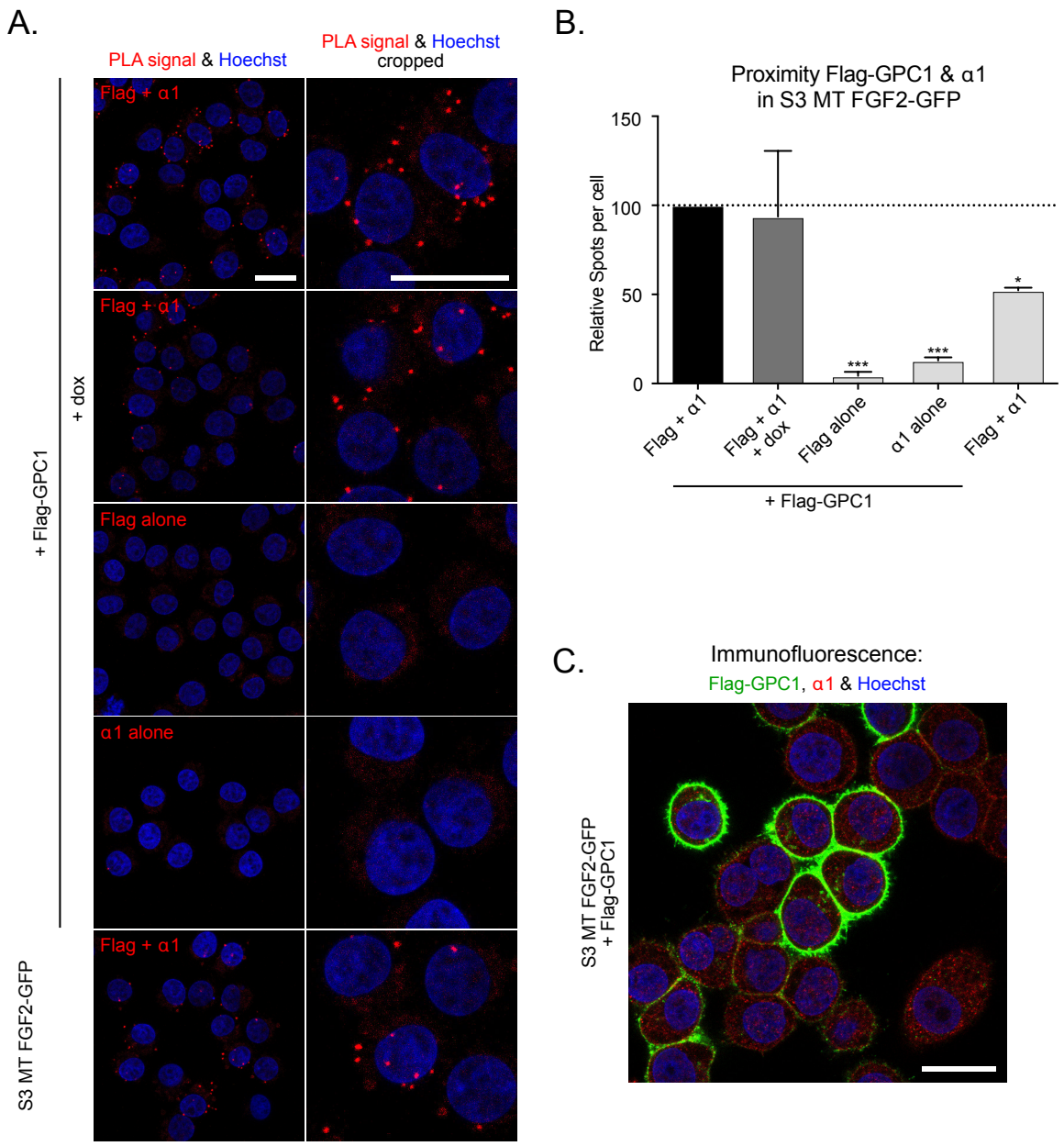

Figure 11: Flag-GPC1 and α1 showed proximity in HeLa S3 FGF2-GFP cells. A. Representative images showing PLA signal (in red) and Hoechst nucleus staining (in blue) for wt + Flag-GPC1 cells using anti-mouse flag antibody and anti-rabbit α1 antibody. Single antibody samples and cells not expressing Flag-GPC1 incubated with both antibodies were used as control. B. Quantification of relative dots per cell per condition normalized to S3 FGF2-GFP wt + Flag-GPC1 conditions for 3 experiments + SDs. Statistical analysis via one-way Anova combined with Tukey's post hoc test (ns $p > 0,05$; * $p \leq 0,05$; ** $p \leq 0,01$; *** $p \leq 0,001$, **** $p \leq 0,0001$). C. Control immunofluorescence image showing antibody staining for Flag-GPC1 (in green) and α1 (in red) together with Hoechst nucleus staining (in blue). Scale bar in all Zeiss LSM800 microscope images 20 µm.

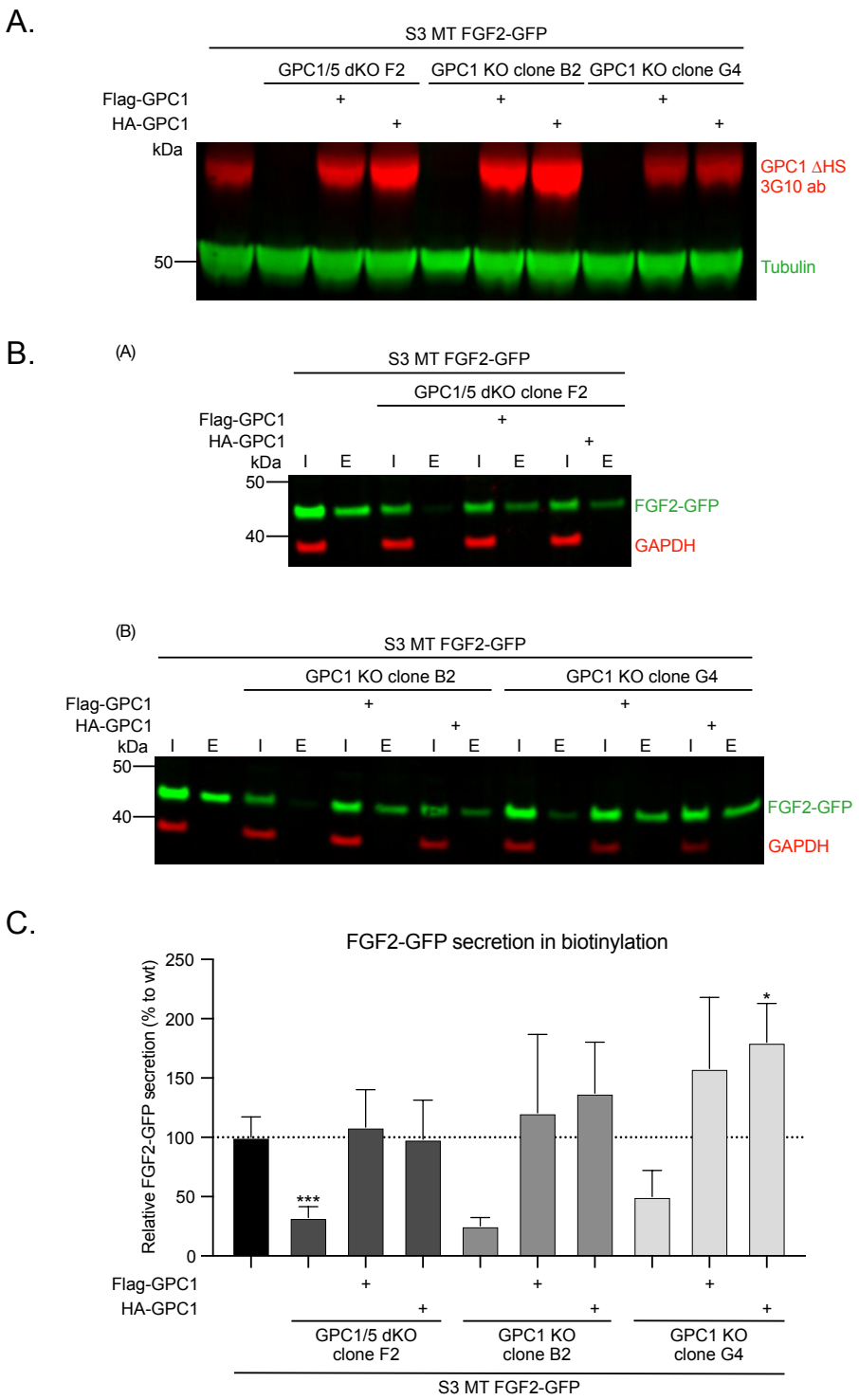

Figure 12: HA-/Flag-tagged GPC1 was expressed in HeLa S3 FGF2-GFP GPC1 KO or GPC1/5 dKO cells. Stable S3 FGF2-GFP cell lines overexpressing Flag-GPC1 or HA-GPC1 in a GPC1 KO or GPC1/5 dKO background were generated and tested for functional protein expression. A. Representative Western blot analysis after digest with heparinase III to detect Flag-GPC1 or HA-GPC1 via 3G10 antibody (in red) and tubulin loading control (in green). B. (A) and (B) Representative Western blot image for cell surface biotinylation experiments using dKO and GPC1 KO cell lines respectively. Both inputs (I) and eluates (E) were loaded for the different cell lines and FGF2-GFP overexpression induced via 24h incubation with 1 µg/ml doxycycline. FGF2-GFP was detected via anti-rabbit FGF2 antibody (in green) and anti-mouse GAPDH (in red) was used as endogenous loading control and cell integrity control. C. Quantification of FGF2-GFP secretion efficiency of the different cell lines via ratio between surface FGF2-GFP (eluate after streptavidin capture) and total FGF2-GFP expression levels (input) normalized to wild-type cells. Data for n = 4 experiments and SDs are shown. Statistical analysis via one-way Anova combined with Tukey's post hoc test (ns $p > 0,05$; * $p \leq 0,05$; ** $p \leq 0,01$; *** $p \leq 0,001$, **** $p \leq 0,0001$).

Since overexpression of HA- or Flag-GPC1 in S3 FGF2-GFP wt cells on top of endogenous GPC1 might mask effects caused by FGF2-GFP overexpression due to competition of endogenous GPC1 with tagged GPC1 forms, experiments were conducted with cell lines devoid of endogenous GPC1. I therefore stably overexpressed Flag-GPC1 and HA-GPC1 in the previously characterized GPC1 KO single clones B2 and G4. To exclude potential effects of GPC5, also GPC1/5 dKO clone F2 was used. Cell lines and GPC1 overexpression were validated via heparinase III digest and Western blotting (Figure 12A.). As seen in Figure 12B. and C. overexpression of HA- or Flag-GPC1 in GPC1 KO or dKO background rescued the secretion phenotype observed before and FGF2-GFP secretion was increased back to or above wt levels showing GPC1 protein functionality.

HA-GPC1 overexpressing cell lines were used for PLA experiments. First, proximity between FGF2 and α1 in wt S3 FGF2-GFP cells was tested, as this had only been published for normal HeLa cells previously [118, 123]. For better understanding, both absolute dots/cell and relative dots/cell normalized to positive conditions are shown in Figure 13A. subpanels (A) and (B). Proximity was detected between α1 and FGF2-GFP in S3 wt cells significantly differing from single antibody controls. Furthermore, GPC1/5 dKO clone F2 and GPC1 KO clones B2 and G4 also showed proximity between α1 and FGF2-GFP (Figure 13B.-D.). Overexpression of HA-GPC1 in these KO cell lines lead to a slight increase of proximity between α1 and FGF2-GFP, yet this effect was not significant. Duolink® data for HeLa S3 were collected via quantification of dots within the focus plane of the nucleus and not throughout the entire cell volume. Low signal number might therefore lead to misinterpretation and underestimation of proximity events.

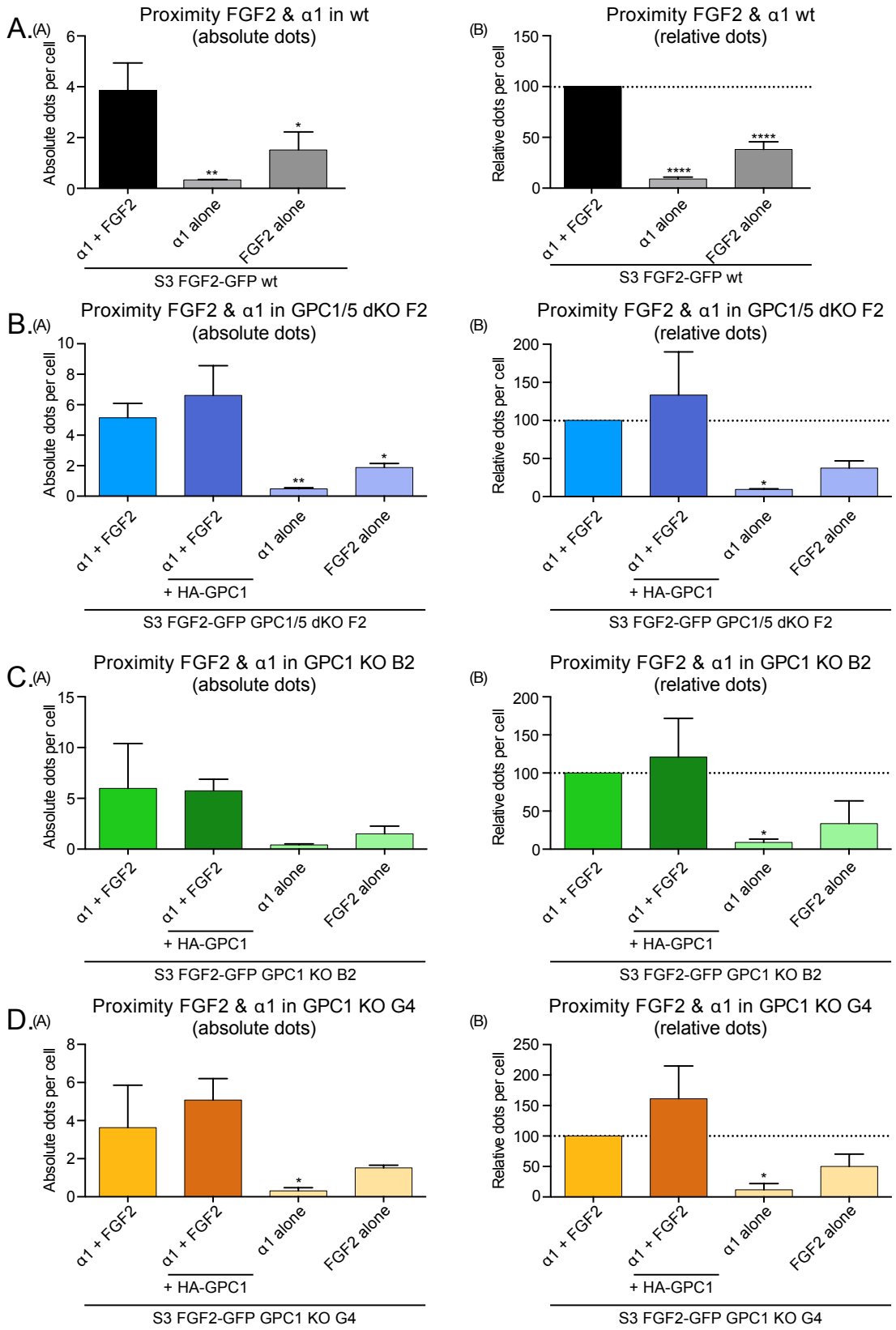

Figure 13: Proximity between FGF2-GFP and α1 in S3 FGF2-GFP wt, GPC1/5 dKO and GPC1 KO cell lines. Proximity between α1 and FGF2-GFP was tested via anti-rabbit FGF2 and anti-mouse α1 antibodies in all experimental setups in cells incubated with doxycycline to induce FGF2-GFP expression. Both absolute dots/cell and relative dots/cell normalized to control condition are shown for all panels in subpanels (A) and (B) respectively. A. S3 FGF2-GFP wt cells. B. S3 FGF2-GFP GPC1/5 dKO F2 background cells. C. S3 FGF2-GFP GPC1 KO B2 background cells. D. S3 FGF2-GFP GPC1 KO G4 background cells. Quantifications were performed for n = 3 experiments and statistical analysis was performed via one-way Anova combined with Tukey's post hoc test (ns $p > 0,05$; * $p \leq 0,05$; ** $p \leq 0,01$; *** $p \leq 0,001$, **** $p \leq 0,0001$).

Furthermore, proximity between FGF2 and GPC1 was assed using the HA-GPC1 overexpressing cell lines mentioned previously. Proximity between FGF2-GFP and HA-GPC1 could be observed in S3 FGF2-GFP GPC1/5 dKO F2, GPC1 KO B2 and GPC1 KO G4 cell lines and was significantly different from controls (Figure 14).

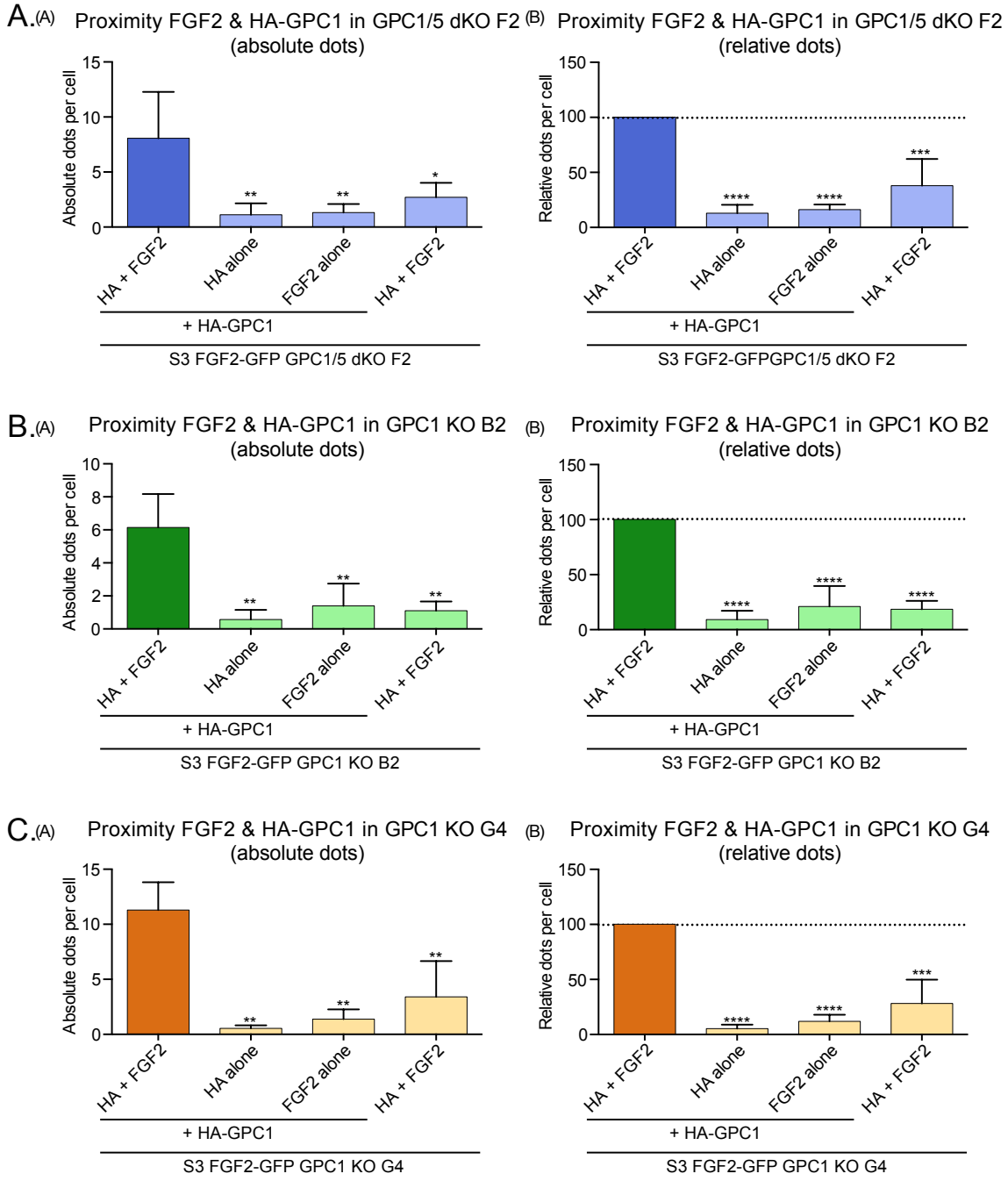

Figure 14: HA-GPC1 and FGF2-GFP showed proximity in PLA experiments. Proximity between HA-GPC1 and FGF2-GFP was tested via anti-mouse FGF2 and anti-rabbit HA antibodies in all experimental setups in cells incubated with doxycycline to induce FGF2-GFP expression. Both absolute dots/cell and relative dots/cell normalized to control condition are shown for all panels in subpanels (A) and (B) respectively A. S3 FGF2-GFP GPC1/5 dKO F2 background cells. B. S3 FGF2-GFP GPC1 KO B2 background cells. C. S3 FGF2-GFP GPC1 KO G4 background cells. Quantifications were performed for n= 4 (for GPC1/5 dKO) or n = 3 (GPC1 KOs B2 and G4) experiments and statistical analysis was performed via one-way Anova combined with Tukey's post hoc test (ns $p > 0,05$; * $p \leq 0,05$; ** $p \leq 0,01$; *** $p \leq 0,001$, **** $p \leq 0,0001$).

Slightly more absolute proximity events were detected between FGF2-GFP and HA-GPC1 compared to FGF2-GFP and α1. Once again this could be due to α1 being involved in many other cellular processes independent of FGF2 secretion and due to HA-GPC1 overexpression.

Experiments testing proximity between intracellular α1 and cell surface HA-GPC1 were repeated in these new cell lines expressing HA-GPC1 in GPC1 KO backgrounds, avoiding competition effects with endogenous GPC1. As seen in Figure 15, proximity between α1 and HA-GPC1 was not increased, but even decreased slightly in conditions were FGF2-GFP was overexpressed. This did not contradict experiments in Figure 10 and Figure 11, where HA- or Flag-GPC1 was overexpressed on top of endogenous GPC1 and FGF2-GFP expression did not significantly alter proximity. Additionally, cadherin (CDH), another abundant plasma membrane protein, was used as a control in these experiments. Proximity between HA-GPC1 and CDH could be detected but was in the range of control conditions were α1 and HA antibodies were used in cells not expressing any HA-GPC1 for dKO F2 and GPC1 KO B2 (Figure 15A. and B.). This demonstrated that proximity between α1 and GPC1 was not due to mere protein abundance, but rather hinted to specific interaction between α1 and GPC1 and localization to similar membrane areas.

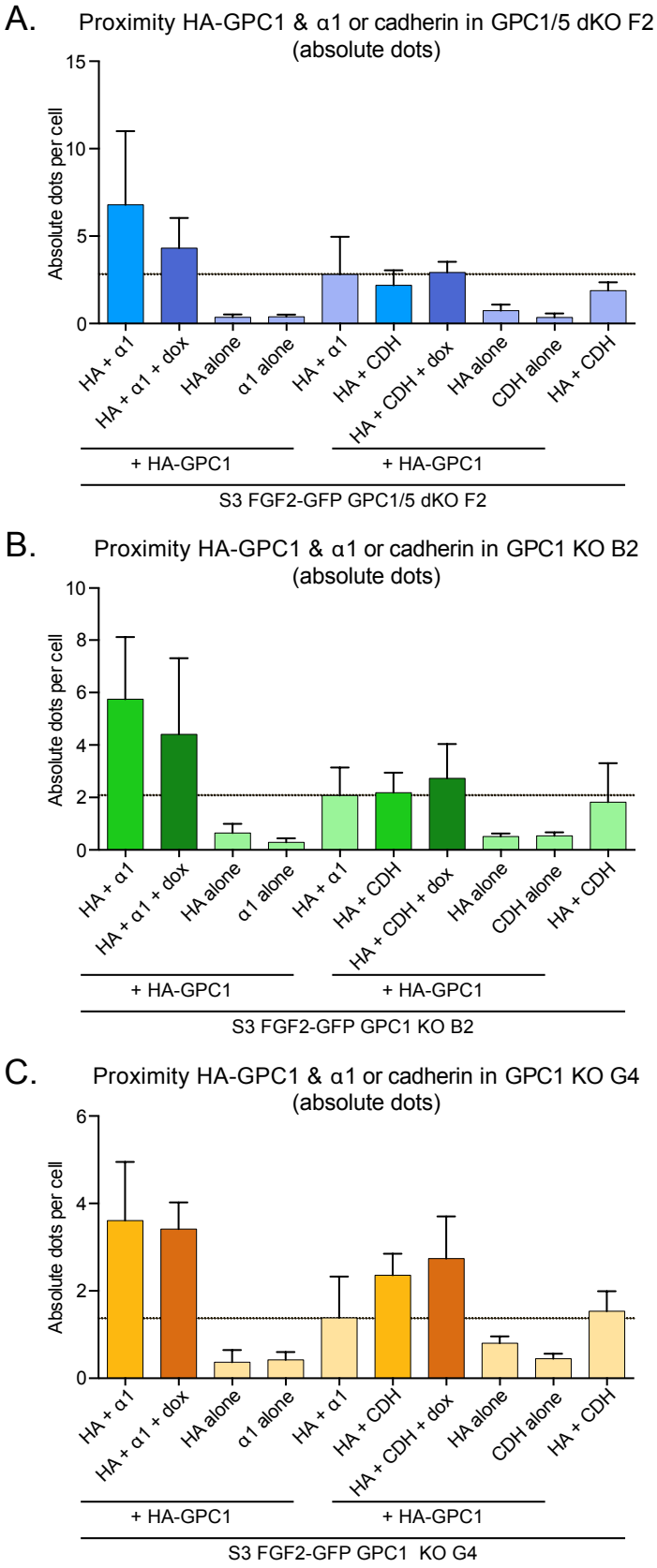

Figure 15: Proximity between α1 and HA-GPC1 differed from proximity of HA-GPC1 with cadherin. HA-GPC1 and α1 proximity or HA-GPC1 and cadherin (CHD) proximity was assessed in PLA experiments. Antibodies used were anti-mouse α1, anti-rabbit HA and anti-mouse CDH. Absolute dots/cell are shown for all KO and HA-GPC1 expressing cell lines and antibody combinations. A. S3 FGF2-GFP GPC1/5 dKO F2 background cells. B. S3 FGF2-GFP GPC1 KO B2 background cells. C. S3 FGF2-GFP GPC1 KO G4 background cells. Quantifications were performed for n = 3 or 4 experiments.

4.1.4 HA-GPC1 expression levels can be correlated to FGF2-GFP secretion

Since HA-GPC1 expressing cell lines proved as valuable tool and allowed to detect GPC1 more quantitatively via specific antibody recognition, follow up experiments were conducted together with Roberto Saleppico, another PhD student in our lab, to correlate HA-GPC1 expression levels to FGF2-GFP secretion efficiency (Figure 16). Therefore, we sorted CHO K1 FGF2-GFP cells into single clones and selected 9 clones with different HA-GPC1 expression levels. I quantified expression levels both via heparinase III digest and Western blotting (Figure 16A. and B.) or via direct quantification of surface HA-GPC1 via HA antibody staining in FACS (Figure 16C). The HA antibody was not able to recognize the single HA-tag in Western blot. These data were compared to FGF2-GFP secretion efficiencies quantified via total internal reflection fluorescence (TIRF) translocation experiments using membrane-impermeable GFP nanobodies (established in [128], for details see 3.2.5.3) performed by Roberto. TIRF microscopy allows for the detection of fluorescent events near the plasma membrane by generation of an evanescent wave that only penetrates the cell to a depth of around 100 nm [245].

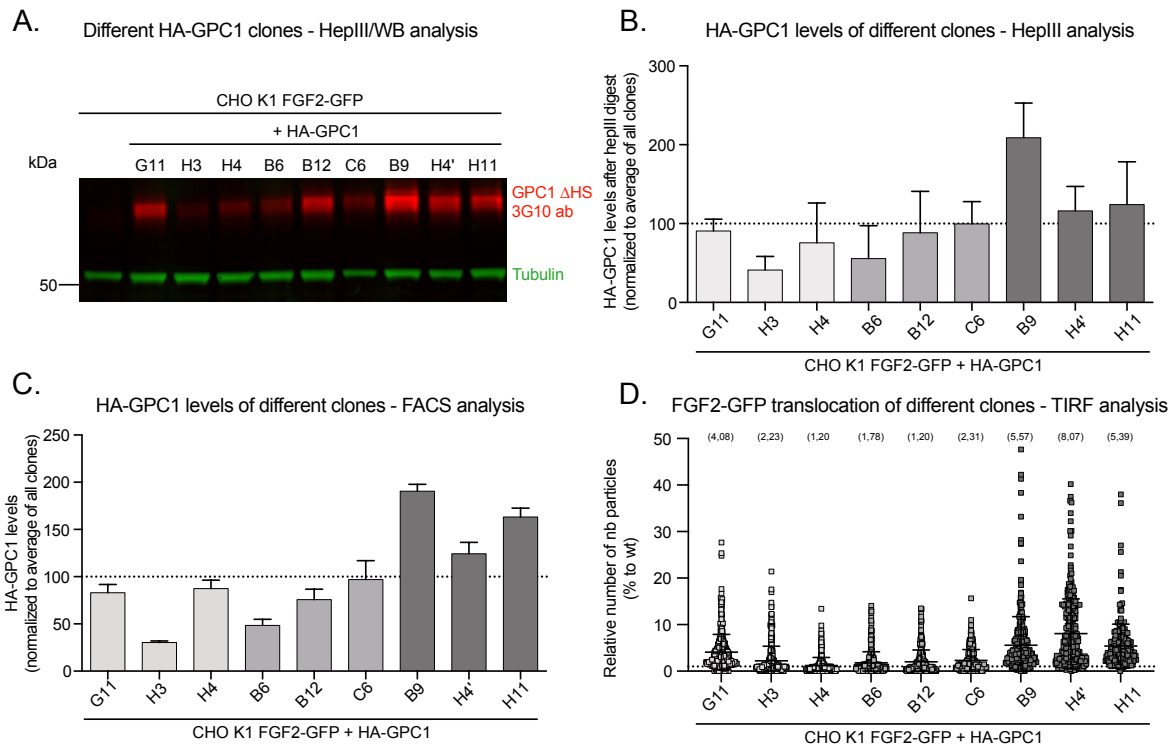

Figure 16: HA-GPC1 levels were correlated to FGF2-GFP secretion efficiency. Nine CHO K1 FGF2-GPC1 + HA-GPC1 single clones containing different HA-GPC1 levels were used in these experiments. A. Representative Western blot analysis after digest with heparinase III to detect HA-GPC1 via 3G10 antibody (in red) and tubulin loading control (in green). B. Quantification of relative HA-GPC1 levels of the different single clones normalized to the average of all HA-GPC1 expressing cell lines for n = 5 experiments showing averages and SDs. C. FACS quantification using anti-rabbit HA antibody to directly detect surface HA-GPC1 of the different clones in n = 4 experiments showing SDs. Levels were normalized to average HA-GPC1 levels from all cell lines. D. FGF2-GFP secretion efficiency analyzed via TIRF translocation experiments using membrane-impermeable GFP nanobodies to detect surface FGF2-GFP in the presence of doxycycline. Secretion efficiencies were normalized to wt cells not overexpressing GPC1 for n = 4 experiments with SDs.

As seen in Figure 16 both Western blot analysis via 3G10 antibody and FACS analysis using HA antibody resulted in similar HA-GFP expression levels for the different clones when normalized to the average HA-GPC1 level of all clones. This normalization style was selected due to lack of HA antibody binding to wt cells in FACS. Clones selected with lower and medium HA-GPC1 levels resulted in having similar expression levels in the end, yet in both assays clones H3 and B6 had the lowest expression levels. Roberto performed TIRF translocation experiments in the presence of doxycycline were single FGF2-GFP secretion events were visualized via incubation with membrane-impermeable GFP nanobodies binding to surface FGF2-GFP. Single translocation events were quantified via trackmate plugin in Fiji [238]. Since he only imaged FGF2-GFP and not HA-GPC1 levels, data were normalized to wt cells only for this experiment. FGF2-GFP secretion efficiencies correlated to HA-GPC1 levels for most clones. Clones B9, H4' and H11 with the highest HA-GPC1 levels also showed highest FGF2 secretion relative to wt cells. On average these cells had 5 – 8 times more FGF2-GFP on their cell surfaces. It's worth mentioning that single cells even showed an increase of FGF2-GFP secretion up to almost 50-fold. Even though sorted and originating always from a single clone, cells showed large heterogeneity regarding FGF2-GFP secretion which could have been caused due to different growth or signaling conditions of the cells.

4.1.5 Both GPC1 and GPC6 impact FGF2-GFP secretion in U2OS cells

As stated previously, HeLa cells only endogenously express GPC1 and GPC5 (and minor neglectable GPC2) from the glypican protein family according to gene expression data bases (see Expression Atlas-EMBL-EBI). Carola Sparn, a former PhD student of our laboratory also working on GPC1, stably overexpressed all other glypican family members in HeLa S3 FGF2-GFP and also performed *in vitro* experiments with purified glypicans to test their binding to FGF2 via biolayer interferometry (BLI). She could show that not only GPC1 but also all other glypicans belonging to the same subfamily (GPC2, GPC4, GPC6) could rescue FGF2-GFP secretion in a GPC1 KO background back to wt levels, yet did not increase secretion as GPC1 overexpression did [51]. This effect was strongest for GPC6, which also bound to FGF2 as purified protein in BLI experiments. At this point I had started to also work with U2OS cells, a human osteosarcoma cell line. They offer the advantage of being very flat cells well-suitable for microscopy, yet are human cells in contrast to hamster CHO cells. To our surprise, U2OS cells expressed mostly GPC1, GPC4 and GPC6 according to expression data. Therefore, I sought to examine the role of both GPC1 and GPC6 in U2OS cells.
First, I generated a stable U2OS cell line expressing FGF2-GFP in a doxycycline-dependent manner too be able to analyze GPC1/GPC6 impact on FGF2 secretion later via cell surface biotinylation experiments. These new cells were compared to HeLa S3 FGF2-GFP cells mostly used in the laboratory and HeLa FGF2-GFP cells used several years ago.

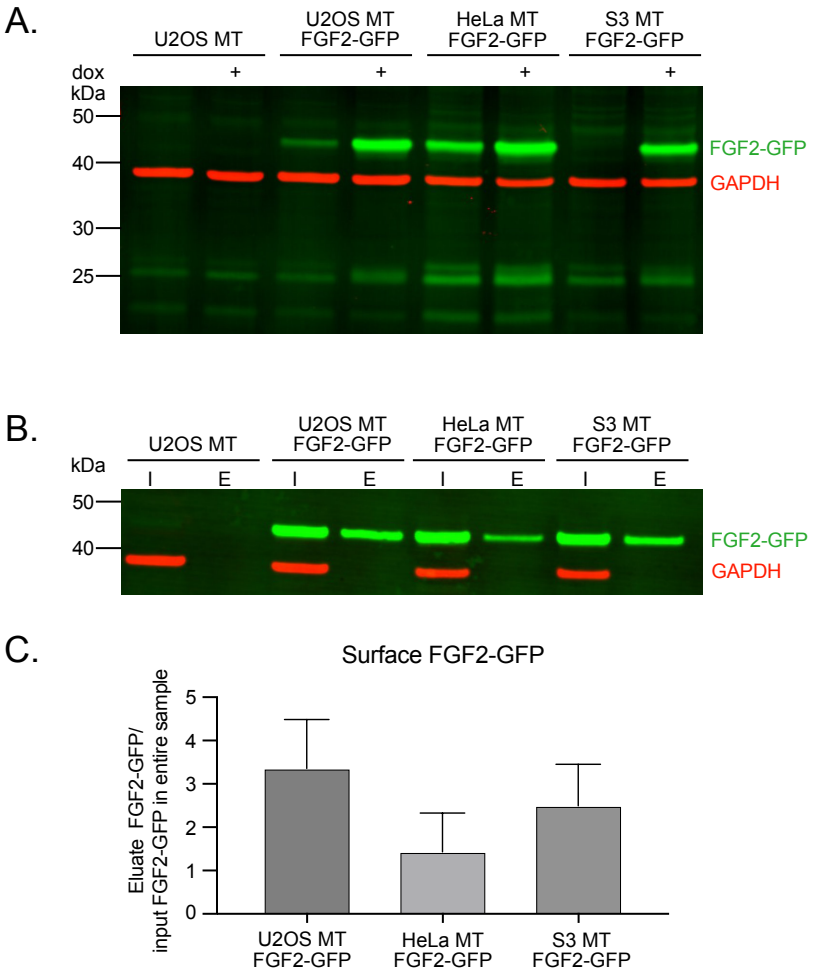

Figure 17: U2OS stably expressed FGF2-GFP in a doxycycline dependent manner. U2OS, U2OS FGF2-GFP, HeLa FGF2-GFP and HeLa S3 FGF2-GFP cell lines were tested for their responsiveness to doxycycline. A. Representative Western blot showing leakiness of the dox-responsive promoter in all cell lines. FGF2-GFP was detected in cell lysates via anti rabbit FGF2 antibody (in green) and GAPDH (in red) served as loading control. B. Western blot showing cell surface biotinylation experiments for cells treated for 24h with 1 µg/ml doxycycline. Both inputs (I) and eluates (E) from all cell lines were loaded. FGF2-GFP was again detected via anti-rabbit FGF2 antibody (in green) and GAPDH (in red) served as loading control and control for cell integrity. C. Quantification from 3 biotinylation experiments showing average % of surface FGF2-GFP in relation to total FGF2-GFP with SDs.

As seen in Figure 17A. empty U2OS cells did not express FGF2-GFP upon addition of doxycycline in contrast to pooled U2OS FGF2-GFP wt cells that went through three FACS sort rounds to select for responsiveness to doxycycline (bright sort + dox, dark sort – dox, bright sort + dox). HeLa S3 FGF2-GFP cell showed no FGF2-GFP expression in absence of doxycycline, while normal HeLa FGF2-GFP cells showed high leakiness (~ 30%) of the promoter. New U2OS FGF2-GFP cells only showed around 5% leakiness in the absence of doxycycline and were therefore suitable to perform biotinylation experiments. On average U2OS cells were slightly more efficient in secreting FGF2-GFP having around 3,4% of total FGF2-GFP on the cell surface, while S3 cells had around 2,5% (Figure 17B. and C.).
U2OS FGF2-GFP expressing cells were also validated via immunofluorescence microscopy detecting FGF2-GFP expression via GFP fluorescence or FGF2 antibody staining (Figure 18).

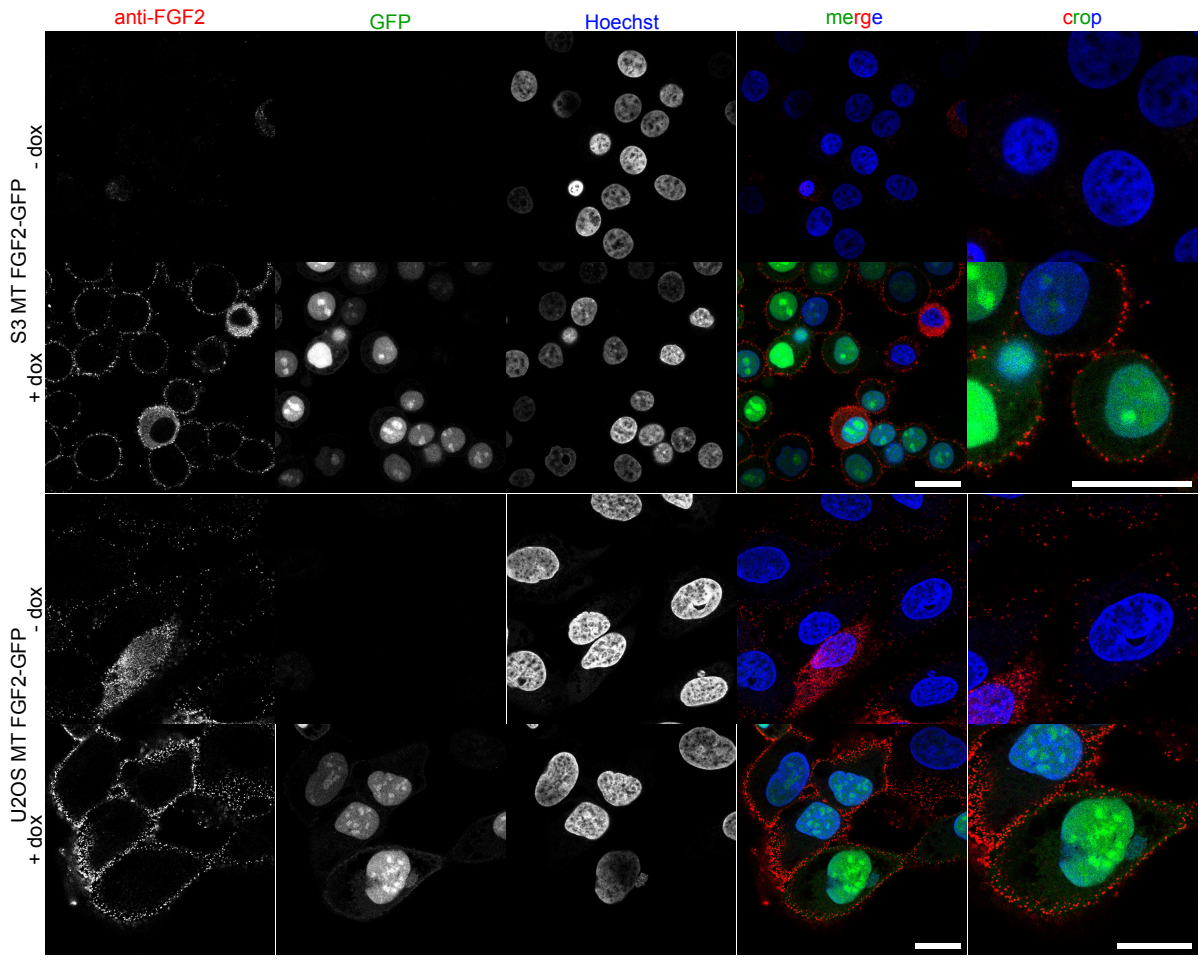

Figure 18: U2OS FGF2-GFP tested in immunofluorescence microscopy were responsive to doxycycline addition. U2OS FGF2-GFP and HeLa S3 FGF2-GFP cells were tested in IF via confocal microscopy using a Zeiss LSM800 microscope. Cells were incubated 24h with or without doxycycline to induce FGF2-GFP expression. Expression was tested after fixation (no permeabilization) via antibody staining with anti-rabbit FGF2 antibody (in red) or GFP fluorescence signal (in green). Nuclei were stained with Hoechst (in blue). Scale bar represents 20 µm in both merged and cropped images for both cell lines.

As seen in Figure 18 FGF2-GFP expression in HeLa S3 cells was not detectable via GFP fluorescence in conditions without doxycycline and FGF2 antibody staining only gave a very weak background signal. U2OS FGF2-GFP cells responded well to doxycycline as FGF2 expression was only detectable by GFP fluorescence in conditions using doxycycline. FGF2 antibody signal gave greater background signals in U2OS in -dox conditions though, reflecting the leakiness observed before in cell lysates (see Figure 17A.). Nonetheless this property might render useful, as U2OS cells could be used for TIRF recruitment experiments were FGF2-GFP membrane recruitment is observed in conditions without doxycycline to visualize single events. Cells were fixed with 4% PFA but not permeabilized in these experiments, explaining the localization of FGF2 antibody signal at the membrane. As the studied 18 kDa LMW form of FGF2 has a C-terminal NLS sequence, the highest GFP signals were observed in the nucleus. These images also show the apparent size difference between S3 and U2OS cells with U2OS being much bigger and having a more spread morphology. S3 cells are round and small in size, with a very big portion of the cytoplasm occupied by the nucleus.

Furthermore, U2OS FGF2-GFP cells were used to generate GPC1 KO cell lines via CRISPR-Cas9. I therefore used the previously tested and well working CRISPR-Cas9 GPC1-gRNA from Sabine Wegehingel. Three GPC1 KO clones (D4, D8 and E3) were selected via genomic DNA sequencing and Western blot analysis after heparinase III digest (Figure 19A.). Cell surface biotinylation experiments revealed a decrease in FGF2-GFP secretion by ~ 50% for GPC1 KO clone D4 (Figure 19B. & C.). GPC1 KO clones D8 and E3 only showed a slight decrease of 10% in FGF2-GFP secretion.

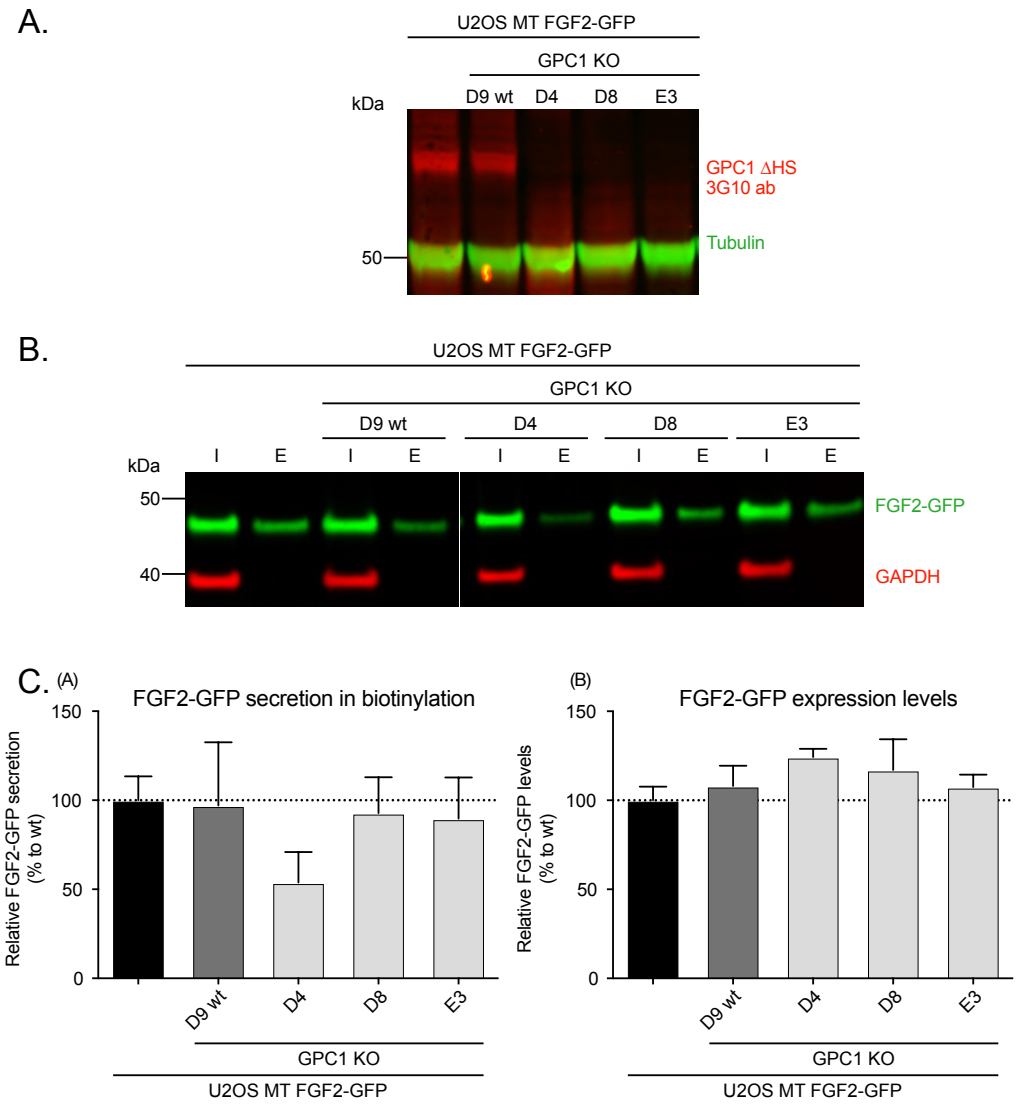

Figure 19: GPC1 KO in U2OS FGF2-GFP decreased FGF2 secretion. U2OS FGF2-GFP cells were used to generate CRISPR-Cas9 GPC1 knockouts and three clones (D4, D8 and E3) were selected for further analysis and compared to wild-type cells (wt) and a clone transfected with gRNA remaining wt (D9 wt). A. Representative Western blot after heparinase III digest showing KO of GPC1 in clones D4, D8 and E3 in contrast to wt cells and D9 wt. GPC1 was detected via 3G10 antibody (in red) and tubulin (in green) was used as loading control. B. Representative Western blot from cell surface biotinylation experiments showing both inputs (I) and eluates (E) for all cell lines. FGF2-GFP detected via anti-rabbit FGF2 antibody (in green) and anti-mouse GAPDH (in red) as loading and cell intactness control. C. Quantification of (A) FGF2-GFP secretion efficiency and (B) FGF2-GFP expression levels for n = 4 experiments showing averages and SDs. Statistical analysis was performed via one-way Anova combined with Tukey's post hoc test (ns $p > 0,05$; * $p \leq 0,05$; ** $p \leq 0,01$; *** $p \leq 0,001$, **** $p \leq 0,0001$).

GPC1 KO led to a decrease in FGF2-GFP secretion in U2OS when compared to S3 cells, yet the phenotype was not as strong as observed before. Possibly, this was due to remaining expression of GPC6. Next, GPC6 KOs and GPC1/6 dKOs in U2OS FGF2-GFP were generated via own gRNA design to challenge this hypothesis. Endogenous GPC6 was not detectable via heparinase III and Western blot. Therefore, successful GPC6 knockout was not only validated via genomic DNA sequencing, but also via RT-qPCR (data not shown). In total 6 GPC6 KO clones were selected for analysis and 5 GPC1/6 dKO clones were generated from GPC1 KO clones E3 and D4. Also, two clones remaining GPC6 wt (from wt and GPC1 KO D4) after transfection with CRISPR-Cas9 vectors were selected.

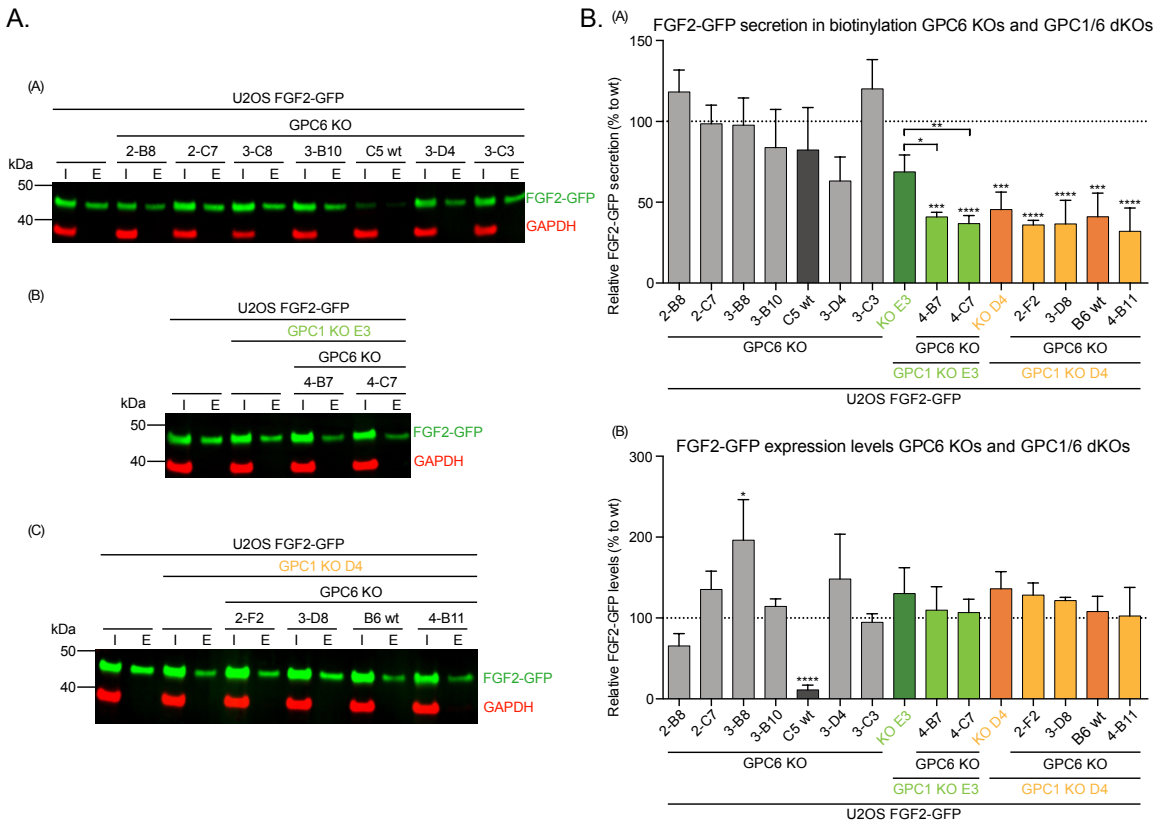

Figure 20: GPC1/6 dKO further decreased FGF2-GFP secretion in comparison to GPC1 KO. U2OS FGF2-GFP wt and GPC1 KO clones E3 and D4 were used to generate GPC6 knockout and GPC1/6 double knockout cells. The number before the clone's name refers to the gRNA used for KO generation. A. Representative Western blots from cell surface biotinylation experiments showing both inputs (I) and eluates (E) from all cells induced with 1 µg/ml doxycycline for 24 h. FGF-GFP detected via anti-rabbit FGF2 antibody (in green) and anti-mouse GAPDH (in red) as control. B. Quantification of (A) FGF2-GFP secretion efficiencies and (B) FGF2-GFP expression levels for n = 4 experiments. Statistical analysis of all clones was performed via one-way Anova combined with Tukey's post hoc test where clones were compared to GPC6 KO clone 2-C7. GPC1/6 dKOs 4-B7 and 4-C7 were compared to GPC1 KO E3 via unpaired t-test with Welch's correction (ns $p > 0,05$; * $p \leq 0,05$; ** $p \leq 0,01$; *** $p \leq 0,001$, **** $p \leq 0,0001$).

Impact of GPC6 KO and GPC1/6 dKO on FGF2-GFP secretion was tested via cell surface biotinylation in U2OS cells (Figure 20). GPC6 KO in wt cells did not significantly decrease FGF2-GFP secretion. This might be due to low protein abundance, as endogenous GPC6 was not detectable via Western blot analysis. GPC6 KO in GPC1 KO E3 background decreased surface FGF2-GFP to 40% and 35% for clones 4-B7 and 4-C7, respectively, and this decrease in secretion was significant in comparison to

the parental GPC1 KO E3 cell line which showed only ~ 70% surface FGF2-GFP (Figure 20B.(A)). Surprisingly, the secretion phenotype for GPC1 KO E3 was stronger in these experiments when compared to previous cell line characterization (Figure 19). GPC1/6 dKO clones derived from GPC1 KO D4 showed around 32-36% surface FGF2-GFP while parental GPC1 KO D4 showed 45%. Also here, additional GPC6 knockout on top of GPC1 knockout further diminished FGF2 secretion, yet for D4 the differences were not significant. All in all, these data pointed out to a major role of GPC1 in FGF2 secretion in U2OS cells, while GPC6 only made minor contributions. Nonetheless, double knockout of both GPC1 and GPC6 in two different clones reached a limit in reducing FGF2-GFP by 60-70%.

As previously done for HeLa S3 cells, U2OS FGF2-GFP cells were also used to generate cell lines overexpressing HA- and Flag-tagged GPC1 to detect GPC1 directly via antibodies. D9 wt and GPC1 KO D4 cells overexpressing Flag- or HA-GPC1 were validated via heparinase III digest and Western blotting (Figure 21A.). All overexpressions lead to a significant increase in FGF2-GFP secretion in cell surface biotinylation experiments when compared to wt cells and proved protein functionality (Figure 21B. and C.). As expected, GPC1 overexpression in D9 wt cells on top of endogenous GPC1 increased secretion more compared to overexpression in a GPC1 KO background.

U2OS FGF2-GFP GPC1 KO D4 + HA-GPC1 cells were also tested in immunofluorescence microscopy (Figure 21D.). HA-GPC1 was co-stained with antibodies directed against the α1 subunit of the Na,K-ATPase. When focusing on the cell nucleus cells displayed a circular staining and localization of GPC1 and α1 at the plasma membrane. When focusing at the bottom of the cells directly imaging the cell surface attached to the glass bottom, both GPC1 and α1 localized in a dot-like fashion throughout the entire cell surface. At this resolution no conclusions about sub-cellular localization of both proteins or potential organization into certain membrane areas could be drawn.

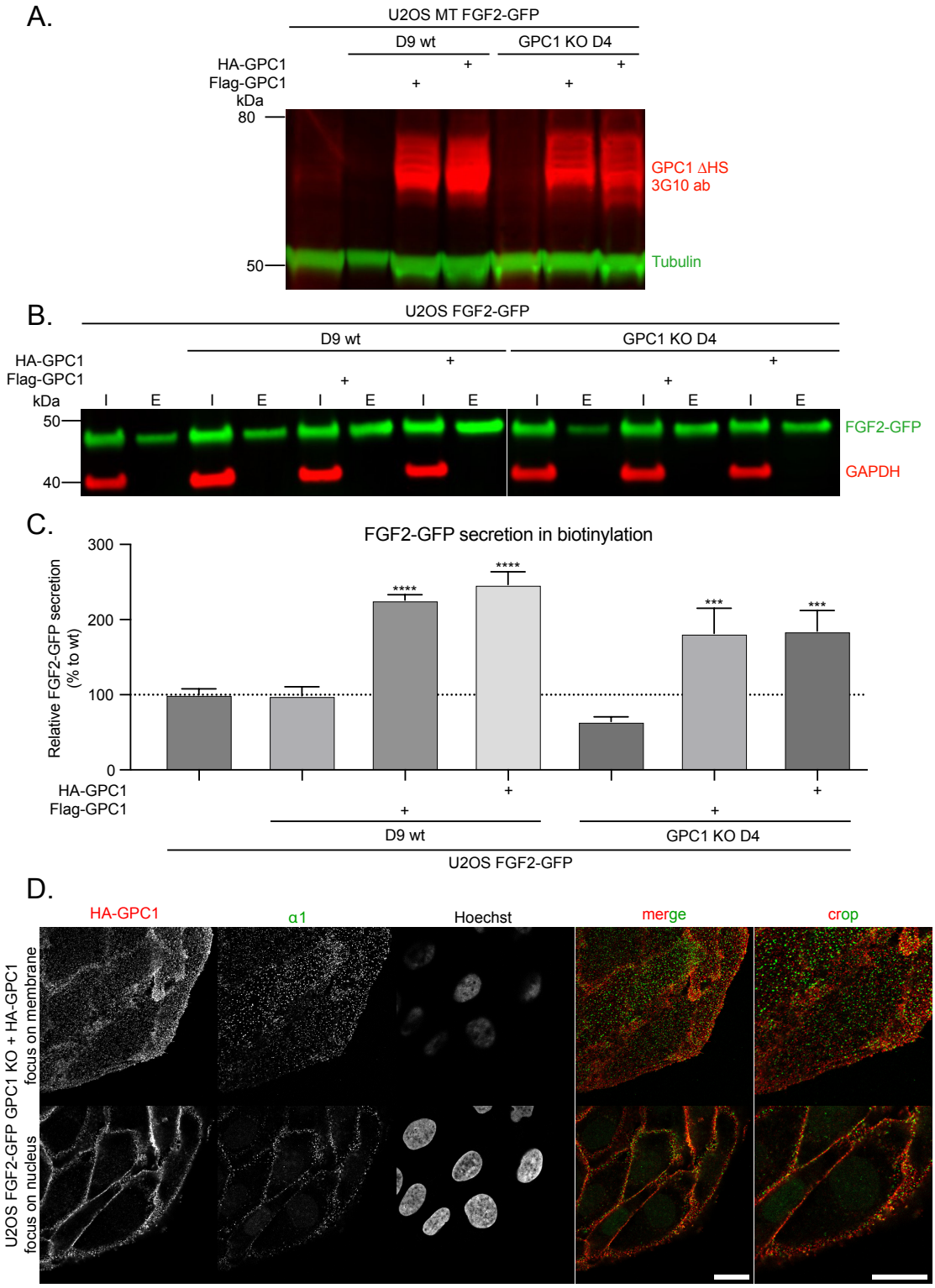

Figure 21: U2OS cell stably overexpressed HA-GPC1 and Flag-GPC1. U2OS FGF2-GFP D9 wt and GPC1 KO D4 cells were used to generate cells stably expressing Flag- or HA-tagged GPC1. A. Representative Western blot after heparinase III digest showing overexpression of Flag-GPC1 and HA-GPC1 in D9 wt and GPC1 KO D4 cells. GPC1 was detected via 3G10 antibody (in red) and tubulin (in green) was used as loading control. B. Representative Western blot from cell surface biotinylation experiments showing both inputs (I) and eluates (E) for all cell lines. FGF2-GFP detected via anti-rabbit FGF2 antibody (in green) and anti-mouse GAPDH (in red) as loading and cell intactness control. C. Quantification of FGF2-GFP secretion efficiency in GPC1 overexpressing cells for n = 3 experiments showing averages and SDs. Statistical analysis was performed via one-way Anova combined with Tukeys post hoc test (ns $p > 0,05$; * $p \leq 0,05$; ** $p \leq 0,01$; *** $p \leq 0,001$, **** $p \leq 0,0001$). D. Confocal immunofluorescence microscopy of fixed and permeabilized GPC1 KO D4 + HA-GPC1 cells stained with anti-rabbit HA antibody and anti-mouse α1 antibody. Nuclei were stained with Hoechst. Cells were focused at the nucleus or at the bottom membrane. Scale bar 20 µm.

4.1.6 Concluding remarks on glypicans in FGF2 secretion

The different experiments conducted in HeLa and U2OS knockout cells of GPC1, GPC5 or GPC6 support the hypothesis of a glypican subclass-specific effect on FGF2 secretion, yet clearly mark GPC1 as the dedicated glypican for FGF2 secretion as was published by our laboratory [51]. While GPC1 KO decreased FGF2-GFP secretion, knockout of GPC5, belonging to a different subclass, did not impact secretion. Upon reintroduction and overexpression of GPC1 secretion was not only restored to wt levels, but even further increased indicating that GPC1 is a rate-limiting factor for FGF2 secretion. This effect was also observed for tagged GPC1 versions. GPC1 levels could be directly correlated to FGF2 secretion in TIRF. GPC6 KO alone did not decrease FGF2-GFP secretion, yet was able to further decrease secretion in GPC1 KO cells until a certain threshold. As GPC1 plays a role in FGF2 secretion, it can also be found in proximity to components of the secretory machinery such as FGF2 itself and α1.

4.2 Components involved in FGF2 secretion organize into membrane nanodomains

Live cell microscopy of single FGF2-GFP translocation events in TIRF microscopy showed FGF2 secretion and translocation to occur within 200 ms [128]. In a fully reconstituted GUV system with $PI(4,5)P_2$ and long-chained heparin FGF2 translocation was shown to be much slower [129]. We thus hypothesize that components needed for FGF2 secretion might be in proximity to each other in a cellular context and proteins might even be localized into nanodomains. To gain information supporting this nanodomain hypothesis became a side-project next to my research on GPC1.

4.2.1 Proteins involved in FGF2 secretion are in proximity to each other in microscopy experiments

4.2.1.1 GPC1 and the α1 subunit of the Na,K-ATPase were imaged in STED microscopy

Confocal microscopy of components such as α1 and GPC1 provided first insights into protein localization at membranes, yet the resolution limit impeded more precise answers to protein position and organization. Therefore, I decided to perform super resolution microscopy, more precisely STED (stimulated emission depletion microscopy) microscopy. Both α1 and HA-GPC1 were detected in U2OS FGF2-GFP GPC1 KO D4 + HA-GPC1 cells via immunofluorescence staining and STED suitable secondary antibodies (from Abberior). As seen in Figure 22A. STED imaging greatly improved resolution compared to confocal imaging and signals first detected as one were now resolved into two distinct protein signals. Also, both α1 and HA-GPC1 showed a dot-like localization throughout the entire imaged membrane sections, as seen before for confocal microscopy images. Colocalization was calculated via Person's correlation coefficient which measures the pixel-by-pixel covariance in the signal levels of two images [246]. The coefficient ranges between 1, declaring that fluorescence signals from two images perfectly correlate with each other, to -1, which indicates that signals are perfectly but negatively related to each other. Here, Pearson's correlation coefficient was calculated for both confocal and STED samples and – dox and + dox conditions were compared to determine if FGF2-GFP expression changed protein distribution and colocalization. For confocal images there was a significant difference in colocalization/correlation detectable between both conditions, showing more colocalization between HA-GPC1 and α1 when FGF2-GFP expression was induced. For STED images this difference was not detectable. In general, very low correlation coefficients were calculated. Values near 0 indicate signal distributions that do not correlate with each other. When using STED of course, we want to improve resolution and do not necessarily expect exact colocalization. By eye it appeared that more events were observed where α1 and GPC1 are near each other when cells were previously incubated with doxycycline to induce FGF2 expression (see arrows), but this statement needs further validation by quantitative methods.

Also, triple color experiments were conducted to image FGF2-GFP together with α1 and GPC1, yet these proved inadequate (data not shown). GFP bleached very fast due to high laser STED intensities and imaging in z-stacks was not possible. In future, more experiments with differently tagged FGF2 must be conducted to be able to analyze all three proteins together in one experiment.

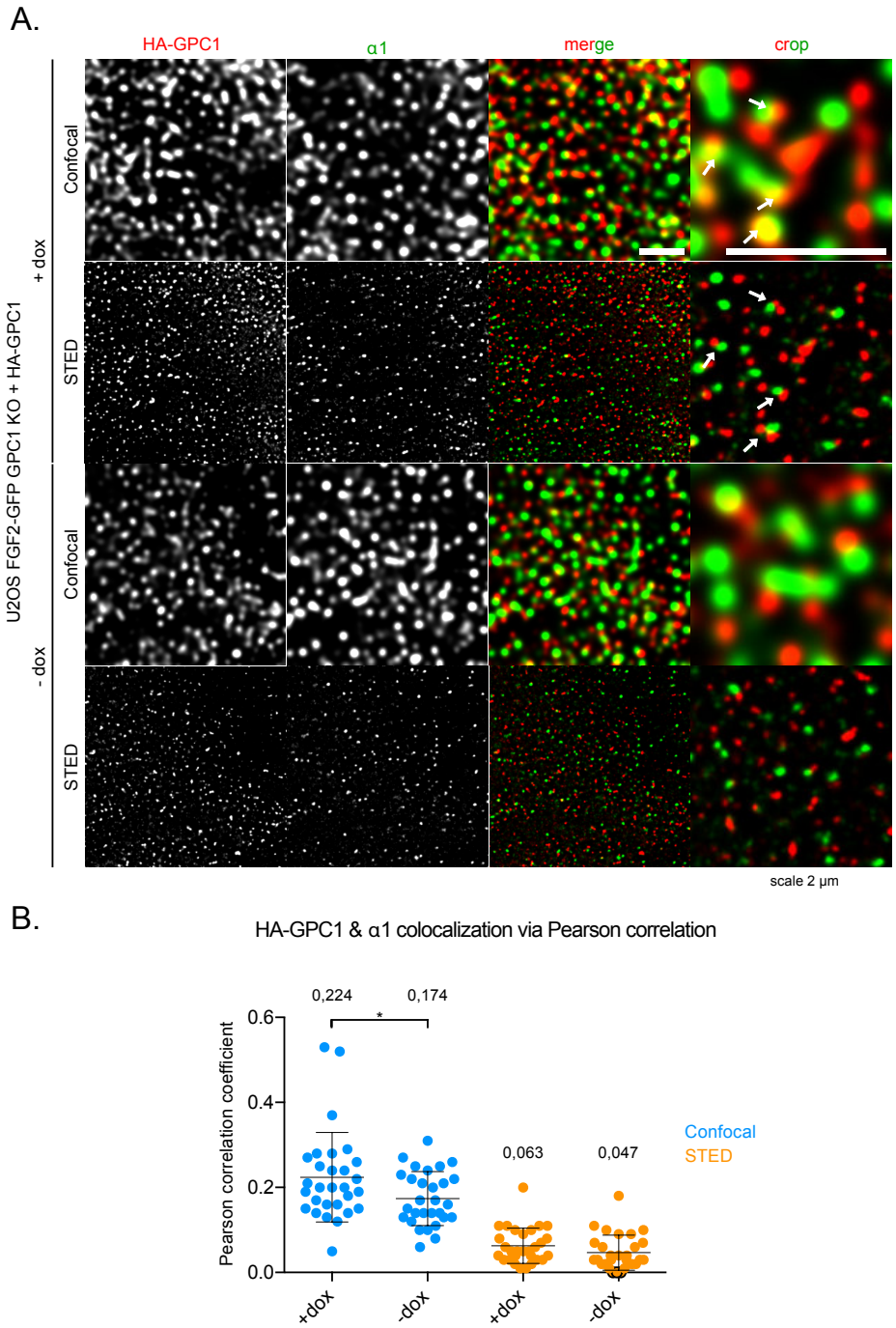

Figure 22: HA-GPC1 and α1 localization in STED microscopy. HA-GPC1 and α1 were detected via immunofluorescence staining using anti-rabbit HA (in red) and anti-mouse α1 (in green) antibody in fixed and permeabilized U2OS FGF2-GFP GPC1 KO D4 + HA-GPC1 cells. Conditions with or without 24h incubation with doxycycline were tested. A. Representative confocal and STED images taken using a Leica TCS SP8 STED 3X microscope and subjected to Huygens deconvolution. Scale bar represents 2 µm in all images and cropped images. B. Protein colocalization was tested via Pearson correlation coefficient in all conditions for n = 3 experiments. Statistical comparison of conditions via unpaired t-test with Welch's correction (ns $p > 0,05$; * $p \leq 0,05$; ** $p \leq 0,01$; *** $p \leq 0,001$, **** $p \leq 0,0001$).

4.2.1.2 FGF2 and PI(4,5)P_2 were found in cholesterol-rich membrane areas in STED microscopy

Experiments conducted by Roberto Saleppico and Dr. Fabio Lolicato in our group showed that cholesterol has an impact on FGF2 secretion and that increased cholesterol levels promote both intracellular recruitment of FGF2 to the plasma membrane and its secretion from cells [247, 248]. These findings support the hypothesis that FGF2 might translocate from specialized nanodomains. Cholesterol is known to be enriched in liquid-ordered lipid rafts, which contain GPI-anchored proteins and cholesterol-linked or palmitate-anchored proteins [249]. With PI(4,5)P_2 as a key player in FGF2 secretion needed for correct translocation and cholesterol promoting PI(4,5)P_2 clustering [247, 248], I sought to image FGF2, PI(4,5)P_2 and cholesterol via STED microscopy.

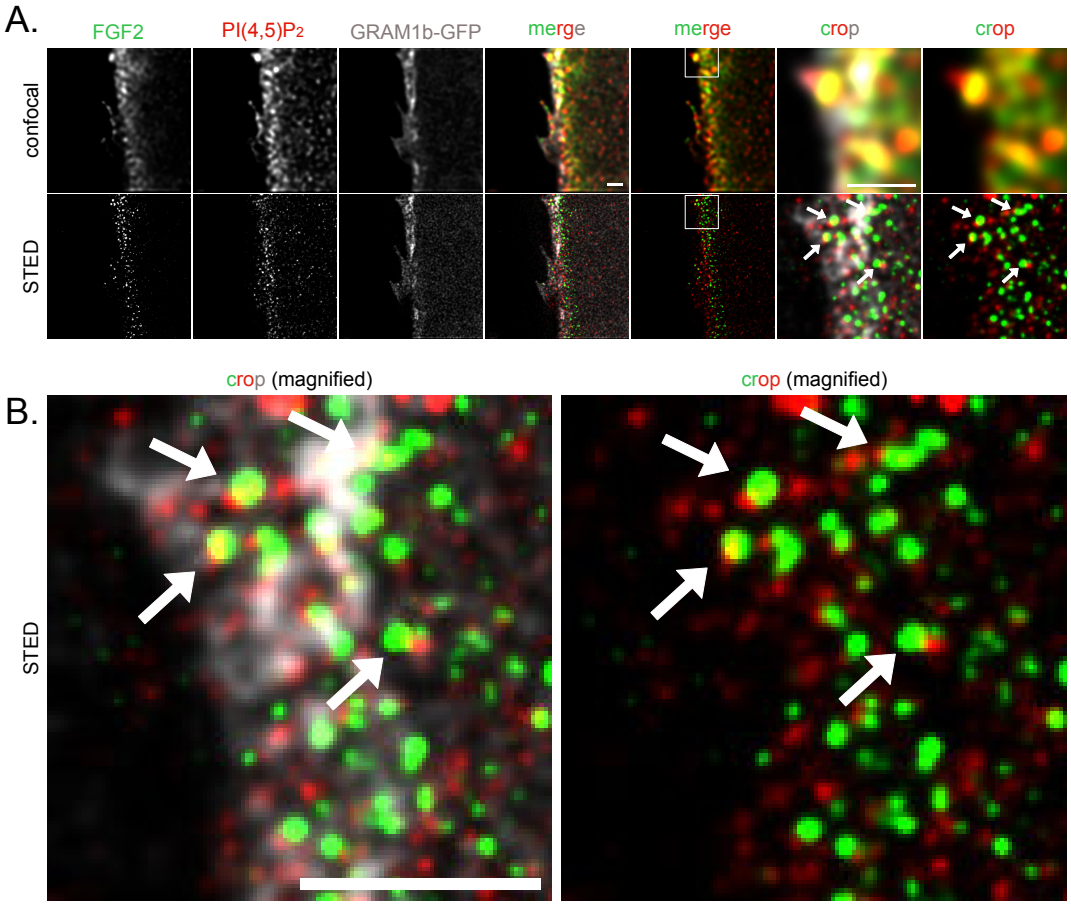

Figure 23: FGF2 and PI(4,5)P_2 were found in membrane areas enriched in cholesterol. U2OS FGF2-Halo cells were transfected with EGFP-Gram$_{1b}$ G187L [217] to detect cholesterol. Cells were treated with doxycycline to induce FGF2-Halo expression and were stained with anti-rabbit FGF2 and anti-mouse PI(4,5)P_2 antibody. Images were acquired on a Leica TCS SP8 STED 3X microscope. A. Representative triple color confocal and STED images showing FGF2 (in green), cholesterol via Gram1b-GFP (in grey) and PI(4,5)P_2 (in red). B. Magnified cropped images from A. showing triple or dual color merged channels. Arrows indicate colocalization events. Scale bar 1 µm. All images deconvolved with Huygens deconvolution software. Adapted data, accepted for publication at J Cell Biol on 30.08.2022 and in press [248].

To detect cholesterol U2OS FGF2-Halo cells were transfected with EGFP-Gram$_{1b}$ G187L which recognizes cellular cholesterol levels above 30 mole % [217]. Cells were induced with doxycycline to detect FGF2-Halo via FGF2 antibody staining together with PI(4,5)P_2 also visualized via antibody staining. As seen in Figure 23 both FGF2 and PI(4,5)P_2 were found at membrane areas enriched in

cholesterol. PI(4,5)P_2 and FGF2 did not localize exclusively to areas enriched in cholesterol, but events where both proteins were found in close proximity to each other (indicated with arrows) overlapped with membrane areas showing cholesterol staining. These data support the hypothesis of cholesterol driven PI(4,5)P_2 clustering promoting FGF2 secretion and localization of FGF2 to membrane domains enriched in cholesterol.

4.2.1.3 Proteins involved in FGF2 secretion were in proximity to each other in U2OS cells

As U2OS cells showed to be very well suitable for microscopy Duolink® PLA experiments were conducted with these cells. U2OS FGF2-GFP GPC1 KO D4 + HA-GPC1 cells were used to test proximity between a wide range of proteins. In all conditions FGF2-GFP expression was induced via incubation with 1 µg/ml doxycycline for 24h. As seen in Figure 24 PLA experiments with U2OS gave much higher signal numbers than seen before for HeLa S3 cells, making quantification more reliable. Due to the flat cell shape of U2OS cells, the PLA signals were quantified at the bottom focus plane right at the cell membrane in contrast to S3 cells (focus at nucleus).
As seen in Figure 24A. and B. all antibody combinations had high PLA signal numbers compared to the single antibody controls giving minimum 4-fold lower values. FGF2 and HA-GPC1 showed the highest proximity. This might be due to the fact that both proteins were overexpressed in these experiments or because the functional relationship between both is much higher as for FGF2 and α1. The Na,K-ATPase is involved in many other cellular processes and only a subpopulation might be related to FGF2 secretion. When looking at GPC1 and FGF2 proximity I could not make conclusion about where exactly these events took place. These might be surface events where FGF2 is bound to the heparan sulfate chains of GPC1 or these might also be proximity events across the plasma membrane of intracellular FGF2 and extracellular GPC1. To evaluate whether proximity between α1 and GPC1 was specific, proximity to other membrane proteins, namely syndecan 4 (SDC4) as other HSPG and cadherin (CDH) as other transmembrane protein, was tested. There was no significant difference in proximity of α1-GPC1 and α1-SDC4. As mentioned previously the Na,K-ATPase is a conserved protein participating in many processes and associated to many different proteins. Perhaps distribution throughout the cell membrane is very homogenous and does not involve sublocalization to certain membrane areas. However, there was a significant difference between α1-GPC1 and GPC1-CDH proximity.

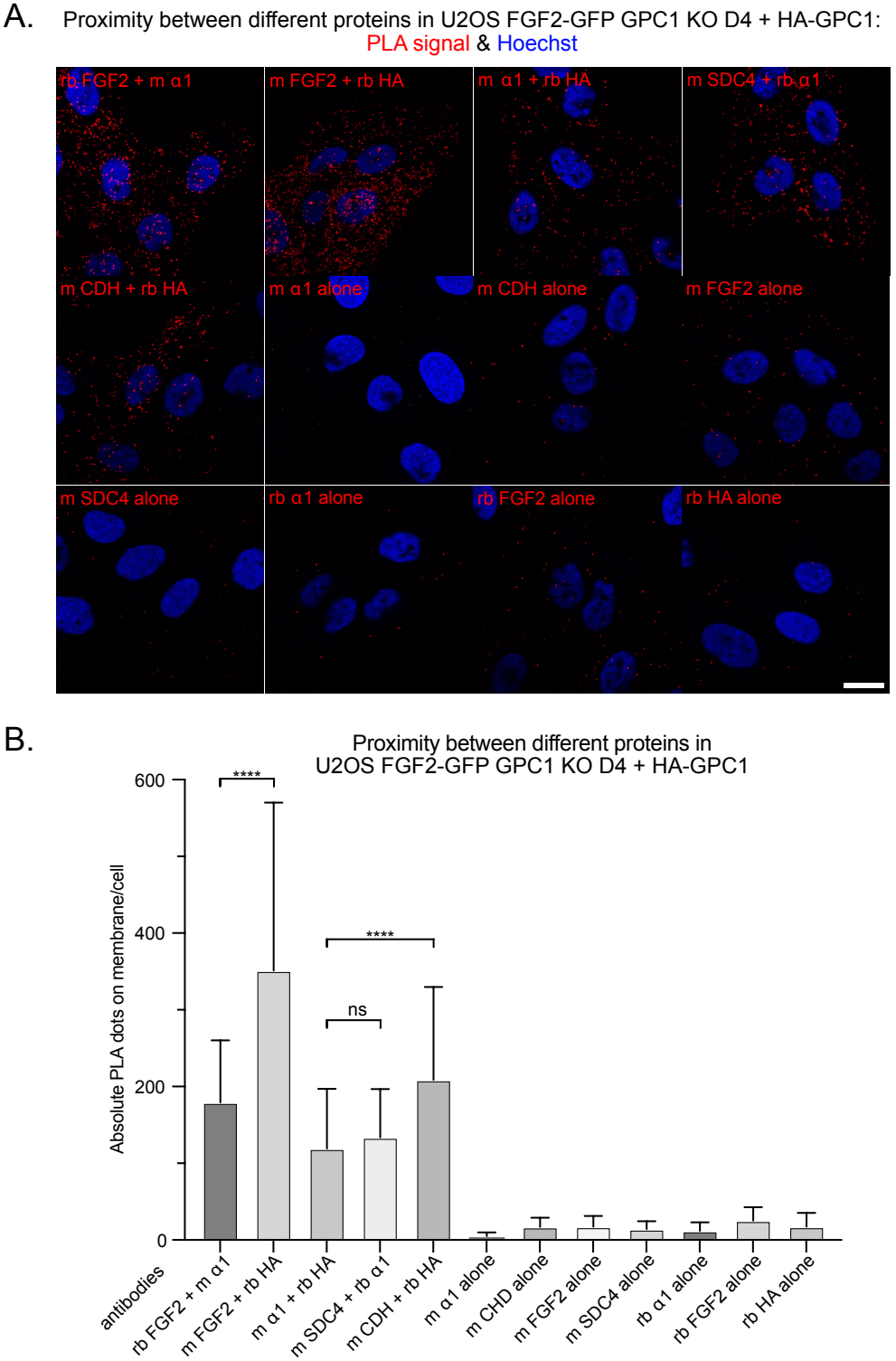

Figure 24: U2OS FGF2-GFP GPC1 KO D4 + HA-GPC1 cells showed proximity of many components needed for FGF2 secretion. U2OS FGF2-GFP GPC1 KO D4 + HA-GPC1 cells were treated with doxycycline to induce FGF2-GFP expression. Antibodies used and the host species of the antibody are depicted. A. Representative images showing merged confocal images of different antibody combinations used for PLA (in red) and nuclei stained with Hoechst (in blue). Scale bar 20 µm. B. Quantification from 4 experiments showing the absolute PLA dots per cell quantified on the membrane. Statistical comparison of conditions via unpaired t-test with Welch's correction (ns $p > 0,05$; * $p \leq 0,05$; ** $p \leq 0,01$; *** $p \leq 0,001$, **** $p \leq 0,0001$).

4.2.2 Proteins involved in FGF2 secretion localize together to detergent resistant membrane fractions

Collectively, data from microscopy experiments such as PLA and STED have shown that components needed for FGF2 secretion are in proximity to each other and that FGF2 and $PI(4,5)P_2$ can be found in areas enriched in cholesterol. To take these observations one step further I decided to perform isolation of detergent resistant membrane (DRM) fractions. Liquid ordered membrane areas enriched in cholesterol are resistant to detergents such as Triton X-100 at 4°C and can be separated from liquid-disordered membrane areas via ultracentrifugation in a sucrose gradient.

For DRM experiments cells were lysed in lysis buffer containing 1% Triton X-100 and mixed 1:1 with 80% sucrose and placed into an ultracentrifugation tube. Lysates were overlayed with 30% and 5% sucrose and centrifuged over-night. The subsequent day 10 fractions were collected and analyzed via SDS-PAGE and Western blotting (Figure 25A.). Caveolin-1 (Cav1) was used as marker for liquid ordered membrane fractions and transferrin receptor (TfR) served as marker for detergent-soluble liquid disordered fractions.

As seen in Figure 25B. and C. FGF2-GFP, α1 and GPC1 were found in liquid ordered membrane fractions characterized via Cav1 presence in both U2OS and HeLa S3 cells. GPC1 was only detected very weakly though, indicating that endogenous levels are low or that the heparinase III digest might not be efficient in the sucrose lysis buffer. It's also worth mentioning that Cav1 distribution was not as clean for U2OS cells, as it was for HeLa S3 cells. While Cav1 localized almost exclusively to the liquid ordered fractions 4-6 in S3 cells, Cav1 was also strongly present in later fractions for U2OS cells, indicating some cell type specific differences. Caveolin-2 in contrast, did not localize exclusively into DRM fractions and is not seen as a marker for liquid ordered membrane areas. Transferrin receptor and cadherin localized mostly to detergent soluble fractions. Both α1 and FGF2-GFP were found in detergent resistant membrane fractions together with GPC1 and Cav1, yet were also found to a great extent in later detergent soluble fractions. These might resemble protein subpopulations not interacting with each other. α1 and TfR could only be detected in U2OS liquid ordered fractions when samples were precipitated via methanol-chloroform, since otherwise protein levels were too low to be detected via Western blotting.

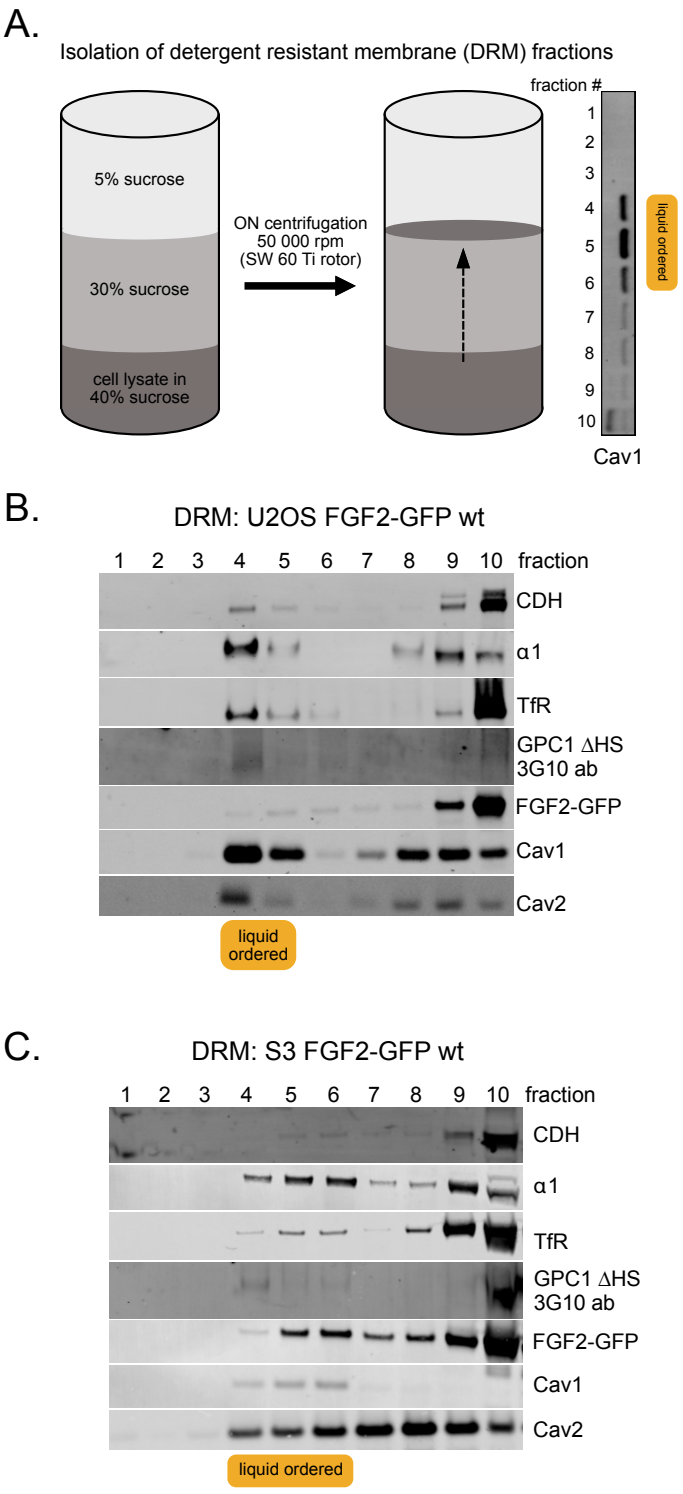

Figure 25: Proteins involved in FGF2 secretion localized into detergent resistant liquid ordered membrane fractions. A. Working model for isolation of DRM fractions. Cell lysates with Triton X-100 in 40% sucrose were overlayed with 30% and 5% sucrose. Via over-night ultracentrifugation lighter detergent resistant fractions were floated up. Fractions were taken from top to bottom and analyzed via Western blotting. B. Representative Western blot analysis of several proteins in U2OS FGF2-GFP wt cells showing protein distribution throughout all fractions. From each fraction (60 µl + 20 µl sample buffer) 10 µl were loaded. To detect α1 and TfR in U2OS, samples were precipitated via methanol-chloroform and the entire fraction was loaded for fractions 1-8. For fractions 9 & 10 ¼ of precipitated fractions were loaded C. Representative Western blot analysis of several proteins in S3 FGF2-GFP wt cells showing protein distribution throughout all fractions. From each fraction (60 µl + 20 µl sample buffer) 10 µl were loaded.

Seeing that α1, FGF2-GFP and GPC1 localize together in detergent resistant membrane fractions, I wondered whether GPC1 knockout changes the localization of FGF2 into DRM fractions. To test this hypothesis, U2OS FGF2-GFP wt, GPC1 KO D4 and GPC1 KO D4 + HA-GPC1 cells were tested in DRM fractionation experiments.

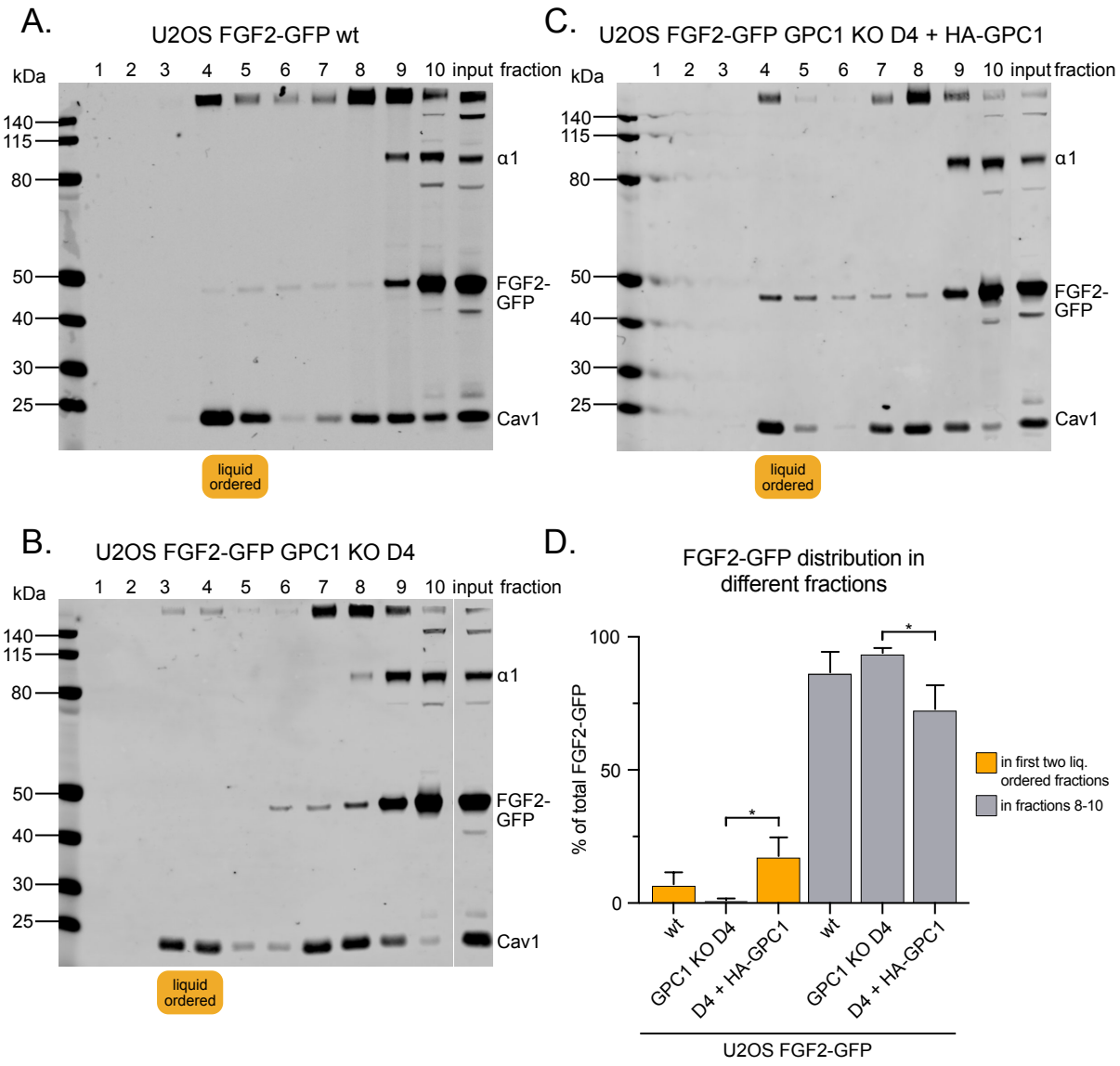

Figure 26: GPC1 modulated localization of FGF2-GFP into detergent resistant membrane fractions. FGF2-GFP, Cav1 and α1 were detected in Western blot after DRM fractionation from A. U2OS FGF2-GFP wt cells, B. U2OS FGF2-GFP GPC1 KO D4 cells and C. U2OS FGF2-GFP GPC1 KO D4 + HA-GPC1 cells. Quantification of FGF2-GFP levels in first two liquid ordered membrane fractions or in fractions 8-10 from 4 experiments. Samples were not precipitated, due to only FGF2-GFP quantification. Statistical analysis was performed via unpaired t-test with Welch's correction always comparing two cell lines (ns $p > 0,05$; * $p \leq 0,05$; ** $p \leq 0,01$; *** $p \leq 0,001$, **** $p \leq 0,0001$).

As seen in Figure 26A.-C. localization of FGF2-GFP into liquid ordered membrane areas shifted upon GPC1 knockout or overexpression. In wt cells around 7% of total FGF2-GFP was found in DRM fractions whereas around 86% of total FGF2-GFP was found in the last three fractions containing detergent soluble protein (Figure 26D.). GPC1 KO reduced DRM FGF2-GFP down to around 1% and increased soluble FGF2-GFP to 94%. When overexpressing GPC1 in the knockout cells, FGF2 in liquid

ordered membrane fractions was increased to around 17%, while soluble FGF2-GFP was reduced to 73% of total protein. This 2,4-fold increase in FGF2-GFP in DRM fractions when comparing wt to GPC1 overexpressing cells correlate with biotinylation experiments and could point out that FGF2-GFP found in DRM fractions could be surface FGF2 bound to the heparan sulfate chains of GPC1. Yet overexpression of GPC1 could also aid the assembly of the FGF2-GFP secretion machinery and thereby recruit more FGF2 into liquid ordered secretion domains.

4.2.3 Concluding remarks on FGF2 secretion nanodomains

Data collectively support the hypothesis that components involved in FGF2 secretion are localized into nanodomains. GPC1, α1 and FGF2 were in proximity to each other and α1 and GPC1 could even be detected near each other via STED microscopy. Also, FGF2 and $PI(4,5)P_2$ were found in cellular areas enriched in cholesterol. Cholesterol has been shown to promote FGF2 secretion via $PI(4,5)P_2$ clustering [247, 248] and is present in liquid ordered membrane domains. Alongside with this, a subpopulation of FGF2 and α1 localized together with GPC1 into detergent resistant membrane areas, which usually contain higher cholesterol levels and are characterized via caveolin-1 signals.

4.3 Caveolin-1 and Caveolin-2 might play a role in FGF2 nanodomain organization

All in all, previous data support the nanodomain hypothesis for FGF2 secretion. I showed that proteins involved in FGF2 secretion localize together into detergent resistant membrane areas. Also, FGF2 and $PI(4,5)P_2$ were found in membrane areas enriched in cholesterol. As seen in DRM experiments caveolin-1 is a marker of detergent resistant membrane fractions. This finding, together with the fact that caveolin-1 is known to be a cholesterol-binding protein and that proteins involved in FGF2 secretion, and even FGF2 itself, contain a caveolin-binding motif (see Figure 5), encouraged me to investigate whether caveolin-1 plays a role in FGF2 secretion.

4.3.1 Caveolin-1 did not impact FGF2-GFP secretion in HeLa S3 cells

Therefore, I generated Cav1 KO cell lines in S3 FGF2-GFP via CRISPR-Cas9 that were tested in cell surface biotinylation experiments.

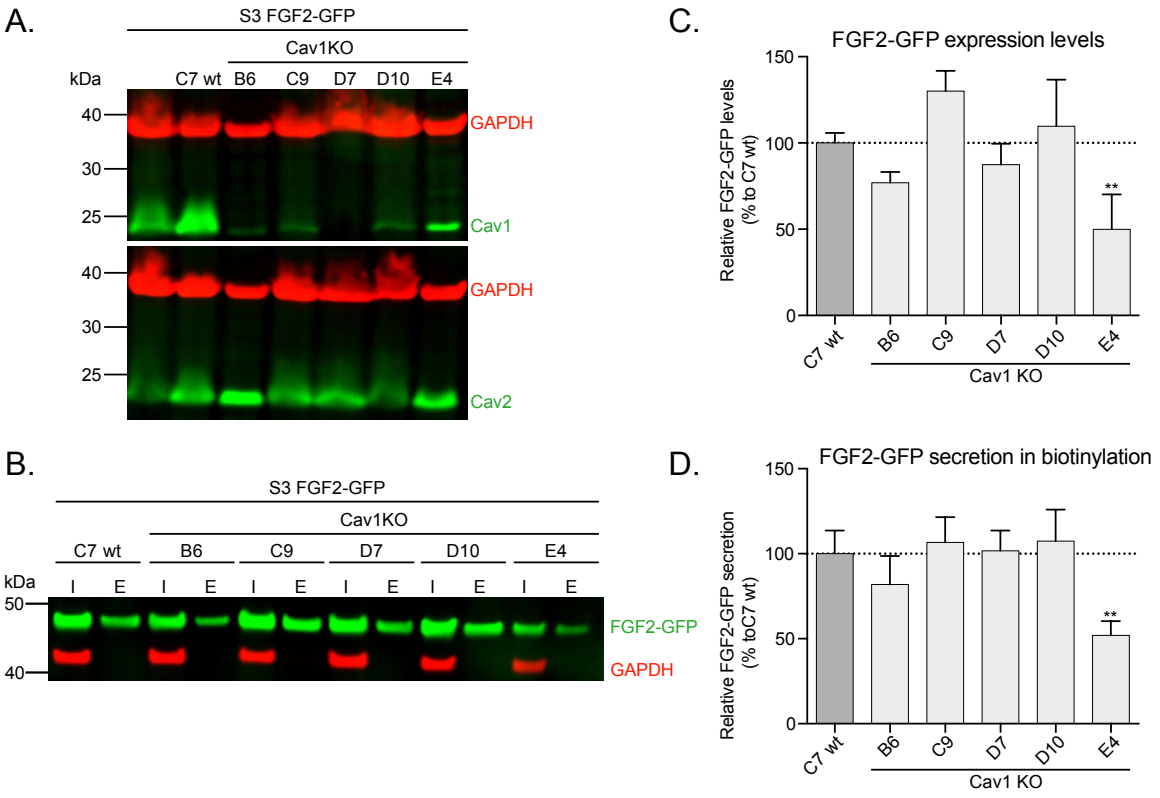

Figure 27: Caveolin 1 KO did not impact FGF2-GFP secretion in HeLa S3 FGF2-GFP cells. In total 5 different Cav1 KO clones (B6, C9, D7, D10 and E4) were selected and one clone remaining wild-type (C7 wt). A. Representative Western blot showing all cell lines using anti-rabbit Cav1 or Cav2 antibody (in green) together with anti-mouse GAPDH (in red). B. Representative Western blot from cell surface biotinylation experiments showing input (I) and eluates (E) for all cell lines induced with doxycycline for 24 h. FGF2-GFP detected via anti-rabbit FGF2 antibody (in green) and anti-mouse GAPDH used as control. C. Quantification of relative FGF2-GFP expression levels normalized to C7 wt. D. Quantification of relative FGF2-GFP secretion normalized to C7 wt. Data from n = 3 experiments and statistical analysis was performed via one-way Anova combined with Tukeys post hoc test (ns $p > 0,05$; * $p \leq 0,05$; ** $p \leq 0,01$; *** $p \leq 0,001$, **** $p \leq 0,0001$).

Successful knockout of Cav1 was tested via genomic DNA sequencing and Western blotting (Figure 27). It seemed small levels of Cav1 remained after KO and Western analysis, but using a different antibody showed no signals for Cav1 (data not shown), suggesting the remaining signals observed were antibody background or cross-reactivity. Slight background signals were also seen in immunofluorescence analysis of Cav1 KO clones. Cav1 was no longer found at the plasma membrane in Cav1 KO cells in contrast to C7 wt cells, were Cav1 localized strongly to the plasma membrane as seen by co-staining with α1 (Figure 28).

Analysis of Cav1 KOs via cell surface biotinylation (Figure 27B.-D.) revealed no differences in FGF2-GFP secretion. Only clone E4 showed reduced surface FGF2-GFP, but also had lower FGF2-GFP expression levels. According to literature, Cav1 KO reduces Cav2 levels drastically, as Cav1 is required for correct protein recruitment to the membrane and in absence of Cav1 Cav2 is degraded via the proteasome [227]. As clearly seen in Figure 27A. caveolin-2 was present in these Cav1 KO cells.

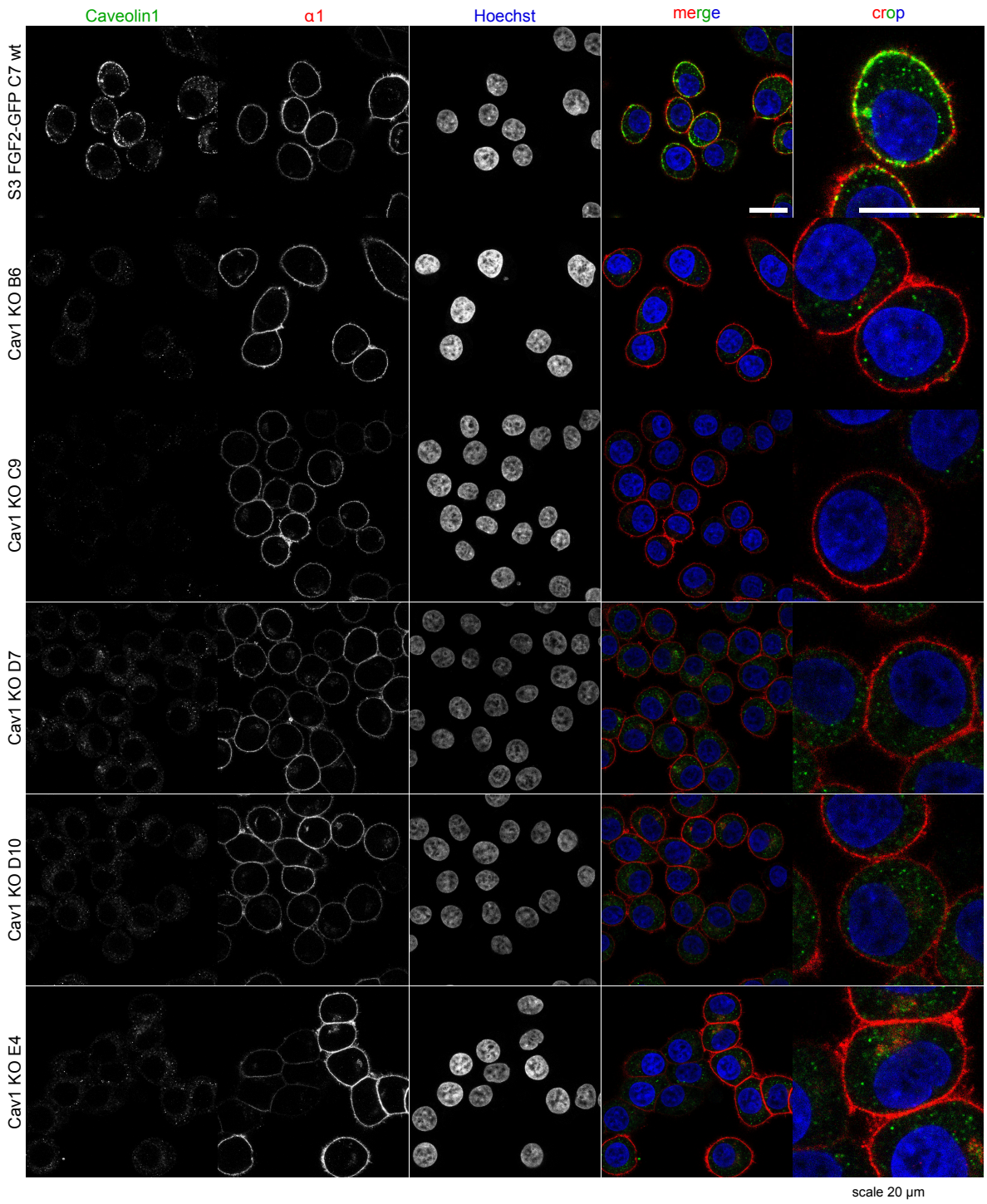

Figure 28: Immunofluorescence staining showing successful knockout of caveolin-1. S3 FGF2-GFP C7 wt cells and Cav1 KO clones were analyzed via staining with anti-rabbit Cav1 (in green) and anti-mouse α1 (in red). Nuclei were stained with Hoechst (in blue). All images taken on a confocal Zeiss LSM800. Scale bar in merged and cropped images represents 20 µm.

4.3.2 Cav2 KO, not Cav1/2 dKO, reduced FGF2-GFP secretion in HeLa S3 cells

Due to persisting Cav2 expression in Cav1 KO cells, I also generated S3 FGF2-GFP Cav2 KO and Cav1/2 dKO cells devoid of all caveolins expressed in HeLa cells. These were once again validated via genomic DNA sequencing, Western blotting and microscopy and analyzed in cell surface biotinylation experiments. When comparing lysates via Western blotting caveolin-2 seemed to be expressed higher than caveolin-1 in HeLa S3 cells (Figure 29A.)

Double knockout using Cav1 KO D7 as parental cell line did not change FGF2-GFP secretion significantly from wt cells (Figure 29B.-D. subpanels (B)). Strikingly, single Cav2 KO did reduce FGF2-GFP secretion by about 40% in clones C2 and D7 (Figure 29B.-D. subpanels (A)). This phenomenon could be explained by two hypotheses. One reason could be that the order of knockout plays a role and this hypothesis will be tested later. Also, all Cav1/2 dKO clones were generated using the Cav1 KO clone D7. If this clone showed a defect before, this would be passed onto the subsequent generation of cells. Another possibility is that when both Cav1 and Cav2 are absent other cellular mechanisms compensate for lack of both proteins.

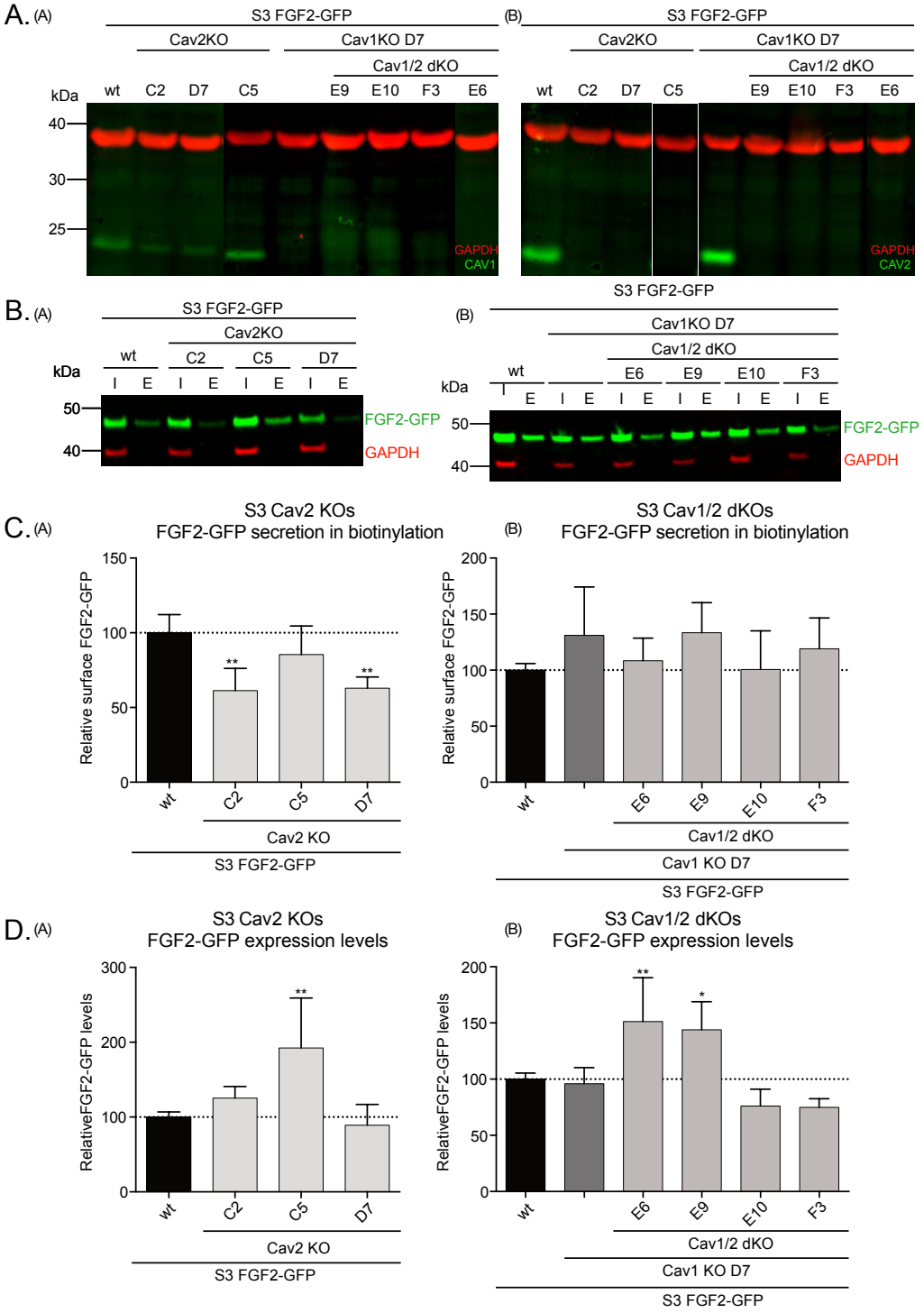

Figure 29: Cav2 KO and Cav1/2 dKO in HeLa S3 FGF2-GFP cells. S3 FGF2-GFP wt cells were used to generate three Cav2 KO clones (C2, C5, D7, subpanels (A)) and Cav1 KO D7 was used to generate four Cav1/2 dKO clones (E6, E9, E10, F3, subpanels (B)). A. Representative Western blot showing Cav1 or Cav2 (in green) via anti-rabbit antibody staining together with anti-mouse GAPDH (in red). B. Representative Western blot from cell surface biotinylation experiments showing input (I) and eluates (E) for all cell lines induced with doxycycline for 24 h. FGF2-GFP detected via anti-rabbit FGF2 antibody (in green) and anti-mouse GAPDH (in red) used as control. C. Quantifications from 4 biotinylation experiments showing relative FGF2-GFP secretion efficiencies normalized to wt cells. D. Quantifications from 4 biotinylation experiments showing relative FGF2-GFP expression levels normalized to wt cells. Statistical analysis was performed via one-way Anova combined with Tukeys post hoc test (ns $p > 0,05$; * $p \leq 0,05$; ** $p \leq 0,01$; *** $p \leq 0,001$, **** $p \leq 0,0001$).

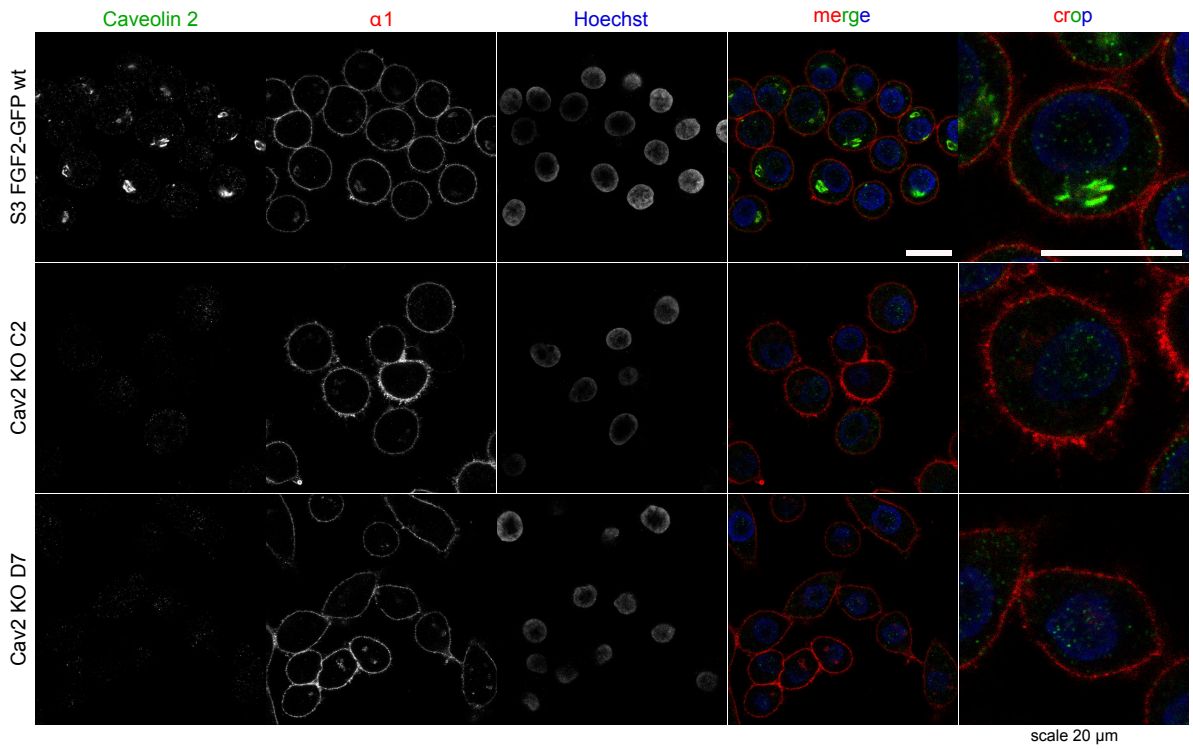

Figure 30: Cav2 knockout was verified via immunofluorescence microscopy for S3 FGF2-GFP Cav2 KO clones C2 and D7. S3 FG2-GFP wt and Cav2 KO clones (C2 and D7) were stained using anti-rabbit Cav2 (in green) and anti-mouse α1 (in red). Nuclei stained with Hoechst (in blue). All images were acquired using a Zeiss LSM800 confocal microscope. Scale bar 20 µm.

As seen in Figure 30 Cav2 KO was confirmed for clones C2 and D7 via immunofluorescence microscopy. As seen from co-staining with α1, Cav2 did not localize predominantly at the membrane, but was found in intracellular vesicles and potentially the Golgi (not validated via co-staining). Not much is known for caveolin-2 and most data in literature focus on characterizing caveolin-1. It has been reported that Cav2 localizes to the Golgi in Fisher Rat Thyroid cells (FRT) cells which barely express Cav1 and that upon Cav1 overexpression Cav2 is partially redistributed to the plasma membrane [250]. Yet this does not apply to S3 wt cells, which express Cav1 endogenously. Exact function and localization of Cav2 require further investigation.

4.3.3 Caveolin-2 KO influenced protein localization into detergent resistant membrane fractions

Since DRM experiments previously provided valuable insights into protein localization into specialized membrane areas and are characterized via Cav1 partitioning into liquid ordered fractions, I performed DRM experiments on the different caveolin KO cells to analyze protein localization. S3 FGF2-GFP wt, Cav1 KO D7, Cav2 KO D7 and Cav1/2 dKO E10 cells were analyzed and representative Western blots for all cell lines are shown in Figure 31 Wt cells showed presence of FGF2-GFP and α1 in Cav1-enriched liquid ordered membrane fractions. In Cav1 and Cav1/2 dKO cells, Cav1 could not be detected as expected. Cav2 KO D7 did show a signal for caveolin-1, yet this was remarkably shifted out of the liquid ordered membrane fractions and localized into the fractions 7-9. This was not expected, as it was only reported before that Cav1 determines localization of Cav2 [227] and not vice versa. This observation was also confirmed for Cav2 KO clone C2 (data not shown).

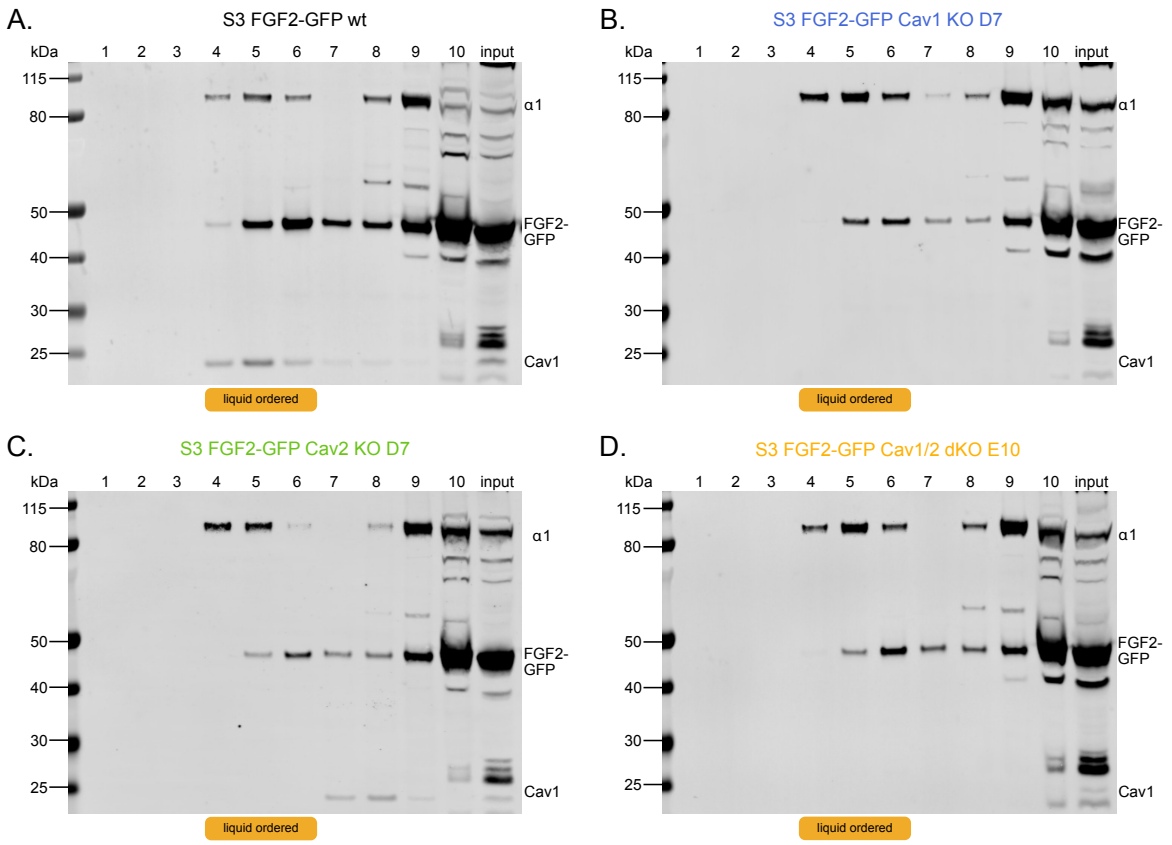

Figure 31: DRM experiments showed protein redistribution into detergent soluble membrane fractions for Cav2 KO. A. S3 FGF2-GFP wt, B. Cav1 KO D7, C. Cav2 KO D7 and D. Cav1/2 dKO E10 cells were analyzed via DRM fractionation. Proteins detected were α1 (anti-mouse antibody), FGF2-GFP (anti-rabbit FGF2 antibody) and Cav1 (anti-rabbit antibody). All 10 fractions and inputs are shown.

Also α1 and FGF2-GFP signals seemed slightly reduced in Cav2 KO cells. Quantification of both α1 and FGF2 protein distributions in DRM fractions showed a decrease in liquid ordered fractions 4-6 and a slight increase in the later fractions 9 and 10 (Figure 32A. and B.). A clear trend for Cav2 KO D7 was observable, yet none of the data were significant due to high variation between the experiments. Cav1/2 dKO E10 and Cav1 KO D7 showed similar values to wt cells when looking at α1 distribution and FGF2-GFP distribution levels did not significantly alter from wt cells. This pointed out to a potential role of Cav2 in organizing liquid ordered membrane domains, as Cav1 failed to localize into DRM fractions in Cav2 KO cells. Also, caveolin-2 could potentially regulate FGF2 and α1 localization into these nanodomains and therefore Cav2 KO reduced FGF2-GFP secretion in previously shown cell surface biotinylation experiments.

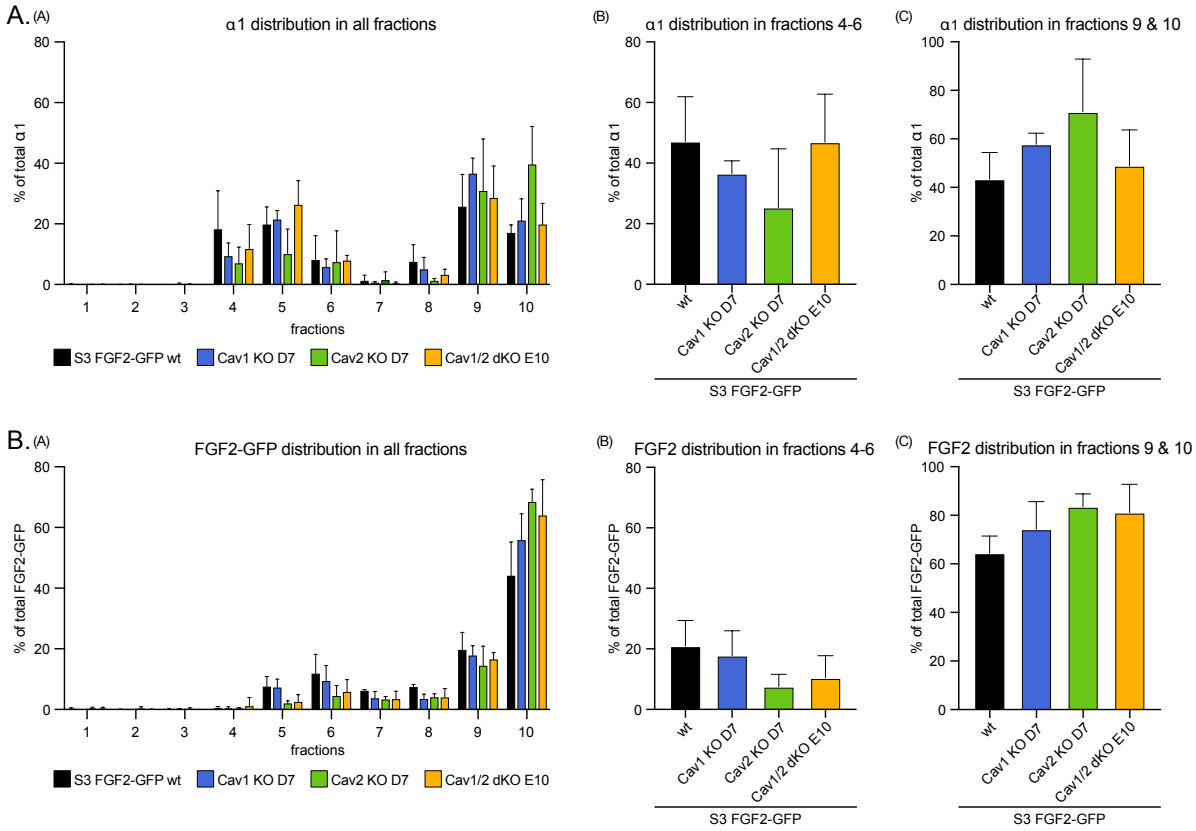

Figure 32: DRM experiment quantification showed protein redistribution into detergent soluble membrane fractions for Cav2 KO. S3 FGF2-GFP wt, Cav1 KO D7, Cav2 KO D7 and Cav1/2 dKO E10 cells were analyzed via DRM fractionation and quantifications were performed for 4 experiments. A. Distribution of α1 in all cell lines (A) throughout all fractions, (B) in fractions 4-6 and (C) in soluble fractions 9 & 10. B. Distribution of FGF2-GFP in all cell lines (A) throughout all fractions, (B) in fractions 4-6 and (C) in soluble fractions 9 & 10. Statistical analysis was performed via one-way Anova combined with Tukey`s post hoc test (ns $p > 0,05$; * $p \leq 0,05$; ** $p \leq 0,01$; *** $p \leq 0,001$, **** $p \leq 0,0001$).

4.3.4 Cav2 overexpression did not rescue the FGF2-GFP secretion phenotype

To confirm the phenotype observed for Cav2 KO in reducing FGF2 secretion in biotinylation experiments and observations made in DRM experiments, I generated S3 FGF2-GFP cells overexpressing Cav2 in the Cav2 KO clones C2 and D7. Additionally, I overexpressed Cav1 and Cav2 in wt cells expressing endogenous protein levels. As seen in Figure 33A. Cav1 was overexpressed successfully in S3 FGF2-GFP wt cells and also Cav2 was successfully overexpressed in wt or Cav2 KO cells. Upon overexpression of Cav2 a double band appeared with one band at the size of before seen protein below 25 kDa and a second band slightly above. This might resemble a differently modified form of Cav2 or a different isoform which was not present under endogenous expression control. Cav1 and Cav2 overexpressing cells were tested in cell surface biotinylation experiments and compared to wt and Cav2 KO cells. Overexpression of Cav1 or Cav2 in wt cells on top of endogenous protein levels did not impact FGF2-GFP secretion (Figure 33B. and C.). In these biotinylation experiments Cav2 KO C2 showed a 30 % reduction in surface FGF2-GFP while Cav2 KO D7 showed an even stronger reduction of approximately 60%. Reintroduction and overexpression of Cav2 in Cav2 KO clones C2 and D7 did not alter the secretion phenotypes though and did not increase surface FGF2-GFP levels.

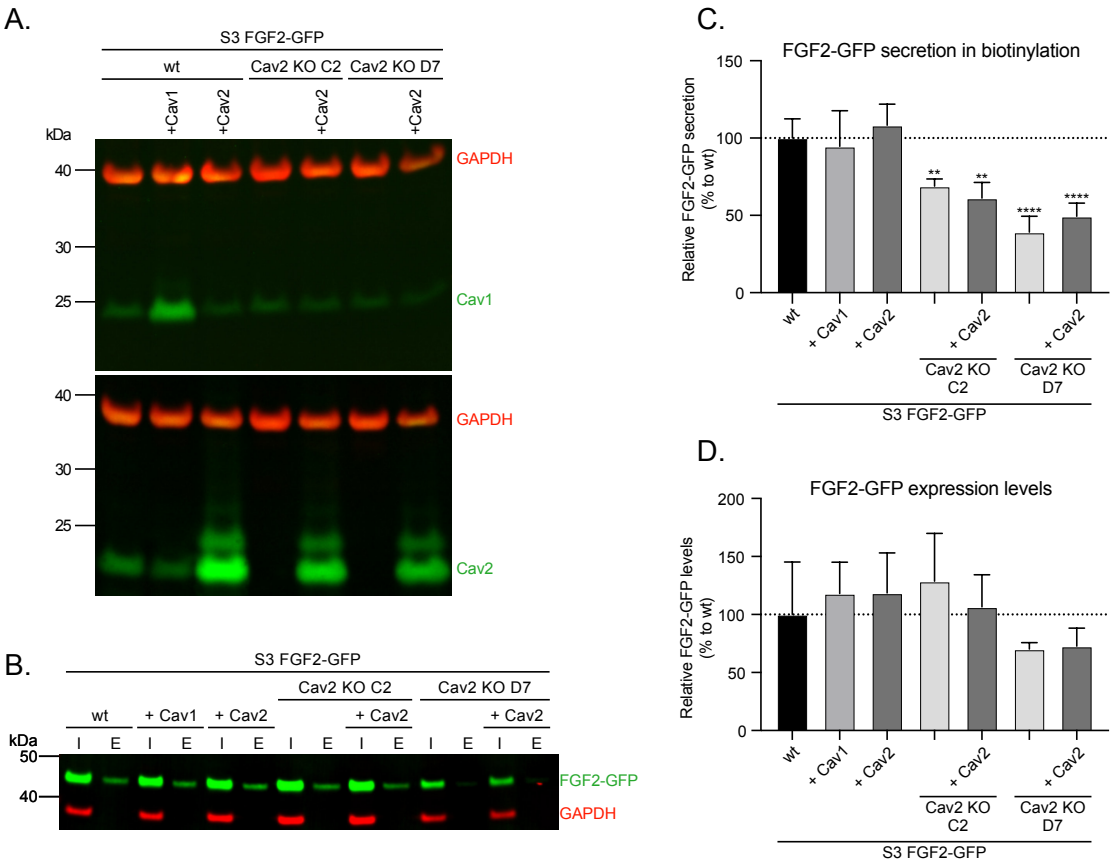

Figure 33: Cav2 overexpression in Cav2 KO cells could not rescue the secretion phenotype. S3 FGF2-GFP Cav2 KO clones C2 and D7 were used to stably overexpress Cav2. Wt cells were also used to overexpress Cav1 or Cav2 additionally to endogenous protein levels. A. Representative Western blot analysis showing Cav1 or Cav2 (in green) overexpression and GAPDH (in red) as loading control. B. Representative Western blot from cell surface biotinylation experiments testing FGF2-GFP secretion efficiency for cells induced with doxycycline. Inputs (I) and eluates (E) were loaded for both FGF2-GFP (anti-rabbit FGF2 antibody, in green) and GAPDH (anti-mouse GAPDH antibody, in red). C. Quantification from 4 experiments showing FGF2-GFP secretion efficiency normalized to wt cells. D. Quantification from 4 experiments showing FGF2-GFP expression levels normalized to wt cells. Statistical analysis was performed via one-way Anova combined with Tukey`s post hoc test testing significance to wt cells (ns $p > 0,05$; * $p \leq 0,05$; ** $p \leq 0,01$; *** $p \leq 0,001$, **** $p \leq 0,0001$).

To find possible explanations for the failed rescue and more insights on the second protein band appearing upon overexpression, I performed DRM experiments to examine overexpressed protein localization and to determine whether Cav2 overexpression could restore Cav1 localization to liquid ordered membrane fractions and shift α1 and FGF2-GFP back into detergent resistant membrane fractions. As seen in Figure 34A. Cav2 knockout caused caveolin-1 to shift out of liquid ordered detergent resistant membrane fractions and more into the heavier soluble fractions, as observed before. Upon overexpression of Cav2 Cav1 shifted back to DRM fractions. In wt cells Cav2 was detected at similar protein levels throughout fractions 4-10, whereas Cav2 KO showed clear absence of the protein. Overexpression of Cav2 in Cav2 KO D7 showed Cav2 to be present again in DRM fractions 4-6 near to wt levels. Increased levels of Cav2 were detected in fractions 7-10, where also the before observed second band appeared. This indicated that Cav2 presence in liquid ordered membrane fractions was restored in Cav2 overexpressing cells, yet overexpressed Cav2 localized preferentially into non-lipid raft fractions.

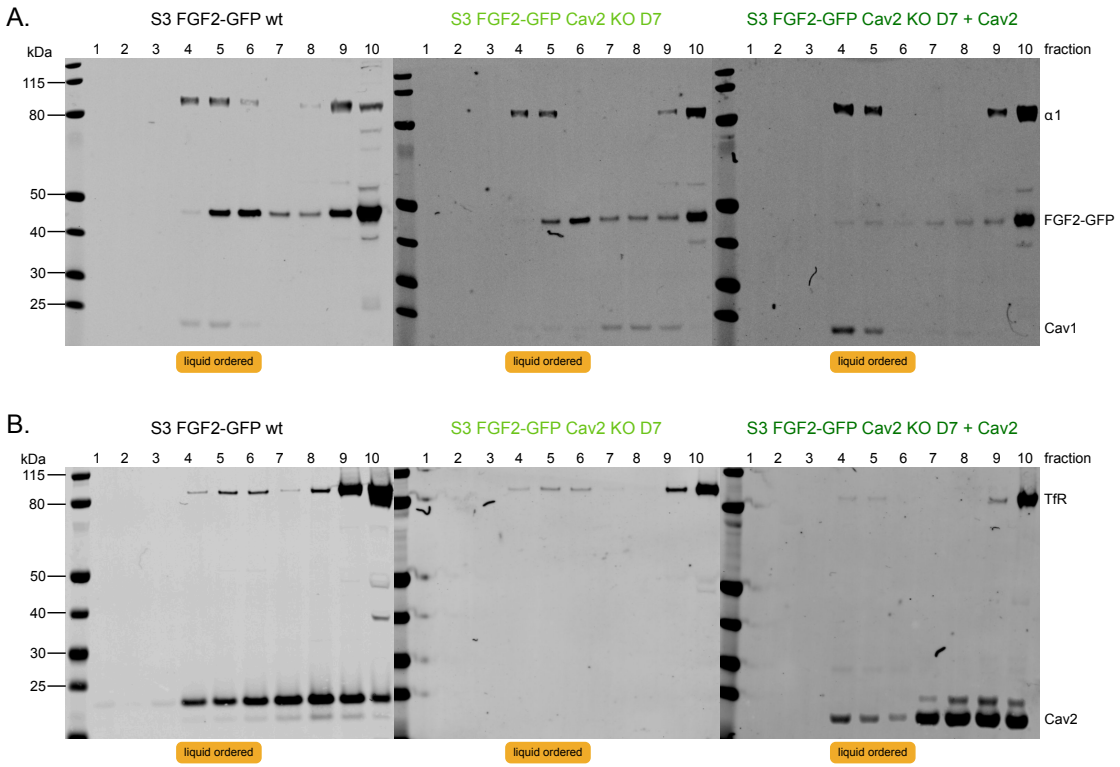

Figure 34: Cav2 overexpression in DRM experiments showed localization of Cav1 into liquid ordered membrane fractions. S3 FGF2-GFP wt, Cav2 KO D7 and Cav2 KO D7 + Cav2 cells were used for isolation of detergent resistant membrane fractions. Representative Western blots showing all 10 fractions from mentioned cell lines. (A) Proteins were detected via anti-mouse α1 antibody, anti-rabbit FGF2 antibody and anti-rabbit Cav1 antibody. (B) Proteins were detected via anti-mouse transferrin receptor (TfR) and anti-rabbit Cav2 antibody.

Samples were also analyzed in regard to α1 and FGF2-GFP levels in liquid ordered rafts in comparison to later detergent soluble membrane fractions. As seen in Figure 35A. and B. α1 and FGF2-GFP protein levels were quantified for all fractions from DRM isolation experiments. α1 levels in DRM fractions 4-6 were reduced in Cav2 KO D7 compared to wt cells and shifted into the later fractions 9 and 10. Overexpression of Cav2 slightly reduced this observation, yet high variations did not allow for strong statements. FGF2-GFP levels showed no difference between Cav2 knockout or overexpressing cells. In both cases FGF2 levels were significantly decreases in contrast to wt cells in the fractions 4-6 and increased in fractions 9 and 10. From these data it can be concluded that Cav2 overexpression could restore correct localization of Cav1 into liquid ordered DRM fractions, yet failed to fully recruit α1 and FGF2-GFP back into these domains. This potentially explained the lack in rescue in before conducted cell surface biotinylation experiments.

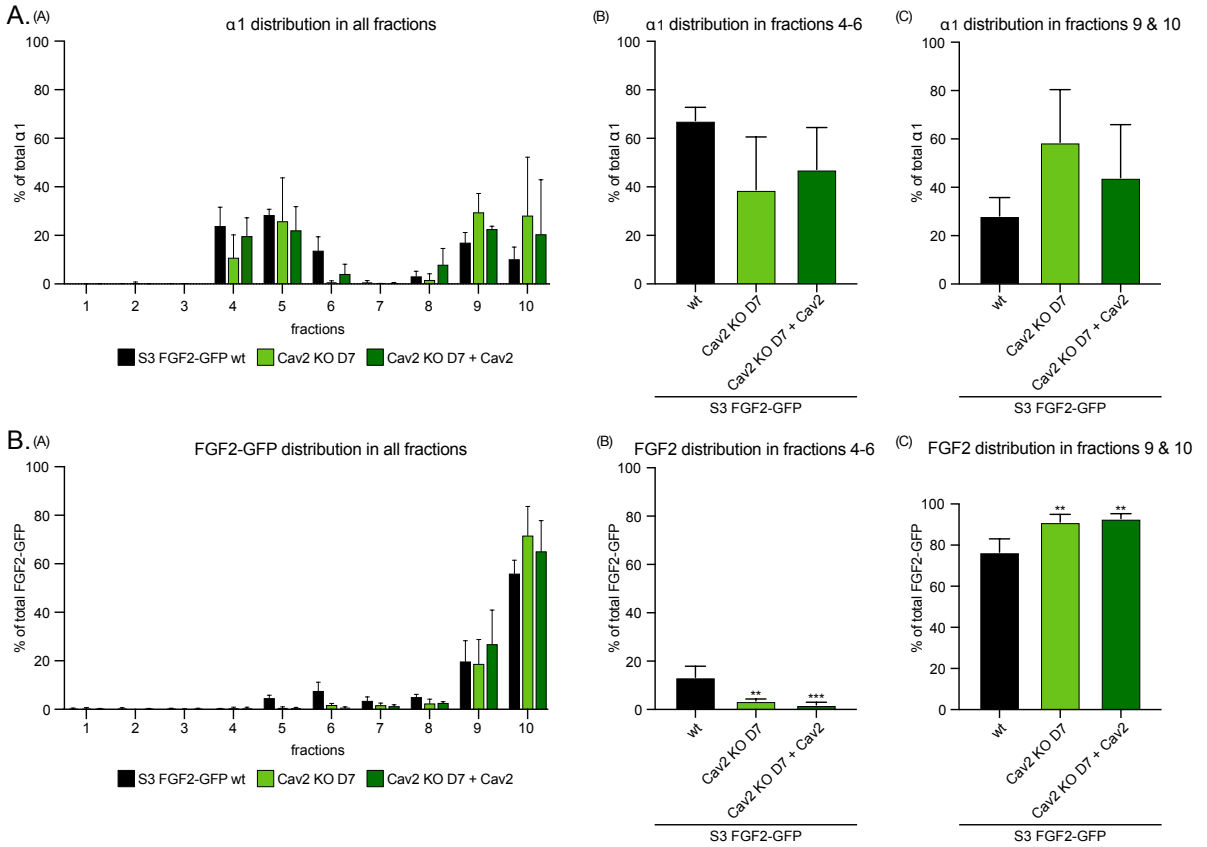

Figure 35: Analysis of α1 and FGF2-GFP levels in DRM fractions isolated from Cav2 KO and Cav2 overexpressing cells. S3 FGF2-GFP wt, Cav2 KO D7 and Cav2 KO D7 + Cav2 cells were analyzed via DRM isolation experiments and α1 and FGF2-GFP levels were quantified. A. Quantification of α1 levels in (A) all DRM experiment fractions and in (B) fractions 4-6 and (C) fractions 9 and 10. B. Quantification of FGF2-GFP levels in (A) all DRM experiment fractions and in (B) fractions 4-6 and (C) fractions 9 and 10. N = 4 experiments. Statistical analysis was performed via one-way Anova combined with Tukey`s post hoc test testing significance to wt cells (ns p > 0,05; * p ≤ 0,05; ** p ≤ 0,01; *** p ≤ 0,001, **** p ≤ 0,0001).

As additional analysis to DRM experiments also immunofluorescence staining was performed on Cav1 and Cav2 overexpressing HeLa S3 cells to analyze protein localization in intact cells (Figure 36). As observed before, Cav1 localized at the membrane in wt cells in a dot-like fashion in patches of different sizes and showed some intracellular staining. Cav2 in contrast preferentially localized into the perinuclear space, possibly the Golgi, and was only found in very few puncta at the membrane. Cav1 overexpression in wt cells led to some intracellular protein aggregation but did not change localization at the membrane. Cav2 intracellular and perinuclear levels seemed reduced in at cells overexpressing Cav1, indicating interconnection of protein expression. A reduction of about 25% of Cav2 levels in wt cells overexpressing Cav1 could also be seen before in cell lysates (Figure 33A.) when Cav2 levels were quantified (only one experiment). When Cav2 was overexpressed in wt cells a massive increase in intracellular Cav2 was observed, yet there was no evidence of increased Cav2 localization to the membrane. Despite being very strongly overexpressed, Cav2 did not evidently impact cellular Cav1 levels or localization. Caveolin-2 knockout strongly reduced Cav2 antibody staining to a weak background staining for both clones C2 and D7, though background was higher for Cav2 KO C2 which might reflect the weaker phenotype observed in cell surface biotinylation experiments. Cav2 KO C2 had reduced membrane caveolin-1 and in Cav2 KO D7 caveolin-1 even fully failed to localize to the

membrane and instead localized intracellularly to the perinuclear space. Overexpression of Cav2 in both clones lead to great increase in Cav2 intracellular staining as was observed for the wt. In Cav2 KO C2 caveolin-2 overexpression was able to increase Cav1 signals at the membrane, indicating that Cav2 regulates Cav1 localization. Overexpression of Cav2 in Cav2 KO D7 did not show a strong membrane localization for Cav1, yet reversed the intracellular localization of Cav1.

In sum, these immunofluorescence data support previous biotinylation and DRM experiments. Apparently, there is protein cross-talk between Cav1 and Cav2 as Cav1 overexpression reduced Cav2 levels both in IF and in cell lysates. Cav2 however regulated Cav1 localization and was needed for Cav1 recruitment to the membrane (seen in IF, Figure 36) and to detergent resistant liquid ordered membrane areas (seen in DRM experiments, Figure 31 and Figure 32). Both Cav2 KO clones showed phenotypes in FGF2-GFP biotinylation experiments (Figure 33) and impacted protein distribution in DRM experiments, whereat the severity of the phenotype was also reflected in IF experiments looking at the subcellular localization of Cav1 and Cav2.

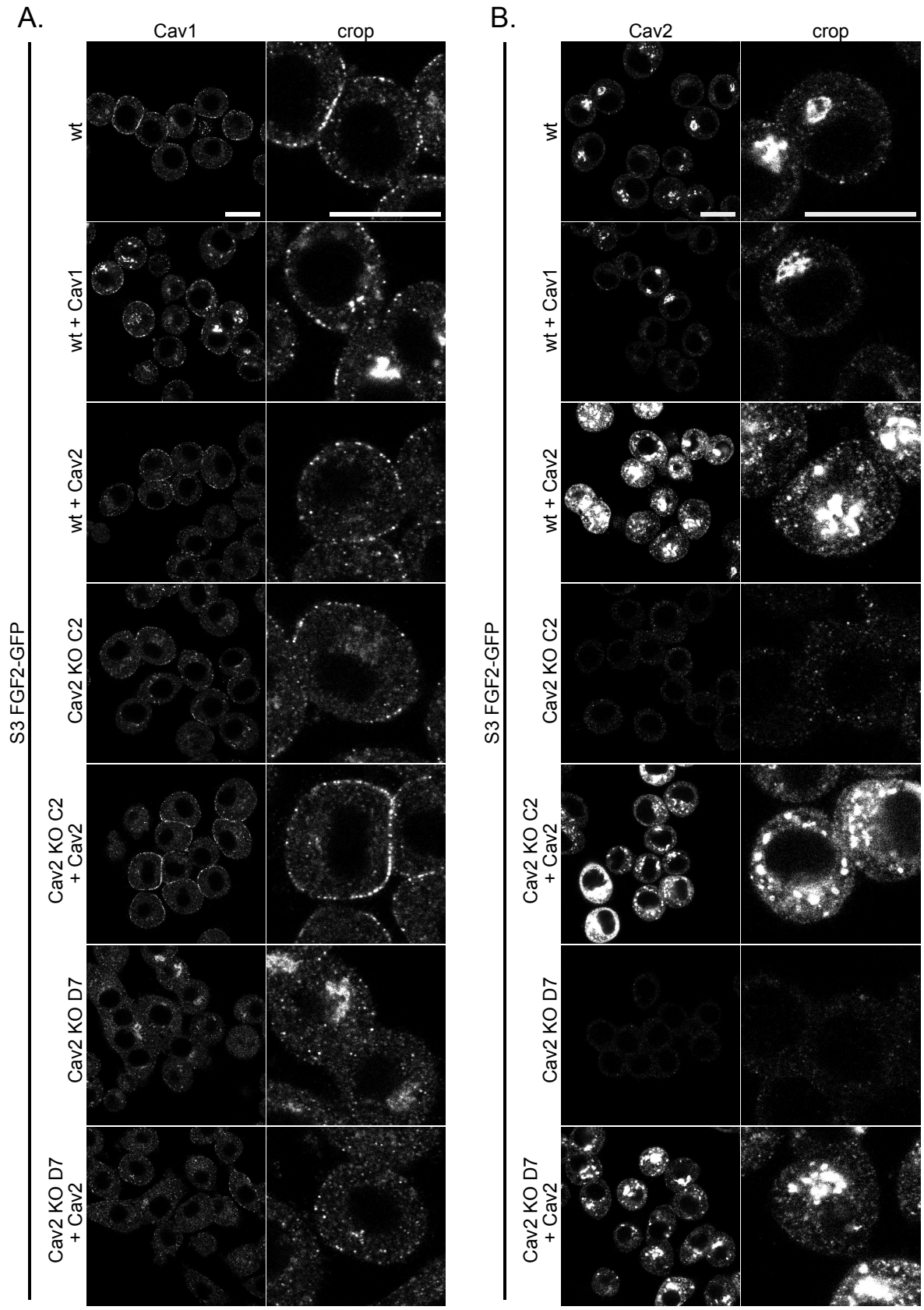

Figure 36: Cav1 and Cav2 cellular localization in immunofluorescence and analysis of protein countereffects. HeLa S3 FGF2 GFP wt, + Cav1, + Cav2 and Cav2 KOs C2 and D7 overexpressing Cav2 cells were analyzed via immunofluorescence confocal microscopy. In different samples (A) Cav1 and (B) Cav2 were detected using corresponding antibodies. Fixed cells imaged on a Zeiss LSM800 confocal microscope. Scale bar represents 20 µm.

To assay whether Cav1/Cav2 overexpression or Cav2 KO also alter FGF2-GFP and α1 localization in an alternative non-DRM experiment, immunofluorescence staining of FGF2 and α1 was performed in above used overexpression cell lines (Figure 37). FGF2-GFP was detected via GFP fluorescence, showing a strong nuclear signal due to FGF2 C-terminal NLS, or by FGF2 antibody staining showing an even intracellular staining for cells with high expression levels, since cells were permeabilized in contrast to Figure 18, where no permeabilization was performed (FGF2 signal seen only at membrane). Anti-mouse α1 antibody staining showed an exclusively membrane-localized signal. Overall FGF2 and α1 staining did not change upon Cav1 or Cav2 overexpression in wt cells. Also, Cav2 KO did not have an impact in IF on FGF2-GFP localization despite impacting FGF2-GFP secretion in biotinylation experiments. Yet, only a small percentage of expressed FGF2 in on cell surfaces (2-4%) and this small portion is not visible in these microscopy images due to resolution and due to permeabilization of the cells. One could repeat these experiments with non-permeabilized cells, but quantitative data collection might require super-resolution STED or TIRF recruitment and translocation experiments. Due to the very round shape of HeLa S3 cells TIRF microscopy was unfortunately not possible. Also, α1 staining at the plasma membrane was not evidently affected by caveolin-2 KO in these immunofluorescence experiments (Figure 37). Again, this would require higher resolved imaging, to analyze whether shifting of α1 into different domains can be observed as was indicated in DRM experiments.

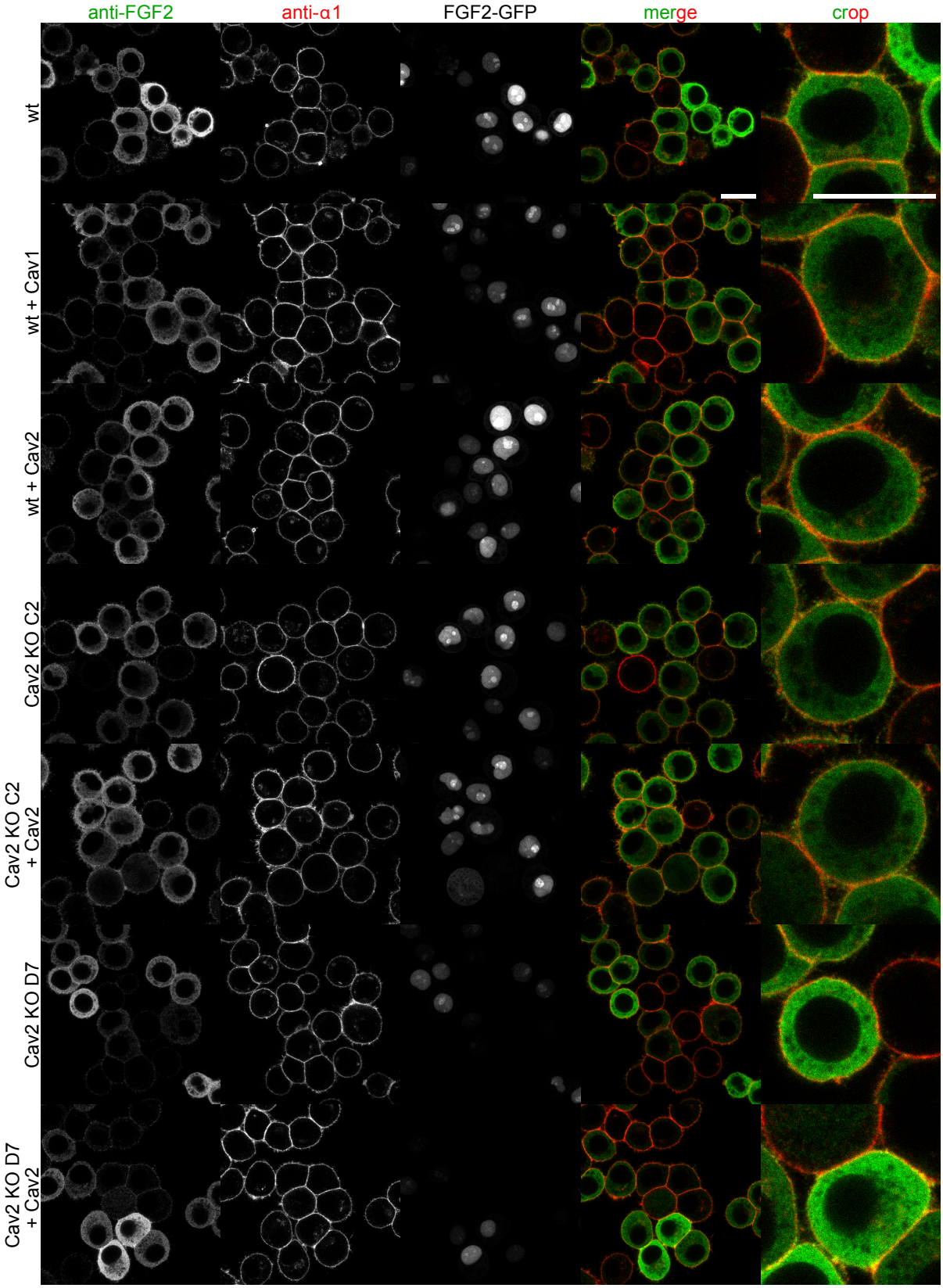

Figure 37: Immunofluorescence staining of FGF2-GFP and α1 in caveolin overexpression cell lines and KOs. HeLa S3 FGF2-GFP wt, wt + Cav1, wt + Cav2, Cav2 KOs C2 and D7, as well as C2 + Cav2 and D7 + Cav2 cell lines were analyzed in immunofluorescence staining and imaged on a Zeiss LSM800 confocal microscope. Cells were fixed and permeabilized. FGF2-GFP was imaged via GFP fluorescence and anti-rabbit FGF2 antibody staining (in green) while α1 was stained via anti-mouse α1 antibody (in red). Merged and cropped images are shown for FGF2 and α1 antibody channels. Scale bar 20 µm.

4.3.5 The order of caveolin KO altered secretion phenotypes

As mentioned in section 4.3.2 Cav2 KO showed a phenotype in FGF2-GFP cell surface biotinylation experiments, whereas Cav1/2 dKO originating from the Cav1 KO D7 single clone did not. Reasons for this could be that the order of knockout is relevant, the Cav1 KO clone D7 was defective from the very start or that there are compensatory events taking place upon knockout of all caveolins expressed in HeLa cells.

To challenge these ideas, caveolin-1/2 double knockouts were generated in HeLa S3 FGF2-GFP cells originating from the Cav2 KOs C2 and D7, which exhibited reduced FGF2-GFP secretion efficiencies before. Double KO of Cav1 and Cav2 was validated via genomic DNA sequencing and Western blot analysis (Figure 6A.). Cell surface biotinylation experiments showed no striking differences between Cav2 KOs and Cav1/2 dKOs (Figure 38B. and C.). Only additional caveolin-1 KO in Cav2 KO C2 significantly reduced surface FGF2-GFP from 55% to 24% in dKO clone B10. This effect was not reproducible for the other clones. dKO B5 showed similar surface FGF2-GFP levels to the parental Cav2 KO clone and dKOs B6 and C3 even showed increased secretion efficiencies. The dKOs originating from Cav2 KO D7 also did not show a further reduction in FGF2-GFP secretion, but rather had slightly increased surface FGF2 despite expressing less FGF2-GFP (Figure 38B.-D. subpanels (B)). Yet secretion levels were still significantly different from wt cells and followed the trend seen for Cav2 KO D7.

These data demonstrate that caveolin-2 on its own has an effect on FGF2-GFP secretion and double knockout of both caveolin-1 and caveolin-2 in tendency shows similar FGF2-GFP secretion phenotypes to the parental cell lines. Secretion is even mildly increased in a few cases, indicating possible additional compensatory effects within the cell. For these new dKOs surface FGF2-GFP levels never reach wt levels, as it was the case for dKOs originating from Cav1 KO cells (Figure 29). As single outlier dKO clone B10 further decreased FGF2-GFP secretion in contrast to the parental Cav2 KO clone C2, yet this was not reproducible for other clones.

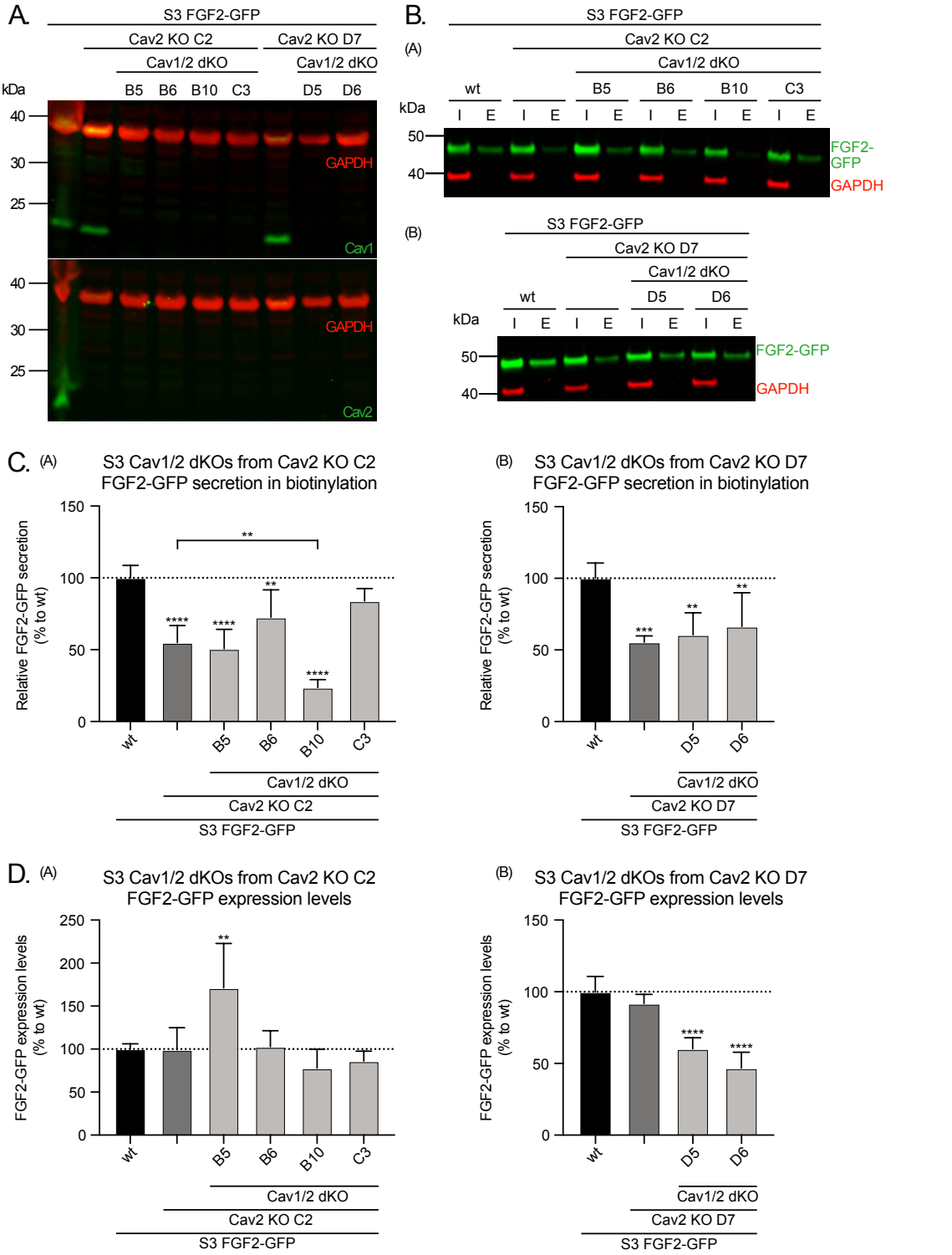

Figure 38: Cav1/2 dKOs generated from Cav2 KOs did not show significant difference in FGF2-GFP secretion efficiencies compared to parental cell lines. S3 FGF2-GFP Cav2 KO C2 and D7 were used to generate in total 6 new dKO single clones. A. Representative Western blot showing Cav1 or Cav2 levels detected via antibody staining (in green) together with GAPDH (in red) in the stated cell lines. B. Representative Western blot images from cell surface biotinylation experiments of cells induced with doxycycline (A) Cav2 KO C2 and dKOs B5, B6, B10 and C3 and for (B) Cav2 KO D7 and dKOs D5 and D6. Both inputs (I) and eluates (E) are shown for all cell lines detecting FGF2-GFP via anti-rabbit FGF2 antibody (in green) and anti-mouse GAPDH (in red) as control. C. Quantification of FGF2-GFP secretion efficiencies relative to wt for (A) Cav2 KO C2 and dKOs B5, B6, B10 and C3 and for (B) Cav2 KO D7 and dKOs D5 and D6. D. Quantification of FGF2-GFP expression levels of (A) Cav2 KO C2 and dKOs B5, B6, B10 and C3 and for (B) Cav2 KO D7 and dKOs D5 and D6 normalized to wt cells. N = 4 experiments. Statistical analysis of all clones was performed via one-way Anova combined with Tukey's post hoc test where clones were compared to wt cells. Cav2 KO C2 was compared to dKO B10 via unpaired t-test with Welch's correction (ns $p > 0,05$; * $p \leq 0,05$; ** $p \leq 0,01$; *** $p \leq 0,001$, **** $p \leq 0,0001$).

4.3.6 Caveolin-1 KO in U2OS FGF2-GFP did not impact FGF2 secretion in biotinylation, but did in TIRF

Due to above mentioned imaging limitations for HeLa S3 cells, I decided to recapitulate the role and impact of caveolin-1 and -2 in U2OS cells. U2OS cells are well suitable for TIRF microscopy and confirming results in an additional cell line would provide more confidence that caveolins play a role in FGF2-GFP secretion and act as potential organizers within liquid ordered membrane domains.
Caveolin-1 knockout was validated for single clones B3, B6, B10 and C3 in U2OS FGF2-GFP cells by genomic DNA sequencing and Western blot analysis using anti Cav1 antibody (Figure 39A.). For clones B6, B10 and C3 caveolin-1 KO seemed to reduce Cav2 expression levels in cell lysates. U2OS Cav1 KOs were analyzed via cell surface biotinylation experiments to assess FGF2-GFP secretion efficiencies in comparison to wt cells (Figure 39B. and C.). Surface FGF2-GFP was only significantly reduced in KO clone B3, despite that clone showing higher FGF2-GFP expression levels quantified from biotinylation experiments. Clones B6, B10 and C3 did not show significant changes in surface FGF2-GFP, whereby C3 even had slightly increased surface FGF2-GFP. To test FGF2 secretion in an alternative assay, Roberto performed TIRF microscopy of U2OS Cav1 KO clones, as described previously in 4.1.4. Strikingly, TIRF translocation assay showed a significant decrease in surface FGF2-GFP detected via anti-GFP nanobody staining for all caveolin-1 KO clones (Figure 39D.). All clones displayed 22 – 34 % less surface FGF2-GFP in comparison to wt cells. TIRF microscopy can not only be used to quantify FGF2-GFP translocation in fixed cells, but also to observe single particle FGF2-GFP recruitment to the inner plasma membrane leaflet in living cells that are not induced with doxycycline. For this, Roberto imaged U2OS Cav1 KO clones in live cell imaging solution and GFP particles were quantified for each cell via trackmate Plugin in Fiji [238]. Quantitative analysis from 4 TIRF recruitment experiments only showed a weak decrease in FGF2-GFP recruitment to the inner plasma membrane leaflet for most clones. Only clone C3 showed a significant decrease to 72% recruitment efficiency compared to wt cells (Figure 39E.).
These data demonstrate that it is not sufficient to rely on data from cell surface biotinylation experiments, but that TIRF experiments should be conducted additionally to use a different method to quantify surface FGF2-GFP. Perhaps, weak phenotypes are not seen in biotinylation because the very small biotin can even detect FGF2-GFP particles from FGF2 oligomers that haven't translocated to the cell surface. Nanobodies (and antibodies) are bigger in size and can detect only surface FGF2-GFP. Therefore, both assays should be conducted whenever possible.

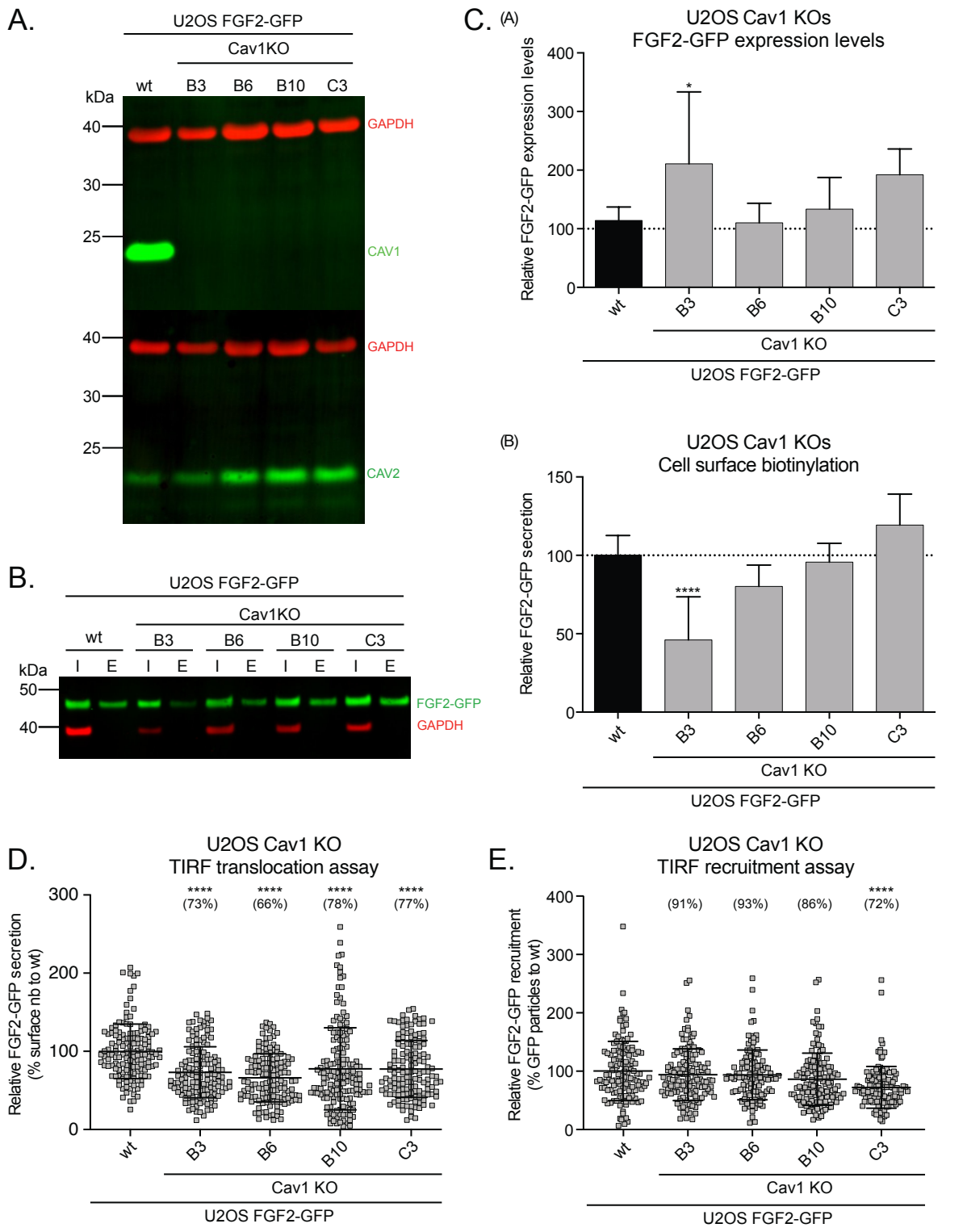

Figure 39: U2OS FGF2-GFP caveolin-1 KO did not show a FGF2-GFP secretion phenotype in cell surface biotinylation but did impact FGF2 secretion and recruitment in TIRF microscopy. U2OS FGF2-GFP cells were used to generate Cav1 KO single clones B3, B6, B10 and C3. A. Cav1 KO was confirmed via anti-rabbit Cav1 antibody staining (in green) in a representative Western blot also showing GAPDH (in red). B. Representative Western blot images from cell surface biotinylation experiments of cells induced with doxycycline. Both inputs (I) and eluates (E) are shown for all cell lines detecting FGF2-GFP via anti-rabbit FGF2 antibody (in green) and anti-mouse GAPDH (in red) as control. C. Quantification of (A) FGF2-expression levels and (B) FGF2-GFP secretion efficiency from n = 5 experiments. D. Quantification of FGF2-GFP secretion efficiency via TIRF translocation assays for n = 4 experiments. E. Intracellular FGF2-GFP particles at the plasma membrane quantified via TIRF recruitment assay for n = 4 experiments. All statistical analysis was performed via one-way Anova combined with Tukey's post hoc test where clones were compared to wt cells (ns $p > 0,05$; * $p \leq 0,05$; ** $p \leq 0,01$; *** $p \leq 0,001$, **** $p \leq 0,0001$).

4.3.7 Overexpression of Cav1 or Cav2 in U2OS cells did not impact FGF2-GFP secretion in biotinylation

When I generated S3 Cav2 KO cell lines overexpressing Cav2 and wt cells overexpressing both Cav1 or Cav2, I decided to also generate U2OS cell lines stably overexpressing Cav1 or Cav2. U2OS FGF2-GFP wt cells were used to overexpress Cav1 or Cav2 on top of endogenous protein to see if general protein overexpression had an impact on FGF-GFP secretion. Additionally, Cav1 KOs B6 and B10 were used to overexpress and reconstitute Cav1.

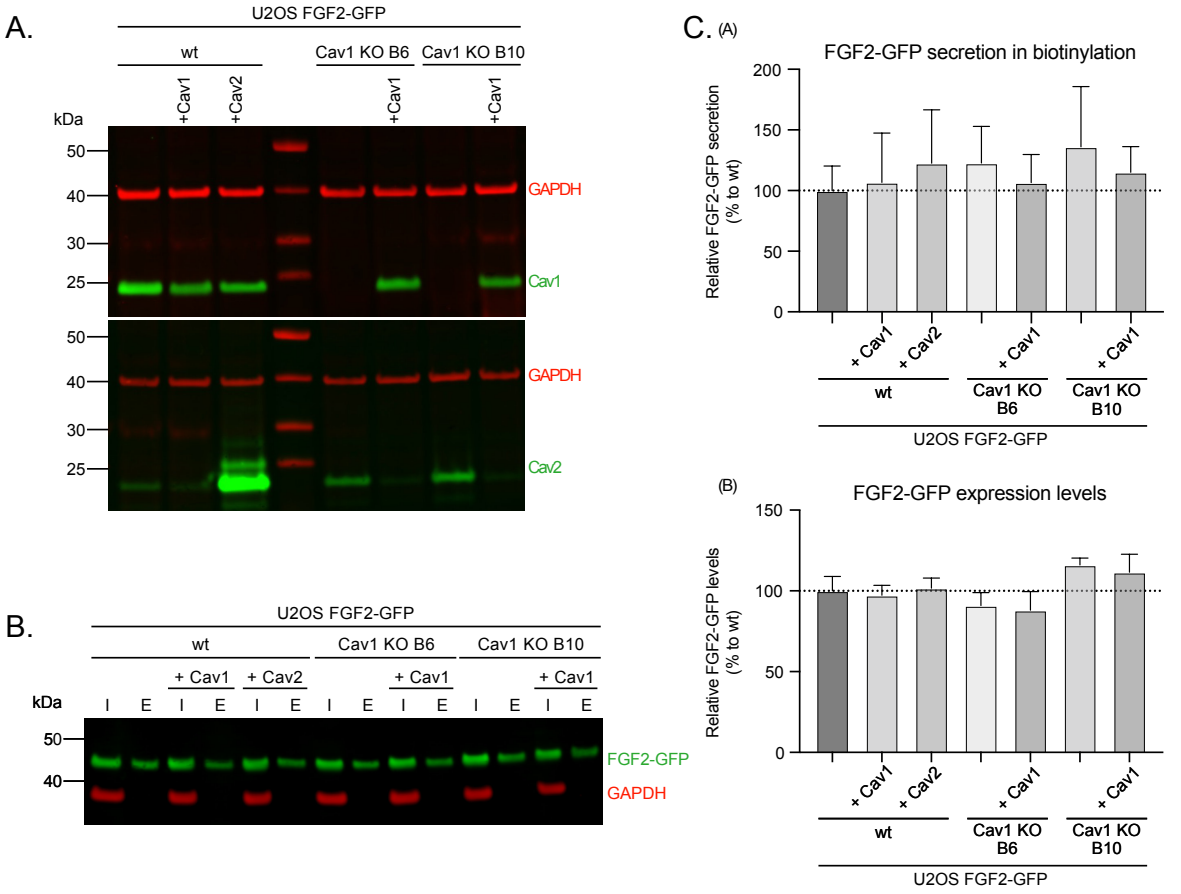

Figure 40: U2OS FGF2-GFP cells overexpressing Cav1 or Cav2 did not have a phenotype in cell surface biotinylation experiments testing FGF2-GFP secretion. U2OS FGF2-GFP wt cells were used to overexpress Cav1 and Cav2. Cav1 KO clones B6 and B10 were used to reintroduce and overexpress Cav1. A. Representative Western blot from generated cell lines showing Cav1 or Cav2 (in green) expression levels and GAPDH (in red) as control. B. Representative Western blot images from cell surface biotinylation experiments of cells induced with doxycycline. Both inputs (I) and eluates (E) are shown for all cell lines detecting FGF2-GFP via anti-rabbit FGF2 antibody (in green) and anti-mouse GAPDH (in red) as control. C. Quantifications from 4 experiments showing (A) relative FGF2-GFP secretion efficiencies to wt cells and (B) relative FGF2-GFP expression levels. Statistical analysis was performed via one-way Anova combined with Tukey's post hoc test where clones were compared to wt cells (ns $p > 0,05$; * $p \leq 0,05$; ** $p \leq 0,01$; *** $p \leq 0,001$, **** $p \leq 0,0001$).

As seen in Figure 40A. Cav2 overexpression was successful in U2OS wt cells. Also here, as seen for HeLa S3 cells, a second and even a weak third band was seen for Cav2 which was not present at endogenous protein expression levels. These might represent different Cav2 isoforms or differently modified protein. Cav1 levels did not increase in wt cells overexpressing Cav1, indicating that either cell

line generation was not successful, despite selection with antibiotic resistance, or that caveolin-1 cannot be overexpressed in U2OS due to regulatory mechanism controlling Cav1 protein levels. In Cav1 KO cells overexpression and reintroduction of Cav1 led to similar protein levels as for wt cells, supporting the hypothesis that Cav1 protein levels are tightly regulated in U2OS. Remarkably, the overexpression of Cav1 in Cav1 KO cells led to a strong decrease in Cav2 signals. Similar effects were observed before in HeLa S3 wt cells overexpressing Cav1 in immunofluorescence staining (Figure 36) and cell lysates (Figure 33A.), yet not as strongly as seen here for U2OS cells. As expected from cell surface biotinylation experiments with U2OS Cav1 KOs, overexpression of Cav1 or also Cav2 in wt cells did not have an impact on FGF2-GFP secretion efficiency (Figure 40B. and C.). Whether Cav1 overexpression can rescue the decrease in surface FGF2-GFP seen in TIRF translocation remains to be clarified and will not be presented within this thesis due to long maintenance and inaccessibility of the TIRF microscope.

4.3.8 Neither Cav2 KO nor Cav1/2 dKO in U2OS altered FGF2-GFP secretion in biotinylation

U2OS FGF2-GFP cells were used to generate Cav2 KO cells and Cav1/2 dKO cells originating from Cav1 KOs B6 and B10, as was done before for HeLa S3 cells. As seen in Figure 41, Cav2 KO surprisingly and in contrast to HeLa S3 cells did not reduce FGF2-GFP secretion in cell surface biotinylation experiments. A slight decrease in surface FGF2-GFP was observable for clone F4 (65 %), yet this clone also displayed significantly reduced FGF2-GFP expression levels (29%) making comparison to wt cells inappropriate. Cav2 KO G6 which had similar expression levels (110%) to wt cells also had a similar FGF2-GFP secretion efficiency of around 115% compared to wt (Figure 42C.).

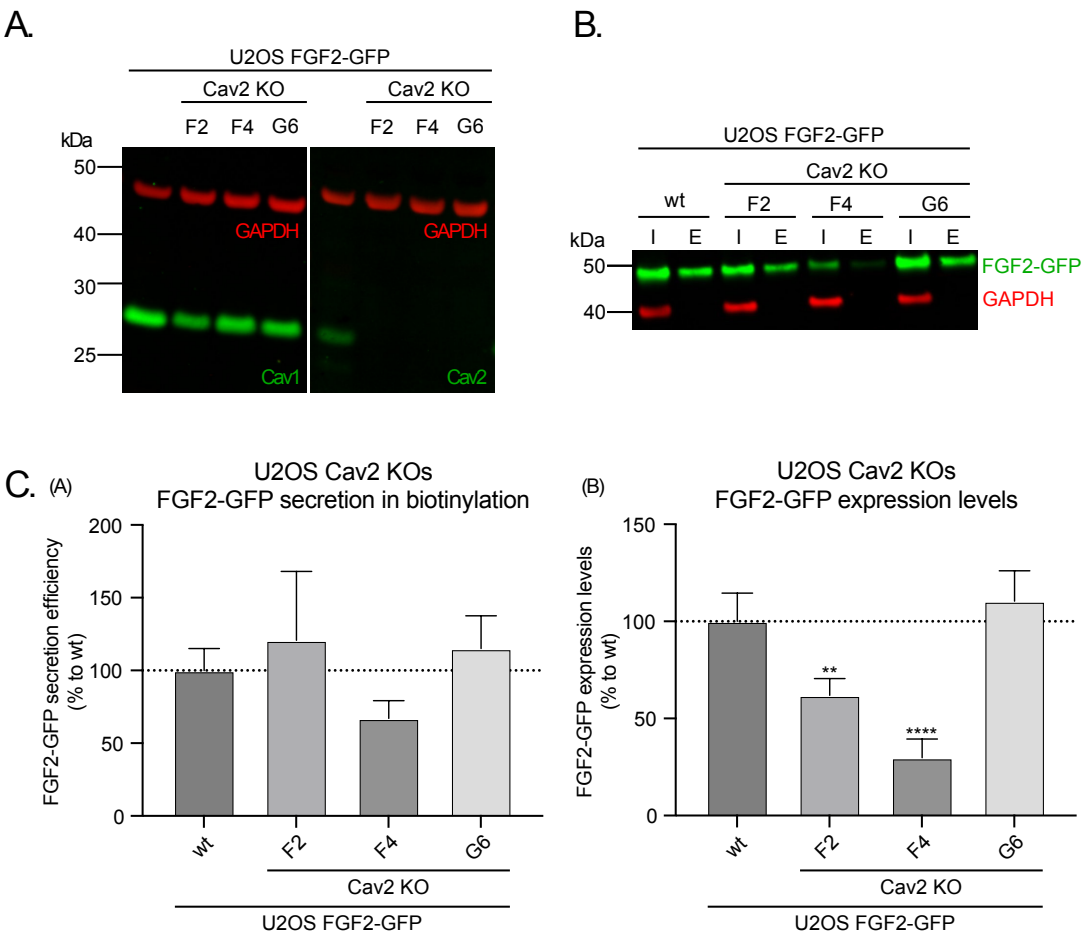

Figure 41: Cav2 KO did not reduce FGF2-GFP secretion in U2OS FGF2-GFP. Cav2 KO clones F2, F4 and G6 were generated from U2OS FGF2-GFP wt cells. A. Representative Western blot from generated cell lines showing Cav1 or Cav2 (in green) expression levels and GAPDH (in red) as control. B. Representative Western blot images from cell surface biotinylation experiments of cells induced with doxycycline. Both inputs (I) and eluates (E) are shown for all cell lines detecting FGF2-GFP via anti-rabbit FGF2 antibody (in green) and anti-mouse GAPDH (in red) as control. C. Quantifications from 4 experiments showing (A) relative FGF2-GFP secretion efficiencies to wt cells and (B) relative FGF2-GFP expression levels. Statistical analysis was performed via one-way Anova combined with Tukey's post hoc test where clones were compared to wt cells (ns $p > 0,05$; * $p \leq 0,05$; ** $p \leq 0,01$; *** $p \leq 0,001$, **** $p \leq 0,0001$).

Cav1/2 dKO in U2OS Cav1 KO B6 and B10 cells also did not affect FGF2-GFP secretion (Figure 42). This is congruent with previous data collected with HeLa S3 Cav1/2 dKO cells originating from Cav1 KO cells. As for Cav1 and Cav2 overexpressing cells, unfortunately no TIRF experiments were possible at the time for U2OS Cav2 or Cav1/2 dKO cells and will have to be conducted at a later timepoint.

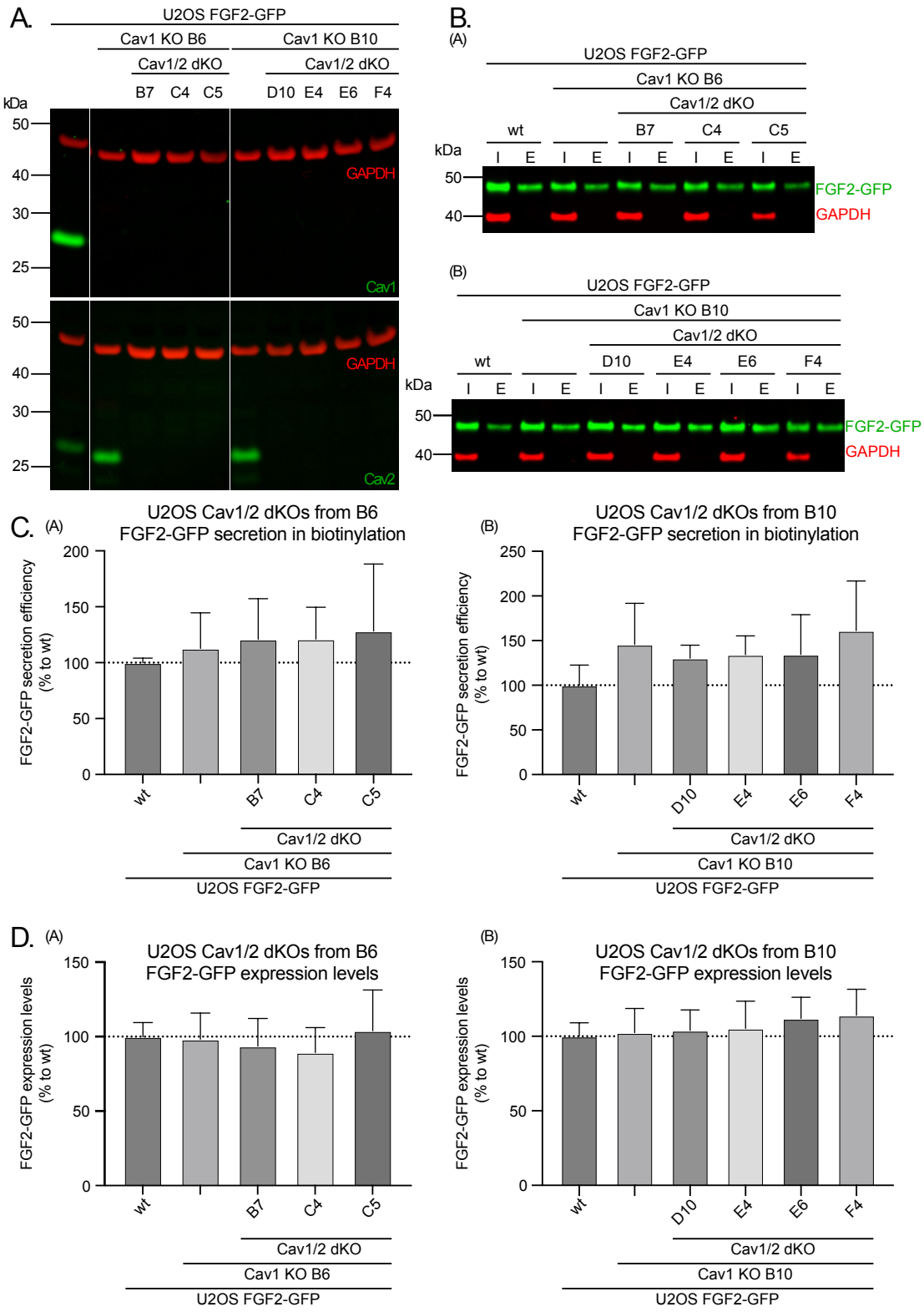

Figure 42: Cav1/2 double KO did not reduce FGF2-GFP secretion in U2OS FGF2-GFP. Cav1 KO clones were used to generate 7 Cav1/2 dKO clones. A. Representative Western blot from generated cell lines showing Cav1 or Cav2 (in green) expression levels and GAPDH (in red) as control. B. Representative Western blot images from cell surface biotinylation experiments of cells induced with doxycycline. Both inputs (I) and eluates (E) are shown for all cell lines detecting FGF2-GFP via anti-rabbit FGF2 antibody (in green) and anti-mouse GAPDH (in red) as control in (A) dKOs originating from Cav1 KO B6 and (B) dKOs originating from Cav1 KO B10. C. Quantifications from 4 experiments showing relative FGF2-GFP secretion efficiencies compared to wt cells for (A) dKOs originating from Cav1 KO B6 and (B) dKOs originating from Cav1 KO B10. D. Quantifications from 4 experiments showing relative FGF2-GFP expression levels compared to wt cells for (A) dKOs originating from Cav1 KO B6 and (B) dKOs originating from Cav1 KO B10. All statistical analysis was performed via one-way Anova combined with Tukey's post hoc test where clones were compared to wt cells (ns $p > 0,05$; * $p \leq 0,05$; ** $p \leq 0,01$; *** $p \leq 0,001$, **** $p \leq 0,0001$).

4.3.9 Cav1 localization into liquid ordered membrane areas was not affected by Cav2 KO in U2OS

The different caveolin knockouts established in U2OS FGF2-GFP cells were tested in DRM experiment to assess whether FGF2-GFP and α1 partitioning into liquid ordered and disordered membrane domains was altered by caveolin removal, although cell surface FGF2 was not affected. U2OS FGF2-GFP wt, Cav1 KO clone B6, Cav2 KO clone G6 and Cav1/2 dKO clone B7 were tested in DRM experiments as they all displayed similar FGF2-GFP expression levels when induced with 1 µg/ml doxycycline.

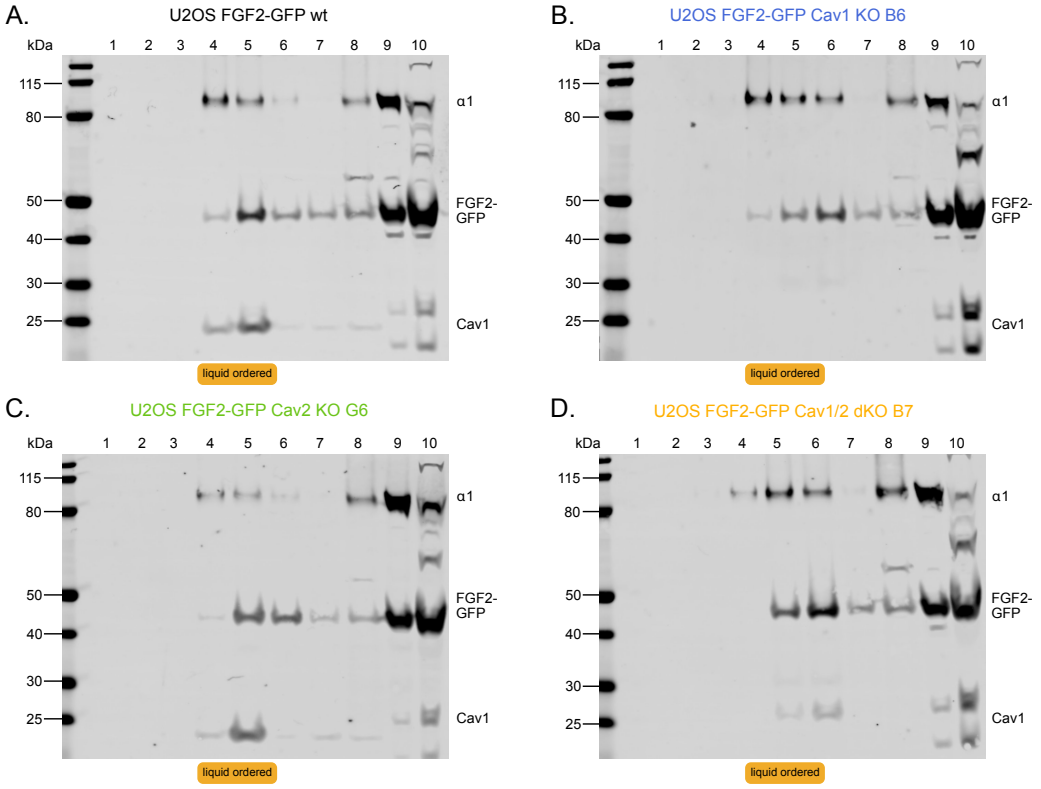

Figure 43: Caveolin knockout in U2OS cells did not impact FGF2 or Cav1 distribution, yet Cav2 KO decreased α1 signals in liquid ordered membrane fractions. A. U2OS FGF2-GFP wt, B. Cav1 KO B6, C. Cav2 KO G6 and D. Cav1/2 dKO B7 cells were analyzed via DRM fractionation. Proteins detected were α1 (anti-mouse antibody), FGF2-GFP (anti-rabbit FGF2 antibody) and Cav1 (anti-rabbit antibody). All 10 fractions are shown. Fractions 1-8 were precipitated and loaded entirely whereas ¼ of fractions 9 and 10 were loaded.

As seen in Figure 43C. Cav2 knockout did not cause Cav1 to move out of liquid ordered membrane areas as it did for HeLa S3 cells. Cav1 was absent in DRM fractions from Cav1 KO B6 cells (Figure 43B.), yet it seemed Cav1 was still expressed in dKO cells (Figure 43D.). When comparing molecular weights though, the bands seen in Cav1/2 dKO were too high to be compared with Cav1 signals in the other cells and must have belonged to another protein. Potentially these represented FGF2-GFP degradation products, as the band was present in fractions also containing a lot of FGF2-GFP. The band also appeared when signal intensity was strongly increased in Cav1 KO B6, even though these cells showed a clear knockout for Cav1 in sequencing results. FGF2-GFP signals throughout the

fractions were comparable in the different cell lines but α1 signals seemed decreased in liquid ordered fractions from Cav2 KO cells.

Quantification from 3 replicates was conducted and results are shown in Figure 44. Only a weak decrease of α1 signals in Cav2 KO liquid ordered fractions was observed with high variation (Figure 44A. subpanel (B)). In Cav1 KO B6 and Cav1/2 dKO B7 the opposite was observed: α1 shifted more into detergent resistant fractions compared to wt cells. This was different from observations made before in HeLa S3 cells (see Figure 32). Big variations for α1 levels were seen, as samples had to be precipitated for detection of α1 in DRM fractions. FGF2-GFP levels in the different fractions separated by sucrose gradient centrifugation did not differ in all the displayed cell lines (Figure 44B.). This deviated from results seen before for HeLa S3 cells, where Cav2 KO decreased FGF2-GFP in DRM liquid ordered fractions and increased levels in soluble fractions (see Figure 32B.). This might explain why there was no phenotype for FGF2-GFP secretion in U2OS Cav2 KO cell surface biotinylation assays, despite α1 to be slightly shifted.

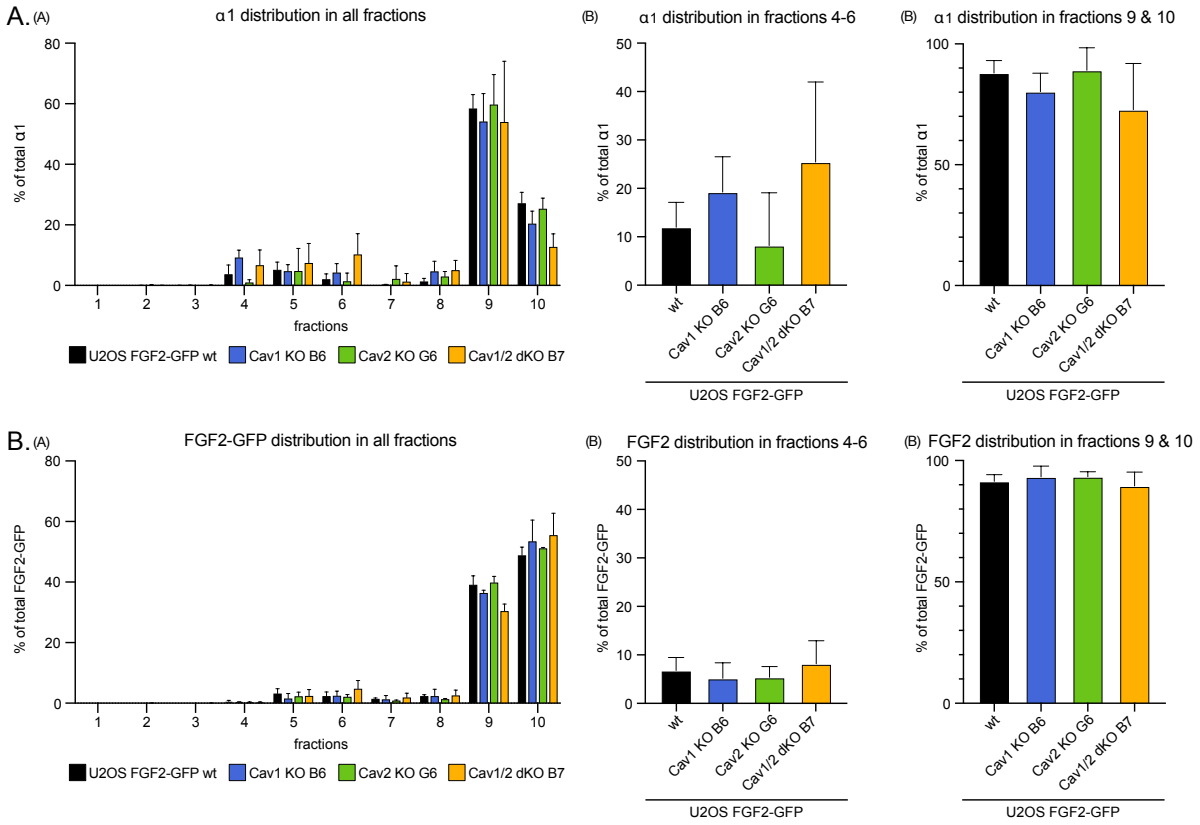

Figure 44: Cav2 KO in U2OS caused a mild decrease in α1 distribution into liquid ordered membrane areas. Quantification from 3 DRM experiments using U2OS FGF2-GFP wt, Cav1 KO B6, Cav2 KO G6 and Cav1/2 dKO B7 cells. Fractions 1-8 were precipitated and loaded entirely whereas ¼ of fractions 9 and 10 were loaded and later calculated in regards to total sample. A. Distribution of α1 in all cell lines (A) throughout all fractions, (B) in fractions 4-6 and (C) in soluble fractions 8-10. B. Distribution of FGF2-GFP in all cell lines (A) throughout all fractions, (B) in fractions 4-6 and (C) in soluble fractions 8-10. Statistical analysis was performed via one-way Anova combined with Tukey`s post hoc test (ns $p > 0,05$; * $p \leq 0,05$; ** $p \leq 0,01$; *** $p \leq 0,001$, **** $p \leq 0,0001$).

4.3.10 Concluding remarks on caveolin-1 and caveolin-2 in S3 or U2OS cells

Taken together, experiments with different caveolin knockout cells in HeLa S3 and U2OS cells showed crosstalk between Cav1 and Cav2 and indicated that expression levels and localization of both proteins are not independent from each other. Yet there seemed to be cell type specific differences between S3 and U2OS cells.

In HeLa cells Cav1 KO or Cav1/2 dKO did not impact FGF2-GFP secretion. Cav2 KO though significantly decreased cell surface FGF2-GFP in biotinylation experiments. Cav2 KO also decreased FGF2-GFP, α1 and strongly Cav1 localization to liquid ordered membrane areas. These reduced FGF2-GFP or α1 levels in DRM fractions might explain reduced cell surface FGF2-GFP in biotinylation experiments. Immunofluorescence images demonstrated that Cav1 also failed to localize to the membrane in Cav2 KO cells and that this effect could be reversed (partially) via overexpression of Cav2. Cav1 overexpression in S3 wt cells on the other hand reduced Cav2 expression levels.

U2OS Cav1 KO, Cav2 KO and Cav1/2 dKO cells did not show any significant phenotypes in FGF2-GFP secretion via cell surface biotinylation. Surprisingly, Cav1 KO did reduce surface FGF2-GFP in TIRF translocation assays. In DRM experiments lipid raft α1 was slightly reduced in Cav2 KOs, while it was increased in Cav1 KO and dKO cells. FGF2-GFP levels in the different fractions were not altered by either Cav KO. Also, Cav1 mislocalization to liquid ordered membrane areas was not observed in U2OS Cav2 KO cells. Overexpression and reintroduction of Cav1 lead to a strong decrease in Cav2 levels in Cav1 KOs. Countereffects and protein localization of Cav1 and Cav2 were not analyzed for U2OS in immunofluorescence microscopy, so no conclusions about subcellular distribution could be drawn from this.

Caveolin-1 and caveolin-2 both are interesting targets to be studied and many novel observations were made throughout this thesis that differ from literature. The here presented data on Cav2 will help to understand this poorly studied protein better. It seems that both Cav1 and Cav2 only play a minor role in FGF2 secretion though, although proteins localize together into liquid ordered membrane areas and are linked to cholesterol distribution throughout the plasma membrane. Yet it is not clear whether these proteins are within the same nanodomain or whether the domains only display similar features, such as being resistant to detergents and containing cholesterol. Further investigations must be conducted for final conclusions.

4.4 The α1-subunit of the Na,K-ATPase interacts with PI(3,4,5)P_3

Phospholipids play a role in FGF2-GFP secretion. While the role of PI(4,5)P_2 has been extensively studied and PI(4,5)P_2 has been shown to be needed for efficient translocation of FGF2 to the cell surface [123, 125, 129], the role of PI(3,4,5)P_3 is not clear yet. To explore the localization and interaction of lipids with other proteins functionalized lipid probes have been developed throughout the last years [236, 251]. Trifunctional (TF) lipid probes contain (1) a coumarin cage, which protects the lipid from metabolism before uncaging at 400 nm, (2) a diazirine group which allows for photo-crosslinking at 360 nm to proteins in proximity, and (3) an alkyne group suitable for click chemistry. A mass spectrometry study from Rainer Müller and Ana Kojic in the laboratory of Carsten Schultz at EMBL Heidelberg identified the α1-subunit of the Na,K-ATPase (ATP1A1) as a hit using trifunctional PI(3,4,5)P_3 [237]. This result was very intriguing to us, as we have never shown direct interaction between α1 and PI(3,4,5)P_3. Therefore, I decided to conduct pulldown experiments with TF-PI(3,4,5)P_3 and check for interaction with α1 in a side project parallel to the GPC and caveolin experiments. TF-PI(4,5)P_2 was hereby used as a control, as it did not appear in the mass spectrometry data.

HeLa S3 MT FGF2-IRES-GFP cells were incubated with the corresponding trifunctional lipid overnight. The subsequent day lipids were uncaged and crosslinked to proteins in proximity prior to cell lysis. Cell lysates were clicked to biotin-azide to allow for pulldown with streptavidin beads after protein precipitation. Inputs, flow through and eluates from the beads were used for SDS-PAGE and Western blotting against α1. As negative control, cells were not crosslinked via UV. For pulldowns using PI(3,4,5)P_3 an additional condition was tested where FGF2 expression was induced via the addition of 1 µg/ml doxycycline.

Representative blots for 4 or 2 pulldowns using TF-PI(3,4,5)P_3 or TF-PI(4,5)P_2 respectively are shown. As seen in Figure 45 both pulldowns were successful from a technical point of view. Streptavidin signals indicated correct clicking of the lipid probe to biotin-azide. Input signal were lower than eluates, as they only represented 10% of the total sample and flow throughs did not contain biotinylated protein indicating that everything bound to the beads. Protein crosslinking was UV dependent, as -UV conditions showed much weaker signal compared to + UV conditions when using TF-PI(3,4,5)P_3 (Figure 45A.). For TF-PI(4,5)P_2 signals in -UV controls were not as clean, but unintentional crosslinking by weak UV irradiation can never be fully excluded. As seen in Figure 45A. α1 anti-rabbit serum generated a lot of background in input and flow through signals. Despite high amounts of α1 in flow throughs, α1 was found in the eluates of +UV samples for TF-PI(3,4,5)P_3 in contrast to control conditions where no crosslinking occurred. Only a very small amount of α1 interacted with TF-PI(3,4,5)P_3 though and overexpression of FGF2 seemed to have no effect. Quantification was not very trustworthy at these low signal intensities. TF-PI(4,5)P_2 on the other hand was not crosslinked to α1 and α1 was not detectable in both – and +UV conditions for TF-PI(4,5)P_2 (Figure 45B).

These experiments support the previous finding, that PI(3,4,5)P_3 interacts with the α1 subunit of the Na,K-ATPase [237]. Also, they help us understand the role of phosphoinositides, in particular PI(3,4,5)P_3, better in the context of FGF2 secretion. Interaction of α1 with PI(3,4,5)P_3 might be

necessary for secretion and might offer a regulatory mechanism by which the FGF2 secretion machinery organizes into nanodomains.

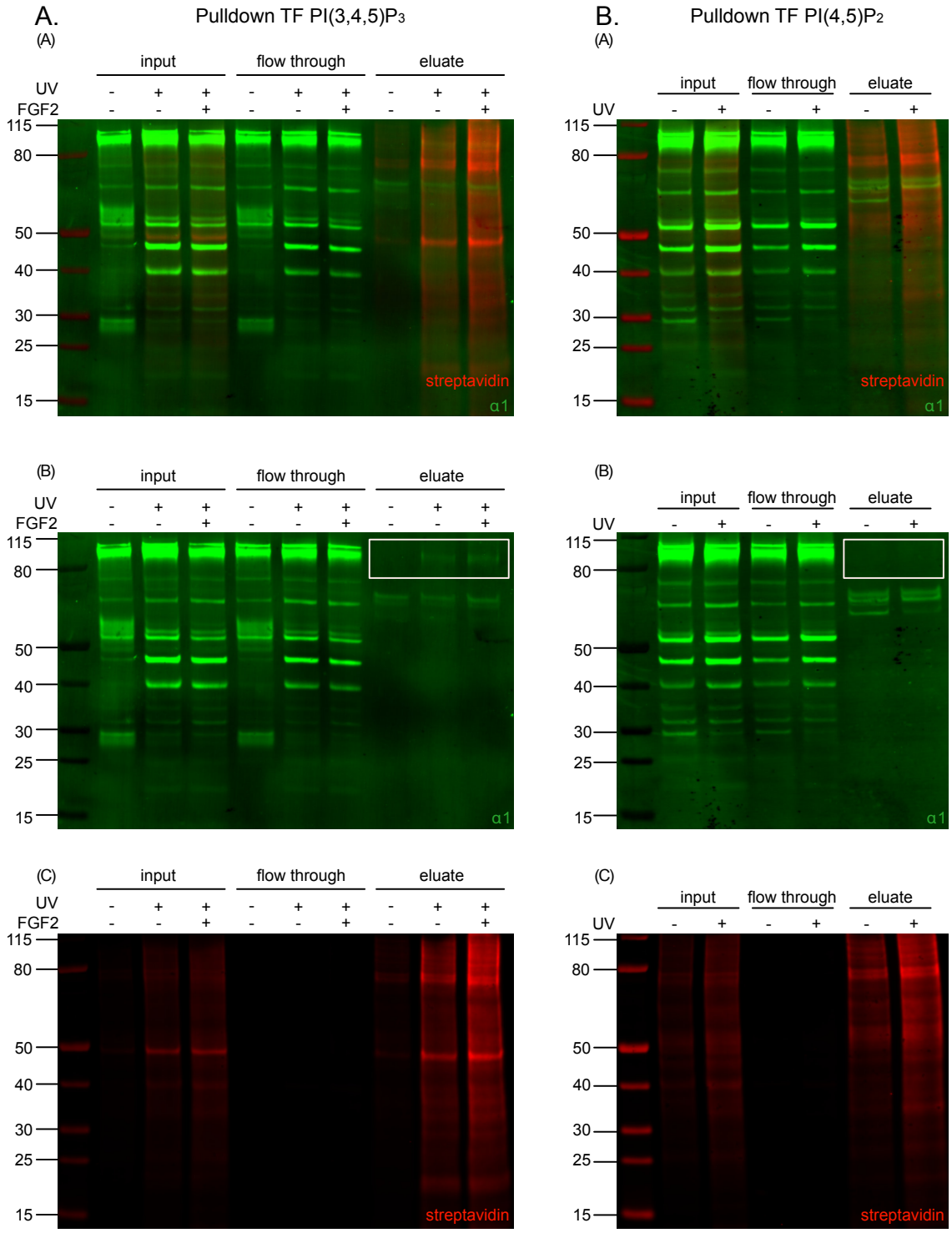

Figure 45: α1 interacted with trifunctional PI(3,4,5)P$_3$ in pulldown experiments. HeLa S3 FGF2-IRES-GFP were incubated with trifunctional (TF) PI(3,4,5)P$_3$ or PI(4,5)P$_2$ before lipid uncaging, crosslinking and click to biotin-azide. Inputs (10%), flow through (10%) and eluates from pulldown with streptavidin beads are depicted. Plus (+) or minus (-) UV irradiation conditions are shown and a condition overexpressing FGF2 was tested for PI(3,4,5)P$_3$. Representative Western blots show α1 (anti-rabbit α1 serum, in green) and biotin (streptavidin-580, in red). A. Pulldown using TF-PI(3,4,5)P$_3$ showing (A) merged channels, (B) α1 only signal and (C) streptavidin only signal. B. Pulldown using TF-PI(4,5)P$_2$ showing (A) merged channels, (B) α1 only signal and (C) streptavidin only signal.

5 Discussion

5.1 Understanding UPS of FGF2 better

Secretion of proteins to the extracellular space has long been thought to occur exclusively through the ER-Golgi route of secretion. Within this well-described pathway proteins are imported into the ER co-translationally or post-translationally to get folded with the help of chaperones and to receive first protein modifications [252]. Thereafter proteins are transported to the Golgi for finally protein modifications, such as glycosylation, and get sorted at the trans-Golgi network to reach their final destination. This process is chronological and organelles have a precise structure and function to provide the proper environment for protein modifications and secretion [253]. It is therefore not surprising that also signaling cascades (both endogenous and exogenous) and developmental programs impact and feedback to the secretory pathway [2].

More recently proteins were discovered that pass through the ER, yet reach the plasma membrane via COPII vesicles or in an Golgi-independent way and some proteins were discovered that lack a signal peptide and are secreted completely without passing the ER-Golgi pathway [254]. Collectively these have been classified to unconventional protein secretion (UPS) and have been categorized into 4 types: type I, type II, type III and type IV [33]. Surprisingly, a lot of proteins are predicted to be secreted unconventionally in programs such as OutCyte or ExoPred and these programs/websites will help to discover new UPS cargos [38, 255]. Up to date not many pathways and proteins have been studied in great detail yet and the probably best understood proteins are IL-1β and FGF2. Of course, the question arises why cells need UPS as alternative secretory route. Evidence comes from studies using FGF2 variants containing a signal peptide to force the protein artificially into the ER-Golgi pathway. Authors here demonstrated that altered FGF2 gets secreted, but gets post-translationally modified with chondroitin sulfates when it passes through the ER-Golgi and therefore fails to bind to surface HSPGs and localizes to the cell supernatant [256]. This secreted form of FGF2 cannot induce signaling. From these data it can be hypothesized that UPS in general adds complexity to cellular secretion and protects proteins from modifications to ensure their biological activity.

FGF2, a potent mitogen activating many cellular pathways that promote angiogenesis and tumor development, was described to be secreted unconventionally via direct translocation across the plasma membrane [98, 113]. In cancer diagnostics and therapy, it is essential to determine biomarkers that allow for early recognition. A study of cancer secretomes showed that in fact hundreds of proteins localized in intracellular organelles are secreted unconventionally or via exosomes and are insensitive to Brefeldin A treatment [257]. Therefore, studying and understanding UPS/UPS proteins is essential for future perspectives. FGF2 is recruited to the inner plasma membrane leaflet via interaction with the α1 subunit of the Na,K-ATPase [118, 123]. This seems to be the first contact to the membrane, followed by interaction with Tec kinase and the phosphoinositide $PI(4,5)P_2$ [125, 258]. FGF2 thereafter oligomerizes into membrane spanning complexes and translocation is promoted substantially by cell surface HSPGs which present FGF2 on the cell surface of cells [51, 127, 234].

For a long time, it remained unknown whether FGF2 is bound to a specific HSPG at the end of its secretory route. BioID experiments, conducted by Eleni Dimou and Matthias Gerstner in our laboratory, led to the identification of novel interaction partners of FGF2 [235]. Other methods to detect protein-protein interactions, such as the yeast-two-hybrid system, involve experimental conditions that do not resemble the native environment of the proteins. This can lead to false or incomplete results. The BioID approach, described by Roux and colleagues, screens for proteins in a relatively natural environment and therefore gives more confidence is the results [242]. The BioID approach conducted by Matthias identified an interesting protein target, glypican-1 or GPC1. This was striking since GPC1, as other HSPGs, is located on the cell surface bound by its GPI-anchor to the plasma membrane, and the biotinylation by BirA* requires intracellular ATP to form reactive biotinyl-AMP. The concentration of extracellular ATP is only 10 nM in contrast to 3-10 mM intracellular ATP, but extracellular ATP levels can be increased for cell-cell communication in the nervous system, vascular systems and in response to inflammatory processes [259]. This was probably not the case in the performed screen though. Nonetheless, it has been shown via BioID-tagging of the E-cadherin ectodomain that extracellular interactomes can be detected [260]. It can therefore not be excluded that extracellular FGF2-BirA* was able to biotinylate GPC1 or that some reactive biotinyl-AMP was exported along with FGF2-BirA*.

5.2 GPC1, GPC5 and GPC6 have different impacts on FGF2 secretion

As mentioned previously, GPC1 was detected in a BioID screen. To assess whether GPC1 impacts FGF2 secretion an established system of cells expressing FGF2-GFP in a doxycycline-dependent manner was used for cell surface biotinylation experiments. This system was used to introduce and analyze GPC1 knockouts. It has been shown that cell treatment with sodium chlorate, which prevents sulfation of HS chains, reduces FGF2 secretion and that CHO 745 cells, not expressing any HSPGs, can't efficiently secrete FGF2 [127, 128]. The removal of a single HSPG and its effect on FGF2 secretion had not been investigated previously. In the presented thesis GPC1 KO led to a strong decrease in FGF2-GFP secretion in cell surface biotinylation experiments (see Figure 6). Stable re- and overexpression of GPC1 in knockouts did not only rescue FGF2 secretion but even increased secretion above wild-type levels. Also, overexpression levels of HA-tagged GPC1, assessed via Western blotting and FACS, could directly be correlated to FGF2 secretion in TIRF translocations assays (Figure 16). FGF2 secretion from high HA-GPC1 expressing cells was very heterogenous, as some cells even secreted up to almost 50-fold more FGF2 compared to wt cells. This demonstrates that GPC1 is a rate-limiting factor for FGF2 secretion and secretion can be increased proportionate to GPC1 expression. Endocytosis experiments using recombinant FGF2 demonstrated that increased surface FGF2 is due to increased secretion and not due to differential endocytosis between wt, GPC1 KO and GPC1 overexpressing cells (Figure 8). As GPC5 is the only other glypican besides GPC1 to be expressed endogenously in HeLa cells, also knockout and overexpression of GPC5 was conducted. GPC5 knockout did not reduce FGF2-GFP secretion in cell surface biotinylation experiments and overexpression of GPC5 could not compensate for loss of GPC1 (Figure 6). Consequently, a double knockout of both GPC1 and GPC5 led to similar phenotype as GPC1 KO cells. Although GPC5 mRNA

levels were highly increased in GPC5 overexpressing cells in contrast to endogenous levels (Figure 7), this was not reflected in FACS experiments detecting overall heparan sulfate levels via HS-binding antibody (Figure 6). Overexpression of GPC1 on the other hand led to an increase in surface HS, indicating that GPC5 only makes minor contributions to overall heparan-sulfate containing proteins on the cell surface of HeLa cells. This is in contrast to data showing that overall glycosaminoglycan and heparan sulfate levels, detected via Blyscan assay, do not differ amongst the different knockout cells [51]. GPC1 overexpression in KO cells only mildly increased HS levels, albeit strongly increasing FGF2 secretion. Differences in detection limits and experimental setups might explain this difference. Additionally, it has been shown that the 10E4 epitope is not always fully accessible in GPC1 and that 10E4 epitope content is lower in cells with excessive nitric oxide-dependent HS degradation [261]. In these experiments immunoisolated radiolabeled 10E4-positive material yielded very little GPC1 in contrast to immunoisolated GPC1 and total proteoglycan products. Assessment of HS levels via 10E4 epitope antibody recognition might therefore be imprecise.

During the discovery of the different glypican family members it was already described that all 6 members can be categorized in two subgroups: GPC1, 2, 4, and 6 together vs. GPC3 and 5 in the other. The different knockout phenotypes of GPC1 and GPC5 might be explained by the fact that the two subgroups share only roughly 20 % identity on the amino acid level and this might have functional implications [184]. Data from Carola Sparn showed that in fact all members of the GPC1 subfamily were able to compensate for loss of GPC1, yet were only able to restore secretion back to wild-type levels and weren't able to further increase secretion as GPC1 overexpression did [51]. Amongst the other subfamily members, the strongest rescue phenotype was observed for GPC6. In order to assess whether knockout of GPC6 also impacts FGF2 secretion, I switched the cell line from HeLa S3 to U2OS. These osteosarcoma cells express GPC4 and GPC6 additionally to GPC1. Knockout of GPC6 led to no significant decrease in FGF2 secretion in U2OS FGF2-GFP expressing cells but double knockout of both GPC1 and GPC6 did decrease secretion a bit further than GPC1 KO alone (Figure 20). This indicates that GPC6, despite in the same subfamily with GPC1, only makes minor contributions to FGF2 secretion in endogenous conditions and is not a limiting factor for FGF2 secretion on its own. In absence of endogenous GPC1 GPC6 can partially promote FGF2 secretion. GPC4 KO was not tested in these cells. As GPC6 is homologous to GPC4 and shares around 60 % sequence identity [184], similar effects to GPC6 KO can be expected. It was shown by Sparn et al. that not only the glypican subfamily determines the involvement in FGF2 secretion, but that the main driving force is the composition and sulfation of the heparan sulfate chains [51]. Experiments digesting the HS chains of GPC1 and GPC5 into disaccharides and comparing them to disaccharide standards with known HPLC elution profiles, revealed differences between the two proteins. GPC1 contained more trisulfated disaccharides with two O-linked and one N-linked group [51], which intriguingly match to *in vitro* experiments were FGF2 was crystalized with heparin and FGF2 was found to bind to a stretch of these three disaccharides [262]. Along with the disaccharide type, also the positioning and frequency along the heparan sulfate chain might impact binding. Repetitive stretches might additionally improve and increase binding and explain less binding of FGF2 to GPC5 for instance [51]. *In vitro* experiments have also shown that only long-chained heparin, not heparin disaccharides, are able to induce FGF2 translocation and outcompete

$PI(4,5)P_2$ binding [129], supporting the idea that repetitive high affinity disaccharides promote FGF2 secretion.

5.3 PLA experiments showed proximity between proteins involved in FGF2 secretion

Proximity ligation assays offer the possibility to assess protein proximity within 40 nm of each other if the PLA probes are used as secondary antibodies against two different primary antibodies. Experiments were performed for several pairs of proteins involved in FGF2 secretion. It was shown before that FGF2 and the α1 subunit of the Na,K-ATPase are in proximity to each other in HeLa cells [118]. This proximity was specific, as other unrelated proteins such as the cell adhesion protein cadherin and the Golgi matrix protein GM130 showed much less proximity events to FGF2 within the same experiments. Also treatment of cells with ouabain, an inhibitor of the Na,K-ATPase, reduced proximity to FGF2 [123]. Proximity between FGF2 and α1 was confirmed also in HeLa S3 cells in this thesis (Figure 13), yet signal number in a single focal plane seemed much lower in S3 wt cells compared to previous data in HeLa cells. Overexpression of HA-tagged GPC1 in GPC1 KO cells within the same set of experiments lead to a slight increase in proximity between FGF2 and α1. GPC1 was shown to promote FGF2 secretion and might therefore also recruit more FGF2 to translocation sites where also α1 is present.
Proximity between FGF2 and HA-GPC1 was also detected and was slightly higher in absolute numbers when compared to FGF2-α1 proximity (Figure 14). This might be explained by the fact that both proteins were overexpressed: FGF2-GFP under doxycycline control and HA-GPC1 in a constant/stable fashion. Also, the functional relationship between GPC1 and FGF2 is very high, as demonstrated in previous experiments. The Na,K-ATPase actively transports Na+ and K+ ions in most higher eukaryotic cells, a function that is crucial to maintain cellular membrane potential, to transport glucose and to transport amino acids into the cell [263, 264]. In fact, the Na,K-ATPase is essential, as homozygous KO mice of all three α isoforms are embryonic lethal [265]. Due to involvement in many other cellular processes, it was therefore not expected that all α1 within a cell will be associated to FGF2 secretion.
Furthermore, proximity was for the first time in our laboratory shown between components residing on different sides of the plasma membrane: cell-surface GPI-anchored GPC1 and α1, which contains mostly intracellular and transmembrane domains (Figure 10 and Figure 11). Since the cell membrane is roughly 5 nm thick, the maximum distance of 40 nm between the two epitopes was kept. This also takes into account that the antibodies themselves are roughly 10 nm in size and might even bring the two proteins closer to each other if oriented favorably. Of note to mention is though that for all detections of intracellular proteins via PLA cell permeabilization is required. Some antibodies can reach the cytoplasm alone by fixation with 4% PFA, but the PLA probes were unable to enter unpermeabilized cells in my hands. Proximity between α1 and HA-GPC1 was slightly reduced in cells overexpressing FGF2-GFP upon addition of doxycycline (Figure 15). This fits to the observation that α1 and FGF2 proximity was reduced in cells overexpressing GPC1. This might indicate that upon overexpression of both FGF2 and GPC1 both of these proteins show the most proximity. α1 recruits FGF2 to the plasma membrane but GPC1 is needed for translocation across the plasma membrane. Increased expression of GPC1 might pull FGF2 away from α1 and promotes its secretion. Also, proximity between FGF2 and

GPC1 might be both across the membrane, when FGF2 is at the inner plasma membrane leaflet or has oligomerized into pores, or extracellular, leading to more proximity events. Experiments using heparin to wash away cell surface FGF2 and image only cross-membrane proximity turned out to be inadequate though (data not shown). Proximity between HA-GPC1 and α1 was higher than controls and more frequent than proximity between HA-GPC1 and cadherin. Even though cadherin is an abundant transmembrane protein, proximity between α1 and GPC1 was different and might be linked to functional relation.

5.4 Components involved in FGF2 secretion localize into nanodomains

FGF2 secretion is a very fast process in living cells (200 ms) [128], indicating that secretion can't be just a coincidental process but is highly coordinated. Organization of the components needed for FGF2 into nanodomains would greatly facilitate this process. Within the presented thesis several experiments were conducted to gain data supporting this hypothesis.

5.4.1 Proximity of components in PLA can reflect nanodomain organization

The previously mentioned PLA experiments were revisited in U2OS cells, which were better suitable for microscopy and showed in general more proximity events, allowing for more robust quantification. In contrast to HeLa cells, absolute dots at the bottom focal plane, so right at the membrane, were used for quantification. Once again, the highest proximity was seen between FGF2 and GPC1 (Figure 24). α1 also showed proximity to FGF2 and HA-GPC1. Proximity between these components supports the hypothesis that proteins are not randomly distributed throughout the cells but are close to each other due to involvement in the same pathway.

To test specificity for the α1-GPC1 proximity, proximity to syndecan-4 or cadherin was likewise tested. Proximity between α1 and GPC1 was significantly different from proximity between cadherin and GPC1. Surprisingly, GPC1 and cadherin proximity was higher. Cancer cells undergo epithelial-to-mesenchymal transition (EMT) to relocate to distant places to form metastasis [266]. Cadherins are involved in regulating cell-cell adhesion and therefore also play a big role in EMT, where N-cadherin is characteristically upregulated and E-cadherin is downregulated [267]. It has been shown that HSPGs also facilitate cell-cell interactions and cell-matrix crosstalk in the context of tumor proliferation [266]. GPC3 and E-cadherin expression for instance are interrelated in non-mucinous adenocarcinoma [268]. As GPC1 has been related to drive cancer cell metastasis it is not out of the question that GPC1 and cadherin can be involved in coherent pathways and are therefore localized in proximity to each other at the plasma membrane. Lipid rafts have been associated with the assembly of N-cadherin at cell-cell contact sites and thereby regulate cell adhesion [269]. The enrichment of GPI-anchored proteins in lipid rafts [270] also supports that GPC1 and cadherin are in proximity to each other in membrane lipid rafts. In fact, both proteins were found in liquid ordered membrane domains when detergent resistant membranes were isolated (Figure 25), although cadherin localized mostly to soluble fractions. α1 was in proximity to HA-GPC1 and syndecan-4 to a similar extent. As seen in DRM experiments α1 localized

to both liquid ordered and disordered fractions (Figure 25). Syndecan-4 can also be found both in liquid ordered and disordered membranes. Unclustered SDC4 is found in non-raft compartments, but moves to rafts when clustered via $PI(4,5)P_2$ induced by FGF2 signaling [165].
As seen in PLA experiments, protein proximity can hint to functional interplay, yet many proteins are involved in multiple pathways or localize to similar membrane areas, making strong statements impossible. Also, PLA detects proteins within roughly 40 nm of each other. Other methods, such as Fluorescence/Förster Resonance Energy Transfer (FRET), first described by Theodor Förster in 1965, allow detection of proximity within 3-6 nm [271]. FRET would therefore enable more precise determination of protein proximity and would also allow for live cell imaging, as some artifacts can be caused by the fixation and permeabilization needed for PLA.

5.4.2 DRM experiments can demonstrate nanodomain organization

FGF2, GPC1 and α1 localized together into liquid ordered membrane domains as demonstrated in DRM experiments (Figure 25). GPC1 has been shown to partition into lipid rafts via its GPI-anchor where it interacts with FGF2 and sequesters it away from FGFR in skeletal muscle differentiation [272]. In these experiments GPC1 was the only HSPG to localize to lipid rafts together with the marker caveolin-1 and both proteins were displaced when cells were treated with Methy-β-cyclodextrin (MβCD), which extracts cholesterol. Yet a sub-portion of GPC1 localized together with syndecans 1-4 to soluble fractions together with α1 [272]. Gutiérrez and Brandan demonstrated that radiolabeled FGF2 added to cells co-fractioned with raft and non-raft domains corresponding to binding to GPC1 or syndecans, respectively. As seen in Figure 25 FGF2-GFP expressed endogenously under doxycycline control was also found in both detergent resistant and soluble fractions. α1 (also referred to as ATP1A1) is often described as a non-raft marker when detergent resistant membranes are isolated with Triton X-100 [272]. Isolation with Brij 98, another detergent used in DRM experiments, in contrast renders α1 insoluble and sequesters it to lipid rafts [273]. α1 localization to lipid rafts was here not inhibited by MβCD, indicating that Brij 98 isolated rafts are independent of cholesterol and one therefore has to keep in mind that the use of detergents might cause artifacts or alternating results. On the other hand, it has been shown that α1 can be palmitoylated and protein palmitoylation is known to allow transmembrane proteins to partition into lipid rafts [274, 275], explaining α1 localization to both liquid ordered and disordered membranes.
Within the presented experiments α1 localized to lipid rafts in HeLa cells (see Figure 25). In U2OS the percentage of α1 recruited to liquid ordered plasma membrane fractions was much lower, as α1 was only detectable in DRM fractions when samples were subjected to protein precipitation. Same was true for the non-raft marker transferrin receptor (TfR). α1 localization to lipid rafts might depend on protein palmitoylation and only involves a subpopulation of the protein. As lipid rafts are rich in cholesterol and sphingolipids, these might also aid recruitment of α1 to areas of FGF2 secretion.
FGF2 recruitment to liquid ordered membrane domains was greatly affected by knockout or overexpression of GPC1 (Figure 26). KO of GPC1 decreased FGF2 content in DRM fractions, while overexpression increased levels in comparison to wt cells. Two explanations exist for this observation. FGF2 detected in liquid ordered fractions can represent mostly surface FGF2 bound to GPC1 since

GPC1 content reflects FGF2 levels. FGF2 levels in DRM fractions made up 7% of total cellular FGF2 content in fractionation experiments, coinciding with the 3-5% surface/total FGF2 seen in biotinylation experiments (see Figure 17). Also, the 2,4-fold increase in DRM-resident FGF2 when comparing wt to GPC1 overexpressing cells correlated with the increase seen in biotinylation experiments (see Figure 21). Another possible explanation would be that this is intracellular FGF2. Extracellular GPC1 might aid the recruitment process of components needed for FGF2 secretion and thereby recruit FGF2 to liquid ordered membrane domains. Yet it has been shown that $NaClO_3$ treatment, inhibiting HSPG and GPC1 sulfation and function, did not impact FGF2 recruitment to the plasma membrane in TIRF experiments [128], making the second explanation less likely.
It has been shown that treatment with docosahexanoic acid (DHA), a polyunsaturated acid that disrupts lipid rafts, leads to reduced unconventional secretion of Tau [59] and that DHA treatment leads to redistribution of phospholipid species increasing monounsaturated SM, PC and PE species in DRM fractions [276]. Also, DHA treatment displaces cholesterol from lipid rafts and promotes formation of sphingomyelin-rich caveolae/lipid rafts, thereby having an anti-inflammatory effect on human vascular retinal endothelial cells [277, 278]. DHA treatment represents an attractive pharmacological approach to test whether FGF2 secretion is impaired in biotinylation experiments or whether components redistribute in DRM experiments upon disruption of lipid rafts.

5.4.3 STED microscopy experiments can support the nanodomain hypothesis

Recently Dr. Fabio Lolicato and Roberto Saleppico demonstrated that cholesterol impacts FGF2 secretion by potential $PI(4,5)P_2$ clustering [247, 248]. $PI(4,5)P_2$ is essential for FGF2 secretion, both in living cells and *in vitro* [48, 123, 125]. Within this project it was my aim to visualize FGF2 together with $PI(4,5)P_2$ and cholesterol. To sense cellular cholesterol contents above 30 mole % cells were transfected with the cholesterol sensor EGFP-$Gram_{1b}$-G187L [217]. STED experiments revealed presence of both FGF2 and $PI(4,5)P_2$ in cholesterol rich membrane domains (Figure 23).
PIP_2 has been shown to be enriched in detergent resistant membrane fractions [279, 280]. On the other hand, it has been shown that treatment with 0,0025% Triton X-100 leads to an increase in FRET signals between GFP-PH-PH and RFP-PH-PH (PH/pleckstrin homology domains bind to PIPs). This indicates artificial PIP_2 clustering, whereas EM data rather show a homogenous distribution of PIP_2 at the plasma membrane [281].
The here presented STED images also showed a rather homogenous signal for $PI(4,5)P_2$, yet also showed that events were FGF2 and $PI(4,5)P_2$ signals overlapped or were very close to each other occurred mostly in cholesterol enriched areas. This supports the hypothesis that components needed for FGF2 secretion localize within cholesterol-enriched nanodomains.
STED imaging was also performed to analyze GPC1 and α1 subcellular localization at high resolution. Both proteins displayed a homogenous distribution throughout the plasma membrane and localized in a dot-like fashion (Figure 22). Colocalization was assessed via calculation of Pearson correlation coefficient for both confocal and STED images comparing conditions without or with overexpressed FGF2-GFP. Colocalization was decreased in conditions were FGF2 was not expressed for confocal

images, indicating that FGF2 expression promotes proximity between α1 and GPC1. This difference was only minor though and not reproducible in STED images. In general Pearson coefficients were very lows, indicating very weak correlation. As mentioned, Pearson's does not directly measure colocalization but rather the strength of association (= correlation) of two signals. Therefore, it is troublesome to apply Pearson's calculations to samples with very little correlation or non-linear correlation, as it might have been the case for the presented experiment. Therefore, a different quantification method should be applied to reevaluate the data. Quantifying the number of events where signals are within a certain distance of each other might for example be more conclusive.
Membrane nanodomains have been described for a long time via indirect methods, such as DRM isolations also used within this project. More recently, solvatochromic dyes have emerged, which can sense membrane polarity and change their spectral emission according to the order of the membrane. For more direct visualization of liquid ordered nanodomains and visualization of proteins involved in FGF2 secretion, these dyes could be used for super resolution experiments.

5.5 Caveolins – interesting, yet complicated

5.5.1 Caveolin phenotypes in HeLa S3 cells

Caveolin-1 and -2 can form heterooligomers to induce caveolae formation, which are involved in many cellular processes such as signaling, transport and lipid regulation. Several mouse models exist to study the phenotypes of Cav knockouts. As many proteins involved in FGF2 secretion have a caveolin binding motif (see Figure 5), caveolins were an interesting target to study in the pathway of FGF2 secretion.
I generated Cav1 knockouts in HeLa S3, yet unfortunately, these did not show a phenotype in regard to FGF2-GFP secretion (Figure 27). Whether caveolae form in these cells, was not analyzed. According to literature, knockout of Cav1 results in decreased Cav2 expression and Cav2 localization is dependent on Cav1, since in absence of Cav1 Cav2 gets trapped within the Golgi and gets degraded by the proteasome [250, 282, 283]. Yet, this was clearly not the case in my hands, as Cav2 expression in all Cav1 KOs remained near wt levels. Interestingly endogenous Cav2 localized mostly to the perinuclear space, and only very little Cav2 was detectable at the membrane, where Cav1 was highly enriched (Figure 28 and Figure 30). It was previously reported that Cav2 localizes to the Golgi in Fischer rat thyroid cells, which express no Cav1, and is then redistributed to the plasma membrane upon co-expression of Cav1 [250]. Detection of Cav1 via Western blotting in HeLa cells was troublesome due to low expression levels, which might explain the predominant intracellular localization of Cav2. In fact, overexpression of Cav1 in wt cells led to reduced intracellular localization of Cav2, although signals at the plasma membrane were not visibly increased (Figure 36). Cav2 levels in Western blot seemed lower upon overexpression of Cav1 (Figure 33). Cav1 overexpression on top of endogenous Cav1 also led to intracellular relocation of Cav1 to the perinuclear space. It has been reported that Cav1 mutations and overexpression of tagged forms can lead to accumulation within the Golgi [284]. Others have suggested that overexpressed Cav1 localized to aggresomes around the microtubule organizing center (MTOC), although this is dependent on the tagging strategy [285]. Cav2 overexpression in wt cells led

to a massive increase in intracellular Cav2, yet did not affect Cav1 localization in immunofluorescence staining (Figure 36). Overexpressed Cav2 was shown to accumulate in the Golgi and in lipid droplets [286].

To exclude a lack in phenotype, due to persistence of Cav2, Cav2 knockouts and double knockouts of both Cav1 and Cav2 were generated. Strikingly, Cav2 knockouts showed reduced FGF2 secretion, whereas double KOs originating from Cav1 KOs did not (Figure 29). In DRM experiments Cav1 localized almost exclusively to liquid ordered membrane fractions, whereas Cav2 distribution was homogenous throughout the fractions (Figure 25). KO of Cav2 led to drastic changes in Cav1 localization and Cav1 shifted to the higher density liquid disordered phases (Figure 31). This is inconsistent with previous reports, where Cav1 levels are not or only very little affected by Cav2 KO and Cav1 trafficking and caveolae formation is unperturbed [287]. In general, more emphasis has been put on the role and importance of caveolin-1 and its impact on caveolin-2. Only little is known about the biological functions of caveolin-2 on its own. Cav2 KO also led to reduced Cav1 levels at the plasma membrane, as seen in immunofluorescence staining (Figure 36), supporting the observed phenotype in DRM experiments. Overexpression of Cav2 led to an increased signal in Western blot, yet two additional bands appeared at a slightly higher molecular weight. Three Cav2 isoforms exist, that are produced by alternative translation initiation or splicing: 18 kDa (canonical), 16,8 kDa, and 12,8 kDa. Yet these do not explain the appearance of higher weight bands, as the canonical version has the highest molecular weight. Alternatively, the extra bands could be caused by protein modifications, such as ubiquitination or incorrect processing within the Golgi due to strong overexpression. Nonetheless, Cav2 overexpression was able to restore Cav1 localization to the membrane and to DRM fractions (Figure 36 and Figure 34), again indicating a role of Cav2 in regulation of Cav1 and not vice versa as postulated before.

All caveolin knockout mice models are viable, indicating that compensatory pathways exist to ensure cell functioning without caveolae [227]. Cav1/2 double knockout cells from Cav1 KO cells did not have a phenotype in biotinylation experiments, although dKOs generated from Cav2 KOs showed a similar phenotype to the parental cell line (Figure 29 and Figure 38). In general, elimination of both caveolin types expressed in HeLa cells, might lead to compensation via other proteins. Caveolin-1 and -2 are the major components in caveolae, yet other interconnected proteins exist, which makes it challenging to study caveolins, especially via crude knockout cells.

Cavin proteins have also been identified as essential structural components of caveolae. The cavin family consist of four homologous proteins: cavin 1 (PTRF) which is essential for caveolae formation just like Cav1, cavin 2 (SDPR), cavin 3 (PRKCDBP) and muscle specific cavin-4 (MURC) [288-292]. Cavins can form homo- or heterooligomers independent of caveolae. Cavin 1 is ubiquitously expressed and is essential for caveolae formation, whereas the importance of the other cavins, seen by knockout experiments, largely depends on the tissue and their expression levels therein [292]. Only Cavin 1 can engage with caveolins and knockout animals show loss of caveolae within all tissues [291]. Cavin 1 presence is required to incorporate the other family members within the caveolar coat [289]. Although only adaptor proteins, it cannot be excluded that in absolute lack of caveolins, as in the here generated dKOs, cavins can help to maintain cells in a healthy state.

Flotillin 1 (also called reggie 2) and Flotillin 2 (also called reggie 1) are proteins associated to the membrane that function in signaling, endocytosis and cytoskeleton associated processes [293]. Due to lack of structure-function causality, diverse cellular localization and missing identified protein interaction partners, it is difficult to understand the role of flotillins. What is clear though, is that flotillins form microdomains and are present in all mammalian cell lines [293]. As the name indicates flotillins float in density gradients while preparation of detergent resistant membrane fractions [294]. This also suggested them to be associated to caveolins or even be present in caveolae [295]. Others have suggested that flotillins can therefore substitute for the lack of caveolins in certain cells [293], although this was neither ruled out nor demonstrated. It is known though that flotillins can form caveolin-independent microdomains that contain Fyn kinase and GPI-anchored proteins [296]. Both flotillin 1 and 2 are palmitoylated and flotillin 2 is additionally myristoylated, which allows the proteins to associate with cholesterol- and sphingolipid-rich membrane domains [297, 298]. Flotillin microdomains, that can be enriched in number if both forms are co-expressed [299], can also indirectly affect phosphatidylinositol signaling via increasing $PI(4,5)P_2$ levels [300]. All these data suggest that flotillins can act independently from caveolins and form important signaling microdomains in cellular plasma membranes. Hence, flotillins could potentially help the cell overcome a critical state, when both caveolin-1 and caveolin-2 are knocked out. The role of flotillins in the context of the here presented Cav KOs remains to be assessed therefore.

5.5.2 Caveolins and the nanodomain organization of the FGF2 secretory machinery

Caveolin-1 was displaced from liquid ordered DRM fractions in Cav2 KO cells. Another striking observation was that both α1 and FGF2 levels were likewise reduced in DRM fractions (Figure 32). Both proteins only mildly shifted out of DRM fractions, yet a clear trend was observable for Cav2 KO cells, although no differences in FGF2 and α1 localization were detected via immunofluorescence staining (Figure 37). These Cav2 KO cells had also demonstrated reduced FGF2 secretion in cell surface biotinylation assays. The reduced amounts in DRM fractions might therefore explain the phenotype observed in biotinylations. FGF2, α1 and GPC1 are in proximity to each other and can be found in detergent resistant membrane fractions. Finding a potential organizer of this association would be very attractive and further promote the nanodomain hypothesis. To challenge this hypothesis also cells overexpressing Cav2 in a Cav2 KO background were analyzed for α1 and FGF2 localization in DRM experiments (Figure 35). Only a very weak rescue of the phenotype was observable. Looking at Cav2 signals in DRM when overexpressed, showed that again a second band for Cav2 was present and that this form exclusively localized to detergent soluble fractions. Some Cav2 localized successfully to detergent resistant fractions, yet this was even weaker than for wt cells. The lack in rescue for Cav2 KOs in biotinylation experiments was therefore also reflected in α1 and FGF2 localization in DRM experiments.

Caveolin-1 is a high-affinity cholesterol binding protein [231]. No direct interaction of caveolin-2 with cholesterol has been demonstrated, yet it can be speculated that an interplay exists as both localize to lipid rafts. Cholesterol has recently been shown to increase FGF2 secretion, potentially via clustering

of PI(4,5)P_2 [247, 248]. As also GPI-anchored GPC1 and (palmitoylated?) α1 localized to detergent resistant rafts, it is tempting to speculate that caveolins play a role in the nanodomain organization of the FGF2 secretory machinery. Some interplays between Cav1 and α1 have been observed previously, as knockdown of the Na,K-ATPase can increase endocytosis of Cav1 and decrease the plasma membrane pool [301]. Vice versa, knockout of Cav1 can interrupt the interaction of the Na-K-ATPase with its signaling interactors [302]. Yet no such interaction with Cav2 has been described so far.

5.5.3 Caveolin phenotypes in U2OS cells

To confirm observations made before in Hela cells and in order to gain more supporting information on the existence of FGF2 secretory nanodomains, caveolin experiments were also conducted in U2OS cells.

As expected from S3 cells, Cav1 KO did not affect FGF2 secretion in cell surface biotinylation experiments but led to increased Cav2 levels in Western blotting (Figure 39). Surprisingly, surface FGF2 was significantly reduced in TIRF translocation assays and phenotypes were similar for all KO clones. One clone also showed reduced recruitment of FGF2 to the inner plasma membrane leaflet. As demonstrated here, and previously by other laboratory members, it is important to conduct both assays whenever possible. Overexpression of Cav1 in Cav1 KO cells did not affect FGF2 secretion in biotinylation once again (Figure 40), yet remains to be investigated in TIRF experiments. Overexpression of Cav1 in U2OS led to a strong decrease in Cav2 levels, clearly indicating protein interdependence. This effect was stronger for U2OS than for HeLa S3 cells.

Cav2 knockout and double knockout of Cav1 and 2 did not have a phenotype in cell surface biotinylation experiments (Figure 41 and Figure 42). This phenotype was not expected for Cav2 KOs, as S3 Cav2 KO cells showed less FGF2 secretion. Once again, TIRF experiments must be conducted to analyze whether this phenotype can be reproduced or whether the differences in FGF2 secretion are merely not detectable in biotinylation.

Also, in DRM experiments U2OS Cav2 KOs showed phenotypes inconsistent with the previous data. Cav2 KO did not cause Cav1 to shift out of liquid ordered membrane fractions (Figure 43), indicating that Cav2 does not regulate Cav1 localization in U2OS cells. This observation must be analyzed in regards to subcellular localization using immunofluorescence microscopy. Cav2 KO caused α1 to slightly shift out of DRM fractions, but did not affect FGF2 distributions (Figure 44), matching with the unchanged FGF2 secretion in biotinylation.

Apparently, some interconnection between α1 and Cav2 exists also in U2OS cells, yet phenotypes seen for Cav1 and FGF2 were inconsistent with previous data. Analysis of the roles of Cav1 and Cav2 seems complicated and cannot be answered by simple knockout or overexpression and must be addressed in a more delicate fashion. Beyond that, cell type specific differences in Cav1/Cav2 function might exist, which additionally aggravated the analysis. Nevertheless, protein interdependencies were demonstrated that have never been shown before and the precise interplay remains interesting for future work.

5.6 PI(3,4,5)P_3 interacts with the Na,K-ATPase

Previous mass spectrometry data have suggested that the α1 subunit of the Na,K-ATPase can interact with PI(3,4,5)P_3 [237]. Pulldown experiments using trifunctional PI(3,4,5)P_3 were able to detect α1 in eluates via Western blotting, indicating that α1 was crosslinked to PI(3,4,5)P_3 which was subsequently clicked to biotin and enriched via streptavidin affinity capture (Figure 45). This was not observed for PI(4,5)P_2. Incubation of cells with doxycycline to induce overexpression of FGF2 did not alter α1 - PI(3,4,5)P_3 interaction, due to low levels of α1.

Pleckstrin homology (PH) domains can bind to phosphoinositides and bind to phosphoinositides with adjacent phosphates, such as PI(4,5)P_2, PI(3,4)P_2 and PI(3,4,5)P_3, with high affinity [303]. Thereby they can transiently recruit proteins to the plasma membrane. Tec family kinases, especially Btk, was shown to bind specifically to PI(3,4,5)P_3 [304], which explains why Tec kinase could be involved in FGF2 secretion and interact with FGF2 at the membrane. For the Na,K-ATPase it has been shown that 3 separate binding sites exist for phosphatidylserine/cholesterol, polyunsaturated phosphatidylethanolamine and saturated PC or sphingomyelin/cholesterol, which all have different inhibitory or stimulatory effects on the ATPase [305]. In fact, cholesterol depletion of purified membrane fragments via Methy-β-cyclodextrin (MβCD) can lead to reduced activity [306]. Direct binding of α1 to PI(3,4,5)P_3 has not been shown previously, but the Na,K-ATPase is associated with PI3K activating pathways, which lead to production of PI(3,4,5)P_3 [307].

STORM experiments using both PI(4,5)P_2 and PI(3,4,5)P_3 antibodies have demonstrated that both lipids segregate largely into different clusters of different sizes [308] and it has been suggested that PI(4,5)P_2 metabolism occurs in a very fast manner in liquid ordered membrane domains [309]. How and where exactly PI(3,4,5)P_3 is remains open. PI(3,4,5)P_3 is much less abundant at the plasma membrane and gas chromatography data have suggested it's levels are 1/2 - 1/6 of those of PI(4,5)P_2. Quantitative data have shown that 85% of PI(4,5)P_2 is polyunsaturated and thereby localized to liquid disordered membrane areas [310, 311]. PI(3,4,5)P_3 in contrast is mostly saturated or monounsaturated, favoring partitioning into liquid ordered domains where also PI3K, which synthesizes PI(3,4,5)P_3 from PI(4,5)P_2, is localized [312, 313].

Clearly, no concluding statement can be made in regards to localization of both PIP species within liquid ordered membrane areas as both has been described and PIPs function in signaling pathways associated with lipid rafts. Modeling approaches by Dr. Fabio Lolicato will help to better understand the interaction of the Na,K-ATPase with different phosphoinositide species and might confirm specific interaction between α1 and PI(3,4,5)P_3.

6 Future perspective

As presented, GPC1 was found to be a novel interaction partner of FGF2 and is a rate-limiting factor for unconventional secretion of FGF2, not being involved in its endocytosis. Other glypicans, such as GPC5 and GPC6 did not have the same effect. The high binding specificity of GPC1 to FGF2 can be explained by the composition of the heparan sulfate chains and the abundance of certain disaccharide units. These data were published beginning of 2022 by Carola Sparn in collaboration with Roberto Saleppico, Sabine Wegehingel, Eleni Dimou, myself and others. Both GPC1 and FGF2 are involved in tumor progression and angiogenesis, demonstrating the importance of these findings. As many proteins secreted unconventionally are associated to disease and inflammation, research on the molecular mechanisms of UPS and UPS cargos will allow for better understanding and the development of therapeutic approaches.

STED, PLA and DRM data suggested that proteins involved in FGF2 secretion are in proximity to each other and localize to liquid ordered membrane domains. Experiments using FRET will aid higher resolution proximity identification and the use of solvatochromic dyes could demonstrate localization of the proteins to liquid ordered membrane areas via microscopy techniques. This will offer an alternative to DRM fractionation experiments which are a more indirect and debated experimental approach to demonstrate nanodomains. Also, treatment of cells with DHA to disrupt liquid ordered membrane areas will give interesting data in biotinylation and DRM experiments.

How exactly proteins are recruited to liquid ordered membrane fractions remains open. Caveolins can potentially organize proteins within these domains, but also protein palmitoylation, cholesterol and sphingomyelin can influence compartmentalization. DRM experiments using 2-bromopalmitate to inhibit protein palmitoylation or pulldown experiments using clickable palmitic acid offer a promising approach. Alternatively, cholesterol and sphingomyelin manipulation can be conducted. On top of DRM experiments, also PLA and FRET could be used to assess protein proximity under changing plasma membrane conditions and compositions.

The role of caveolins in FGF2 secretion remains ambiguous. The different knockout cell lines in HeLa S3 and U2OS cells both indicated effects on FGF2 secretion determined either by cell surface biotinylation or TIRF, yet data were inconsistent. TIRF microscopy of the remaining Cav2 KOs and Cav1/2 dKOs in U2OS needs to be conducted. Also, the effect of Cav knockout on other proteins such as cavins or flotillins must be analyzed, as this might explain for compensatory mechanisms. This could be assessed via RT-qPCR of these proteins in Cav KO cells or via RNA sequencing. The interplay of caveolins and cholesterol within FGF2 secretion is not well understood yet. Cholesterol impacts FGF2 secretion, yet a change in cholesterol levels in Cav1 KOs was not detectable via Filipin staining (data not shown). As this method can only detect big phenotypes and is very sensitive, lipidomics could be used as alternative approach to assess lipid contents of the different caveolin knockout cell lines to assess impact on FGF2 secretion.

7 References

1. Shivakumar, K., *A catalogue of human secreted proteins and its implications.* AIMS Biophysics, 2016. **3**(4): p. 563-570.
2. Farhan, H. and C. Rabouille, *Signalling to and from the secretory pathway.* J Cell Sci, 2011. **124**(Pt 2): p. 171-80.
3. Blobel, G. and D. Sabatini, *Dissociation of mammalian polyribosomes into subunits by puromycin.* Proc Natl Acad Sci U S A, 1971. **68**(2): p. 390-4.
4. Benham, A.M., *Protein secretion and the endoplasmic reticulum.* Cold Spring Harb Perspect Biol, 2012. **4**(8): p. a012872.
5. Jackson, R.C. and G. Blobel, *Post-translational cleavage of presecretory proteins with an extract of rough microsomes from dog pancreas containing signal peptidase activity.* Proc Natl Acad Sci U S A, 1977. **74**(12): p. 5598-602.
6. Loaeza-Reyes, K.J., et al., *An Overview of Glycosylation and its Impact on Cardiovascular Health and Disease.* Front Mol Biosci, 2021. **8**: p. 751637.
7. Helenius, J., et al., *Translocation of lipid-linked oligosaccharides across the ER membrane requires Rft1 protein.* Nature, 2002. **415**(6870): p. 447-50.
8. Frank, C.G., et al., *Does Rft1 flip an N-glycan lipid precursor?* Nature, 2008. **454**(7204): p. E3-E4.
9. Dempski, R.E., Jr. and B. Imperiali, *Oligosaccharyl transferase: gatekeeper to the secretory pathway.* Curr Opin Chem Biol, 2002. **6**(6): p. 844-50.
10. Aebi, M., *N-linked protein glycosylation in the ER.* Biochim Biophys Acta, 2013. **1833**(11): p. 2430-7.
11. Schoberer, J., et al., *Analysis of Protein Glycosylation in the ER.* Methods Mol Biol, 2018. **1691**: p. 205-222.
12. Vembar, S.S. and J.L. Brodsky, *One step at a time: endoplasmic reticulum-associated degradation.* Nature Reviews Molecular Cell Biology, 2008. **9**(12): p. 944-U30.
13. Feige, M.J. and L.M. Hendershot, *Disulfide bonds in ER protein folding and homeostasis.* Curr Opin Cell Biol, 2011. **23**(2): p. 167-75.
14. Sato, K. and A. Nakano, *Mechanisms of COPII vesicle formation and protein sorting.* Febs Letters, 2007. **581**(11): p. 2076-2082.
15. Sato, K., *COPII coat assembly and selective export from the endoplasmic reticulum.* J Biochem, 2004. **136**(6): p. 755-60.
16. Nakano, A. and M. Muramatsu, *A novel GTP-binding protein, Sar1p, is involved in transport from the endoplasmic reticulum to the Golgi apparatus.* J Cell Biol, 1989. **109**(6 Pt 1): p. 2677-91.
17. Barlowe, C. and R. Schekman, *SEC12 encodes a guanine-nucleotide-exchange factor essential for transport vesicle budding from the ER.* Nature, 1993. **365**(6444): p. 347-9.
18. Kuehn, M.J., J.M. Herrmann, and R. Schekman, *COPII-cargo interactions direct protein sorting into ER-derived transport vesicles.* Nature, 1998. **391**(6663): p. 187-90.
19. Malhotra, V. and P. Erlmann, *Protein export at the ER: loading big collagens into COPII carriers.* EMBO J, 2011. **30**(17): p. 3475-80.
20. Saito, K., et al., *TANGO1 facilitates cargo loading at endoplasmic reticulum exit sites.* Cell, 2009. **136**(5): p. 891-902.
21. Huang, S. and Y. Wang, *Golgi structure formation, function, and post-translational modifications in mammalian cells.* F1000Res, 2017. **6**: p. 2050.
22. Lucocq, J.M., E.G. Berger, and G. Warren, *Mitotic Golgi fragments in HeLa cells and their role in the reassembly pathway.* J Cell Biol, 1989. **109**(2): p. 463-74.
23. Wang, Y., et al., *A direct role for GRASP65 as a mitotically regulated Golgi stacking factor.* EMBO J, 2003. **22**(13): p. 3279-90.
24. Tang, D.M., et al., *Molecular mechanism of mitotic Golgi disassembly and reassembly revealed by a defined reconstitution assay*. Journal of Biological Chemistry, 2008. **283**(10): p. 6085-6094.
25. Xiang, Y. and Y. Wang, *GRASP55 and GRASP65 play complementary and essential roles in Golgi cisternal stacking.* J Cell Biol, 2010. **188**(2): p. 237-51.
26. Cooper, G.M., *The Golgi Apparatus*, in *The Cell: A Molecular Approach*. 2000, Sinauer Associates: Sunderland (MA).
27. Rothman, J.E. and F.T. Wieland, *Protein sorting by transport vesicles.* Science, 1996. **272**(5259): p. 227-34.

28. Arakel, E.C. and B. Schwappach, *Formation of COPI-coated vesicles at a glance.* J Cell Sci, 2018. **131**(5).
29. Beck, R., et al., *The COPI system: molecular mechanisms and function.* FEBS Lett, 2009. **583**(17): p. 2701-9.
30. Sohn, K., et al., *A major transmembrane protein of Golgi-derived COPI-coated vesicles involved in coatomer binding.* J Cell Biol, 1996. **135**(5): p. 1239-48.
31. De Matteis, M.A. and A. Luini, *Exiting the Golgi complex.* Nat Rev Mol Cell Biol, 2008. **9**(4): p. 273-84.
32. Kim, J., H.Y. Gee, and M.G. Lee, *Unconventional protein secretion - new insights into the pathogenesis and therapeutic targets of human diseases.* J Cell Sci, 2018. **131**(12).
33. Rabouille, C., *Pathways of Unconventional Protein Secretion.* Trends Cell Biol, 2017. **27**(3): p. 230-240.
34. Rubartelli, A. and R. Sitia, *Secretion of Mammalian Proteins that Lack a Signal Sequence*, in *Unusual Secretory Pathways: From Bacteria to Man*, K. Kuchler, A. Rubartelli, and B. Holland, Editors. 1997, Springer Berlin Heidelberg: Berlin, Heidelberg. p. 87-114.
35. Helms, J.B. and J.E. Rothman, *Inhibition by brefeldin A of a Golgi membrane enzyme that catalyses exchange of guanine nucleotide bound to ARF.* Nature, 1992. **360**(6402): p. 352-4.
36. Mollenhauer, H.H., D.J. Morre, and L.D. Rowe, *Alteration of intracellular traffic by monensin; mechanism, specificity and relationship to toxicity.* Biochim Biophys Acta, 1990. **1031**(2): p. 225-46.
37. Eilers, U., J. Klumperman, and H.P. Hauri, *Nocodazole, a microtubule-active drug, interferes with apical protein delivery in cultured intestinal epithelial cells (Caco-2).* J Cell Biol, 1989. **108**(1): p. 13-22.
38. Zhao, L., et al., *OutCyte: a novel tool for predicting unconventional protein secretion.* Sci Rep, 2019. **9**(1): p. 19448.
39. Agosta, F., et al., *Myeloid microvesicles in cerebrospinal fluid are associated with myelin damage and neuronal loss in mild cognitive impairment and Alzheimer disease.* Ann Neurol, 2014. **76**(6): p. 813-25.
40. Chen, H., et al., *Interleukin-33 is released in spinal cord and suppresses experimental autoimmune encephalomyelitis in mice.* Neuroscience, 2015. **308**: p. 157-68.
41. Freigang, S., et al., *Fatty acid-induced mitochondrial uncoupling elicits inflammasome-independent IL-1alpha and sterile vascular inflammation in atherosclerosis.* Nat Immunol, 2013. **14**(10): p. 1045-53.
42. Schroder, K. and J. Tschopp, *The inflammasomes.* Cell, 2010. **140**(6): p. 821-32.
43. Witsch, E., M. Sela, and Y. Yarden, *Roles for growth factors in cancer progression.* Physiology (Bethesda), 2010. **25**(2): p. 85-101.
44. Rodriguez, L.S., et al., *Immunomodulators released during rotavirus infection of polarized caco-2 cells.* Viral Immunol, 2009. **22**(3): p. 163-72.
45. Zhang, X., et al., *Hsp20 functions as a novel cardiokine in promoting angiogenesis via activation of VEGFR2.* PLoS One, 2012. **7**(3): p. e32765.
46. Dimou, E. and W. Nickel, *Unconventional mechanisms of eukaryotic protein secretion.* Curr Biol, 2018. **28**(8): p. R406-R410.
47. Zeitler, M., et al., *HIV-Tat Protein Forms Phosphoinositide-dependent Membrane Pores Implicated in Unconventional Protein Secretion.* J Biol Chem, 2015. **290**(36): p. 21976-84.
48. Steringer, J.P., et al., *Phosphatidylinositol 4,5-bisphosphate (PI(4,5)P2)-dependent oligomerization of fibroblast growth factor 2 (FGF2) triggers the formation of a lipidic membrane pore implicated in unconventional secretion.* J Biol Chem, 2012. **287**(33): p. 27659-69.
49. Nickel, W., *The unconventional secretory machinery of fibroblast growth factor 2.* Traffic, 2011. **12**(7): p. 799-805.
50. La Venuta, G., et al., *The Startling Properties of Fibroblast Growth Factor 2: How to Exit Mammalian Cells without a Signal Peptide at Hand.* J Biol Chem, 2015. **290**(45): p. 27015-27020.
51. Sparn, C., et al., *Glypican-1 drives unconventional secretion of fibroblast growth factor 2.* Elife, 2022. **11**.
52. Chang, H.C., et al., *HIV-1 Tat protein exits from cells via a leaderless secretory pathway and binds to extracellular matrix-associated heparan sulfate proteoglycans through its basic region.* AIDS, 1997. **11**(12): p. 1421-31.
53. Martin-Sanchez, F., et al., *Inflammasome-dependent IL-1beta release depends upon membrane permeabilisation.* Cell Death Differ, 2016. **23**(7): p. 1219-31.

54. Latz, E., T.S. Xiao, and A. Stutz, *Activation and regulation of the inflammasomes.* Nature Reviews Immunology, 2013. **13**(6): p. 397-411.
55. Heilig, R., et al., *The Gasdermin-D pore acts as a conduit for IL-1beta secretion in mice.* Eur J Immunol, 2018. **48**(4): p. 584-592.
56. Liu, X., et al., *Inflammasome-activated gasdermin D causes pyroptosis by forming membrane pores.* Nature, 2016. **535**(7610): p. 153-8.
57. Ding, J., et al., *Pore-forming activity and structural autoinhibition of the gasdermin family.* Nature, 2016. **535**(7610): p. 111-6.
58. Katsinelos, T., et al., *Unconventional Secretion Mediates the Trans-cellular Spreading of Tau.* Cell Rep, 2018. **23**(7): p. 2039-2055.
59. Merezhko, M., et al., *Secretion of Tau via an Unconventional Non-vesicular Mechanism.* Cell Rep, 2018. **25**(8): p. 2027-2035 e4.
60. Goedert, M., et al., *Assembly of microtubule-associated protein tau into Alzheimer-like filaments induced by sulphated glycosaminoglycans.* Nature, 1996. **383**(6600): p. 550-3.
61. Holmes, B.B., et al., *Heparan sulfate proteoglycans mediate internalization and propagation of specific proteopathic seeds.* Proc Natl Acad Sci U S A, 2013. **110**(33): p. E3138-47.
62. Merezhko, M., R.L. Uronen, and H.J. Huttunen, *The Cell Biology of Tau Secretion.* Front Mol Neurosci, 2020. **13**: p. 569818.
63. Locher, K.P., *Review. Structure and mechanism of ATP-binding cassette transporters.* Philos Trans R Soc Lond B Biol Sci, 2009. **364**(1514): p. 239-45.
64. Chen, W., S. Wang, and D. Xing, *New Horizons for the Roles and Association of APE1/Ref-1 and ABCA1 in Atherosclerosis.* J Inflamm Res, 2021. **14**: p. 5251-5271.
65. Kuchler, K., R.E. Sterne, and J. Thorner, *Saccharomyces cerevisiae STE6 gene product: a novel pathway for protein export in eukaryotic cells.* EMBO J, 1989. **8**(13): p. 3973-84.
66. Flieger, O., et al., *Regulated secretion of macrophage migration inhibitory factor is mediated by a non-classical pathway involving an ABC transporter.* FEBS Lett, 2003. **551**(1-3): p. 78-86.
67. Stegmayer, C., et al., *Direct transport across the plasma membrane of mammalian cells of Leishmania HASPB as revealed by a CHO export mutant.* J Cell Sci, 2005. **118**(Pt 3): p. 517-27.
68. Ktistakis, N.T. and S.A. Tooze, *Digesting the Expanding Mechanisms of Autophagy.* Trends in Cell Biology, 2016. **26**(8): p. 624-635.
69. Kinseth, M.A., et al., *The Golgi-associated protein GRASP is required for unconventional protein secretion during development.* Cell, 2007. **130**(3): p. 524-34.
70. Duran, J.M., et al., *Unconventional secretion of Acb1 is mediated by autophagosomes.* J Cell Biol, 2010. **188**(4): p. 527-36.
71. Andrei, C., et al., *The secretory route of the leaderless protein interleukin 1beta involves exocytosis of endolysosome-related vesicles.* Mol Biol Cell, 1999. **10**(5): p. 1463-75.
72. Zhang, M., et al., *Translocation of interleukin-1beta into a vesicle intermediate in autophagy-mediated secretion.* Elife, 2015. **4**.
73. Dupont, N., et al., *Autophagy-based unconventional secretory pathway for extracellular delivery of IL-1beta.* EMBO J, 2011. **30**(23): p. 4701-11.
74. Grieve, A.G. and C. Rabouille, *Golgi bypass: skirting around the heart of classical secretion.* Cold Spring Harb Perspect Biol, 2011. **3**(4).
75. Kim, J., et al., *Monomerization and ER Relocalization of GRASP Is a Requisite for Unconventional Secretion of CFTR.* Traffic, 2016. **17**(7): p. 733-53.
76. Jung, J., et al., *The HSP70 co-chaperone DNAJC14 targets misfolded pendrin for unconventional protein secretion.* Nat Commun, 2016. **7**: p. 11386.
77. Schotman, H., L. Karhinen, and C. Rabouille, *dGRASP-mediated noncanonical integrin secretion is required for Drosophila epithelial remodeling.* Dev Cell, 2008. **14**(2): p. 171-82.
78. Tian, G., et al., *An unconventional secretory pathway mediates the cilia targeting of peripherin/rds.* J Neurosci, 2014. **34**(3): p. 992-1006.
79. Gospodarowicz, D., *Localisation of a fibroblast growth factor and its effect alone and with hydrocortisone on 3T3 cell growth.* Nature, 1974. **249**(453): p. 123-7.
80. Gospodarowicz, D., H. Bialecki, and G. Greenburg, *Purification of the fibroblast growth factor activity from bovine brain.* J Biol Chem, 1978. **253**(10): p. 3736-43.
81. Gospodarowicz, D. and J.S. Moran, *Mitogenic effect of fibroblast growth factor on early passage cultures of human and murine fibroblasts.* J Cell Biol, 1975. **66**(2): p. 451-7.
82. Maciag, T., et al., *An endothelial cell growth factor from bovine hypothalamus: identification and partial characterization.* Proc Natl Acad Sci U S A, 1979. **76**(11): p. 5674-8.

83. Katoh, M. and M. Katoh, *FGF signaling network in the gastrointestinal tract (review).* Int J Oncol, 2006. **29**(1): p. 163-8.
84. Smallwood, P.M., et al., *Fibroblast growth factor (FGF) homologous factors: new members of the FGF family implicated in nervous system development.* Proc Natl Acad Sci U S A, 1996. **93**(18): p. 9850-7.
85. Olsen, S.K., et al., *Fibroblast growth factor (FGF) homologous factors share structural but not functional homology with FGFs.* J Biol Chem, 2003. **278**(36): p. 34226-36.
86. Ornitz, D.M. and N. Itoh, *The Fibroblast Growth Factor signaling pathway.* Wiley Interdiscip Rev Dev Biol, 2015. **4**(3): p. 215-66.
87. Mohammadi, M., S.K. Olsen, and O.A. Ibrahimi, *Structural basis for fibroblast growth factor receptor activation.* Cytokine & Growth Factor Reviews, 2005. **16**(2): p. 107-137.
88. Eswarakumar, V.P., I. Lax, and J. Schlessinger, *Cellular signaling by fibroblast growth factor receptors.* Cytokine Growth Factor Rev, 2005. **16**(2): p. 139-49.
89. Tulin, S. and A. Stathopoulos, *Extending the family table: Insights from beyond vertebrates into the regulation of embryonic development by FGFs.* Birth Defects Res C Embryo Today, 2010. **90**(3): p. 214-27.
90. Popovici, C., et al., *An evolutionary history of the FGF superfamily.* Bioessays, 2005. **27**(8): p. 849-57.
91. Prudovsky, I., et al., *Protein-phospholipid interactions in nonclassical protein secretion: problem and methods of study.* Int J Mol Sci, 2013. **14**(2): p. 3734-72.
92. Miyakawa, K., et al., *A hydrophobic region locating at the center of fibroblast growth factor-9 is crucial for its secretion.* J Biol Chem, 1999. **274**(41): p. 29352-7.
93. Jaye, M., J. Schlessinger, and C.A. Dionne, *Fibroblast growth factor receptor tyrosine kinases: molecular analysis and signal transduction.* Biochim Biophys Acta, 1992. **1135**(2): p. 185-99.
94. Mistry, N., et al., *Of urchins and men: evolution of an alternative splicing unit in fibroblast growth factor receptor genes.* RNA, 2003. **9**(2): p. 209-17.
95. Yeh, B.K., et al., *Structural basis by which alternative splicing confers specificity in fibroblast growth factor receptors.* Proc Natl Acad Sci U S A, 2003. **100**(5): p. 2266-71.
96. Kalinina, J., et al., *The alternatively spliced acid box region plays a key role in FGF receptor autoinhibition.* Structure, 2012. **20**(1): p. 77-88.
97. Yun, Y.R., et al., *Fibroblast growth factors: biology, function, and application for tissue regeneration.* J Tissue Eng, 2010. **2010**: p. 218142.
98. Xie, Y., et al., *FGF/FGFR signaling in health and disease.* Signal Transduct Target Ther, 2020. **5**(1): p. 181.
99. Presta, M., et al., *Fibroblast growth factor/fibroblast growth factor receptor system in angiogenesis.* Cytokine Growth Factor Rev, 2005. **16**(2): p. 159-78.
100. Liao, S., et al., *Biological functions of the low and high molecular weight protein isoforms of fibroblast growth factor-2 in cardiovascular development and disease.* Dev Dyn, 2009. **238**(2): p. 249-64.
101. Schlessinger, J., et al., *Crystal structure of a ternary FGF-FGFR-heparin complex reveals a dual role for heparin in FGFR binding and dimerization.* Mol Cell, 2000. **6**(3): p. 743-50.
102. Plotnikov, A.N., et al., *Crystal structures of two FGF-FGFR complexes reveal the determinants of ligand-receptor specificity.* Cell, 2000. **101**(4): p. 413-24.
103. Bugler, B., F. Amalric, and H. Prats, *Alternative initiation of translation determines cytoplasmic or nuclear localization of basic fibroblast growth factor.* Mol Cell Biol, 1991. **11**(1): p. 573-7.
104. Sorensen, V., T. Nilsen, and A. Wiedlocha, *Functional diversity of FGF-2 isoforms by intracellular sorting.* Bioessays, 2006. **28**(5): p. 504-14.
105. Claus, P., et al., *Differential intranuclear localization of fibroblast growth factor-2 isoforms and specific interaction with the survival of motoneuron protein.* J Biol Chem, 2003. **278**(1): p. 479-85.
106. Choi, J., M.K. Ko, and E.P. Kay, *Subcellular localization of the expressed 18 kDa FGF-2 isoform in corneal endothelial cells.* Mol Vis, 2000. **6**: p. 222-31.
107. Bouche, G., et al., *Activation of rDNA transcription by FGF-2: key role of protein kinase CKII.* Cell Mol Biol Res, 1994. **40**(5-6): p. 547-54.
108. Korc, M. and R.E. Friesel, *The role of fibroblast growth factors in tumor growth.* Curr Cancer Drug Targets, 2009. **9**(5): p. 639-51.
109. Zhang, X., et al., *Receptor specificity of the fibroblast growth factor family. The complete mammalian FGF family.* J Biol Chem, 2006. **281**(23): p. 15694-700.

110. Akl, M.R., et al., *Molecular and clinical significance of fibroblast growth factor 2 (FGF2 /bFGF) in malignancies of solid and hematological cancers for personalized therapies.* Oncotarget, 2016. **7**(28): p. 44735-44762.
111. Ahmad, I., T. Iwata, and H.Y. Leung, *Mechanisms of FGFR-mediated carcinogenesis.* Biochim Biophys Acta, 2012. **1823**(4): p. 850-60.
112. Behbod, F., et al., *Transcriptional profiling of mammary gland side population cells.* Stem Cells, 2006. **24**(4): p. 1065-74.
113. Schafer, T., et al., *Unconventional secretion of fibroblast growth factor 2 is mediated by direct translocation across the plasma membrane of mammalian cells.* J Biol Chem, 2004. **279**(8): p. 6244-51.
114. Rapoport, T.A., B. Jungnickel, and U. Kutay, *Protein transport across the eukaryotic endoplasmic reticulum and bacterial inner membranes.* Annu Rev Biochem, 1996. **65**: p. 271-303.
115. Wienhues, U., et al., *Protein folding causes an arrest of preprotein translocation into mitochondria in vivo.* J Cell Biol, 1991. **115**(6): p. 1601-9.
116. Backhaus, R., et al., *Unconventional protein secretion: membrane translocation of FGF-2 does not require protein unfolding.* J Cell Sci, 2004. **117**(Pt 9): p. 1727-36.
117. Sparn, C., et al., *Unconventional secretion mediated by direct protein self-translocation across the plasma membranes of mammalian cells.* Trends Biochem Sci, 2022. **47**(8): p. 699-709.
118. Zacherl, S., et al., *A direct role for ATP1A1 in unconventional secretion of fibroblast growth factor 2.* J Biol Chem, 2015. **290**(6): p. 3654-65.
119. Florkiewicz, R.Z., J. Anchin, and A. Baird, *The inhibition of fibroblast growth factor-2 export by cardenolides implies a novel function for the catalytic subunit of Na+,K+-ATPase.* J Biol Chem, 1998. **273**(1): p. 544-51.
120. Dahl, J.P., et al., *Participation of Na,K-ATPase in FGF-2 secretion: rescue of ouabain-inhibitable FGF-2 secretion by ouabain-resistant Na,K-ATPase alpha subunits.* Biochemistry, 2000. **39**(48): p. 14877-83.
121. Engling, A., et al., *Biosynthetic FGF-2 is targeted to non-lipid raft microdomains following translocation to the extracellular surface of CHO cells.* J Cell Sci, 2002. **115**(Pt 18): p. 3619-31.
122. Blanco, G., J.C. Koster, and R.W. Mercer, *The alpha subunit of the Na,K-ATPase specifically and stably associates into oligomers.* Proc Natl Acad Sci U S A, 1994. **91**(18): p. 8542-6.
123. Legrand, C., et al., *The Na,K-ATPase acts upstream of phosphoinositide PI(4,5)P2 facilitating unconventional secretion of Fibroblast Growth Factor 2.* Commun Biol, 2020. **3**(1): p. 141.
124. Ebert, A.D., et al., *Tec-kinase-mediated phosphorylation of fibroblast growth factor 2 is essential for unconventional secretion.* Traffic, 2010. **11**(6): p. 813-26.
125. Temmerman, K., et al., *A direct role for phosphatidylinositol-4,5-bisphosphate in unconventional secretion of fibroblast growth factor 2.* Traffic, 2008. **9**(7): p. 1204-17.
126. Muller, H.M., et al., *Formation of disulfide bridges drives oligomerization, membrane pore formation, and translocation of fibroblast growth factor 2 to cell surfaces.* J Biol Chem, 2015. **290**(14): p. 8925-37.
127. Zehe, C., et al., *Cell-surface heparan sulfate proteoglycans are essential components of the unconventional export machinery of FGF-2.* Proc Natl Acad Sci U S A, 2006. **103**(42): p. 15479-84.
128. Dimou, E., et al., *Single event visualization of unconventional secretion of FGF2.* J Cell Biol, 2019. **218**(2): p. 683-699.
129. Steringer, J.P., et al., *Key steps in unconventional secretion of fibroblast growth factor 2 reconstituted with purified components.* Elife, 2017. **6**.
130. Esko, J.D., K. Kimata, and U. Lindahl, *Proteoglycans and Sulfated Glycosaminoglycans*, in *Essentials of Glycobiology*, nd, et al., Editors. 2009: Cold Spring Harbor (NY).
131. Sarrazin, S., W.C. Lamanna, and J.D. Esko, *Heparan Sulfate Proteoglycans.* Cold Spring Harbor Perspectives in Biology, 2011. **3**(7).
132. Lin, X., *Functions of heparan sulfate proteoglycans in cell signaling during development.* Development, 2004. **131**(24): p. 6009-21.
133. Ravikumar, M., et al., *Heparan Sulfate Proteoglycans: Key Mediators of Stem Cell Function.* Front Cell Dev Biol, 2020. **8**: p. 581213.
134. Costell, M., et al., *Perlecan maintains the integrity of cartilage and some basement membranes.* J Cell Biol, 1999. **147**(5): p. 1109-22.
135. Farach-Carson, M.C. and D.D. Carson, *Perlecan--a multifunctional extracellular proteoglycan scaffold.* Glycobiology, 2007. **17**(9): p. 897-905.

136. Rapraeger, A., M. Jalkanen, and M. Bernfield, *Cell surface proteoglycan associates with the cytoskeleton at the basolateral cell surface of mouse mammary epithelial cells.* J Cell Biol, 1986. **103**(6 Pt 2): p. 2683-96.
137. Saoncella, S., et al., *Syndecan-4 signals cooperatively with integrins in a Rho-dependent manner in the assembly of focal adhesions and actin stress fibers.* Proc Natl Acad Sci U S A, 1999. **96**(6): p. 2805-10.
138. Filmus, J., M. Capurro, and J. Rast, *Glypicans.* Genome Biol, 2008. **9**(5): p. 224.
139. Filmus, J. and M. Capurro, *The role of glypicans in Hedgehog signaling.* Matrix Biol, 2014. **35**: p. 248-52.
140. Topczewski, J., et al., *The zebrafish glypican knypek controls cell polarity during gastrulation movements of convergent extension.* Dev Cell, 2001. **1**(2): p. 251-64.
141. Lin, X. and N. Perrimon, *Dally cooperates with Drosophila Frizzled 2 to transduce Wingless signalling.* Nature, 1999. **400**(6741): p. 281-4.
142. Nagarajan, A., P. Malvi, and N. Wajapeyee, *Heparan Sulfate and Heparan Sulfate Proteoglycans in Cancer Initiation and Progression.* Front Endocrinol (Lausanne), 2018. **9**: p. 483.
143. Matsuda, K., et al., *Glypican-1 is overexpressed in human breast cancer and modulates the mitogenic effects of multiple heparin-binding growth factors in breast cancer cells.* Cancer Res, 2001. **61**(14): p. 5562-9.
144. Su, G., et al., *Glypican-1 is frequently overexpressed in human gliomas and enhances FGF-2 signaling in glioma cells.* Am J Pathol, 2006. **168**(6): p. 2014-26.
145. Iozzo, R.V. and R.D. Sanderson, *Proteoglycans in cancer biology, tumour microenvironment and angiogenesis.* J Cell Mol Med, 2011. **15**(5): p. 1013-31.
146. Aikawa, T., et al., *Glypican-1 modulates the angiogenic and metastatic potential of human and mouse cancer cells.* J Clin Invest, 2008. **118**(1): p. 89-99.
147. Wang, S., Y. Qiu, and B. Bai, *The Expression, Regulation, and Biomarker Potential of Glypican-1 in Cancer.* Front Oncol, 2019. **9**: p. 614.
148. Lewis, J.M., et al., *Integrated Analysis of Exosomal Protein Biomarkers on Alternating Current Electrokinetic Chips Enables Rapid Detection of Pancreatic Cancer in Patient Blood.* ACS Nano, 2018. **12**(4): p. 3311-3320.
149. Maeda, N., *Proteoglycans and neuronal migration in the cerebral cortex during development and disease.* Frontiers in Neuroscience, 2015. **9**.
150. Mikami, T. and H. Kitagawa, *Biosynthesis and function of chondroitin sulfate.* Biochimica Et Biophysica Acta-General Subjects, 2013. **1830**(10): p. 4719-4733.
151. Nadanaka, S. and H. Kitagawa, *Heparan sulphate biosynthesis and disease.* Journal of Biochemistry, 2008. **144**(1): p. 7-14.
152. Esko, J.D. and R.J. Linhardt, *Proteins that Bind Sulfated Glycosaminoglycans*, in *Essentials of Glycobiology*, nd, et al., Editors. 2009: Cold Spring Harbor (NY).
153. Loo, B.M., et al., *Binding of heparin/heparan sulfate to fibroblast growth factor receptor 4.* J Biol Chem, 2001. **276**(20): p. 16868-76.
154. Pye, D.A., et al., *Heparan sulfate oligosaccharides require 6-O-sulfation for promotion of basic fibroblast growth factor mitogenic activity.* J Biol Chem, 1998. **273**(36): p. 22936-42.
155. Guimond, S., et al., *Activating and inhibitory heparin sequences for FGF-2 (basic FGF). Distinct requirements for FGF-1, FGF-2, and FGF-4.* J Biol Chem, 1993. **268**(32): p. 23906-14.
156. Maccarana, M., B. Casu, and U. Lindahl, *Minimal sequence in heparin/heparan sulfate required for binding of basic fibroblast growth factor.* J Biol Chem, 1993. **268**(32): p. 23898-905.
157. Rudd, T.R., M.D. Preston, and E.A. Yates, *The nature of the conserved basic amino acid sequences found among 437 heparin binding proteins determined by network analysis.* Mol Biosyst, 2017. **13**(5): p. 852-865.
158. Nickel, W. and M. Seedorf, *Unconventional mechanisms of protein transport to the cell surface of eukaryotic cells.* Annu Rev Cell Dev Biol, 2008. **24**: p. 287-308.
159. Lambaerts, K., S.A. Wilcox-Adelman, and P. Zimmermann, *The signaling mechanisms of syndecan heparan sulfate proteoglycans.* Curr Opin Cell Biol, 2009. **21**(5): p. 662-9.
160. Afratis, N.A., et al., *Syndecans - key regulators of cell signaling and biological functions.* FEBS J, 2017. **284**(1): p. 27-41.
161. Dews, I.C. and K.R. Mackenzie, *Transmembrane domains of the syndecan family of growth factor coreceptors display a hierarchy of homotypic and heterotypic interactions.* Proc Natl Acad Sci U S A, 2007. **104**(52): p. 20782-7.
162. Simons, M. and A. Horowitz, *Syndecan-4-mediated signalling.* Cell Signal, 2001. **13**(12): p. 855-62.

163. Lim, S.T., et al., *Direct binding of syndecan-4 cytoplasmic domain to the catalytic domain of protein kinase C alpha (PKC alpha) increases focal adhesion localization of PKC alpha.* J Biol Chem, 2003. **278**(16): p. 13795-802.
164. Tkachenko, E. and M. Simons, *Clustering induces redistribution of syndecan-4 core protein into raft membrane domains.* J Biol Chem, 2002. **277**(22): p. 19946-51.
165. Tkachenko, E., et al., *Fibroblast growth factor 2 endocytosis in endothelial cells proceed via syndecan-4-dependent activation of Rac1 and a Cdc42-dependent macropinocytic pathway.* J Cell Sci, 2004. **117**(Pt 15): p. 3189-99.
166. Elfenbein, A., et al., *Syndecan 4 regulates FGFR1 signaling in endothelial cells by directing macropinocytosis.* Sci Signal, 2012. **5**(223): p. ra36.
167. Filmus, J. and S.B. Selleck, *Glypicans: proteoglycans with a surprise.* Journal of Clinical Investigation, 2001. **108**(4): p. 497-501.
168. Mayor, S. and H. Riezman, *Sorting GPI-anchored proteins.* Nat Rev Mol Cell Biol, 2004. **5**(2): p. 110-20.
169. Hancock, J.F., *Lipid rafts: contentious only from simplistic standpoints.* Nat Rev Mol Cell Biol, 2006. **7**(6): p. 456-62.
170. Mertens, G., et al., *Heparan sulfate expression in polarized epithelial cells: the apical sorting of glypican (GPI-anchored proteoglycan) is inversely related to its heparan sulfate content.* J Cell Biol, 1996. **132**(3): p. 487-97.
171. Nam, E.J. and P.W. Park, *Shedding of cell membrane-bound proteoglycans.* Methods Mol Biol, 2012. **836**: p. 291-305.
172. Svensson, G., et al., *Crystal structure of N-glycosylated human glypican-1 core protein: structure of two loops evolutionarily conserved in vertebrate glypican-1.* J Biol Chem, 2012. **287**(17): p. 14040-51.
173. Khan, S., et al., *The solution structure of heparan sulfate differs from that of heparin: implications for function.* J Biol Chem, 2011. **286**(28): p. 24842-54.
174. Awad, W., D.T. Logan, and K. Mani, *GPC1 (glypican 1).* Atlas Genet Cytogenet Oncol Haematol, 2014. **7**: p. 461-3.
175. Lu, H., et al., *Elevated glypican-1 expression is associated with an unfavorable prognosis in pancreatic ductal adenocarcinoma.* Cancer Med, 2017. **6**(6): p. 1181-1191.
176. Qiao, D., et al., *Glypican-1 regulates anaphase promoting complex/cyclosome substrates and cell cycle progression in endothelial cells.* Mol Biol Cell, 2008. **19**(7): p. 2789-801.
177. Qiao, D., et al., *Heparan sulfate proteoglycans as regulators of fibroblast growth factor-2 signaling in brain endothelial cells. Specific role for glypican-1 in glioma angiogenesis.* J Biol Chem, 2003. **278**(18): p. 16045-53.
178. Veugelers, M., et al., *Characterization of glypican-5 and chromosomal localization of human GPC5, a new member of the glypican gene family.* Genomics, 1997. **40**(1): p. 24-30.
179. Saunders, S., S. Paine-Saunders, and A.D. Lander, *Expression of the cell surface proteoglycan glypican-5 is developmentally regulated in kidney, limb, and brain.* Dev Biol, 1997. **190**(1): p. 78-93.
180. Li, F., et al., *Glypican-5 stimulates rhabdomyosarcoma cell proliferation by activating Hedgehog signaling.* J Cell Biol, 2011. **192**(4): p. 691-704.
181. Li, Y., et al., *The overexpression of glypican-5 promotes cancer cell migration and is associated with shorter overall survival in non-small cell lung cancer.* Oncol Lett, 2013. **6**(6): p. 1565-1572.
182. Yang, X., et al., *Glypican-5 is a novel metastasis suppressor gene in non-small cell lung cancer.* Cancer Lett, 2013. **341**(2): p. 265-73.
183. Zhang, C., et al., *A lung cancer gene GPC5 could also be crucial in breast cancer.* Mol Genet Metab, 2011. **103**(1): p. 104-5.
184. Veugelers, M., et al., *Glypican-6, a new member of the glypican family of cell surface heparan sulfate proteoglycans.* J Biol Chem, 1999. **274**(38): p. 26968-77.
185. Capurro, M., et al., *Glypican-6 promotes the growth of developing long bones by stimulating Hedgehog signaling.* J Cell Biol, 2017. **216**(9): p. 2911-2926.
186. Li, Y.Y., et al., *Glypican 6 is a putative biomarker for metastatic progression of cutaneous melanoma.* Plos One, 2019. **14**(6).
187. Capurro, M., et al., *Glypican-3 binds to Frizzled and plays a direct role in the stimulation of canonical Wnt signaling.* J Cell Sci, 2014. **127**(Pt 7): p. 1565-75.
188. Huang, K. and S. Park, *Heparan Sulfated Glypican-4 Is Released from Astrocytes by Proteolytic Shedding and GPI-Anchor Cleavage Mechanisms.* eNeuro, 2021. **8**(4).

189. Watanabe, K., H. Yamada, and Y. Yamaguchi, *K-glypican: a novel GPI-anchored heparan sulfate proteoglycan that is highly expressed in developing brain and kidney.* J Cell Biol, 1995. **130**(5): p. 1207-18.
190. Cebecauer, M., et al., *Membrane Lipid Nanodomains.* Chem Rev, 2018. **118**(23): p. 11259-11297.
191. Simons, K. and E. Ikonen, *Functional rafts in cell membranes.* Nature, 1997. **387**(6633): p. 569-72.
192. Simons, K. and G. van Meer, *Lipid sorting in epithelial cells.* Biochemistry, 1988. **27**(17): p. 6197-202.
193. Sezgin, E., et al., *The mystery of membrane organization: composition, regulation and roles of lipid rafts.* Nat Rev Mol Cell Biol, 2017. **18**(6): p. 361-374.
194. Simons, K. and W.L. Vaz, *Model systems, lipid rafts, and cell membranes.* Annu Rev Biophys Biomol Struct, 2004. **33**: p. 269-95.
195. Kucherak, O.A., et al., *Switchable nile red-based probe for cholesterol and lipid order at the outer leaflet of biomembranes.* J Am Chem Soc, 2010. **132**(13): p. 4907-16.
196. Danylchuk, D.I., et al., *Redesigning Solvatochromic Probe Laurdan for Imaging Lipid Order Selectively in Cell Plasma Membranes.* Anal Chem, 2020. **92**(21): p. 14798-14805.
197. Weber, G. and F.J. Farris, *Synthesis and spectral properties of a hydrophobic fluorescent probe: 6-propionyl-2-(dimethylamino)naphthalene.* Biochemistry, 1979. **18**(14): p. 3075-8.
198. Owen, D.M., et al., *Quantitative imaging of membrane lipid order in cells and organisms.* Nature Protocols, 2012. **7**(1): p. 24-35.
199. Dietrich, C., et al., *Lipid rafts reconstituted in model membranes.* Biophys J, 2001. **80**(3): p. 1417-28.
200. Kim, H.M., et al., *A two-photon fluorescent probe for lipid raft imaging: C-laurdan.* Chembiochem, 2007. **8**(5): p. 553-9.
201. Bongiovanni, M.N., et al., *Multi-dimensional super-resolution imaging enables surface hydrophobicity mapping.* Nat Commun, 2016. **7**: p. 13544.
202. Carravilla, P., et al., *Long-term STED imaging of membrane packing and dynamics by exchangeable polarity-sensitive dyes.* Biophys Rep, 2021. **1**(2): p. None.
203. Sezgin, E., et al., *Polarity-Sensitive Probes for Superresolution Stimulated Emission Depletion Microscopy.* Biophys J, 2017. **113**(6): p. 1321-1330.
204. Vance, D.E.V.J.E., *Biochemistry of lipids, lipoproteins and membranes*. Cholesterol: evolution of structure and function, ed. K. Bloch. 1991, Amsterdam: Elsevier.
205. Crane, J.M. and L.K. Tamm, *Role of cholesterol in the formation and nature of lipid rafts in planar and spherical model membranes.* Biophys J, 2004. **86**(5): p. 2965-79.
206. van Meer, G., D.R. Voelker, and G.W. Feigenson, *Membrane lipids: where they are and how they behave.* Nat Rev Mol Cell Biol, 2008. **9**(2): p. 112-24.
207. Ikonen, E., *Cellular cholesterol trafficking and compartmentalization.* Nat Rev Mol Cell Biol, 2008. **9**(2): p. 125-38.
208. Radhakrishnan, A. and H.M. McConnell, *Chemical activity of cholesterol in membranes.* Biochemistry, 2000. **39**(28): p. 8119-24.
209. Lange, Y., J. Ye, and T.L. Steck, *How cholesterol homeostasis is regulated by plasma membrane cholesterol in excess of phospholipids.* Proceedings of the National Academy of Sciences of the United States of America, 2004. **101**(32): p. 11664-11667.
210. Das, A., et al., *Three pools of plasma membrane cholesterol and their relation to cholesterol homeostasis.* Elife, 2014. **3**.
211. Maxfield, F.R. and D. Wustner, *Analysis of cholesterol trafficking with fluorescent probes.* Methods Cell Biol, 2012. **108**: p. 367-93.
212. Smutzer, G., B.F. Crawford, and P.L. Yeagle, *Physical properties of the fluorescent sterol probe dehydroergosterol.* Biochim Biophys Acta, 1986. **862**(2): p. 361-71.
213. Schroeder, F., et al., *Fluorescence properties of cholestatrienol in phosphatidylcholine bilayer vesicles.* Biophys Chem, 1988. **32**(1): p. 57-72.
214. Li, Z., E. Mintzer, and R. Bittman, *First synthesis of free cholesterol-BODIPY conjugates.* J Org Chem, 2006. **71**(4): p. 1718-21.
215. Marks, D.L., R. Bittman, and R.E. Pagano, *Use of Bodipy-labeled sphingolipid and cholesterol analogs to examine membrane microdomains in cells.* Histochemistry and Cell Biology, 2008. **130**(5): p. 819-832.
216. Shaw, J.E., et al., *Correlated fluorescence-atomic force microscopy of membrane domains: structure of fluorescence probes determines lipid localization.* Biophys J, 2006. **90**(6): p. 2170-8.

217. Ercan, B., et al., *Molecular basis of accessible plasma membrane cholesterol recognition by the GRAM domain of GRAMD1b.* EMBO J, 2021. **40**(6): p. e106524.
218. Naito, T., et al., *Movement of accessible plasma membrane cholesterol by the GRAMD1 lipid transfer protein complex.* Elife, 2019. **8**.
219. Lucero, H.A. and P.W. Robbins, *Lipid rafts-protein association and the regulation of protein activity.* Arch Biochem Biophys, 2004. **426**(2): p. 208-24.
220. Anderson, R.G., et al., *Potocytosis: sequestration and transport of small molecules by caveolae.* Science, 1992. **255**(5043): p. 410-1.
221. Couet, J., et al., *Identification of peptide and protein ligands for the caveolin-scaffolding domain. Implications for the interaction of caveolin with caveolae-associated proteins.* J Biol Chem, 1997. **272**(10): p. 6525-33.
222. Razani, B., et al., *Caveolin-1-deficient mice are lean, resistant to diet-induced obesity, and show hypertriglyceridemia with adipocyte abnormalities.* J Biol Chem, 2002. **277**(10): p. 8635-47.
223. Drab, M., et al., *Loss of caveolae, vascular dysfunction, and pulmonary defects in caveolin-1 gene-disrupted mice.* Science, 2001. **293**(5539): p. 2449-52.
224. Wang, S., et al., *Knockdown of caveolin-1 by siRNA inhibits the transformation of mouse hepatoma H22 cells in vitro and in vivo.* Oligonucleotides, 2009. **19**(1): p. 81-8.
225. Tang, Z., et al., *Molecular cloning of caveolin-3, a novel member of the caveolin gene family expressed predominantly in muscle.* J Biol Chem, 1996. **271**(4): p. 2255-61.
226. Volonte, D., et al., *Caveolin-1 and caveolin-3 form heterooligomeric complexes in atrial cardiac myocytes that are required for doxorubicin-induced apoptosis.* Am J Physiol Heart Circ Physiol, 2008. **294**(1): p. H392-401.
227. Le Lay, S. and T.V. Kurzchalia, *Getting rid of caveolins: phenotypes of caveolin-deficient animals.* Biochim Biophys Acta, 2005. **1746**(3): p. 322-33.
228. Collins, B.M., et al., *Structure-based reassessment of the caveolin signaling model: do caveolae regulate signaling through caveolin-protein interactions?* Dev Cell, 2012. **23**(1): p. 11-20.
229. Carninci, P., et al., *The transcriptional landscape of the mammalian genome.* Science, 2005. **309**(5740): p. 1559-63.
230. Frank, P.G., et al., *Caveolin-1 and regulation of cellular cholesterol homeostasis.* Am J Physiol Heart Circ Physiol, 2006. **291**(2): p. H677-86.
231. Murata, M., et al., *VIP21/caveolin is a cholesterol-binding protein.* Proc Natl Acad Sci U S A, 1995. **92**(22): p. 10339-43.
232. Fielding, C.J., A. Bist, and P.E. Fielding, *Caveolin mRNA levels are up-regulated by free cholesterol and down-regulated by oxysterols in fibroblast monolayers.* Proc Natl Acad Sci U S A, 1997. **94**(8): p. 3753-8.
233. de Almeida, C.J.G., *Caveolin-1 and Caveolin-2 Can Be Antagonistic Partners in Inflammation and Beyond.* Front Immunol, 2017. **8**: p. 1530.
234. Steringer, J.P. and W. Nickel, *A direct gateway into the extracellular space: Unconventional secretion of FGF2 through self-sustained plasma membrane pores.* Semin Cell Dev Biol, 2018. **83**: p. 3-7.
235. Gerstner, M., *Unraveling the Interactome of Fibroblast Grwoth Factor 2, a Potent Tumor Cell-Survival Factor*, in *Department of Biology*. 2017, Ruprecht-Karls University Heidelberg.
236. Hoglinger, D., et al., *Trifunctional lipid probes for comprehensive studies of single lipid species in living cells.* Proc Natl Acad Sci U S A, 2017. **114**(7): p. 1566-1571.
237. Muller, R., et al., *Synthesis and Cellular Labeling of Multifunctional Phosphatidylinositol Bis- and Trisphosphate Derivatives.* Angew Chem Int Ed Engl, 2021. **60**(36): p. 19759-19765.
238. Schindelin, J., et al., *Fiji: an open-source platform for biological-image analysis.* Nat Methods, 2012. **9**(7): p. 676-82.
239. Urlinger, S., et al., *Exploring the sequence space for tetracycline-dependent transcriptional activators: novel mutations yield expanded range and sensitivity.* Proc Natl Acad Sci U S A, 2000. **97**(14): p. 7963-8.
240. Albritton, L.M., et al., *A putative murine ecotropic retrovirus receptor gene encodes a multiple membrane-spanning protein and confers susceptibility to virus infection.* Cell, 1989. **57**(4): p. 659-66.
241. Tinevez, J.Y., et al., *TrackMate: An open and extensible platform for single-particle tracking.* Methods, 2017. **115**: p. 80-90.
242. Roux, K.J., et al., *A promiscuous biotin ligase fusion protein identifies proximal and interacting proteins in mammalian cells.* J Cell Biol, 2012. **196**(6): p. 801-10.

243. Choi-Rhee, E., H. Schulman, and J.E. Cronan, *Promiscuous protein biotinylation by Escherichia coli biotin protein ligase.* Protein Sci, 2004. **13**(11): p. 3043-50.
244. Mayle, K.M., A.M. Le, and D.T. Kamei, *The intracellular trafficking pathway of transferrin.* Biochim Biophys Acta, 2012. **1820**(3): p. 264-81.
245. Axelrod, D., *Cell-substrate contacts illuminated by total internal reflection fluorescence.* J Cell Biol, 1981. **89**(1): p. 141-5.
246. Dunn, K.W., M.M. Kamocka, and J.H. McDonald, *A practical guide to evaluating colocalization in biological microscopy.* Am J Physiol Cell Physiol, 2011. **300**(4): p. C723-42.
247. Lolicato, F., et al., *Cholesterol promotes both head group visibility and clustering of PI(4,5)P₂ driving unconventional secretion of Fibroblast Growth Factor 2.* bioRxiv, 2021: p. 2021.04.16.440132.
248. Lolicato, F., et al., *Cholesterol promotes clustering of PI(4,5)P2 driving unconventional secretion of FGF2.* J Cell Biol, 2022.
249. Simons, K. and R. Ehehalt, *Cholesterol, lipid rafts, and disease.* J Clin Invest, 2002. **110**(5): p. 597-603.
250. Mora, R., et al., *Caveolin-2 localizes to the golgi complex but redistributes to plasma membrane, caveolae, and rafts when co-expressed with caveolin-1.* J Biol Chem, 1999. **274**(36): p. 25708-17.
251. Laguerre, A. and C. Schultz, *Novel lipid tools and probes for biological investigations.* Curr Opin Cell Biol, 2018. **53**: p. 97-104.
252. Rapoport, T.A., *Protein translocation across the eukaryotic endoplasmic reticulum and bacterial plasma membranes.* Nature, 2007. **450**(7170): p. 663-9.
253. Mellman, I. and G. Warren, *The road taken: past and future foundations of membrane traffic.* Cell, 2000. **100**(1): p. 99-112.
254. Nickel, W. and C. Rabouille, *Mechanisms of regulated unconventional protein secretion.* Nat Rev Mol Cell Biol, 2009. **10**(2): p. 148-55.
255. Ras-Carmona, A., M. Gomez-Perosanz, and P.A. Reche, *Prediction of unconventional protein secretion by exosomes.* BMC Bioinformatics, 2021. **22**(1): p. 333.
256. Wegehingel, S., C. Zehe, and W. Nickel, *Rerouting of fibroblast growth factor 2 to the classical secretory pathway results in post-translational modifications that block binding to heparan sulfate proteoglycans.* FEBS Lett, 2008. **582**(16): p. 2387-92.
257. Villarreal, L., et al., *Unconventional secretion is a major contributor of cancer cell line secretomes.* Mol Cell Proteomics, 2013. **12**(5): p. 1046-60.
258. La Venuta, G., et al., *Small Molecule Inhibitors Targeting Tec Kinase Block Unconventional Secretion of Fibroblast Growth Factor 2.* J Biol Chem, 2016. **291**(34): p. 17787-803.
259. Trautmann, A., *Extracellular ATP in the immune system: more than just a "danger signal".* Sci Signal, 2009. **2**(56): p. pe6.
260. Shafraz, O., et al., *Mapping transmembrane binding partners for E-cadherin ectodomains.* Proc Natl Acad Sci U S A, 2020. **117**(49): p. 31157-31165.
261. Mani, K., et al., *The heparan sulfate-specific epitope 10E4 is NO-sensitive and partly inaccessible in glypican-1.* Glycobiology, 2004. **14**(7): p. 599-607.
262. Raman, R., et al., *Structural specificity of heparin binding in the fibroblast growth factor family of proteins.* Proc Natl Acad Sci U S A, 2003. **100**(5): p. 2357-62.
263. Skou, J.C. and M. Esmann, *The Na,K-ATPase.* J Bioenerg Biomembr, 1992. **24**(3): p. 249-61.
264. Rindler, T.N., et al., *Knockout of the Na,K-ATPase alpha(2)-isoform in the cardiovascular system does not alter basal blood pressure but prevents ACTH-induced hypertension.* Am J Physiol Heart Circ Physiol, 2011. **301**(4): p. H1396-404.
265. Moseley, A.E., et al., *Deficiency in Na,K-ATPase alpha isoform genes alters spatial learning, motor activity, and anxiety in mice.* J Neurosci, 2007. **27**(3): p. 616-26.
266. Papiewska-Pajak, I., et al., *Glypican-1 Level Is Elevated in Extracellular Vesicles Released from MC38 Colon Adenocarcinoma Cells Overexpressing Snail.* Cells, 2020. **9**(7).
267. Loh, C.Y., et al., *The E-Cadherin and N-Cadherin Switch in Epithelial-to-Mesenchymal Transition: Signaling, Therapeutic Implications, and Challenges.* Cells, 2019. **8**(10).
268. Foda, A.A., et al., *Relation of glypican-3 and E-cadherin expressions to clinicopathological features and prognosis of mucinous and non-mucinous colorectal adenocarcinoma.* Tumour Biol, 2015. **36**(6): p. 4671-9.
269. Causeret, M., et al., *N-cadherin association with lipid rafts regulates its dynamic assembly at cell-cell junctions in C2C12 myoblasts.* Mol Biol Cell, 2005. **16**(5): p. 2168-80.
270. Wang, Y., et al., *Significance of glycosylphosphatidylinositol-anchored protein enrichment in lipid rafts for the control of autoimmunity.* J Biol Chem, 2013. **288**(35): p. 25490-25499.

271. Sekar, R.B. and A. Periasamy, *Fluorescence resonance energy transfer (FRET) microscopy imaging of live cell protein localizations.* J Cell Biol, 2003. **160**(5): p. 629-33.
272. Gutierrez, J. and E. Brandan, *A novel mechanism of sequestering fibroblast growth factor 2 by glypican in lipid rafts, allowing skeletal muscle differentiation.* Mol Cell Biol, 2010. **30**(7): p. 1634-49.
273. Dalskov, S.M., et al., *Lipid raft localization of GABA A receptor and Na+, K+-ATPase in discrete microdomain clusters in rat cerebellar granule cells.* Neurochem Int, 2005. **46**(6): p. 489-99.
274. Fang, C., et al., *Identification of Palmitoylated Transitional Endoplasmic Reticulum ATPase by Proteomic Technique and Pan Antipalmitoylation Antibody.* J Proteome Res, 2016. **15**(3): p. 956-62.
275. Levental, I., et al., *Palmitoylation regulates raft affinity for the majority of integral raft proteins.* Proc Natl Acad Sci U S A, 2010. **107**(51): p. 22050-4.
276. Cucchi, D., et al., *Omega-3 polyunsaturated fatty acids impinge on CD4+ T cell motility and adipose tissue distribution via direct and lipid mediator-dependent effects.* Cardiovasc Res, 2020. **116**(5): p. 1006-1020.
277. Opreanu, M., et al., *Docosahexaenoic Acid (DHA 22:6n3) Inhibits Sphingomyelin Signaling Pathway and Ceramide Production in the Retina.* Investigative Ophthalmology & Visual Science, 2007. **48**(13): p. 45-45.
278. Opreanu, M., et al., *Docosahexaenoic Acid (dha 22:6n3) Increases Sphingomyelin Content of Caveolae/ Lipid Rafts Isolated From Human Retinal Vascular Endothelial (hrve) Cells.* Investigative Ophthalmology & Visual Science, 2008. **49**(13): p. 3982-3982.
279. Hope, H.R. and L.J. Pike, *Phosphoinositides and phosphoinositide-utilizing enzymes in detergent-insoluble lipid domains.* Mol Biol Cell, 1996. **7**(6): p. 843-51.
280. Laux, T., et al., *GAP43, MARCKS, and CAP23 modulate PI(4,5)P(2) at plasmalemmal rafts, and regulate cell cortex actin dynamics through a common mechanism.* J Cell Biol, 2000. **149**(7): p. 1455-72.
281. van Rheenen, J., et al., *PIP2 signaling in lipid domains: a critical re-evaluation.* EMBO J, 2005. **24**(9): p. 1664-73.
282. Parolini, I., et al., *Expression of caveolin-1 is required for the transport of caveolin-2 to the plasma membrane. Retention of caveolin-2 at the level of the golgi complex.* J Biol Chem, 1999. **274**(36): p. 25718-25.
283. Razani, B., et al., *Caveolin-1 null mice are viable but show evidence of hyperproliferative and vascular abnormalities.* J Biol Chem, 2001. **276**(41): p. 38121-38.
284. Hanson, C.A., et al., *Overexpression of caveolin-1 is sufficient to phenocopy the behavior of a disease-associated mutant.* Traffic, 2013. **14**(6): p. 663-77.
285. Tiwari, A., et al., *Caveolin-1 is an aggresome-inducing protein.* Sci Rep, 2016. **6**: p. 38681.
286. Ostermeyer, A.G., et al., *Accumulation of caveolin in the endoplasmic reticulum redirects the protein to lipid storage droplets.* J Cell Biol, 2001. **152**(5): p. 1071-8.
287. Razani, B., et al., *Caveolin-2-deficient mice show evidence of severe pulmonary dysfunction without disruption of caveolae.* Mol Cell Biol, 2002. **22**(7): p. 2329-44.
288. Aboulaich, N., et al., *Vectorial proteomics reveal targeting, phosphorylation and specific fragmentation of polymerase I and transcript release factor (PTRF) at the surface of caveolae in human adipocytes.* Biochem J, 2004. **383**(Pt 2): p. 237-48.
289. Bastiani, M., et al., *MURC/Cavin-4 and cavin family members form tissue-specific caveolar complexes.* J Cell Biol, 2009. **185**(7): p. 1259-73.
290. Hansen, C.G., et al., *SDPR induces membrane curvature and functions in the formation of caveolae.* Nat Cell Biol, 2009. **11**(7): p. 807-14.
291. Hill, M.M., et al., *PTRF-Cavin, a conserved cytoplasmic protein required for caveola formation and function.* Cell, 2008. **132**(1): p. 113-24.
292. Kovtun, O., et al., *Cavin family proteins and the assembly of caveolae.* J Cell Sci, 2015. **128**(7): p. 1269-78.
293. Otto, G.P. and B.J. Nichols, *The roles of flotillin microdomains--endocytosis and beyond.* J Cell Sci, 2011. **124**(Pt 23): p. 3933-40.
294. Bickel, P.E., et al., *Flotillin and epidermal surface antigen define a new family of caveolae-associated integral membrane proteins.* J Biol Chem, 1997. **272**(21): p. 13793-802.
295. Volonte, D., et al., *Flotillins/cavatellins are differentially expressed in cells and tissues and form a hetero-oligomeric complex with caveolins in vivo. Characterization and epitope-mapping of a novel flotillin-1 monoclonal antibody probe.* J Biol Chem, 1999. **274**(18): p. 12702-9.

296. Stuermer, C.A., et al., *Glycosylphosphatidyl inositol-anchored proteins and fyn kinase assemble in noncaveolar plasma membrane microdomains defined by reggie-1 and -2.* Mol Biol Cell, 2001. **12**(10): p. 3031-45.
297. Neumann-Giesen, C., et al., *Membrane and raft association of reggie-1/flotillin-2: role of myristoylation, palmitoylation and oligomerization and induction of filopodia by overexpression.* Biochem J, 2004. **378**(Pt 2): p. 509-18.
298. Morrow, I.C., et al., *Flotillin-1/reggie-2 traffics to surface raft domains via a novel golgi-independent pathway. Identification of a novel membrane targeting domain and a role for palmitoylation.* J Biol Chem, 2002. **277**(50): p. 48834-41.
299. Babuke, T., et al., *Hetero-oligomerization of reggie-1/flotillin-2 and reggie-2/flotillin-1 is required for their endocytosis.* Cell Signal, 2009. **21**(8): p. 1287-97.
300. Kwiatkowska, K., et al., *Flotillins: At the Intersection of Protein S-Palmitoylation and Lipid-Mediated Signaling.* Int J Mol Sci, 2020. **21**(7).
301. Cai, T., et al., *Regulation of caveolin-1 membrane trafficking by the Na/K-ATPase.* J Cell Biol, 2008. **182**(6): p. 1153-69.
302. Bai, Y., et al., *Differential roles of caveolin-1 in ouabain-induced Na+/K+-ATPase cardiac signaling and contractility.* Physiol Genomics, 2016. **48**(10): p. 739-748.
303. Lemmon, M.A., *Pleckstrin homology (PH) domains and phosphoinositides.* Biochem Soc Symp, 2007(74): p. 81-93.
304. Salim, K., et al., *Distinct specificity in the recognition of phosphoinositides by the pleckstrin homology domains of dynamin and Bruton's tyrosine kinase.* EMBO J, 1996. **15**(22): p. 6241-50.
305. Cornelius, F., et al., *General and specific lipid-protein interactions in Na,K-ATPase.* Biochim Biophys Acta, 2015. **1848**(9): p. 1729-43.
306. Garcia, A., et al., *Cholesterol depletion inhibits Na(+),K(+)-ATPase activity in a near-native membrane environment.* J Biol Chem, 2019. **294**(15): p. 5956-5969.
307. Wu, J., et al., *Cell signaling associated with Na(+)/K(+)-ATPase: activation of phosphatidylinositide 3-kinase IA/Akt by ouabain is independent of Src.* Biochemistry, 2013. **52**(50): p. 9059-67.
308. Wang, J. and D.A. Richards, *Segregation of PIP2 and PIP3 into distinct nanoscale regions within the plasma membrane.* Biol Open, 2012. **1**(9): p. 857-62.
309. Myeong, J., et al., *Compartmentalization of phosphatidylinositol 4,5-bisphosphate metabolism into plasma membrane liquid-ordered/raft domains.* Proc Natl Acad Sci U S A, 2021. **118**(9).
310. Hansen, S.B., *Lipid agonism: The PIP2 paradigm of ligand-gated ion channels.* Biochim Biophys Acta, 2015. **1851**(5): p. 620-8.
311. Haag, M., et al., *Quantification of Signaling Lipids by Nano-Electrospray Ionization Tandem Mass Spectrometry (Nano-ESI MS/MS).* Metabolites, 2012. **2**(1): p. 57-76.
312. Milne, S.B., et al., *A targeted mass spectrometric analysis of phosphatidylinositol phosphate species.* J Lipid Res, 2005. **46**(8): p. 1796-802.
313. Peres, C., et al., *Modulation of phosphoinositide 3-kinase activation by cholesterol level suggests a novel positive role for lipid rafts in lysophosphatidic acid signalling.* FEBS Lett, 2003. **534**(1-3): p. 164-8.

8 Abbreviations

%	Percent
α1	Alpha 1 subunit of the Na,K-ATPase
Å	Angstrom
ABC	Adenosine trisphosphate-binding cassette
AcbA/Acb1/ACBP	Acyl-CoA-binding protein
ARF	ADP ribosylation factors
ATP	Adenosine triphosphate
bp	Base pairs
BSA	Bovine serum albumin
Cav1/Cav2/Cav3	Caveolin-1/caveolin-2/caveolin-3
CDB	Cell dissociation buffer
Cdk1	Cyclin-dependent kinase 1
CHD	Cadherin
CHO cells	Chinese hamster ovary cells
CIP	Calf intestinal phosphatase
CNX	Calnexin
COPI/COPII	Coat protein complex I/coat protein complex II
CRT	Calreticulin
CUPS	Compartments for unconventional protein secretion
DEAE	Diethylaminoethyl cellulose
DHFR	Dihydrofolate reductase
DMEM	Dulbecco’s modified eagle’s medium
DMSO	Dimethyl sulphoxide
DNA	Deoxyribonucleic acid
dNTP	Deoxyribonucleotide triphosphate
dox	Doxycycline
DRM	Detergent resistant membrane
DTT	Dithiothreitol
E. coli	Escherichia coli
ECM	Extracellular matrix
EDTA	Ethylenediaminetetraacetic acid
ER	Endoplasmic reticulum
ERAD	ER-associated degradation
ERES	ER-exit sites
ERGIC	ER-Golgi intermediate compartment
ESCRT	Endosomal sorting complexes required for transport
FACS	Fluorescent activated cell sorting
FCS	Fetal calf serum

FGF	Fibroblast growth factor
FGFR	Fibroblast growth factor receptor
GAG	Glycosaminoglycan
GalNAc	N-acetylgalactosamine
GAPDH	Glycerinaldehyd-3-phosphate-dehydrogenase
GCSI/II	Glucosidase I/II
GEF	Guanine nucleotide exchange factor
GF/GFR	Growth factor/ growth factor receptor
GFP	Green fluorescent protein
Glc	Glucose
GlcA	Glucuronic acid
GlcNAc	N-acetylglucosamine
GPC	Glypican
GPI	Glycosylphosphatidylinositol
GRAM	Glucosyltransferases, Rab-like GTPase activators and Myotubularins
GRASP	Golgi reassembly stacking protein
GSDMD	Gasdermin D
GTP	Guanosine trisphosphate
GTP	Guanosine triphosphate
GUV	Giant unilamellar vesicle
h	Hours
HEK cells	Human embryonic kidney cells
HeLa cells	Henrietta Lacks cells
hep III	Heparinase III
HIV	Human immunodeficiency virus
HMW	High molecular weight
HS	Heparan sulfate
Hsp	Heat shock protein
HSPG	Heparan sulfate proteoglycan
IdoA	Iduronic acid
IL-1β	Interleukin-1β
kDa	Kilo Dalton
KO	Knockout
LB	Lysogeny broth
LCIS	Live cell imaging solution
L_d or L_o	Liquid ordered or disordered
LMW	Low molecular weight
LUV	Unilamellar vesicle
Man	Mannose
MAPK	Mitogent-activated protein kinase

min	Minutes
ml	Milliliter
mRNA	Messenger RNA
ms	Milli-seconds
MVB	Multivesicular body
MβCD	Methy-β-cyclodextrin
n	Number/replicates
NAc	N-acetlyglucosamine
NLS	Nuclear localization signal/sequence
nM, mM or µM	Nano-, milli- or micro-molar
OST	Oligosaccharide transferase
PAGE	Polyacrylamide gel electrophoresis
PAMP	Pathogen-associated molecular patterns
PC	Phosphatidylcholine
PCR	Polymerase chain reaction
PDI	Protein disulfide isomerase
PE	Phosphatidylethanolamine
PFA	Paraformaldehyde
PH	Pleckstrin homology
PI	Phosphatidylinositol
$PI(X)P_x$	Phosphatidylinositol phosphate
PLA	Proximity ligation assays
Plk1	Polo-like kinase 1
PP2A	Protein phosphatase 2
Rft1	Protein RFT1 homolog
RNA	Ribonucleic acid
RT	Room temperature
SDC	Syndecan
SNARE	Soluble n-ethylmaleimide-sensitive fusion protein attachment protein receptor
SRP	Signal recognition particle
STED	Stimulated emission depletion
TANGO1	Transport and Golgi organization protein 1
Tat	Transactivator of tanscription
TF	Trifunctional
TfR	Transferrin receptor
TIRF	Total internal reflection fluorescence
U2OS cells	Human bone osteosarcoma epithelial cells
UPS	Unconventional protein secretion
wt	Wild-type
β	Beta

ΔHS	HS chains removed (via hepIII digest)

All amino acids are abbreviated in conventional three letter or single letter code.

9 Acknowledgements

First of all, I would like to thank Walter Nickel for enabling me to do my PhD in his lab. Walter, you have always been a fair, supporting and motivating supervisor. Discussing my project with you was always very inspiring and I greatly appreciate that your door was always open to me. Thank you for all the nice conversations, being private or work-related, and the great trips to conferences we had together.
Next, I would like to thank my TAC meeting members Michael Brunner and Holger Lorenz for the great support the last years and all your feedback and input in the meetings. A special thanks to Holger who was always available for discussions regarding experimental setups and quantification methods. Thank you for sitting with me at the microscope whenever I had doubts and introducing me to the ZMBH imaging facility.
Thank you to the entire Nickel laboratory for all the years together. It was a very pleasant work atmosphere and I enjoyed when we met privately, be it at the Neckarwiese or going out for dinner. A special thanks to Sabine for introducing me to the laboratory and teaching me many new methods such as generating all those knockout cell lines. A special thanks also to Roberto, who was not only my office and bench partner, but with whom I also very much enjoyed working together and who was always available for discussion and advice.
I would also like to thank all the people and former members of the third floor for the introductions to new machines and for the nice environment. Thanks for all the administrative support to Anke and also Barbara. Pia und Jutta, ich war immer gerne bei euch im Labor, sei es mal ab und an zur cookie time oder auch um gemeinsam pulldowns zu machen. Janathan, te agradezco por todos los momentos divertidos que pasamos juntos en el tercer piso y te valoro tener de amigo.
Tamara, vielen Dank dass du einfach bist wie du bist. Wir haben diese Reise nach Heidelberg zur Masterarbeit und zum Doktor gemeinsam begonnen und es bedeutet mir viel, dass wir uns in all der Zeit unterstützt haben und immer alles besprechen konnten. Danke für die vielen Abende im Bräustadel oder beim gemeinsamen Film gucken.
Vielen Dank auch an meine Eltern und meinen Bruder, die mich während meiner ganzen schulischen und universitären Laufbahn unterstützt haben. Die vielen Gespräche und Zusprüche haben mich immer motiviert weiterzumachen und meinen Weg zu finden und zu gehen.
Und zu guter Letzt aber am wichtigsten: danke Angelo. Danke für all die Sonntagsausflüge die wir gemeinsam ins Labor gemacht haben und all deine Geduld und Unterstützung. Du warst wirklich toll und ich freu mich auf unser gemeinsames Leben, bei dem ich weiß, dass du mich immer bestärken wirst.